BIOCHEMICAL AND MATHEMATICAL MODELING OF MICROAEROBIC CONTINUOUS ETHANOL PRODUCTION BY SACCHAROMYCES CEREVISIAE

Thesis by
Ron Grosz

In Partial Fulfillment of the Requirements
for the Degree of
Doctor of Philosophy

California Institute of Technology
Pasadena, California

1987

ACKNOWLEDGMENTS

I must thank Professor Gregory Stephanopoulos for the support, freedom, and responsibility given to me in conducting the research, and for his patience, especially since the most important results came at the very end. It was a pleasure working in his group. I must also thank Brian Davison for teaching me a variety of laboratory techniques, and Ka-Yiu San for familiarizing me with numerous instruments and the microcomputers. I am grateful to Nam Sun Wang for the general exchange of research ideas and for his help in conducting the most grueling experiments. I express my deep appreciation to Joe Vallino for his assistance with the MIT computing facilities and for the great deal of help he offered during my experimentation. I am indebted to Munaf Shaikh for his laboratory assistance and to Bob Kiss for his consultation in the use of the English language. Partial financial support by the NSF is acknowledged.

For My Family

ABSTRACT

The effect of the aeration intensity in the vicinity of 10ppb of dissolved oxygen upon the steady state, continuous ethanol production by *Saccharomyces cerevisiae* is explored. The specific ethanol productivity increased by 30 to 50% as the aeration rate was reduced, but decreased to the original level as the aeration was further reduced to the lowest rates. These metabolic changes occurred when the respiration rate contributed negligibly to ATP energy production, excluding the Pasteur mechanism, and when the residual glucose level saturated the glucose transporter, excluding glucose kinetics as the cause.

To expose the mechanism of the metabolic changes, the intracellular concentrations of ethanol, glycerol, ATP, glucose 6-phosphate, pyruvate, and NADH, the activities of the hexokinase, alcohol dehydrogenase, fumarase, and isocitrate dehydrogenase, and the cell viability were assayed. Rate-limiting steps were identified by the accumulation of upstream and the depletion of downstream metabolites. The enzyme activity and cofactor measurements elucidated the causes of the rate limitation.

Based on the assays, the metabolic acceleration with decreasing aeration was the result of an increasing glucose transporter activity, and ATP was the most likely activator. The reversal at yet lower aerations resulted from the continued accumulation of ATP until the downstream glycolytic kinases were inhibited.

High concentrations of silicone polymer antifoam decreased the resistance to glycerol transport across the cell membrane, enhancing glycerol production at the expense of ethanol production. Such cultures attained lower ATP concentrations.

The biomass concentration in the fermentor was occasionally found to undergo hysteresis, characterized by extinction and ignition as critical aeration rates were passed. Hysteresis and associated phenomena were prevented by the addition of yeast extract and the removal of the antifoam from the medium. The higher ATP concentration of the low antifoam culture and the biosynthetic intermediates of yeast extract must participate in this transition.

Mathematical models account for all observed phenomena. Featured by the model are the ATP activation of the glucose transporter, ATP wastage by ATPases and such processes, and oxygen induction of ATP waste reactions. Singularity theory was invoked to account for the transition from the hysteresis to monotonic biomass versus aeration bifurcation diagrams.

TABLE of CONTENTS

LIST of FIGURES

Chapter 1.

Chapter 2.

LIST of TABLES

NOMENCLATURE

A	functionality of dissolved oxygen in growth model
ATP	ATP concentration μmol/g
B	functionality of ATP in growth model
C	functionality of ethanol inhibition in growth model
C'_{ext}	pyruvate conc. in perchloric acid extract g/l
d	dilution rate hr^{-1}
D	function in growth model introducing hysteresis
E_{max}	maximum tolerated ethanol concentration for growth mmol/l
EtOH	ethanol concentration mmol/l
G_{ext}	glucose conc. in perchloric acid extract g/l
G_{sup}	glucose conc. in fermentor g/l
I	lumped glycolytic intermediate conc. in catabolic model μmol/g
K_1	coefficient of ATP activation of glucose transport
K_2	coefficient of G6P inhibition of glucose transport
K_3	activity of glycerol production pathway
K_4	coefficient of glycerol inhibition of its own pathway
K_5	transport coefficient of glycerol out of cell
K_6	activity of glycolytic kinase
K_7	conc. of multiply phosphorylated adenylate pool μmol/g
K_8	reductance of unmeasured products relative to glycerol
K_9	low antifoam combination of parameters $K_4K_5/(K_4 + K_5)$
K_{10}	high antifoam combination of parameters as above
K_{11}	coefficient of antifoam inhibition of glucose uptake
K_{12}	maximum activity of ATP waste reactions

K_{13}	half-saturation coeff. of O_2 induction of ATP waste activity
K_{atp}	ATP conc. at half-maximal growth enhancement μmol/g
k_1a	gas-to-liquid transport coefficient of O_2 hr^{-1}
K_o	dissolved O_2 at half maximal-growth enhancement ppb
m	ATP maintenance coefficient mol/g-hr
MW	molecular weight of 1 carbon mole of biomass
P/O	efficiency of oxidative phosphorylation
O_2	dissolved oxygen concentration ppb
O_{2s}	parameter specifying center of "S" shaped function D
Q_a	aeration rate ccpm
R_1	specific glucose uptake rate mmol/g-hr
R_2	specific glycerol prod. rate mmol/g-hr
R_3	specific ethanol prod. rate mmol/g-hr
R_4	glucose utilization for other products mmol/g-hr
R_{atp}	catabolic ATP production rate mmol/g-hr
t	time delay in sample filtration before metabolite extraction l
U_{atp}	ATP utilization by all processes mmol/g-hr
V_{bio}	intracellular volume of biomass l
V_{int}	volume of medium in interstitial spaces of filtered yeast l
V_{neu}	volume of extract neutralization l
V_{per}	volume of perchloric acid extraction solution l
V_{sam}	sample volume from fermentor l
X	biomass concentration g/l
Y_{atp}	ATP yield of growth g/mol

GREEK LETTERS

α	parameter specifying height of "S" shaped function D
β	parameter in "S" shaped function D
μ_{max}	maximum specific growth rate hr^{-1}
ν_g	specific glucose uptake rate g/g-hr.
ν_o	specific oxygen uptake rate g/g-hr
ν_{pyr}	specific pyruvate production rate g/g-hr.

1.1 INTRODUCTION

The fermentative production of ethanol as both a chemical and a fuel has gained considerable attention in the past decade. The traditional approach to ethanol fermentation, the batch process(1), is inefficient for the production of the large volumes of fermentative ethanol envisioned for the future, and has sparked the proposal of numerous new processes(1,2), many of which involve the yeast species *Saccharomyces cerevisiae*.

In the Melle-Boinet process, the yeast crop at the end of batch is recovered and recycled to the next batch, so that the fermentation time to the production of 95% w/v ethanol is reduced to 36 to 72 hours. With the largest inocula of the order of $1x10^8$ cells/ml, the fermentation can be completed in 3-6 hours. A continuous fermentation of ethanol in the sense of a traditional chemostat has also been considered, but suffers from low biomass and ethanol concentrations, and consequently, low ethanol productivities per unit reactor volume(3). Continuous operation has been modified to include cell recycle, allowing for higher biomass concentrations and ethanol productivities of 30-35 g/l-hr, 7.5 times as high as in the conventional chemostat culture(4). A further process improvement is the removal of the toxic product ethanol from the cell recycle reactor by applying a vacuum(5). The vacuum fermentation has seen ethanol productivities of 80 g/l-hr, but has not justified the energetic cost in the compression of CO_2 generated by the fermentation, nor the condensation of the vaporized ethanol(4). Finally, yeast has been immobilized on solid supports and retained within the fermentor to enhance volumetric productivities(6).

The role of oxygen in all of these processes is vital. In the Melle-Bionet process, the recycled crop is useless if the cells lose viability. The viability is enhanced by supplying small quantities of oxygen to fermentation(1), but too much oxygen is to be avoided, since a reduction in the specific ethanol productivity is seen. In the continuous processes, optimal aeration rates for maximum ethanol productivity exist. Below this aeration, lower biomass concentrations and viabilities are supported, while above this level, the specific ethanol productivities begin to decline.

Despite the qualitative knowledge of the importance of oxygen, very few studies have explored the details of its metabolic effects, especially in the context of the continuous fermentation. In this study, the behavior of the product forming pathways in response to changes in the level of aeration is explored. Special emphasis is placed upon the effect of oxygen upon the specific ethanol productivity. The conventional chemostat is chosen as the system most suitable for a fundamental study. The chemostat attains steady states in which the cells' environment and metabolic states are unchanging with time. In this way, the effects of changing only one input to the system, the aeration rate, is gauged in the attainment of a new steady state. Misinterpretation of metabolic events arising from transient environmental conditions are avoided. The chemostat is not optimal for industrial ethanol production, but the fundamental metabolic mechanisms manifested by the chemostat culture will also affect cell recycle or immobilized cell cultures, thereby influencing the process performance.

Special interest is placed upon the strange behaviors of the specific ethanol productivity and glucose uptake rate as a function of dissolved oxygen in a chemostat reported by Nishizawa et al.(7). The important results of these authors is reproduced in Figure 1. As the dissolved oxygen concentration is reduced, the specific ethanol productivity and glucose uptake rate pass through sharp maxima at around 10ppb of dissolved oxygen. Implied is the sudden intensification of the metabolism instigated by the reduction of oxygen and the sudden reversal of the intensification as the dissolved oxygen is further reduced. The result is also odd in that the trace quantities of dissolved oxygen are far below the levels that are thought to influence the specific ethanol productivities through known mechanisms. Cysewski and Wilke(5) also observed the sharp intensification of metabolism by lowering the dissolved oxygen in the parts-per-billion range, as recreated in Figure 2, but did not demonstrate the reversal at the lowest levels. Perhaps the experimental system was unable to attain the extraordinarily low, 1ppb dissolved oxygen concentration necessary for the metabolic reversal. An interesting feature of Figure 2 is that the specific ethanol productivity increases with dissolved oxygen reduction in two stages, separated by a plateau. Presumably, the more aerobic stage relates to respiration, while the more anaerobic stage results from the same enigmatic mechanism governing the results of Nishizawa et al.(7). A substantial fraction of the effort in the studies described herein is allocated to the reproduction of these strange events and the partial elucidation of their cause. Another curiosity is that the phenomena just described are relatively unknown, and their

significance is unrecognized by the authors reporting them. A relatively recent report on the participation of oxygen in ethanol fermentation(8) makes no mention of them.

In the remainder of this chapter, a literature review is presented of the known biochemistry of *Saccharomyces cerevisiae* under the relevant environmental conditions. The second chapter describes the chemostat studies that were undertaken to reproduce the results of Nishizawa et al.(7). Steady states were attained in the chemostat at varying degrees of aeration, and the specific ethanol productivities, specific glycerol productivities, specific glucose uptake rates, and biomass concentrations measured at each steady state. The results of the previous investigators were reproduced in that the specific ethanol productivity increased by 30-45%, attained a maximum, and then decreased by a similar magnitude as the aeration rate was decreased. In addition to this phenomenon, several new and important events were uncovered. Oscillatory states were found to bifurcate as the aeration rate was decreased, or when the reactor was started up under lower aerations. In addition, the biomass concentration versus aeration diagram was found to undergo hysteresis, characterized by the extinction of the biomass concentration as a critical aeration rate was passed from above, and ignition as another critical aeration was passed from below. Between these two aerations, both high and low biomass concentration steady states existed. Hysteresis was prevented by removing the majority of the antifoam from the medium, or by adding yeast extract to the nutrient.

In Chapter 3, the experiments designed to elucidate the cause of the behaviors of the specific ethanol productivity are described. Intra-

cellular enzyme and metabolite assays were undertaken to identify the rate-limiting steps of metabolism causing the increase in the metabolic rate followed by the reversal. Measured as functions of the aeration rate were the intracellular ATP glucose 6-phosphate, pyruvate, NADH, ethanol, and glycerol concentrations. The activities of the glycolytic enzymes hexokinase and alcohol dehydrogenase, and the TCA cycle enzymes fumarase and isocitrate dehydrogenase were assayed. From these results, it was concluded that the metabolic intensification resulted from an enhanced glucose transporter activity, and the most likely activator of the transporter was ATP, whose concentration increased in parallel to the metabolic activity. Evidence is provided that ATP is the source, not only the consequence, of enhanced metabolic rates. The metabolic slowdown at the lowest aeration rates was attributed to rate limitation by one of the downstream kinase enzymes, and the accumulation of ATP to the point that the kinase activity was inhibited was most likely the cause of the rate limitation. Rate limitation was inferred from crossover points in the metabolic pathway. Metabolites upstream of the crossover point accumulate, and those downstream deplete when the rate limiting reaction is slowed. The opposite is true when it is accelerated. A number of other conclusions regarding the energetic efficiency of growth, intracellular ethanol inhibition, and factors affecting glycerol production are drawn, with the aid of the assays.

The final chapter presents mathematical models accounting for all phenomena verified or uncovered in these studies. The maximum in the specific ethanol productivity is predicted by a model that incorporates the ATP activation of the glucose transporter and the regulation of the

downstream kinase by the ATP/ADP ratio. In addition, a model is presented to account for the changing energetic efficiencies of growth that must accompany the sharply changing metabolic rates. The prime elements of the model are the significant wastage of ATP energy by ATPases and such processes and the induction by oxygen of the ATP waste reactions. Finally a model is presented that allows the biomass concentration to undergo a hysteresis-type profile with respect to the aeration rate, and the elimination of hysteresis by yeast extract addition or antifoam removal. The tools of singularity theory are exploited by the model.

1.2 YEAST BIOCHEMISTRY REVIEW

A review of some important elements of yeast biochemistry is presented to facilitate the discussion in subsequent chapters. The review does not encompass all aspects of yeast metabolism, but those viewed by the author as most pertinent to the studies presented. The phenomena considered are those that affect *Saccharomyces cerevisiae* growing on glucose under oxygen limitation. However, during the discussion, examples will be drawn from other strains and growth conditions not employed in these studies, but that may reflect operative mechanisms.

1.2.1 PATHWAYS AND PRODUCTS OF GLUCOSE METABOLISM

The metabolic pathways of the cell provide it with all components needed for growth and viability. These are the building blocks for biosynthesis, ATP energy, and a balancing of surplus or deficient NADH/NADPH reducing power(9). With different substrate concentrations, oxygen levels, nitrogen sources, and degrees of medium richness, the cell can reconfigure its metabolism to meet its needs optimally. In this section, the metabolic configuration of yeast grown under conditions of excess glucose and oxygen limitation, those employed in these studies, is considered.

By far most of the glucose utilized by the cell is converted to carbon dioxide and ethanol by the glycolytic sequence(10). A diagram of the glycolytic pathway with abbreviated intermediate and enzyme names is shown in Fig. 3. The complete names associated with the

abbreviations are presented in Fig. 4. The stoichiometry of the reaction is given by the following equation:

$$C_6H_{12}O_6 \longrightarrow 2CO_2 + 2C_2H_5OH + 2ATP. \qquad (1)$$

This pathway supplies most of the cell's ATP energy as well as the glycolytic intermediates for biosynthesis.

The TCA cycle enzymes, which aerobically couple with the respiratory chain to produce significant ATP through oxidative phosphorylation, have an alternate role with oxygen limitation and surplus glucose. Glucose is a repressor and oxygen an activator of the TCA cycle and respiratory chain enzymes(10-12). Thus, the environmental conditions combine to produce less active respiratory enzymes than are necessary for significant oxidative phosphorylation. The effects of glucose and oxygen will be considered in greater detail in upcoming sections. In addition, oxygen is the terminal acceptor of the respiratory chain, and its presence in only trace quantities eliminates respiration as a major contributor to metabolism. However, the residual TCA cycle activity is thought to provide biosynthetic building blocks such as glutamate and ketoglutarate not attainable elsewhere(9). The TCA cycle activity may also influence the regulation of glycolysis by altering the NADH/NAD ratio and, thus, the action of the glycolytic dehydrogenases. In addition, the TCA cycle enzymes can alter the concentration of citrate, a modulator of the glycolytic enzyme phosphofructokinase(13).

After ethanol, the most significant product is glycerol. In the present study, ethanol accumulates to between 3 and 35 grams per liter

in the fermentor, while the glycerol concentration varies between 1 and 3 grams per liter. Glycerol is produced by the reduction of the glycolytic intermediate dihydroxyacetone phosphate to alpha-glycerol phosphate, the hydrolysis of this compound to glycerol, and the diffusion of glycerol across the cell membrane(14). The pathway is included in Fig. 3. The stoichiometry of the reaction is given by:

$$C_6H_{12}O_6 + 2NADH_2 + 2ATP \longrightarrow 2C_3H_8O_3. \qquad (2)$$

Glycerol synthesis has no direct benefit to the cell, as one mole of its production wastes one mole of ATP, and no biosynthetic building blocks are obtained from the pathway(13). However, glycerol production may serve to oxidize any excess of NADH to NAD, and thereby, perpetuate glycolysis at the reaction of glyceraldehyde 3-phosphate dehydrogenase. The latter enzyme requires NAD as a cofactor. This function may be particularly important during oxygen limitation, since an inactive respiration cannot perform it, and the degree of reductance of yeast biomass is slightly lower than that of glucose(15).

There are further evidences that glycerol production adjusts the redox balance of the cell. Glycerol production increases with increasing growth rates and, hence, the greater need to counterbalance the net NADH produced by the biosynthetic pathways(15). Furthermore, under conditions in which other products such as acetate, acetaldehyde, acetoin, and butylene glycol are formed, glycerol is also produced in a proportion reflecting the redox balance(15). Finally, transition to aerobic conditions or the addition of reducible substances to the medium, both providing alternate routes to NADH reduction, diminishes the excretion

of glycerol(15).

Succinate can accumulate under anaerobic conditions to approximately 1 gram per liter(15). However, more important than the product itself is that its production may imply an altered operation of the TCA cycle under anaerobic, compared to aerobic, conditions. Under aerobic conditions, succinate is produced oxidatively from oxaloacetate to citrate to ketoglutarate and is then further oxidized to fumarate, malate and back to oxaloacetate. This TCA cycle sequence is shown in Fig. 5. However, Chapman and Bartley(16) found no ketoglutarate oxidase activity in anaerobic cells, while the other TCA cycle enzymes were active. This implies that the TCA cycle is halted at the level of this inactive enzyme. From this, the authors further concluded that anaerobically, the portion of the TCA cycle between succinate and oxaloacetate reverses itself and produces succinate reductively. The proposed alteration in the TCA cycle operation during anaerobiosis is shown in Fig 6. Further evidence for this mechanism is provided by the observation that succinate is formed in larger quantities under glucose repression, with respiratory deficient mutants, and upon the addition of inhibitors of mitochondrial protein synthesis, all of which may give rise to lower activities of ketoglutarate oxidase(17).

However, the reductive pathway for succinate production is not universally agreed upon. Other investigators found ketoglutarate oxidase activities under anaerobic conditions sufficient to support the oxidative route(18). Furthermore, succinate production is stimulated by the addition of glutamate to the medium, a process that must occur by the action of ketoglutarate oxidase(15). Finally, it has been argued that

reductive succinate production is inconsistent with the redox balance of the cell(15).

Acetate is a minor metabolic product and is formed primarily at higher PH values than are employed in these studies(13). Acetate production generates NADH and must therefore be accompanied by glycerol production anaerobically. The net reaction is:

$$C_6H_{12}O_6 \longrightarrow CH_3CHO + CO_2 + C_3H_8O_3. \qquad (3)$$

This process is known as Neuberg's second form of fermentation(13).

Other minor products are 2,3-butanediol, acetoin, butyric acid, formic acid, lactic acid, acetaldehyde, and, when amino acids are present in the medium, fusel oils(15). These products are considered not to play a major role in the present study.

The hexose monophosphate pathway has two potential modes of operation in baker's yeast. One mode is the production of NADPH and pentose phosphates needed strictly for biosynthesis(19). The other mode is to provide a route alternate to glycolysis for the conversion of glucose to glyceraldehyde phosphate. However, studies with radioactive tracers and detailed metabolic balances(10,19) indicate a hexose monophosphate pathway flux sufficient to satisfy the former function, but not the latter.

The regeneration of TCA cycle intermediates tapped for biosynthesis is thought to occur through the action of pyruvate carboxylase, whose product is oxaloacetate(20). The glyoxylate bypass enzymes and phosphoenolpyruvate carboxykinase, which duplicate this task, are strongly repressed by glucose.

In conclusion, glycerol and ethanol are the main products of metabolism with high glucose concentrations and oxygen limitation. Ethanol production supplies the ATP energy, and glycerol production adjusts the NADH reductance balance. Respiration is inactive, but most enzymes of the TCA cycle remain active and supply biosynthetic building blocks.

1.2.2 REGULATION OF GLYCOLYSIS

Because glycolysis is the major supplier of ATP energy and intermediates for biosynthesis, the cell must regulate the pathway so that the supply of these factors meets the demand. Such regulation can be the alteration of the enzyme levels, as with repression and induction, or by the regulation of the activity of the enzymes already present, as in activation or inhibition. In this section, the latter mechanisms are considered.

The glycolytic regulation mechanisms are best exemplified and are studied most in conjunction with two special phenomena that yeast exhibits, the Pasteur effect and glycolytic oscillations. In the first part of this section, the Pasteur effect is considered and in the second, glycolytic oscillations.

The Pasteur effect is defined as a decrease in the rate of nutrient uptake by the cell when an anaerobic system is changed to aerobic conditions(21). The effect is usually measured by the Pasteur quotient, PQ, or the ratio of substrate uptake aerobically compared to anaerobically(22).

Resting cells experience the strongest Pasteur regulation with a PQ of 0.5, while cells growing on abundant glucose have virtually no such

regulation(PQ=0.96)(23). Cells growing on sugars that are not strong repressors of the respiratory enzymes, as galactose, have intermediate regulation(PQ=0.66). These vast differences in the strength of the effect have led to confusion in the literature about its very existence(24). However, as will be discussed, these differences have a rational explanation. Additional confusion has arisen in the literature as a result of different methods used to measure the effect(25). The most correct method is to measure directly the differences in the rate of glucose uptake under aerobic and anaerobic conditions. However, the expedient method of Warburg manometry in the measurement of the difference in carbon dioxide production aerobically and anaerobically has frequently been used and has led to erroneous results. Carbon dioxide production is related mainly to ethanol production and cannot account for other fates of glucose such as glycerol and polysaccharide formation(25). The two different methods of calculation can alter the resulting PQ from 0.34 with the Warburg method to 0.55 with the direct method in the same experimental situation(25).

To explain the Pasteur effect, the interaction between the respiratory and glycolytic pathways must be considered. Earlier investigators realized that upon changing from the anaerobic to the aerobic state, respiration and the associated phosphorylation of ADP to ATP is initiated(26). The diminished phosphorus and ADP levels were thought to limit glycolysis at the ADP utilizing steps and in the phosphorus-requiring conversion of

glyceraldehyde phosphate to phosphoglyceric acid(26).

The earlier investigations suffered from two flaws. The first is that no explanation is supplied for the decrease in glucose uptake that accompanies Pasteur regulation. Some inhibition of the glucose transport system or hexokinase is needed. Second, they did not take into account the phenomenon of allosteric regulation that is now known to be a repeated theme in metabolic control(21).

The allosterically regulated enzyme phosphofructokinase is currently thought to be the main target of respiratory inhibition. A variety of compounds have been identified as inhibitors or activators of this enzyme. Among the activators are ammonium ion, potassium, phosphate, AMP, cyclic AMP, fructose diphosphate, ADP, and fructose 6-phosphate(26). Inhibitors are magnesium, citrate, and ATP(26). Some of the activators may be deinhibitors as, for example, phosphate reduces ATP inhibition.

Thus, it is thought that respiratory conversion of ADP to ATP slows glycolysis at PFK, since the latter is an inhibitor and the former an activator. The adenylates are interconverted by adenylate kinase according to(19):

$$ATP + AMP \quad \langle\text{------}\rangle \quad 2ADP. \qquad (4)$$

Thus, a secondary effect of respiratory phosphorylation is a reduced AMP concentration, which can further reduce the PFK activity.

The aforementioned mechanism accounts for a diminished flux through the reactions downstream of PFK, but cannot account for a decreased glucose uptake. It is necessary to propose the inhibition of glucose uptake or phosphorylation by glucose 6-phosphate or fructose 6-phosphate, the accumulating metabolites upstream of PFK. Hexokinase is known to

be inhibited by G6P in certain animal cells(21), but no such inhibition is known in yeast. Sols(28), however, has presented evidence that G6P is indeed an inhibitor of glucose transport in yeast, and thus the Pasteur

mechanism is complete. Sols also recognized the potential importance of citrate in PFK regulation. Depletion of AMP caused by respiration slows the allosterically regulated TCA cycle reaction of isocitrate dehydrogenase causing citrate accumulation and the further inhibition of PFK.

Evidence for ATP involvement in Pasteur regulation has been provided by Fiechter(22). This investigator cultivated yeast in a chemostat under conditions in which respiration was active. The ATP concentration in the microbe paralleled the respiration rate, as the dilution rate was changed, and as the oxygen supply was removed. A twofold increase in the ATP concentration accounted for a Pasteur quotient of 0.85.

Perhaps the most comprehensive studies to date of the Pasteur effect were performed by den Hollander et al.(24,25) and Reibstein et al.(29). Their findings supported the aforementioned mechanism only partially. ADP and phosphate decreased three fold upon aerating an anaerobic system, but the ATP concentration increased by a meager 30%. Hence, the altered PFK activity can be accounted for only by the behaviors of ADP and P, but ATP plays a minimal role. Also, in these investigations, decreased glycolysis and sugar transport rates were correlated with increased intracellular glucose 6-phosphate concentrations, confirming inhibition of transport by this compound. However, in cells cultivated on raffinose,

no such correlation was observed, indicating that with this compound an alternate regulation of glucose uptake is operative, or else the entire concept of G6P regulation is questionable. Finally, these investigators found that 3PGA and F6DP, metabolites downstream of phosphofructokinase, increased in concentration or remained the same upon transition to respiration. This implies the existence of another regulatory site in glycolysis downstream of PFK, perhaps pyruvate kinase(25).

Other competing mechanisms for the Pasteur effect cannot be ignored. A compartmentation mechanism, whereby ATP generated by respiration becomes trapped within the mitochondria and unavailable to glycolysis, can account for the Pasteur effect in reticulocytes(21). Also, the mechanism for competition between respiration and glycolysis for phosphate has been bolstered since its original appearance(21). The lack of phosphate can slow the GAPDH reaction and inhibit both PFK and hexokinase, accounting for all aspects of the Pasteur effect(21). Such a mechanism is invoked in those instances in which Pasteur regulation takes place without a visible change in the concentration in ATP or G6P. In such instances, the property of phosphate as a deinhibitor of ATP can accomplish the regulation.

Finally, it becomes clear why the Pasteur effect is more prevalent in resting cells and cells growing on nonrepressive substrates compared to those growing on glucose. The former two cases have more active TCA cycle and respiratory chain enzymes than the glucose-repressed cells. Hence, a greater proportion of the metabolism is contributed by respiration in unrepressed cells upon aerobic transition, amplifying all aspects of the Pasteur mechanism. In addition, resting cells have only 10% of the

transport activity of growing cells, even anaerobically(30). Again, respiration occupies a greater proportion of the entire metabolism in the resting cells.

The second special phenomenon that manifests glycolytic regulatory mechanism is glycolytic oscillations. Yeast suspensions exhibit periodic oxidation and reduction of NADH, which can be monitored continuously by fluorometry(31). Hence, the trace of NADH fluorescence as a function of time is a damped sinusoid with a typical period of 0.5 minutes. The degree of damping depends on the method of cell preparation with the number of cycles varying from a few to as many as 48(32).

To obtain oscillations, the cell suspension must be prepared as follows. Cells are grown aerobically or anaerobically, washed, resuspended in sugar-free buffer, and starved aerobically for several hours, ensuring complete oxidation of the NADH. Glucose is then added to the system and anaerobic conditions imposed by addition of cyanide or naturally through the respiratory depletion of all dissolved oxygen(32). Upon anaerobiosis, the oscillatory reduction of NAD begins. Cells harvested in the diauxic lag between the fermentative growth on glucose and the respiratory growth on the produced ethanol show the greatest potential for undamped oscillations(32).

Additional factors that influence the nature of the oscillations are the amount of sugar added to initiate the oscillations, the type of sugar, the microbial strain, and the addition of other agents. Oscillations are induced only by intermediate concentrations of glucose near 20mM, whereas vastly higher or lower concentrations inhibit the oscillations(33). Initiation with fructose instead of glucose results in an increase of

the oscillatory period by a factor of 1.5 to 2.0(34). Preincubation with ethanol prevents oscillations until all ethanol has been consumed by respiration(33).

In one study, 16 out of 32 strains of yeast, including several of *Saccharomyces cerevisiae* exhibited oscillations(35). Oscillations were qualitatively similar among the various strains and differed mainly in the period and the optimal glucose concentration for initiation. Oscillations have also been observed in cell-free extracts, in which only the water soluble enzymes are retained(34). Cell-free extracts have oscillatory periods of 5 minutes, compared to 30 seconds for cell suspensions.

Oscillations in the degree of reductance of the nicotinamide pool are necessarily caused by fluctuation in the activity of glyceraldehyde phosphate dehydrogenase, which is the only reducer of NAD in the glycolytic pathway. Such a change in activity must be accomplished by changing the concentration of the substrate of the reaction, glyceraldehyde 6-phosphate. This implies that the entire glycolytic pathway undergoes oscillations in order to supply a sinusoidally varying input to the dehydrogenase. The first steps to deduce the mechanism of the oscillation were to measure the concentrations of the other glycolytic intermediates as a function of time when the NADH fluorescence was oscillating. Ghosh and Chance(31) found that glucose 6-phosphate and fructose 6-phosphate accumulated at the position along the oscillatory cycle in which the glycolytic flux was a minimum, and all intermediates downstream of PFK were depleted. Conversely, when the glycolytic flux was maximal, metabolites upstream of PFK were depleted, while those downstream accumulated. This crossover clearly indicates that PFK is the pacemaker of glycolysis.

Pye(32), performing a similar study, found that in phase with NADH were FDP, ADP, and PEP, while in phase with NAD were G6P, 3PGA, pyruvate, and acetaldehyde. This result indicates the existence of three crossover points across which oscillating metabolites experience a phase change. These crossovers were at PFK, pyruvate kinase, and phosphoglycerate kinase, which are all activated or enhanced by ADP, the ultimate controller of the oscillations.

Pye also found that adding exogenous ADP to an oscillating cell-free extract caused a phase shift in the oscillations. It speeded the rate of increase in the glycolytic rate when added at the point of minimal flux, while it retarded the flux decrease when added after the apex of the cycle. A final, important observation of Pye regarded the feeding of the glycolytic pathway. Oscillations in a cell-free extract could be sustained only with trehalose as the carbon source; glucose arrested the oscillations. Trehalose, a dimer, is broken down slowly by trehalase to glucose, suggesting that a slow, steady supply of glucose rather than a sudden flood is necessary to support oscillations. This theory was confirmed by demonstrating oscillations with the slow infusion of glucose to the system.

The fact that the crossover points are all ADP-controlled led to early mechanistic interpretations of the oscillations. Ghosh and Chance(31) reasoned that ADP is both a product and an activator of phosphofructokinase. Thus, a mechanism of feedback activation of PFK by the product ADP and the downstream removal of the ADP by kinases could simulate the oscillations(37).

The conceptual aspects of the oscillatory cycle were well summarized

by Pye and are easily followed with reference to Fig. 3. Description of the mechanism begins with the position of the cycle at which ADP is at a low level, and in which case, the activity of PFK is also low. The flux of metabolites to the PFK reaction by glucose transport and hexokinase is relatively unimpeded and exceeds the flux through PFK. Fructose 6-phosphate accumulates, and as the substrate for PFK, activates this enzyme. The activation of PFK leads to a greater concentration of its products ADP and FDP. Since the products are also feedback activators, the PFK reaction is further stimulated in a positive feedback fashion. When the PFK flux is maximal, it exceeds the input by the transporter and hexokinase, so that fructose 6-phosphate becomes depleted. Simultaneously, downstream reactions remove ADP, and the cycle is reversed.

Numerous mathematical models have been proposed for the glycolytic oscillations. The minimum requirements for the model to generate oscillations qualitatively similar to experimental result are(38):

1) A constant influx of metabolites to PFK
2) Feedback activation of PFK by one of its products
3) Removal of the activator by downstream reactions.

However, to correctly model the details of the pattern of the oscillations of all metabolites, more complex models are needed that account for interactions among PFK and the other reactions of the pathway. The model must take into account the action of an oscillating ADP on the other kinases, an oscillating NADH on the dehydrogenases, adenylate kinase interconversion among the adenylate phosphates, ATPases, polysaccharide formation, activation of pyruvate kinase by fructose diphosphate, and a

variety of others(39).

The conclusion of this section is that phosphofructokinase is the main regulator of the glycolytic pathway, but that its control is shared by pyruvate kinase and, possibly, phosphoglycerate kinase. The degree to which PFK acts independently depends on the environmental conditions and the state of the microorganism.

1.2.3 GLUCOSE TRANSPORT

The glucose transport system in yeast supplies the cell with its energy, and in the absence of inorganic nitrogen sources, its biosynthetic building blocks in addition. The role of the metabolic regulatory machinery, then, is twofold. One role is to control the transport of glucose at a level that just satisfies the summation of the needs of the biosynthetic and energy-producing pathways. The other role is to allocate the glucose already transported to those pathways.

It has already been established that, under the experimental conditions considered here, the main consumer of glucose is the glycolytic pathway. Thus, any large changes in the rate of glycolysis must necessarily be accompanied by a change in the transport rate of glucose, because transported glucose cannot be diverted to or from any other pathway. Therefore, the regulation of glucose uptake becomes a critical aspect of this study.

The cell has three potential methods of solute transport, diffusion, facilitated diffusion, and active transport(23). Simple diffusion involves the diffusion of the solute through proteinaceous membrane pores, down a

concentration gradient. The process requires no metabolic energy, and the rate of transport is proportional to the concentration gradient. Diffusion is typically limited to compounds of three carbons or smaller, or else larger compounds with exceptionally narrow cross sections(14). Larger cross-section compounds are excluded simply by the limiting size of the membrane pores.

Facilitated diffusion also requires the favor of a concentration gradient, and thus, does not require the input of metabolic energy. The solute binds from the outside to a membrane protein carrier and is transported by translation or rotation of the solute carrier complex to the inside of the membrane(23). Unlike simple diffusion, the rate of transport becomes saturated at high solute concentrations, as is typical of enzyme-mediated reactions. Most common hexoses are transported by facilitated diffusion in *Saccharomyces cerevisiae*(40,41,42).

Active transport, mediated by proteinaceous entities within the membrane, is capable of transporting solutes against a concentration gradient and, therefore, requires the input of metabolic energy. The classic example of an active transporter is the phosphotransferase system of bacteria(43). Energy is supplied to the sugar transporter by its being phosphorylated by phosphoenol pyruvate. There has been speculation about the existence of a phosphate translocation transporter of sugars in *S. cerevisiae*, but it has not been universally accepted(44). However, numerous compounds are transported actively by *S. cerevisiae*, including amino acids(45).

There is overwhelming evidence that glucose transport occurs by facilitated diffusion. The transport of glucose and a variety of other

sugars is saturable, with clearly identifiable Michaelis-Menten constants(40-42). Furthermore, when more than one sugar is present in the medium simultaneously, the uptake rates of the two sugars competitively inhibit one another. This shows that the transporter not only acts on a variety of sugars, but also provides evidence for facilitated diffusion, as the different sugars compete for a limited number of active sites on the carrier.

The sugar transporter is inhibited by very low concentrations of uranyl ions and other agents that have associations with the outer membrane(22). The concentrations of these inhibitors are too low to cause any major damage to the cell membrane, the only instance in which pure diffusional uptake would be inhibited. Instead, this is indicative of interference with a small number of transporter surface sites, relative to the entire membrane area, providing further evidence for facilitated and not simple diffusional uptake.

The sugar transporter is not active, however. The carrier cannot transport sugars against a concentration gradient and can, at most, equilibrate the sugar concentration on either side of the membrane(46). Transport also occurs in the absence of metabolism, as when metabolic inhibitors are added, and in membrane vesicles devoid of intracellular metabolic machinery(22). Clearly, energy addition cannot be involved. Finally, when metabolic inhibitors are added to prevent downstream utilization of the transported glucose, unphosphorylated glucose can be detected inside the cell(46). This precludes the possibility of a phosphate translocation transporter, analogous to the bacterial systems, which would allow only for the appearance of phosphorylated sugar in the cell.

A few additional properties of the sugar transporter are noteworthy. Among the many sugars transported by the carrier, a few nonmetabolizable ones as l-xylose and l-arabinose gain entrance into only 50% of the intracellular compartment volumes and are excluded from the others(45). The implication of this phenomenon on the properties of the transporter is unknown. Countertransport is also possible, so that a cell saturated intracellularly with a sugar will leak the sugar when transferred to a sugar-free medium. In addition, when a second sugar is added to a cell equilibrated with the first sugar, the first sugar will be transiently transported out of the cell against a concentration gradient(22). The first and second sugars compete for the external transporter sites, while intracellularly, the first sugar has no competition. The final important property is that, under both aerobic and anaerobic conditions, only traces or no intracellular unphosphorylated glucose can be found(46). This property has three possible implications. It is possible that the sugar transporter is the rate-limiting process under all conditions, so that transported sugars are instantly phosphorylated by a more active hexokinase. The second possibility is that glucose is phosphorylated before it enters the cell in a group translocation mechanism. Finally, it is possible that the uptake of sugar is closely regulated by an intracellular metabolite, such as glucose 6-phosphate, so that transported glucose never accumulates(46).

As mentioned, the fact that intracellular glucose is not ordinarily found within the cell has led to disagreement over the existence of phosphate translocational transport. Meredith and Romano(44) claimed evidence for active transport. They found that the addition of metabolic

inhibitors causes the dephosphorylation and release of accumulated glucose 6-phosphate from the cell, tying together transport, phosphorylation, and energy generation. Furthermore, when radio labelled pulses of glucose were added, the label found itself intracellularly in the form of phosphorylated glucose, before any intracellular labelled free glucose was detectable. However, none of these observations precluded the possibility of energy-independent transport followed by rapid intracellular phosphorylation by an active hexokinase(22).

The glucose transport mechanism is not a static pump, supplying constant amounts of glucose to the cell under all conditions. Rather, the activity and properties of the pump change with altered needs and environmental conditions. This first became evident when it was found that, in the presence of glucose, the transport of the nonmetabolizable d-xylose was more rapid anaerobically than aerobically, while with glucose absent, there was no difference(46). Subsequently, many more such verifications were found.

Serrano and De La Fuente(47) clearly demonstrated the dependence of transport properties on the energetic state of the cell. They discovered that the Michaelis-Menten constants for the unmetabolized sugars xylose and arabinose were lower by a factor of 2 or 3, when the metabolized sugar mannose was present. In addition, the transport of glucose and fructose was biphasic, with a K_m of 100 mM when the concentrations of the sugars were high, and a K_m of 10 mM and 3mM for fructose and glucose, respectively, when the concentrations of those sugars were low. Addition of iodoacetate, a metabolic inhibitor, forced the transporter to assume the higher K_m, regardless of the sugar concentration. Finally, the

Michaelis-Menten constants for glucose and fructose were an order of magnitude higher aerobically compared to anaerobically. The sum totality of the evidence supported the conclusion that the transporter can exist in two states, characterized by high and low affinity for the substrate, that the state of the transporter is controlled by the level of glycolysis, and that under certain conditions, both states can exist simultaneously. The authors then proceeded to speculate about the role of the transporter in the Pasteur effect. Anaerobically, K_m is low, and the rate of transport is maximal for a given extracellular glucose concentration. Upon introducing air, the increased concentration of some regulatory metabolite pushes the transporter to the low affinity state and achieves the lower transport rate characteristic of the Pasteur effect. The authors explored the possibility that glucose 6-phosphate is this regulator, but could supply no evidence.

Spoerl et al.(48) demonstrated that the activity of the glucose transporter is altered by both the energy state of the cell and the state of the protein-synthesizing machinery. Cells preincubated with glucose expelled preloaded, unmetabolized, sorbose more rapidly than cells not preincubated in glucose. Metabolic inhibitors prevented this acceleration by glucose, as did cycloheximide, an inhibitor of protein synthesis. Pretreatment with ethanol also accelerated solute transport, but not as effectively as glucose. Nonmetabolizable sugars had no such stimulating effect. Addition of amino acids accentuated the effect of glucose. Finally, the activated transporter decayed to the activity of the transporter with no glucose pretreatment after four hours. Thus, the transporter is subjected to continual synthesis and decay, and its eventual

tivity reflects the balance between the two processes. As synthesis quires both ATP energy and protein synthesis, the activity of the ansporter is expected to be greatest in the cells with the most active ergy metabolism and protein-synthesizing machinery.

Bisson and Fraenkel(49-51) provided evidence that the sugar transporter does not exist in a high and low affinity state, as thought by Serrano and De La Fuente, but that the transporter consists of two separate entities, one with low affinity and one with high affinity. Wild-type yeast possesses three hexose kinases, hexokinase A, hexokinase B, and glucokinase. Only the first two can phosphorylate fructose. The wild-type strain demonstrated both the high and the low affinity transport for both glucose and fructose. A mutant deficient in both hexokinases, but not glucokinase, had two K_m's for glucose transport but only low affinity fructose transport. A mutant lacking all three kinases transported both sugars only with low affinity. Cloning of the kinase genes into the deficient mutants further demonstrated that high affinity transport depends on the presence of the cognate hexose kinase. The authors suggested that binding of the hexose kinase to the plasma membrane in association with the high affinity transporter was required for its existence.

Bisson and Fraenkel(51) explored the influence of the environment on the activities of the two transporters. Cells growing exponentially on glucose possessed the most active low affinity transporter and the least active high affinity transporter. During the diauxic phase and the aerobic growth phase on ethanol, high affinity transport became progressively more active, while the opposite was true for low affinity transport. Lower glucose concentrations and the substitution of other sugars that

are not as strongly repressive as glucose resulted in a higher activity of the high affinity carrier. The authors concluded that the high affinity carrier is subject to catabolite repression, not much unlike the respiratory enzymes.

Busturia and Lagunas(52) investigated the decay characteristics of both components of the transporter when cycloheximide, an inhibitor of protein synthesis, was present. Decay of the transporters depended on the presence of active metabolism, as it was prevented by metabolic inhibitors and the presence of only nonmetabolizable sugars. However, ATP alone is not sufficient to cause the deactivation of the carriers, since cells growing on ethanol did not deactivate. In addition, the decay was slower with galactose and maltose, indicating that the rates of decay reflected the rank order of the degree of repression of the carbon source.

The final degree of control that the cell might have, to tune the rate of transport to the metabolic demand, is the transport modulation by glucose 6-phosphate. Inhibition of glucose uptake by G6P has been suggested(46,28,53), but is far from conclusively proven. Typical proofs for the regulation are as follows. In cells undergoing glycolytic oscillations, G6P concentrations do not oscillate(34) This can occur only if the uptake of glucose is regulated to match the oscillating demand of glycolysis by a high sensitivity with respect to G6P. In cells that have transport activity in excess of glycolytic activity, intracellular free sugar does not accumulate. However, if the same cells are exposed to an inhibitor of hexokinase, then intracellular accumulation of the sugar does occur(47). Consequently, the product of the hexokinase reaction is

implicated. Evidence against G6P inhibition of transport is provided by phosphoglucose isomeraseless mutants, which can accumulate high G6P levels without affecting uptake of xylose(54).

In conclusion, we see that glucose uptake rates can be regulated by changing the transporter's affinity to the substrate and by changing the level or activity of the transporters. Such regulation can occur at two levels. One level is the differential rate of synthesis and decay of the low and high affinity transporters, which depends on the energy level, the degree of repression, and the state of protein synthesis. The second level is the modulation of the existing activity by an intracellular metabolite as G6P, the concentration of which depends on the metabolic state of the cell. Hence, the activity of the glucose transporter is a potential source of any observed changes in the metabolic rate of the cell.

1.2.4 CRABTREE EFFECT AND CATABOLITE REPRESSION

The Crabtree effect refers to a decrease in the respiration rate caused by the repression of the TCA cycle and respiratory chain enzymes by fermentable substrates in the medium(23). With the high residual glucose levels found in the fermentations studied within, the Crabtree effect is maximally operative. Therefore, the Crabtree effect is one of the reasons for the negligible respiration rates observed. In addition, catabolite repression must be included in any mechanism proposed to explain experimentally observed phenomena.

The Crabtree effect manifests itself by influencing the macroscopic

properties of both batch and continuous cultures growing on fermentable carbon sources. Batch growth on glucose occurs in two exponential phases separated by a lag, characteristic of diauxic growth(56,57). During the first exponential phase, the growth rate is near maximum(0.4/hr), the respiratory quotient high(around 15), and the respiration rate low(20 ml/g-hr). Energy metabolism is almost purely fermentative, with a stoichiometric expulsion of ethanol in relation to sugar uptake. After the glucose is exhausted, the exponential phase terminates, and a lag phase ensues. During this lag, the cell synthesizes the machinery enabling it to grow on the ethanol previously expelled. Thus, the cell must synthesize respiratory enzymes(since ethanol cannot be fermented) and gluconeogenetic enzymes, enabling it to synthesize six-carbon compounds from the two-carbon ethanol. Once the transition is accomplished, the cell initiates a second exponential phase in which the growth rate is reduced(0.15/hr), and the rate of oxygen uptake is high(250 ml/g-hr), representing the sole source of energy production. The disappearance of glucose is strongly correlated with the appearance of a strengthened respiration and the presence of other repressible processes.

In continuous culture with glucose as a limiting substrate, growth is mostly oxidative at dilution rates below 0.25/hr, with a respiratory quotient near 1.0(57). As the dilution rate is increased from 0.05 to 0.25/hr, the respiration rate increases, consistent with the fact that respiration is the energy producer. Above the dilution rate of 0.25/hr, the metabolism becomes progressively more fermentative, with an RQ increasing to 14 linearly as the dilution rate approaches 0.45. Simultaneously, the residual glucose and ethanol concentrations rise sharply,

while the rate of respiration declines by a factor of 3. Again, the repression of respiration is correlated with the level of residual glucose in the medium.

The onset of fermentation above a dilution rate of 0.25 may not be entirely due to the repression of the respiratory enzymes(58). Even a fully active respiratory system may be incapable of sustaining a flux necessary to support the higher growth rates. In such a case, a bottleneck would occur at pyruvate oxidase, the point at which glycolytic intermediates are channeled towards respiration. The higher pyruvate concentration would be diverted towards ethanol production by pyruvate decarboxylase. Such a competition between pyruvate oxidase and carboxylase has been proposed as a significant regulator of respiration and fermentation(59). Pyruvate decarboxylase's higher K_m for pyruvate makes it only 2% active when the oxidase is fully active(11). The branch point is poised to channel pyruvate towards respiration until the process is saturated, whereupon a switch is made to fermentation. High glycolytic fluxes are also accompanied by increased pyruvate carboxylase activity(12).

A multitude of studies of both batch and continuous culture have revealed that the TCA cycle and respiratory chain enzymes are significantly repressed when metabolism is fermentative(11,12,60-64). In comparing the respiratory to the fermentative exponential phases of batch growth, the TCA cycle enzymes, such as isocitrate dehydrogenase, fumarase, malate dehydrogenase, oxoglutarate oxidase, and aconitase are more active by a factor of 3-6(11,61,63). Respiratory enzymes as succinate cytochrome c reductase, cytochrome c oxidase, and NADH cytochrome c reductase are activated by factors of 5 to 100(12,61). Cytochrome absorbance increases

by a factor of 5 to 20(61). In continuous culture, similar activity changes can be observed in the transition between dilution rates supporting fermentation and those supporting respiration(62).

In addition to the respiratory enzymes, the gluconeogenetic enzymes phosphoenolpyruvate carboxykinase and hexose diphosphatase(65), the glyoxylate bypass enzymes, isocitrate lyase and malate synthase(11,65), and the enzymes required for other degradative pathways, such as maltase and invertase(66) are all strongly repressed by glucose and may be completely absent as long as glucose is present. None of these enzymes are useful during fermentative growth.

The morphology of mitochondria changes in the transition from repression to derepression. Perlman and Mahler(61) found repressed mitochondria to be larger in volume, fewer in number, and more irregularly shaped than the symmetric, derepressed mitochondria. The total mitochondrial volume per cell was also lower during repression. In contrast, Fiechter et al.(23) found smaller and more spherical mitochondria under repressed conditions. Finally, Polakis et al.(64) saw no mitochondria at all with repression, but this may have been due to an inferior method of sample preparation for electron microscopy.

Limited studies have been made of the dynamics of repression and derepression. Perlman and Mahler(61) subdivided the derepression process during batch growth transition into two phases, the fermentative phase and the oxidative phase. The fermentative phase begins when glucose is nearly exhausted from the medium, but is yet present at 0.4 g/l. At this stage, all respiratory enzymes with the exception of cytochrome oxidase begin to increase in activity. The oxidative phase is initiated

when the residual glucose level falls below 0.1 g/l, at which point cytochrome oxidase begins to increase in activity, and the other enzymes continue their activation. The addition of chloramphenicol, an inhibitor of the mitochondrial protein-synthesizing machinery, had no effect during the fermentative phase, but halted all new enzyme synthesis in the oxidative phase.

Chapman and Bartley(67) studied the dynamics of repression in submerging respiratory-competent cells into fermentative medium. The enzymes were classified into three groups, based on their responses. The loss of activity of the first group, isocitrate dehydrogenase, glutamate dehydrogenase, and cytochrome oxidase was slower than would be expected if all new synthesis stopped and activity was diluted by growth. The second group, aconitase, oxoglutarate oxidase, and fumarase lost activity as though all new synthesis was arrested. The third, isocitrate dehydrogenase and all remaining respiratory chain enzymes, lost activity more quickly than would be possible by growth dilution, indicating a mechanism of catabolite inactivation, in addition to repression.

The nature of the repressing compound and its mode of action have been the subject of much research with no success(23). A few clues have surfaced, however. Repression appears to be correlated more with the rate of metabolism than the concentration of substrate in the medium. Glucose and fructose are more rapidly metabolized than maltose or galactose, while simultaneously, the former are stronger repressors than the latter. In addition, the enzyme patterns in the first and second exponential phases of batch growth correspond identically to those existing in continuous culture at the same specific growth rates(62). This is true

despite the fact that the substrate for growth in the second batch phase is ethanol, while that in oxidative continuous growth is glucose. Finally, the initiation of catabolite repression in aerobic and anaerobic continuous culture occurs at a glucose uptake rate of about 2.4 mmoles/g-hr, despite the different dilution rates at which this uptake rate exists(23).

Gorts(68) contrasted the batch fermentations of glucose and the less repressive maltose, in search of the identity of the repressor. The two fermentations made equal use of the pentose phosphate pathway and possessed identical concentrations of RNA, protein, glucan, mannan, glycogen, and trehalose. The only difference was the higher glucose 6-phosphate concentration in glucose culture, which correlated with a lower aconitase activity. However, this did not prove that G6P is the repressor.

Numerous investigators have sought the role of cyclic AMP in the repression. Recall that in bacteria, cyclic AMP combines with the repressor protein to enable transcription of the Lac operon(23). Some success has been achieved in the reversal of glucose repression by exogenously added cyclic AMP(69,70). However, doubt has been cast on the physiological role of cyclic AMP, as mutants devoid of adenylate cyclase and cyclic AMP undergo the identical derepression as wild type cells(71).

Entian(66) discovered the involvement of the hexokinase P2 isoenzyme in the repression mechanism. Cells with alterations in this enzyme do not experience catabolite repression. However, these mutations did not influence the phosphorylating activity of this enzyme, thus preserving the intracellular distribution of metabolites. Thus, repression is related to the structure but not to the phosphorylating activity of this enzyme.

Repression, in some cases, has been demonstrated to be caused by the cessation of the transcription of the affected DNA(72), as opposed to post translational modification or some other mechanism. Six proteins found in derepressed cells are absent in repressed cells. The same six proteins were absent from RNA1 temperature sensitive mutants grown initially at the nonpermissive temperature, subsequently, transferred to a repressive medium at a permissive temperature(72). RNA1 is a factor critical for the transport of messenger RNA from the nucleus to the cytoplasm. Thus, messenger RNA is clearly not produced for those six proteins in repression medium.

The work of Barford and Hall(73) and Barford et al.(74), which disputes the sum totality of the literature regarding repression, must be mentioned. In chemostat culture above a dilution rate of 0.25, previously thought to be the threshold for repression, the respiratory activity did not decrease, but remained constant at the maximal observed rate for any dilution rate. Repression was found above the critical dilution rate only transiently, with maximal activity resulting after 30-200 generations. Furthermore, with appropriate adaptation, glucose cultures respired identically to galactose cultures. Maximal respiration was also observed in carefully prepared and adapted batch cultures. Thus, the authors concluded that previous observations of the Crabtree effect were really transients, which would have disappeared with longer cultivation times. By their definition, the Crabtree effect does not qualify as a genuine regulatory phenomenon.

1.2.5 EFFECT OF OXYGEN ON THE RESPIRATORY ENZYMES AND LIPID CONTENT

The concentration of oxygen employed in these studies is below the level required to support a significant degree of respiration. Nonetheless, the trace concentrations can have a profound effect on the activities of the TCA cycle enzymes, mitochondrial ATPases, and the levels of unsaturated fatty acids and sterols. The TCA cycle enzymes are thought to provide intermediates to the biosynthetic pathways even when respiration is absent(75). Therefore, changes in the TCA activities in response to changes in the dissolved oxygen can have a direct effect on the growth rate. Similarly the mitochondrial ATPase(76) can actively dephosphorylate ATP and, therefore, influence the ATP yield of the cell. Finally, the unsaturated fatty acid and sterol content under oxygen limitation is low, may limit growth, and can be changed by altering the oxygen concentration(77).

To facilitate the subsequent discussion, a brief outline of the structure of the mitochondrial inner membrane is provided. The inner membrane contains five important enzyme complexes, the NADH coenzyme Q reductase, succinate coenzyme Q reductase, coenzyme QH_2 cytochrome C reductase, cytochrome C oxidase, and the F1 ATPase(78). The sequence of the redox enzymes along the respiratory chain are shown schematically in Fig. 7. Cytochrome C and coenzyme Q, also known as ubiquinone, are mobile carriers shuttling electrons between the enzyme complexes. Cytochromes A and A_3 are associated with cytochrome C oxidase, cytochromes B and C_1 are associated with coenzyme Q cytochrome C reductase, and cytochrome C stands alone.

The effect of oxygen on respiration has been studied under conditions

in which glucose repression was eliminated(77,79,80). Repression is avoided by low dilution rates and by low feed-glucose concentrations in continuous culture and by a low galactose concentration in batch culture. As the dissolved oxygen concentration is increased from anaerobiosis to approximately 1% of air saturation, the rate of respiration increases, linearly(80) or with a Michaelis-Menten saturation parameter of 0.4%, from zero to 50-150 nmol/min-g(77,80).

Apart from the rate of respiration, however, a measure of the respiratory competence is provided by the potential respiration rate. To measure the latter, cells are removed from the fermentor, centrifuged, and resuspended in a buffer saturated with oxygen. The potential respiration rate increases from 50 to 300 nmol/min-g as the dissolved oxygen is increased from zero to 1% of air saturation(77). However, the increase shows saturation kinetics and reaches a half-maximal value at a very low 0.04% of air saturation. The experimental comparison of the potential and actual respiration rate as a function of the dissolved oxygen is reconstructed in Fig. 8. Thus, the ability of yeast to respire is more sharply induced by oxygen than is the actual respiration rate.

The activities of a number of TCA cycle, respiratory chain, and glyoxylate bypass enzymes were measured as a function of DO(77,79,80). All enzymes are induced by oxygen, with responses that can be subdivided into two categories. The first category shows extremely sharp induction similar to the potential respiration rate(77,80). It includes succinate cytochrome C reductase, succinate dehydrogenase, and fumarase. The second category shows a more gradual induction characteristic of the actual respiration rate and includes cytochrome oxidase and all of the

glyoxylate bypass enzymes(77,80). Thus, the behavior of the potential respiration rate is founded upon the induction of the respiratory enzymes with the exception of cytochrome oxidase. Furthermore, the different behavior of the actual respiration rate reflects the fact that the respiratory enzymes are saturated at a higher oxygen concentration than is required for their maximal induction.

In a separate study(77), the malate dehydrogenase activity was measured as a function of the percent oxygen in gas supply to the fermentor. The activity of the enzyme jumped when the oxygen content was increased from zero to 0.2%, but subsequently increased gradually through an oxygen content of 50%. This dual behavior is thought to be the result of the existence of two isoenzymes of malate dehydrogenase, one of which is degradative and induced sharply, and the other is biosynthetic and slowly induced. Aconitase, yet unmentioned, is another TCA cycle enzyme induced by oxygen(63).

Cytochromes A, A_3, B, and C_1 are induced sharply, but ubiquinone and cytochrome C respond gradually(80). The induction of cytochromes B and C_1 is consistent with the increase in activity of succinate cytochrome C reductase, in which they reside. However, a discrepancy exists between the induction of cytochrome oxidase and the constituent cytochrome AA_3. This discrepancy may indicate a sequential process by which the apoprotein associates with the prosthetic group and is then incorporated into the inner mitochondrial membrane with structural proteins. Thus, the activity of the incorporated enzyme does not necessarily parallel the quantity of the component parts.

In addition to the enzyme activities and the potential respiration

rate, the unsaturated fatty acid content, the total fatty acid content, and the sterol content sharply increase with oxygenation, with a half-maximal stimulation occurring at 0.04 to 0.2% of air saturation(77). The stimulation is consistent with the requirement of molecular oxygen in the biosynthetic pathways of unsaturated fatty acids and sterols.

Oxygen affects the morphology and size of the mitochondria themselves. Early studies have claimed that mitochondria do not exist under anaerobic conditions or under severe glucose repression, but that mitochondriagenesis ensues by supplying oxygen or removing glucose from the system(63,81). However, later studies revealed that mitochondrialike structures exist anaerobically, but are more fragile than normal mitochondria, and are destroyed by the permanganate method of fixation for electron microscopy(82). Freeze etching preserved these mitochondria-like structures, which were named promitochondria. Promitochondria are unable to respire, lacking succinate dehydrogenase, cytochrome oxidase, NADH oxidase, and all cytochromes except B_1(76). They do possess mitochondrial DNA and the oligomycin-sensitive F1 ATPase associated with mitochondria, but the latter is less active than in respiring mitochondria. In addition, promitochondria have a different lipid composition than the aerobic counterpart(83), having a far lower ergosterol content, even when ergosterol is supplemented in the medium. Furthermore, they have a paucity of unsaturated fatty acids unless supplemented with Tween 80, in which case they derive 90% of the unsaturated lipid content from the medium(83).

When oxygen is introduced, promitochondria are converted into aerobic mitochondria by the addition of lipids and proteins to the pre-existing

structures(84). The mitochondrial protein synthesizing machinery, subservient to mitochondrial DNA, produce cytochromes AA_3, B, and membrane factors associated with the ATPase, while all remaining proteins are synthesized in the cytoplasm, taking signals from chromosomal DNA(84). Therefore, oxygen induces and glucose represses the manufacture of proteins in both the cytoplasm and the mitochondria. Finally, mitochondria increase in number by division(84).

Investigators have questioned whether all components of mitochondria are synthesized in equal proportion in a coordinated fashion, or whether different regulatory mechanisms apply to different components. Ferdouse et al.(85) studied the kinetics of change of mitochondrial number, volume, and the content of the cytochromes during glucose derepression and anaerobic-to-aerobic transitions in the presence and absence of added ergosterol and Tween 80. Upon glucose derepression, not all components are synthesized in proportion, as indicated by the 11-fold increase in cytochrome A, compared to a 4-fold increase in the number of mitochondria per cell. On anaerobic-to-aerobic transition without lipid supplements, the ratio of cytochromes to mitochondrial volume continually increases. During the same adaptation in the presence of added ergosterol and Tween 80, mitochondrial numbers increase in steps that correspond to decreases in the volumes of the individual mitochondria indicating division. Corresponding to the division is an increase in protein synthesis.

Gordon and Stewart(86) investigated the relationship between the incorporation of lipids and proteins into the mitochondria. The addition of chloramphenicol, an inhibitor of mitochondrial protein synthesis, to anaerobic cells undergoing aerobic transition causes protein synthesis

to be totally inhibited, ubiquinone and unsaturated fatty acid synthesis to be partially inhibited, and sterol synthesis to be uninhibited. From this evidence, there appears to be a coupling among the production of the various components, but the coupling is not absolute, and the regulatory mechanisms involved must be complex(86).

Perlman and Mahler(61) presented the opinion that upon glucose derepression, cytochrome oxidase, ATPase, and the cytochromes increased in the amount per cell, but not in the amount per mitochondrial mass, suggestive of these components' being constitutive of mitochondria. Other components may alter their loading of the mitochondria.

Since the majority of the mitochondrial proteins are synthesized in the cytoplasm, and the synthesis of mitochondrial matter is not perfectly coordinated, the localization of the oxidative enzymes comes to question. Nurminen and Suomalainen(87) studied the location of the TCA cycle and respiratory chain enzymes within the cell, upon the transfer of anaerobic cells to aerobic, glucose limited medium. Approximately 80% of the induced respiratory chain enzymes are located in the mitochondrial fraction. In contrast, only 20-40% of the TCA cycle activity is found in the mitochondrial fraction, the remainder residing in the cytoplasm.

The relative strength of glucose repression compared to oxygen induction, especially when both factors limit respiration simultaneously, is the subject of debate. Chapman and Bartley(67) transferred aerobically grown cells into both aerobic and anaerobic media containing high glucose concentrations. Glucose was found to be the predominant influence on the enzymatic pattern. The greatest differences were detected in the respiratory chain enzymes, for which oxygen partially alleviates the

repressive effects of glucose. In most cases, however, it is thought that only the lack of oxygen, not an excess of glucose, can completely block the synthesis of the cytochromes(88).

Despite the absence of respiration in the studies presented within, we find that oxygen can alter growth and product formation directly or indirectly, by altering the TCA cycle and ATPase activity and stimulating unsaturated fatty acid and sterol synthesis.

1.2.6 EFFECT OF OXYGEN AND GLUCOSE ON THE GLYCOLYTIC ENZYMES

Contained herein are studies of ethanol production by yeast. Of great importance, therefore, are the levels and changes in the activities of the glycolytic enzymes in response to changes in the environment. More numerous studies document the effects of oxygen and glucose on the respiratory enzymes, but influences upon the glycolytic enzymes have also been revealed. This section considers such influences.

In their enzymatic study of the transition of yeast from aerobic to anaerobic, glucose derepressed medium, Chapman and Bartley(67) noted that several glycolytic enzymes behaved oppositely from respiratory enzymes. Pyruvate kinase, pyruvate decarboxylase, and alcohol dehydrogenase all increased in specific activity three to five-fold in a coordinated manner. The increased activity was interpreted as an adaptation that enabled the microbe to operate more optimally in the new environment.

Hommes(89) observed a similar activation in the strain C. parapsilosis. The responses of the enzymes in the transition from 0.6% to 1.2% glucose in the medium can be subdivided into three classes. The majority

of the enzymes experience a 1.5 to 3-fold activation. Aldolase, triose-phosphate isomerase, and pyruvate kinase increase in activity by a factor of 10 or more. In contrast, phosphofructokinase remained almost constant, and alcohol dehydrogenase was repressed. Upon further increase in the glucose concentration to 20%, only aldolase and triose phosphate isomerase further increase in activity. The distinct responses suggest control under different operons.

The most comprehensive report of the effects of glucose on the glycolytic enzymes was presented by Maitra and Lobo(90,91) The addition of glucose to a S. fragilis, S. dobzhanskii cross growing on basal medium elicits a 3 to 100-fold increase in the glycolytic enzyme activities, with phosphoglucose isomerase having the smallest response, and glyceraldehyde 3-phosphate dehydrogenase having the strongest. Exceptions are alcohol and aldehyde dehydrogenases, which lose activity. The activities of the enzymes that gained in activity were plotted against the hexokinase activity, in a variety of experimental conditions. In all cases, a linear relationship between all enzymes and hexokinase activity, with a positive slope and high correlation coefficient, was found indicating a coordinated synthesis of the enzymes.

The kinetics of enzyme synthesis was recorded from the transients in the enzyme activities upon resuspension in a glucose-containing medium(90). All enzymes increase in activity without delay, except for enolase, phosphoglycerate kinase, and pyruvate decarboxylase, which show two-hour delays. The kinetic response to the addition of galactose instead of glucose is similar but with added delay. Upon removal of sugars from the medium, deactivation initiates and can be accounted for by dilution

due to growth.

In seeking the identity of the metabolites causing the induction, Maitra and Lobo(90) measured the intracellular metabolite pools in both glucose- and galactose-grown cultures. The main difference between the two cultures is the delay in the attainment of the same, high intracellular glucose 6-phosphate concentration in the galactose culture, compared to the glucose culture. This was interpreted as the cause of the delayed induction of the enzymes in the galactose culture. These investigators also questioned whether, among the enzymes that exist in two or more isoenzymes, both isoenzymes are induced, or one is induced in preference to the other. Isoenzymes of hexokinase, phosphoglucose isomerase, and phosphoglycerate kinase are equally induced, while only one isoenzyme of triose phosphate isomerase is induced. The conclusion of this work was that G6P is the inducer of the enzymatic activity, and the differing patterns of induction among enzymes indicate different thresholds for G6P induction, differential induction among isoenzymes, and different rates of enzyme degradation.

Maitra and Lobo(91) further investigated the role of G6P as an inducer. 2-Deoxyglucose and other glucose analogues that are phosphorylated by hexokinase, but otherwise not metabolized, succeed in inducing the enzymes, while nonphosphorylated analogues fail. In hexokinase-deficient mutants, only glucose is phosphorylated; fructose is not. In such a mutant, only glucose succeeds in glycolytic induction, while fructose fails. All of these evidences point to G6P or a phosphorylated analog as the inducer. However, the investigators proceeded to show, with phosphoglucose isomeraseless mutants, that hexokinase, and possibly

phosphofructokinase, are more likely induced by mannose 6-phosphate.

A conflict exists over the response of alcohol dehydrogenase to the addition of glucose. Maitra and Lobo(91) saw inactivation, Chapman and Bartley(67) saw activation, and Hommes(89) saw both under different circumstances. The discrepancy is possibly explained by the existence of two and possibly three isoenzymes of alcohol dehydrogenase(92,93). One isoenzyme is repressed by glucose and operates when ethanol is the carbon source. The other is induced and operates when glucose is the carbon source. Thus, the enzymes catalyze reactions in opposite directions. Both, however, have NAD as the coenzyme.

Finally, Oura(93) noted an effect of oxygen upon glycolytic enzymes when glucose induction is eliminated. Oxygen addition causes a decrease in hexokinase, phosphofructokinase, and alcohol dehydrogenase activity. In contrast, pyruvate decarboxylase activity shows a minimum at intermediate aeration rates. The phenomenon was interpreted as an adaptation to a new respiratory environment, which obviated the presence of excess glycolytic enzyme activity.

1.2.7 NEGATIVE PASTEUR EFFECT

The negative Pasteur effect refers to an increase in the alcoholic fermentation rate after supplying oxygen to an anaerobic system. Such behavior is opposite to what is allowed by the ordinary Pasteur regulation and must derive from an alternate mechanism. The study of such mechanisms is made important by the fact that, in the chemostat cultures operated in these studies, there was indeed a stimulation of fermentation by oxygen

in the lowest aeration ranges.

The negative Pasteur effect in the *Saccharomyces* strains occur primarily with resting cells in succinate buffer of low PH(4.5-5.5)(94). Other TCA cycle acids have no ability to produce the effect at physiological concentrations. Addition of potassium cyanide, the respiratory inhibitor, to aerobic cells did not abolish the effect, indicating that respiration has no part.

In attempting to find the cause of the effect from differences between aerobically and anaerobically grown cells, it was found(94) that the intracellular pH of the anaerobic cells is lower. This PH difference was confirmed to be due to a higher intracellular succinate in the anaerobic cells. Thus, an inhibition of anaerobic fermentation is correlated with a more rapid uptake and accumulation of succinate from the medium under anaerobic conditions. An additional clue was supplied by the lessened ability of the anaerobic cells to phosphorylate deoxyglucose. The evidence suggests the inhibition of hexokinase either directly or indirectly by succinate. However, the addition of glucose 6-phosphate to the cell suspension has a minimal effect, and the addition of ATP, ADP, NAD, dihydroxyacetone, and a variety of glycolytic compounds had no effect in alleviating the anaerobic inhibition of fermentation. These compounds, especially the phosphorylated ones, may not permeate the cell membrane, however. As a result, experiments on cell-free extracts were initiated.

Cell-free extracts of *Saccharomyces* experienced a negative Pasteur effect in fumaric, malic, and citric acid buffers, in addition to succinate(94), the sole inducer in cell suspensions. With the permeability

barrier of the cell membrane eliminated, G6P, fructose mono and diphosphate, 3-phosphoglyceric acid, and ATP reverse the negative Pasteur effect by stimulating anaerobic fermentation. Dihydroxyacetone and NAD have no effect. In addition, anaerobic extracts with inhibited fermentation rates have lower ATP concentrations than extracts relieved by the presence of oxygen. Thus, the bottleneck in *Saccharomyces* is caused by the inhibition of hexokinase either directly, or through the depletion of ATP by the heightened succinate content of the anaerobic cells; that is, succinate is either a hexokinase inhibitor, or the cause of an ATP depletion.

Bonnet and de Jonge(95) studied the effect of a variety of organic buffers on the appearance of a negative Pasteur effect in *S. uvarum*. With the exception of succinic acid, none of the TCA cycle intermediates cause the effect. However, numerous physiological compounds, including acetate, formate, and glutarate, induce the effect. Most striking are the facts that a mere 0.08 M acetate produces a negative Pasteur quotient of 0.56, and only 0.01 M formate results in a quotient of 0.80. The quotient is defined as the ratio between anaerobic and aerobic fermentation rates. The investigators had no speculation about mechanisms.

The *Brettanomyces* strains of yeast experience a negative Pasteur effect without the need for succinate or any other buffer(94). In contrast to the *Saccharomyces* strains, anaerobic fermentation is stimulated by dihydroxyacetone, acetaldehyde, pyruvate, ketoglutarate, and others that can enzymatically oxidize NADH. In addition, unlike *Saccharomyces* strains, respiratory deficient mutants ferment equally under anaerobic and aerobic conditions. Thus, respiration of the supplied oxygen is the alleviator

of inhibition of anaerobic fermentation characteristic of the negative Pasteur effect. The likely bottleneck anaerobically is the glyceraldehyde reaction, which lacks NAD. Supplying oxygen oxidizes NADH by respiration, supplementing the deficient NAD, and allowing resumed fermentation. Similar effects are expected by the addition of the enzymatically reducible compounds.

Silhankova et al.(96) compared the aerobic and anaerobic fermentation rates of four strains of bottom brewer's yeast and 26 of their respiratory deficient mutants. Of the respiring strains, only one is distinguished by a high ordinary Pasteur quotient of 1.42. It obtains this quotient by possessing a higher anaerobic fermentation rate, rather than a lower aerobic fermentation rate, than the other strains. Furthermore, this strain does not respire more quickly than the other strains, barring a strengthened ordinary Pasteur mechanism. Respiratory deficient mutants have both lower aerobic and anaerobic fermentation rates than the respiring counterparts, but anaerobic fermentation is inhibited to a greater extent, resulting in a general reduction of the Pasteur quotient. Two mutants experience such a strong inhibition of anaerobic fermentation that an ordinary Pasteur effect of the respiratory-sufficient parents is converted into a negative Pasteur effect.

In seeking to explain the inhibition, the investigators(96) took into consideration the mechanisms discussed above, and also the fact that numerous respiratory deficient-mutants are auxotrophic for lysine and glutamic acid. The auxotrophy is the result of blockages in the TCA cycle, preventing biosynthesis. The same blockages could cause accumulated TCA cycle intermediates, such as succinic acid, which are inhibitors in

the negative Pasteur effect. However, they found no auxotrophy among the strains inhibited anaerobically.

Thus, in those instances in which oxygen stimulates fermentation, as in the continuous culture studies presented here, an inhibited hexokinase, or depleted NAD or ATP may be the cause.

1.2.8 YIELD STUDIES

The ATP supplied by the glycolytic pathway must be consumed in three processes. First, in growing cells, part of the ATP is consumed in the biosynthesis of monomers, their incorporation into polymers, and the assembly of the polymers into cell structure. All of these processes are energetically driven. The second energy consumer is the maintenance of cell viability. The cell must transport ions against a concentration gradient, maintain intracellular pH, and reconstruct degraded structures. Third, any surplus ATP produced in glycolysis, not consumed in either of these two processes, must be wasted outright by ATPases or by other ATP dumping mechanisms. Hence, the level of glycolysis reflects the sum utilization by these three processes. Changes in the level of glycolysis, as have been concretely observed in the research described within, necessarily reflect changes in the ATP consumption in at least one of these three processes. Therefore, it is important to study the ATP sinks, so that variability in ATP consumption can be explained.

In the study of the energetics of anaerobic growth on glucose, it is convenient to subdivide the metabolism into constituent anabolic and catabolic pathways, as has been suggested by Roels(97) and Dekkers

et al.(98). The glycolytic pathway to ethanol production is represented as:

$$C_6H_{12}O_6 \longrightarrow 2ATP + 2CO_2 + 2C_2H_5OH. \qquad (5)$$

The ATP produced represents the stoichiometric contribution of substrate level phosphorylation. Naturally, the ATP produced is counterbalanced by ADP and P on the opposite side. The second pathway produces glycerol(98):

$$C_6H_{12}O_6 + 2NADH_2 + 2ATP \longrightarrow 2C_3H_8O. \qquad (6)$$

Contrary to ethanol production, glycerol production consumes ATP. In addition, $NADH_2$ is supplied to this reaction by the biosynthetic pathways. Recall that there is net $NADH_2$ production in biosynthesis, owing to the lower degree of reductance of yeast biomass than glucose. Finally, the sum of all biosynthetic reactions can be lumped into one equation(98):

$$0.183C_6H_{12}O_6 + (MW/Y_{atp})ATP + 0.17NH_3 \longrightarrow CH_{1.83}O_{0.56}N_{0.17} + 0.09NADH_2 + 0.095CO_2 + 0.35H_2O. \qquad (7)$$

The formula $CH_{1.83}O_{0.56}N_{0.17}$ represents the elemental composition of yeast biomass as measured by Dekkers et al.(98). The carbon dioxide generated in this reaction comes from the small net production of carbon dioxide among the weighted sum of the biosynthetic pathways as computed by Oura(99). Ammonia is assumed to be the sole nitrogen source. MW is the mass per carbon-mole of biomass, and Y_{atp} is defined as the number

of grams of cell matter synthesized per one mole of ATP input from catabolism. Thus, Y_{atp}, in addition to the strict stoichiometric ATP consumption in the weighted synthetic pathways, accounts for additional utilization by maintenance and waste. In order to separate synthesis and maintenance, Y_{atp} is sometimes written as(100):

$$\frac{1}{Y_{atp}} = \frac{1}{Y^{max}_{atp}} + \frac{m_{atp}}{u} \quad . \qquad (8)$$

Y^{max} now represents the ATP consumed only in biosynthesis, while maintenance is accounted for by m_{atp}. U, the specific growth rate and the divisor of maintenance, decouples maintenance from growth, since maintenance depends only on how much biomass is present, not on its rate of change. Clearly, under anaerobic conditions, the ATP yield can be obtained by measuring the extents of the product-forming reactions and balancing the ATP produced and consumed among all pathways. The maximum ATP yield and the ATP maintenance coefficient can be further found by measuring Y_{atp} at a number of specific growth rates.

Aerobic conditions are not utilized in the studies within. However, it is still important to study aerobic growth, as the energetics of this peripherally related growth condition may elucidate mechanisms occurring in the microaerobic state. Aerobically, glycerol production virtually disappears. Oxidative degradation of glucose by glycolysis and the TCA cycle, producing $NADH_2$, and the respiratory oxidation of $NADH_2$ coupled to phosphorylation are the new reactions:

$$C_6H_{12}O_6 + 6H_2O \longrightarrow 6CO_2 + 12NADH_2 + 4ATP \quad (10)$$

$$NADH_2 + 1/2O_2 \longrightarrow H_2O + (P/O)ATP\ . \quad (11)$$

P/O is the number of ATP molecules generated by the processing of an oxygen atom by the respiratory chain and is related to the number of phosphorylation sites along the inner mitochondrial membrane and the extent of dephosphorylation by mitochondrial ATPases(101). During aerobic growth, evaluation of Y_{atp} is complicated by the addition of another unknown, the P/O ratio, in the ATP balance. To evaluate Y_{atp}, a constant P/O value must be assumed.

Lagunas(102) studied the ATP yield of biomass in aerobic batch cultures of yeast growing on glucose, galactose, and ethanol. The investigator assessed the substrate level and oxidative phosphorylation from the measured rates of fermentation and respiration and by assuming that either two or three sites of phosphorylation exist in the inner membrane.

Comparing ATP generation to the amount of biomass formed, an ATP yield of 9.0 grams biomass per mole of ATP is found with three sites of mitochondrial phosphorylation and 10.2, with 2 sites. However, according to the theoretical calculations of several authors(100), taking into account the ATP spent in macromolecule synthesis, an ATP yield of biomass is expected to be 29 g/mol. Thus, a vast discrepancy exists between the theoretical and measured yields. Lagunas investigated the question of whether maintenance can account for the additional ATP expenditure with cells resting in the absence of carbon and nitrogen sources. The degree of respiration of these cells indicates that only 1.2 mmol/g-hr are necessary to maintain cell viability. This quantity is 1/20 of that required to close the gap between theoretical and actual yields. The

author concluded that there is a great consumption of energy in some undefined process associated with growth and not with maintenance.

Lagunas(102) also studied the influence of respiration on the energetics of yeast with both anaerobic and aerobic cultures growing in glucose or galactose. In aerobic, galactose-grown cells, repression of respiration occurs to a lower extent than with glucose, so that 30% of the galactose is catabolized by respiration, compared to 3% of the glucose. Assuming three sites of oxidative phosphorylation(P/O=3), an assumption which has been demonstrated in derepressed mitochondrial suspensions(103), a six-fold increase in ATP generation should accompany an anaerobic to aerobic transition in galactose cultures. Nonetheless, only a doubling of the cell yield from 25g/mol to 58 g/mol is seen, rather than the expected sixfold increase. Therefore, either the P/O is lower than 3, or ATP requirements for growth are greater under aerobic conditions than anaerobic conditions. Again, there is a conflict between experimental results and theory.

Von Meyenburg(101) employed glucose utilizing continuous cultures for his assessment of yeast energetics. Below a dilution rate of 0.24/hr, growth is purely respiratory with no ethanol production. Above this dilution rate, glucose repression becomes progressively stronger, and ethanol production assumes a greater fraction of the energy production. However, if the ATP yield is fundamentally associated with biosynthesis, then the total ATP production, regardless of its source, should be a linear function of the specific growth rate(or dilution rate). The P/O ratio that best satisfies this linear relationship is 1.1, which is lower than the theoretical value of 3.0 and confirms the findings of Lagunas.

Furthermore, at this P/O ratio, the Y_{atp} can be calculated to be 12, similar to what Lagunas found and vastly lower than the theoretical prediction. Von Meyenburg speculated that the lower than expected phosphorylation efficiency is due to a large degree of dephosphorylation of ATP that had been recorded in the literature.

Rogers and Stewart(104) employed microaerobic and aerobic chemostat cultures of wild-type and respiratory-deficient mutants of *S. cerevisiae* in their energetics studies. Efficiencies of oxidative phosphorylation were evaluated in similar ways to those presented by von Meyenburg(101). Maintenance energy requirements were estimated by extrapolating yields to zero dilution rate, where only maintenance prevails. Aerobic cultures of wild type cells at nonrepressive dilution rates phosphorylate with a P/O ratio of 1.0, grow with a Y_{atp} of 8.4, and maintain viability with an m_{atp} of 1.12 mmol ATP/g-hr. Microaerobic, wild-type cultures have a higher ATP yield of 14.0 and a lower maintenance coefficient of 0.43. Respiratory-deficient mutants also perform more efficiently than the aerobic wild-type cells, both aerobically and anaerobically, with a Y_{atp} of 12.5 and a maintenance coefficient of 0.7. Thus, the degree of respiratory competence dictates the energetic yield. Microaerobic cells have uninduced respiratory enzymes, with negligible succinate dehydrogenase, NADH cytochrome C reductase, and cytochrome oxidase activities. Neither do the mutant cells have respiratory activities. In contrast, these enzymes in the aerobic wild-type cells are fully active. Thus, the authors concluded that the induction of respiratory activity represents an increase of cell complexity and differentiation, which can be supported omly with a higher ATP expenditure.

Grosz et al.(105) explored fed batch cultures in a range of respiratory states that spanned a respiratory quotient of 2.5 to 1.2 in a single fermentation. If Equation 10 is multiplied by an extent "a," Equation 11 by an extent "b," Equation 5 by an extent "c," and the biosynthetic reaction 7 by an extent 1.0, then an ATP balance produces the following result:

$$4a + 2(P/O)b + 2c = MW/Y_{atp} \quad . \qquad (12)$$

Thus, if the experimentally measured variables 4a + 2c are plotted against b, then the slope is -2(P/O) and the intercept is MW/Y_{atp}. When this was done, a considerable scatter in the data about a straight line existed, and a positive slope gave a negative value of P/O. These results imply that either or both the Y_{atp} and the P/O change as the respiratory quotient, and thus, the respiratory activity changes. Such a finding is congruous with the findings of Rogers and Stewart(104).

Stouthamer(100) has extensively reviewed the growth energetics of a variety of microorganisms and offers some explanations of the discrepancies between theoretical and experimental findings with yeast. A wide variety of microorganisms growing anaerobically on glucose have a Y_{atp} near 10.5, whereas the same theoretical value of about 29 is expected. Thus a significant amount of ATP is utilized in some unknown process, or else the majority of the ATP is wasted. Stouthamer suggested one new source of ATP utilization in his study of continuous cultures of wild-type and ATPase negative mutants of

E. coli(106). Stouthamer reasoned that aerobically, the ATPase negative mutants can utilize respiratory proton translocation to energize the

cell membrane, but cannot convert the membrane energy into ATP. The wild-type microbe growing anaerobically can energize its membrane only by hydrolyzing, with the membrane bound-ATPase, ATP generated by substrate level phosphorylations. The different possibilities of membrane energization are shown schematically in Fig. 9. Thus, the difference in the ATP yields of the mutant grown aerobically and the wild type anaerobically reflects the ATP utilization for membrane energization. The mutant has an ATP yield of 17.5, while the wild type has one of 8.5. As a result, 51% of the generated ATP is consumed in membrane energization, vastly more than is admitted in any theoretical calculation, and this ATP sink can account for a large portion of the difference between theoretical and experimental yields.

In a more complete elaboration, Stouthamer(100) outlined mechanisms with which the cell can waste the large quantities of ATP that they do. ATP waste can occur its hydrolysis by membrane ATPases. Concomitant with hydrolysis is a decay of the energized membrane by the leakage of protons across the membrane. The possibility of controlling the leakiness of the membrane to regulate the degree of energy wastage was also suggested and substantiated by experimental observations with *E. coli*(100). Another method of energy wasting with relevance to yeast is futile cycling within the metabolic pathways. An example of such cycling is the glycolytic phosphorylation of glucose to fructose diphosphate, followed by the hydrolysis of the latter compound by diphosphatase.

The possibility of ATP hydrolysis by the membrane ATPases and the decay of the membrane proton gradient cannot be excluded from yeast because proton-translocating membrane ATPases have been found(107,108).

Hydrolysis and proton leakage can also occur across the mitochondrial inner membrane. This could possibly account for the altered cell yield in response to changing respiratory activity.

In conclusion, much ATP is wasted by yeast, and the greater the degree of respiratory competence, the greater the wastage.

1.2.9 ETHANOL INHIBITION

Ethanol, the primary product in the studies presented, is inhibitory to both growth and product formation. Inhibition strengthens at the low oxygen concentrations employed and varies as the oxygen tension is altered. Therefore, the kinetics of ethanol inhibition must, invariably, enter into any mathematical model proposed. In this section, the quantitative and mechanistic aspects of ethanol inhibition are explored.

Ethanol inhibition has been quantified by a multitude of investigators(109-113). Numerous strains of *S. cerevisiae*, including respiratory-deficient mutants, have been employed in batch and continuous culture in these studies. The common method of assessing ethanol inhibition in batch cultures is the measurement of the fermentation variables, such as biomass, ethanol, and residual glucose concentrations, as functions of time with different concentrations of ethanol preloading. In continuous culture, the effect upon the steady state fermentation parameters by the addition of various concentrations of ethanol into the feed medium is gauged. In all cases, the specific growth rate and the specific fermentation rate are inhibited in a monotonically increasing proportion to the ethanol concentration. In continuous culture, higher feed concen-

trations of ethanol require a higher residual glucose concentration to sustain the specific growth rate. Thus, the steady-state biomass concentration is lower when ethanol is added to the feed. In addition, washout is attained at a lower dilution rate.

Double reciprocal plots of the inverse specific growth rate or the inverse specific ethanol production rate versus the inverse residual glucose concentration are linear in all tested strains and configurations(109-113). In addition, as the ethanol concentration is varied, the slope, but not the x intercept, of these plots changes. Therefore, ethanol inhibits the maximum rates of growth and fermentation, but not the affinities of these processes for the substrate; i.e., inhibition is noncompetitive. The mathematical relationships relating the inhibition of the maximum fermentation and growth rates as functions of the ethanol concentrations are the main subjects of disagreement among the investigators. Some investigators found progressively stronger inhibition as the ethanol concentration increases, some found progressively weaker inhibition, and some found a linear profile of inhibition at all ethanol concentrations. Thus, a multiplicity of mathematical functions have been applied to ethanol inhibition. In general, the fermentation rate is inhibited to a lesser extent than the growth rate, so that fermentation continues at an ethanol concentration at which growth ceases. The maximal ethanol concentration allowing growth lies between 80 and 100 g/l, and the maximum allowing fermentation lies between 90 and 120 g/l.

In rapid batch fermentations and with high added ethanol concentrations, the cell viability decays(114-116). A rapid fermentation is defined as one that produces 95 g/l of ethanol within 6 hours of inoculation, and

is accomplished by inoculating in the order of 5 x 10^8 cells/ml(114). In an actual fermentation carried out at 30 degrees Celsius with an initial cell count of 8 x 10^8/ml, the 95 g/l of ethanol were produced in 3 hours. However, the viability decayed exponentially during this time period, so that finally, only 10% of the cells remained viable(114). The same fermentation at 15 C was completed in 6 hours, and the cells retained complete viability. Thus, the death rate is correlated with the rapidity with which the cells ferment. With an inoculum of 6 x 10^7 cells/ml and a 30 C fermentation temperature, cell viability was also maintained. Thus, the size of the inoculum is also related to the viability. A possible explanation for this phenomenon would be an increased extracellular fluid volume with the lower cell counts, which would allow for relatively unhindered diffusion of ethanol out of the cell.

Leao and van Uden(115) studied the influence of temperature and the concentration of added alkanols upon the death kinetics of *S. cerevisiae*. Viability decay was found to be exponential with time. The first-order rate constant of death has an Arrhenius-type dependence upon the temperature. The intercepts, but not the slopes, of these Arrhenius plots change with the addition of different concentrations of ethanol, propanol, isopropanol, or butanol. Thus, the addition of alkanols expedites the death rate, but not its profile of temperature dependence. The authors interpreted this to mean that the thermal and chemical mechanisms of cell death are identical, and that the presence of the alkanol renders the target reaction more heat-sensitive. Furthermore, the degree to which the alkanols enhance the death rate is related to their lipid solubility, implying that the cell membrane is the target.

The role of the membrane and membrane components in ethanol inhibition was also investigated by Thomas et al.(116,117). Anaerobic cultures subjected to 1 M ethanol concentrations lose viability at a rate dependent upon the lipid and sterol supplementation. Addition of the doubly unsaturated, 18 carbon lipid linoleic acid protects viability more than the singly unsaturated, 18 carbon oleic acid. Sterols with unsaturated side chains, such as ergosterol or stigmasterol, also protected the cells better than cholesterol or campesterol, with unsaturated side chains. In addition, the shorter chain of palmitoleic acid enhances viability more than the longer-chain fatty acids. The supplemented sterols and fatty acids are incorporated into the cell membrane. Thus, the role of the structure of the cell membrane in the conferral of ethanol tolerance was surmised. The presence of sterols with unsaturated side chains in the membrane provides for a more sturdy membrane structure, which possibly forms a more protective barrier against the entrance of ethanol into the cell. The role of the unsaturated and short-chain fatty acids is to increase the membrane fluidity and, thus, better accommodate ethanol molecules that have penetrated the outer monolayer. Alternately, the increased fluidity counteracts the decreased repulsion among polar head groups, as the surrounding water molecules are replaced by ethanol molecules. Finally, increased fluidity may stabilize membrane-bound enzymes.

In addition to the death rate, the growth rate and the solute accumulation rates are also affected by the membrane lipid composition(117). Ethanol added to growing batch cultures slows growth, but to a greater extent in cells supplemented with oleic acid than with linoleic acid. Ethanol also hinders the transport into the cell of glucose, glucosamine,

lysine, and arginine, but again, the effect is more pronounced with oleic acid than with linoleic. Finally, the intracellular ethanol content of linoleic acid supplemented cells is consistently lower than that in oleic supplemented cells. The greater membrane fluidity with the polyunsaturated fatty acid better preserves the activity of several solute transporters, possibly even the transporter of ethanol out of the cell, if it exists.

Addition of unsaturated fatty acids to the medium improves the performance of industrially important ethanol fermentations(118,119). The fermentation of lactose to ethanol is, in principle, similar to the ethanol production of *S. cerevisiae*, especially with regard to product inhibition. Increases in the lactose concentration from 5 to 15% increases proportionally both the fermentation time and the final alcohol concentration(119). A further increase to 20% causes a tripling of the fermentation time and a disproportionately small increase in the final ethanol concentration. The poor performance with the highest substrate concentration is ascribed to ethanol inhibition. However, the addition of ergosterol and a number of combinations of unsaturated lipids reduces the fermentation time to that normally expected, based on the lower lactose concentrations. The added fatty acids and sterols enrich the cell membrane.

As discussed in a previous section, oxygen is known to increase the unsaturated lipid and sterol content of the cells. Therefore, oxygen is expected to play a role in ethanol tolerance similar in nature to the added lipids. Indeed, in rapid fermentations, the presence of oxygen preserves cell viability(114). Anaerobic cells maintain only 2% of

their initial viability after producing 95 g/l of ethanol, while cells maintained at 13, 20, and 100% of air saturation survive to extents of 13, 34, and 60%, respectively. Oxygen is also known to support higher biomass concentrations in continuous fermentation with cell recycle, in which ethanol inhibition is a major contributor(113).

An alternate view of ethanol inhibition was proposed by investigators of the intracellular ethanol content(114,120,121). Nagodawithana and Steinkraus(114) observed that cells producing 95 g/l of ethanol at the end of batch fermentation retain only 15% of the cell viability, while cells bathed in externally added ethanol of even 120 g/l for the same time duration retained 55% viability. Intracellular ethanol inhibits cell function to a greater extent than extracellularly added ethanol, which may not even gain entrance into the cell. Novak et al.(121) attempted to quantify the relative contributions of intracellular and extracellular ethanol to inhibition. The time courses of batch fermentations with different concentrations of ethanol preloading were followed. In the early exponential phase, only a negligible amount of ethanol is produced, allowing for the separate assessment of the inhibition parameter associated with added ethanol. The inhibition of produced ethanol was evaluated by the fitting the ethanol concentration and specific growtg rate profiles to proposed inhibition kinetics. The half-maximal inhibition parameter with respect to produced ethanol is 3.76g/l, while that for added ethanol is 105 g/l. This striking difference in sensitivity underscores the relative importance of intracellular ethanol.

The strongest claims of intracellular ethanol inhibition were made by Navarro and Durand(120). According to these authors,in batch fermenta-

tions, the intracellular ethanol concentration increases to a maximum of 300 g/l within a matter of a few hours. After the attainment of this maximum, growth is arrested and fermentation severely impaired. Thus, the stationary phase of fermentation is induced by the tremendous accumulation of intracellular ethanol to a concentration expected to severely retard numerous growth and fermentative enzymes. Novak et al.(121) also found a maximum of 125 g/l of intracellular ethanol in the early phase of batch culture, while Beaven et al.(122) found a 40 g/l driving force for ethanol expulsion.

Recently, however, Dasari et al.(123) disputed all claims of accumulation of intracellular ethanol above extracellular levels, citing flaws in the methods used to measure this parameter. Most investigators rapidly cool samples withdrawn from the fermentor, centrifuge them, and process the pellet for ethanol analysis. However, significant ethanol production in the dense pellet, even at low temperatures, is incorrectly accounted for as intracellular ethanol. With a more rapid(2 second) sampling and metabolic quenching, the authors demonstrated that there is no accumulation of ethanol intracellular ethanol above extracellular levels, even in the beginning of batch fermentation, confirming other reports of a very rapid equilibration of ethanol across the cell membrane(123).

Finally, there have been studies of specific enzymes that are inactivated by ethanol(114,124-126). A decrease in the alcohol dehydrogenase activity parallels the decay in viability in rapid fermentations(114). Ethanol noncompetitively and reversibly inhibits hexokinase and alpha-glycerol phosphate dehydrogenase, but not phosphofructokinase or aldolase(125). Since the inhibited enzymes are the first in glycolysis

and the glycerol production pathway, a feedback control of ethanol and glycerol production by ethanol was proposed(125). Ethanol and higher alkanols noncompetitively inhibit the glucose transporter, the extent of inhibition being proportional to the lipid solubility of the alkanol(126).

1.3 INITIAL HYPOTHESES AND EXAMPLE MECHANISMS

As seen from the review of its biochemistry, *Saccharomyces cerevisiae* possesses a wealth of documented responses to changes in the glucose, ethanol, and dissolved oxygen concentrations. When a new yeast behavior arises, as it does in these investigations, an attempt must be made to explain it in terms of what is already known. It is possible that the known mechanisms subtly combine and interact to produce the new behavior. Initially, the investigator must ruthlessly piece together old mechanisms into new combinations and generate first hypotheses regarding the cause of the behavior. These hypotheses may also serve in the design of the experimental program aimed at elucidating the new mechanisms. In this section, the initial thoughts that were applied to the present investigation are presented. Specifically, information from the biochemistry review is configured in new ways to explain the maximum in the specific ethanol productivity in the parts-per-billion range of dissolved oxygen in continuous culture. These fabricated mechanisms have little or no resemblance to the one finally proposed in the upcoming chapters and supported by the experimentation. However, these initial guesses were instrumental in the planning of the experimentation that led to the final results. Only a few mechanisms are presented as examples, with many other possibilities omitted. Also, the mechanisms explain only the peak in the specific ethanol production and do not address the changes in the biomass concentrations under the same conditions.

The maximum in the specific ethanol production rate at the trace concentrations of dissolved oxygen is actually composed of two phenomena.

The first phenomenon is that the specific ethanol productivity increases as the dissolved oxygen concentration from anaerobiosis to that which produces the maximum. Such an increase is actually a negative Pasteur effect, as explained in the review. In the past, the negative Pasteur effect has been seen mainly in cells resting in organic acid buffers(94). The stimulation in fermentation by air was attributed to the reversal of the deleterious effects of the buffer. Since the buffers here have no resemblance to those culpable in other studies, the mechanisms are not necessarily the same. The negative Pasteur effect was also seen in respiratory-deficient mutants without the acid buffers, and was again attributed to some unknown, oxygen-reversed inhibition of anaerobic fermentation(96). However, a precedent was set in which a respiratory alteration affected fermentation. The second phenomenon associated with the peak in the specific fermentation rate is the decrease in that rate as oxygen is increased above that at the peak. Such a decrease is consistent with an ordinary Pasteur effect, the mechanism of which has been belabored in the literature. The only requirement for a Pasteur mechanism is the onset of significant respiration above the 10 ppb of dissolved oxygen. In the experiments described in the upcoming sections, no significant respiration was observed. Since this was not known prior to the experimentation, the Pasteur mechanism is invoked in some of the mechanisms described in this section.

The first example mechanism to account for the negative Pasteur effect draws heavily from the work of Rogers and Stewart(77) and has NADH as the fermentation-controlling factor. These investigators observed that the activities of the TCA cycle and some respiratory chain enzymes are maxi-

mally induced by the introduction of oxygen, in the parts-per-billion range, to an anaerobic system. Despite the respiratory-enzyme activity, the actual respiration rate responds much less sharply to the dissolved oxygen, being half-maximally stimulated at approximately 100 ppb. Essentially, the respiratory enzymes are saturated at an oxygen concentration far greater than is required to induce their activity. A comparison of the TCA cycle dehydrogenase activity and the respiration rate is shown in Fig. 10. One consequence of this disparate response to oxygen might concern the action of the TCA cycle enzymes. At 10 ppb, the high activity of these enzymes has a great tendency to produce NADH from NAD, precisely the function of the cycle in respiration. However, insufficient terminal acceptor is present at these trace levels to oxidize NADH and counterbalance this reductive tendency. Thus, one might imagine a high NADH concentration to exist at this DO. At higher DO, respiration begins to oxidize the NADH, with a proportionately smaller gain in the TCA cycle activity. The NADH level is expected to decrease. At lower dissolved oxygen concentrations, the TCA cycle enzymes lose activity proportionally more than the respiration rate, and again, the NADH concentration decreases. Based on this reasoning, a maximum in the NADH concentration should exist at the point at which the relative induction of TCA cycle activity equals the relative increase in the respiration rate, or where the two curves in Fig 10 are parallel. The NADH concentration should be proportional to the difference between these curves.

Thus, it remains only to connect the NADH concentration to the fermentation rate to complete the mechanism. NADH could limit the glycolytic pathway only if its concentration affected the activity of alcohol de-

hydrogenase. Recall that ADH is the last enzyme of the ethanol production pathway and has NADH as one of its substrates. Thus, if ADH were stimulated by NADH, then a peak in the specific ethanol production rate could indeed exist at the same point as the NADH peak. Metabolites upstream of ADH would accumulate or deplete in relation to the disposition of this enzyme. Thus, nutrient uptake would be feedback-controlled by the accumulating G6P. Alcohol dehydrogenase has never been implicated as a limiting reaction in fermentation, but neither has this effect ever been seen. This mechanism is consistent with the finding that respiratory lesions can lead to a negative Pasteur effect, as discussed previously. Finally, this mechanism excludes branching and reductive succinic acid production, as has been claimed in some reports(9).

Experimental verification of the mechanism would require the demonstration of a crossover point at alcohol dehydrogenase, a maximum in the NADH concentration, and the necessary TCA cycle activity and respiration rate profiles, to produce the NADH maximum. As mentioned, metabolites upstream of ADH should accumulate and those downstream deplete when glycolysis is slow, and reverse their tendencies when glycolysis is rapid. Thus, as aeration is increased from near anaerobiosis, Glucose 6-Phosphate and pyruvate should decrease in concentration. Simultaneously, NADH levels and TCA cycle activities would increase, and the respiration rate would remain minimal. As the dissolved oxygen concentration increases past the point of maximum fermentation, all of these should reverse. From this reasoning was born the idea of measuring precisely these enzyme activities and metabolite levels in relation to the oxygenation and accounts for the bulk of the results in Chapter 3.

An alternate mechanism, related to the first one, would have ATP as the controlling metabolite. As the concentration of oxygen increases from zero, the enzymes of the TCA cycle and respiratory chain are newly synthesized, processed, and assembled with membrane components to form complete mitochondria. These new structures add complexity to the cell. It has been suggested that the more differentiated structure places a higher demand on the ATP pool for either or both maintenance and biosynthesis(80). Yet, the concentration of oxygen sufficient to stimulate organelle synthesis is insufficient, in the parts-per-billion range, to return the invested ATP through respiration and phosphorylation. Hence, a DO exists in which the ATP concentration is minimized, in analogy to the maximized NADH of the previous mechanism. A minimum ATP concentration would communicate with the glycolytic pathway through the phosphofructokinase reaction, which is inhibited by ATP and activated by AMP and ADP. The potential for a peak in the fermentation rate can be shown from an analogue to Fig. 10, with the upper curve labelled "ATP utilization in respiratory enzyme synthesis," and the lower one labelled "ATP production from respiration." The difference in these curves is inversely related to the ATP concentration and directly related to the fermentation rate.

To confirm the second mechanism, a crossover at the level of PFK would have to be demonstrated. The same intracellular metabolite measurements mentioned previously would be relevant here. In response to increased aeration from near anaerobiosis, ATP and metabolites upstream of PFK must pass a minimum, while those downstream must attain a maximum, as the specific ethanol production rate passes its peak. Respiration and respiratory enzyme activities must behave identically to the those of

the first mechanism. It should be noted that in this mechanism, the decrease in the specific ethanol production above the 10 ppb of DO occurs through the standard Pasteur mechanism. The only difference is the extension to the additional effects near anaerobiosis.

The final example mechanism draws from the stimulation of unsaturated fatty acid and sterol synthesis by oxygen in the parts-per-billion range(77). These membrane components increase the fluidity and strength of the cell membrane and may protect the membrane-bound enzymes from the deleterious effects of ethanol(116). The addition of these components directly to cells bathed in physiological concentrations of ethanol has been shown to increase the activities of numerous solute transporters(117). Thus, a mechanism for the negative Pasteur effect can be envisioned, whereby the glucose transporter is activated by adding oxygen to an anaerobic system.

To verify that the glucose transporter is rate-limiting, one would one would show that all intracellular metabolites increase in concentration, whenever the fermentative flux increases. The same intracellular metabolite assays need be made. This mechanism cannot account for the ordinary Pasteur effect above the optimal dissolved oxygen concentration; to explain it, the standard mechanism is invoked. This model, therefore, lacks the symmetry of the previous ones.

From these example mechanisms, the utility of enzyme and intracellular metabolite assays becomes obvious. The pattern of metabolites changes, in relation to glycolytic changes, can reveal the rate-limiting steps. In addition, the correlation of respiratory and glycolytic enzyme activities, ATP and NADH levels, viability, and ethanol concentrations with

fermentation can further elucidate the connection between the rate-limiting step and other cellular events.

REFERENCES

1. Jones, R.P., Pamment, N., and Greenfield, P.F., "Alcohol Fermentation by Yeasts - the Effect of Environmental and Other Variables," *Process Biochem.*, 16, 42, 1981.

2. Ryu, D.D.Y., Kim, Y.J., and Kim, J.H., "Effect of Air Supplement on the Performance of Continuous Ethanol Fermentation System," *Biotechnol. Bioeng.*, 26, 12, 1984.

3. Cysewski, G.R., and Wilke, C.R., "Utilization of Cellulosic Materials through Enzymatic Hydrolysis. I. Fermentation of Hydrolysate to Ethanol and Single-Cell Protein," *Biotechnol. Bioeng.*, 18, 1297, 1976.

4. Ghose, T.K. and Tyagi, R.D., "Rapid Ethanol Fermentation of Cellulose Hydrolysate. I. Batch versus Continuous Systems," *Biotechnol. Bioeng.*, 21, 1401, 1979.

5. Cysewski, G.R. and Wilke, C.R., "Process Design and Economic Studies of Alternative Fermentative Methods for the Production of Ethanol," *Biotechnol. Bioeng.*, 20, 1421, 1978.

6. Tyagi, R.D., and Ghose, T.K., "Studies on Immobilized *Saccharomyces cerevisiae*. I. Analysis of Continuous Rapid Ethanol Fermentation in Immobilized Cell Reactor," *Biotechnol. Bioeng.*, 24, 781, 1982.

7. Nishizawa, Y., Dunn, I.J., and Bourne, J.R., "The Influence of Oxygen and Glucose on Anaerobic Ethanol Production," in Continuous Cultivation of Microorganisms, Proc. 7th Internat. Symp. Prague, 1980, p. 605.

8. Tyagi, R.D., Participation of Oxygen in Ethanol Fermentation," *Process Biochem.*, 19, 136, 1984.

9. Oura, E., "Some Aspects of the Growth Process of Baker's Yeast," in Proceedings Third International Specialized Symposium on Yeasts, Part II, Helsinki, 1973, p. 215.

10. Fraenkel, D.G., "Carbohydrate Metabolism," in Molecular Biology of The Yeast *Saccharomyces*: Metabolism and Gene Expression, eds. Strathern, J.N., Jones, E.W., Broach, J.R., Cold Springs Harbor, New York, 1982, p. 1.

11. Polakis, E.S. and Bartley, W., "Changes in the Enzyme Activities of *Saccharomyces cerevisiae* during Aerobic Growth on Different Carbon Sources," *Biochem. J.*, 97, 284, 1965.

12. Polakis, E.S., Bartley, W. and Meek, G.A., "Changes in the Activities of Respiratory Enzymes during the Aerobic Growth of Yeast on Different Carbon Sources," *Biochem. J.*, 97, 298, 1965.

13. Sols, A., Gancedo, C., and De La Fuente, G., "Energy Yielding Metabolism in Yeasts," in The Yeasts, vol. 2, eds. Rose, A.H. and Harrison, J.S., Academic, New York, 1971, p. 271.

14. Gancedo, C., Gancedo, J.M., and Sols, A., "Glycerol Metabolism in Yeasts. Pathways of Utilization and Production," *Eur. J. Biochem.*, 5, 165, 1968.

15. Oura, E., "Reaction Products of Yeast Fermentation," *Process Biochem.*, 13, 19, 1977.

16. Chapman, C. and Bartley, W., "The Kinetics of Enzyme Changes in

Yeast under Conditions that Cause the Loss of Mitochandria," *Biochem. J.*, 107, 455, 1968.

17. Lupianez, J.A., Machado, A., Nunez de Castro, I., and Mayor, F., "Succinic Acid Production by Yeasts Grown under Different Hypoxic Conditions," *Molec. Cell. Biochem.*, 3, 113, 1974.

18. Heerde, E. and Radler, F., "Metabolism of the Anaerobic Formation of Succinic Acid by *Saccharomyces cerevisiae*," *Arch. Microbiol.*, 117, 269, 1978.

19. Lagunas, R. and Gancedo, J.M., "Reduced Pyridine Nucleotide Balance in Glucose Growing *Saccharomyces cerevisiae*," *Eur. J. Biochem.*, 37, 90, 1973.

20. Haarasilta, S. and Oura, E., "Activity and Regulation of Anaplerotic and Gluconeogenetic Enzymes during the Growth Process of Baker's Yeast - Biphasic Growth," *Eur. J. Biochem.*, 52, 1, 1975.

21. Racker, E., "History of the Pasteur Effect and Its Pathobiology," *Molec. Cell. Biochem.*, 5, 17, 1974.

22. Fiechter, A., "Chemostat Studies of Glycolysis in Yeasts," in Continuous Cultivation of Microorganisms, Proc. 7th Internat. Symp., Prague, 1980. p. 81.

23. Fiechter, A., Fuhrmann, G.F., and Kappeli, O., "Regulation of Glucose Metabolism in Growing Yeast Cells," *Adv. Microb. Physiol.*, 22, 81, 1981.

24. Den Hollander, J. A., Ugurbil, K., and Shulman, R.G., "^{31}P and ^{13}C NMR Studies of Intermediates of Aerobic and Anaerobic Glycolysis

in *Saccharomyces cerevisiae*," *Biochemistry*, 25, 212, 1986.

25. Den Hollander, J.A., Ugurbil, K., Brown, T.R., Bednar, M., Redfiled, C. and Shulman, R.G., "Studies of Aerobic and Aerobic Glycolysis in *Saccharomyces cerevisiae*," *Biochemistry*, 25, 203, 1986.

26. Krebs, H.A., "Pasteur Effect and Relation Between Respiration and Fermentation in Living Systems," in Essays in Biochemistry, eds. Campbell, P.N. and Dickens, F., 8, 34, 1972.

27. Lehninger, A.L., *Biochemistry*, Worth: New York, 1975, p. 411.

28. Sols, A., "Regulation of Carbohydrate Transport and Metabolism in Yeast," in *Aspects of Yeast Metabolism*, eds., Mills, A.K. and Krebs, H., Blackwell: Oxford, 1967, p. 47.

29. Reibstein, D, den Hollander, J.A., Pilkis, S.J., and Shulman, R.G., "Studies on the Regulation of Yeast Phosphofructo-1-kinase: Its Role in Aerobic and Anaerobic Glycolysis," *Biochemistry*, 25, 219, 1986.

30. Lagunas, R., Dominguez, C., Busturia, A. and Saez, M., "Mechanisms of Appearance of the Pasteur Effect in *Saccharomyces cerevisiae*- Inactivation of Sugar Transport System," *J. Bact.*, 152, 19, 1982.

31. Ghosh, A. and Chance, B., "Oscillations of Glycolytic Intermediates in Yeast Cells," *Biochem. Biophys. Res. Comm.*, 16, 174, 1964.

32. Pye, E.K., "Biochemical Mechanisms Underlying Metabolic Oscillations in Yeast," *Can. J. Botany*, 47, 271, 1969.

33. Hommes, F.A., "Oscillatory Reductions in Pyridine Nucleotides during Anaerobic Glycolysis in Brewer's Yeast," *Arch. Biochem.*, 108, 36,

1964.

34. Becker, J.V. and Betz, A., "Membrane Transport as Controlling Pacemaker of Glycolysis in *Saccharomyces carlsbergenisis*," *Biochem. Biophys. Acta*, 274, 584, 1972.

35. Chance, B., Hess, B., and Betz, A., "DPNH Oscillations in Cell-Free Extracts of *Saccharomyces carlsbergenisis*," *Biochem. Biophys. Res. Comm.*, 16, 2, 1964.

36. Hommes, F.A., "Oscillatory Reductions of Pyridine Nucleotides During Anaerobic Glycolysis in Yeasts," *Comp. Biochem.*, 14, 231, 1965.

37. Higgins, J., "Chemical Mechanism of Oscillation of Glycolytic Intermediates in Yeast Cells," *Proc. Nat. Acad. Sci.*, 51, 989, 1964.

38. Hess, B. and Plesser, T., "Temporal and Spatial Order in Biochemical Systems," *Ann. N.Y. Acad. Sci.*, 316, 203, 1979.

39. Chance, B., Pye, E.K., Ghosh, A.K., and Hess, B., *Biological and Biochemical Oscillators*, Academic: New York, 1973.

40. Cirillo, V.P., "Relationship Between Sugar Structure and Competition for Sugar Transport System in Baker's Yeast," *J. Bact.*, 95, 603, 1968.

41. Heredia, F., Sols, A., and De La Fuente, G., "Specificity of Constitutive Hexose Transport in Yeast," *Eur. J. Biochem.*, 5, 321, 1968.

42. Kotyk, A., "Properties of Sugar Carrier in Baker's Yeast," *Folia Microbiol.*, 12, 121, 1967.

43. Stryer, L., *Biochemistry*, Freeman, New York: 1981, p. 871.

44. Meredith, S.A. and Romano, A.H., "Uptake and Phosphorylation of 2-

Deoxy D-Glucose by Wild-Type and Respiratory-Deficient Baker's Yeast," *Biochem. Biophys. Acta*, 497, 745, 1977.

45. Kotyk, A., "Molecular Aspects of Nonelectrolyte Transport in Yeasts," in Proceedings of the Third International Symposium on Yeasts, Part II, Helsinki, 1973, p. 103.

46. Kleinzeller, A. and Kotyk, A., "Transport of Monosaccharides in Yeast Cells and its Relationship to Cell Metabolism," in *Aspects of Yeast Metabolism*, eds. Mills, A.K., and Krebs, H., Blackwell: Oxford, 1968, p. 33.

47. Serrano, R. and De La Fuente, G., "Regulatory Properties of the Constitutive Hexose Transport in *Saccharomyces cerevisiae*," *Molec. Cell. Biochem.*, 5, 161, 1974.

48. Spoerl, E., Williams, J.P., and Benedict, S.H., "Increased Rates of Sugar Transport in *Saccharomyces cerevisiae* a Result of Sugar Metabolism," *Biochem. Biophys. Acta*, 298, 956, 1973.

49. Bisson, L.F. and Fraenkel, D.G., "Involvement of Kinases in Glucose and Fructose Uptake by *Saccharomyces cerevisiae*," *Proc. Nat. Acad. Sci.*, 80, 1730, 1983.

50. Bisson, L.F. and Fraenkel, D.G., "Transport of 6-Deoxyglucose in *Saccharomyces cerevisiae*," *J. Bact.*, 155, 995, 1983.

51. Bisson, L.F. and Fraenkel, D.G., "Expression of Kinase Dependent Glucose Uptake in *Saccharomyces cerevisiae*," *J. Bact.*, 159, 1013, 1984.

52. Busturia, A. and Lagunas, R., "Catabolite Inactivation of the

Glucose Transport System in *Saccharomyces cerevisiae*," *J. Gen. Microbiol.*, 132, 379, 1986.

53. Azam, F. and Kotyk, A., "Glucose 6-Phosphate as Regulator of Monosaccharide Transport in Baker's Yeast," *FEBS Lett.*, 2, 333, 1969.

54. Perea, J. and Gancedo, C., "Glucose Transport in a Glucosephosphate Isomeraseless Mutant of *Saccharomyces cerevisiae*," *Curr. Microbiol.*, 1, 209, 1978.

55. De Deken, R.H., "The Crabtree Effect: A Regulatory System in Yeast," *J. Gen. Microbiol.*, 44, 149, 1966.

56. Beck, C. and von Meyenburg, H.K., "Enzyme Pattern and Aerobic Growth of *Saccharomyces cerevisiae* under Various Degrees of Glucose Limitation," *J. Bact.*, 96, 479, 1968.

57. Lievense, J.C., and Lim, H.C., "Growth Dynamics of *Saccharomyces cerevisiae*," *Annual Reports on Fermentation Processes*,5, 211, 1982.

58. Meyenburg, K. von, "Control of Respiration and Fermentation in *Saccharomyces cerevisiae*," *Antonie van Leeuwenhoek*, 35, G19, 1969.

59. Holzer, H., "Regulation of Carbohydrate Metabolism by Enzyme Competition," *Cold Springs Harbor Symp. Quant. Biol.*, 26, 277, 1961.

60. Gorts, C.P.M., "Effect of Different Carbon Sources on the Regulation of Carbohydrate Metabolism in *Saccharomyces cerevisiae*," *Antonie van Leeuwenhoek*, 33, 451, 1967.

61. Perlman, P.S. and Mahler, H.R., "Derepression of Mitochondria and their Enzymes in Yeast: Regulatory Aspects," *Arch. Biochem. Biophys.*, 162, 248, 1974.

62. Beck, C., and von Meyenburg, H.K., "Enzyme Pattern and Aerobic Growth of *Saccharomyces cerevisiae* Under Various Degrees of Glucose Limitation," *J. Bact.*, 96, 479, 1968.

63. Wales, D.S., Cartledge, T.G., and Lloyd, D., "Effects of Glucose Repression and Anaerobiosis on Activities and Subcellular Distribution of Tricarboxylic Acid and Associated Enzymes in *Saccharomyces carlsbergenisis*," *J. Gen. Microbiol.*, 116, 93, 1980.

64. Polakis, E.S., Bartley, W. and Meek, G.A., "Changes in the Structure and Enzyme Activity of *Saccharomyces cerevisiae* in Response to Changes in the Environment," *Biochem. J.*, 90, 369, 1964.

65. Haarasilta, S. and Oura, E., "On the Activity and Regulation of Anaplerotic and Gluconeogenetic Enzymes during the Growth Process of Baker's Yeast," *Eur. J. Biochem.*, 52, 1, 1975.

66. Entian, K.D., "Genetic and Biochemical Evidence for Hexokinases PII as a Key Enzyme Involved in Carbon Catabolite Repression," *Molec. Gen. Genet.*, 178, 633, 1980.

67. Chapman, C., and Bartley, W., "The Kinetics of Enzyme Changes in Yeast under Conditions that Cause the Loss of Mitochandria," *Biochem. J.*, 107, 455, 1968.

68. Gorts, C.P.M., "Some Aspects of Catabolite Repression of Mitochondrial Enzymes in *Saccharomyces cerevisiae*," *Antonie van Leeuwenhoek*, 37 161, 1971.

69. Mahler, H.R., and Lin, C.C., "Exogenous Adenosine 3':5'-Monosphosphate Can Release Yeast from Catabolite Repression," *Biochem.*

Biophys. Res. Comm., 83, 1039, 1978.

70. Fang, M. and Butow, R.A., "Nucleotide Reversal of Mitochondrial Repression in *Saccharomyces cerevisiae*," *Biochem. Biophys. Res. Comm.*, 41, 1579, 1970.

71. Matsumoto, K., Uno, I., Tatsuo, I., and Oshima, Y., "Cyclic AMP may not be Involved in Catabolite Repression in *Saccharomyces cerevisiae* - Evidence from Mutants Unable to Synthesize It," *J. Bact.*, 156, 898, 1983.

72. Boucherie, H., "A Study of Catabolite Repressed Proteins in *Saccharomyces cerevisiae*," *Biochem. Biophys. Acta*, 825, 360, 1985.

73. Barford, J.P. and Hall, R.J., "An Examination of the Crabtree Effect in *Saccharomyces cerevisiae*: the Role of Respiratory Adaptation," *J. Gen. Microbiol.*, 114, 267, 1979.

74. Barford, J.P., Jefferey, P.M. and Hall, R.J., "The Crabtree Effect in *Saccharomyces cerevisiae* - Primary Control Mechanism or Transient?" in *Advances in Biotechnology*, Vol. 1, ed. Moo Young, M., Pergamon: New York, 1981, p. 255.

75. Oura, E., "Effect of Aeration Intensity on the Biochemical Composition of Baker's Yeast. II. Activities of Oxidative Enzymes," *Biotechnol. Bioeng.*, 16, 1213, 1974.

76. Criddle, S. and Schatz, G., "Promitochandria of Anaerobically Grown Yeast. I. Isolation and Biochemical Properties," *Biochemistry*, 8, 324, 1969.

77. Rogers, P.J. and Stewart, P.R., "Mitochondrial and Peroxisomal

Contributions to the Energy Metabolism of *Saccharomyces cerevisiae* in Continuous Culture," *J. Gen. Microbiol.*, 79, 205, 1973.

78. Tzagoloff, A., *Mitochondria*, Plenum: New York, 1982, p. 62.

79. Oura, E., "Effect of Aeration Intensity on the Biochemical Composition of Baker's Yeast. I. Factors Affecting the Type of Metabolism," *Biotechnol. Bioeng.*, 16, 1197, 1974.

80. Rogers, P.J. and Stewart, P.R., "Respiratory Development in *Saccharomyces cerevisiae* Grown at Controlled Oxygen Tension," *J. Bact.*, 115, 88, 1973.

81. Wallace, P.G. and Linnane, A.W., "Oxygen Induced Synthesis of Yeast Mitochondria," *Nature*, 201, 1191, 1964.

82. Schatz, G. and Plattner, H., "Promitochondria of Anaerobically Grown Yeast. III. Morphology," *Biochemistry*, 8, 339, 1969.

83. Paltauf, F. and Schatz, G., "Promitochondria of Anaerobically Grown Yeast. II. Lipid Composition," *Biochemistry*, 8, 335, 1969.

84. Tzagoloff, A., *Mitochondria*, Plenum: New York, 1982, p. 245.

85. Ferdouse, M., Rickard, P.A.D., Moss, F.J., and Blanch, H.W., "Quantitative Studies of the Development of *Saccharomyces cerevisiae* Mitochondria," *Biotechnol. Bioeng.*, 14, 1007, 1972.

86. Gordon, P.A. and Stewart, P.R., "The Effect of Antibiotics on Lipid Synthesis during Respiratory Development in *Saccharomyces cerevisiae*," *Microbios.*, 4, 115, 1971.

87. Nurminen, T. and Suomalainen, H., "Location and Activity of the Respiratory Enzymes of Baker's Yeast and Bottom Brewer's Yeast

under Anaerobic and Aerobic Conditions," *J. Gen. Microbiol.*, 53, 275, 1968.

88. Suomalainen, H., Nurminen, T., and Oura, E., "Aspects of Cytology in Metabolism of Yeast," *Prog. Indus. Microbiol.*, 12, 109, 1973.

89. Hommes, F.A., "Effect of Glucose on the Level of Glycolytic Enzyme Synthesis in Yeast," *Arch. Biochem. Biophys.*, 114, 231, 1966.

90. Maitra, P.K. and Lobo, Z., "A Kinetic Study of Glycolytic Enzyme Synthesis in Yeast," *J. Biol. Chem.*, 246, 475, 1971.

91. Maitra, P.K. and Lobo, Z., "Control of Glycolytic Enzyme Synthesis in Yeast by Products of the Hexokinase Reaction," *J. Biol. Chem.*, 246, 489, 1971.

92. Schimpfessel, L., "Presence et Regulation de la Synthese de Deux Alcool Dehydrogenases Chez La Levure *Saccharomyces cerevisiae*," *Biochem. Biophys. Acta*, 151, 317, 1968.

93. Oura, E., "The Effect of Aeration Intensity on the Biochemical Composition of Baker's Yeast: Activities of Enzymes of the Glycolytic and Pentose Phosphate Pathways," *Biotechnol. Bioeng.*, 18, 415, 1976.

94. Wiken, T.O., "On Negative Pasteur Effects in Yeasts," in *Aspects of Yeast Metabolism*, eds. Mills, A.K. and Krebs, H., Blackwell: Oxford, 1967, p. 133.

95. Bonnet, J.A.B.A.F., and de Jonge, P.H., "The Influence of Some Organic Acids on the Alcoholic Fermentation in Yeasts of the Genus *Saccharomyces*," *Antonie van Leeuwenhoek*, 35, 627, 1964.

96. Silhankova, L, Mostek, J., and Pizingerova, A., "Metabolic Quotients of Respiratory Deficient Mutants of Brewer's Yeast and the Appearance of a Negative Pasteur Effect," *J. Inst. Brew.*, 81, 218, 1975.

97. Roels, J.A., "Simple Model for the Energetics of Growth on Substrates with Different Degrees of Reduction," *Biotechnol. Bioeng.*, 22, 33, 1980.

98. Dekkers, J.G.J., de Kok, H.E., and Roels, J.A., "Energetics of *Saccharomyces cerevisiae* CBS 426: Comparison of Anaerobic and Aerobic Glucose Limitation," *Biotechnol. Bioeng.*, 23, 1023, 1981.

99. Oura, E., "Estimation of the Flux of the Substrate at Different Steps of Metabolism During Microbial Growth," in Continuous Cultivation of Microorganisms, Proc. 7th Internat. Symp., Prague, 1980, p. 91.

100. Stouthamer, A.H., "The Search for Correlation Between Theoretical and Experimental Growth Yields," in Microbial Biochemistry, ed. Quayle, J.R., University Park: Baltimore, 1979, p. 1.

101. von Meyenburg, H.K., "Energetics of the Budding Cycle of *Saccharomyces cerevisiae* during Glucose Limited Aerobic Growth," *Arch. Mikrobial.*, 66, 289, 1969.

102. Lagunas, R., "Energy Metabolism of *Saccharomyces cerevisiae*. Discrepancy between ATP Balance and Known Metabolic Functions," *Biochem. Biophys. Acta*, 440, 661, 1976.

103. Mackler, B. and Haynes, D., "Studies of Oxidative Phosphorylation

in *Saccharomyces cerevisiae* and *Saccharomyces carlsbergenisis*," *Biochem. Biophys. Acta*, 292, 88, 1973.

104. Rogers, P.J. and Stewart, P.R., "Energetic Efficiency and Maintenance Energy Characteristics of *Saccharomyces cerevisiae* (Wild Type and Petite) and *Candida parapsilosis* Grown Aerobically and Microaerobically in Continous Culture," *Arch. Microbiol.*, 99, 25, 1974.

105. Grosz, R., Stephanopoulos, G. and San, K.-Y., "Studies on On-Line Biorector Identification. III. Sensitivity Problems with Respiratory and Heat Evolution Measurements," *Biotechnol. Bioeng.*, 26, 1198, 1984.

106. Stouthamer, A.H. and Bettenhausen, C.W., "A Continuous Culture Study of ATPase-Negative Mutant of *E. coli*," *Arch. Microb.*, 113, 185, 1977.

107. Riemersma, J.C. and Alsbach, E.J.J., "Proton Translocation during Anaerobic Energy Production in *Saccharomyces cerevisiae* in Continuous Culture," *J. Gen. Microbiol.*, 79, 205, 1974.

108. Serrano, R., "Effect of ATPase Inhibitors on the Proton Pump of Respiratory-Deficient Yeast," *Eur. J. Biochem.*, 105, 419, 1980.

109. Aiba, S. and Shoda, M., "Reassessment of the Product Inhibition in Alcoholic Fermentation," *J. Ferm. Technol.*, 46, 241, 1968.

110. Nagatani, M., Shoda, M., and Aiba, S., "Kinetics of Product Inhibition in Alcoholic Fermentation," *J. Ferm. Technol.*, 47, 790, 1969.

111. Bazua, C.D. and Wilke, C.R., "Ethanol Effect on the Continuous

Fermentation with *Saccharomyces cerevisiae*," *Biotechnol. Bioeng. Symp.*, 7, 105, 1977.

112. Aiba, S., Shoda, M., and Nagatani, M., "Kinetics of Product Inhibition in Alcohol Fermentation," *Biotechnol. Bioeng.*, 10, 845, 1968.

113. Ghose, T.K. and Tyagi, R.D., "Rapid Ethanol Fermentation of Cellulose Hydrolysate. II. Product and Substrate Inhibition and Optimization of Fermentor Design," *Biotechnol. Bioeng.*, 21, 1401, 1979.

114. Nagodawithana, T.W. and Steinkraus, K.H., "Effect of Dissolved Oxygen, Temperature, Initial Cell Count, and Sugar Concentration on the Viability of *Saccharomyces cerevisiae* in Rapid Fermentations," *Appl. Microb.*, 28, 383, 1974.

115. Leao, C. and van Uden, N., "Effects of Ethanol and Other Alkanols on the Kinetics of the Activation Parameters of Thermal Death in *Saccharomyces cerevisiae*," *Biotechnol. Bioeng.*,24, 1581, 1982.

116. Thomas, D.S., Hossack, J.A. and Rose, A.H., "Plasma Membrane Lipid Composition and Ethanol Tolerance in *Saccharomyces cerevisiae*," *Arch. Microbiol.*, 117, 239, 1978.

117. Thomas, D.S. and Rose, A.H., "Inhibitory Effect of Ethanol on Growth and Solute Accumulation by *Saccharomyces cerevisiae* as Affected by Plasma Membrane Lipid Composition," *Arch. Microbiol.*, 122, 49, 1979.

118. Deepak, S. and Viswanthan, L., "Effect of Oils and Fatty Acids on Molasses Fermentation by Distiller's Yeast," *Enzyme Microb. Technol.*, 6, 78, 1984.

119. Janssens, J.H., Burris, N., Woodward, A., and Bailey, R.B., "Lipid-Enhanced Ethanol Production by *Kluyveromyces fragilis*," *Appl. Env. Microbiol.*, 45, 598, 1983.

120. Navarro, J.M. and Durand, G., "Fermentation Alcoolique" Influence de la Temperature Sur l'Accumulation d'Alcool Dans les Cellules de Levure," *Ann. Microbiol. (Inst. Pasteur)*, 129B, 215, 1978.

121. Novak, M., Strehaiano, P., Moreno, M., and Goma, G., "Alcoholic Fermentation: on the Inhibitory Effect of Ethanol," *Biotechnol. Bioeng.*, 23, 201, 1981.

122. Beaven, M.J., Charpentier, C., and Rose, A.H., "Production and Tolerance of Ethanol in Relation to Phospholipid Fatty Acyl Composition in *Saccharomyces cerevisiae* NCYC 431," *J. Gen. Microbiol.*, 128, 1447, 1982.

123. Dasari, G., Keshavarz, E., Connor, M.A. and Pamment, N.B., "A Reliable Method for Detecting the Intracellular Accumulation of Fermentation Products: Application to Intracellular Ethanol Analysis," *Biotechnol. Lett.*, 7, 541, 1985.

124. Larue, F., Lafon-Lafourcade, S., and Ribereau-Gayon, P., "Relationship Between the Inhibition of Alcoholic Fermentation by *Saccharomyces cerevisiae* and the Activities of Hexokinase and Alcohol Dehydrogenase," *Biotechnol. Lett.*, 6, 687, 1984.

125. Nagodawithana, T.W., Whitt, J.T. and Cutaia, A.J., "Study of the Feedback Effect of Ethanol on Selected Enzymes of the Glycolytic Pathway," *Am. Soc. Brew. Chem.*, 35, 179, 1977.

126. Leao, C. and van Uden, N., "Effects of Ethanol and Other Alkanols

on the Glucose Transport System of *Saccharomyces cerevisiae*," *Biotechnol. Bioeng.*, 24, 2601, 1982.

Nishizawa et al.(7)

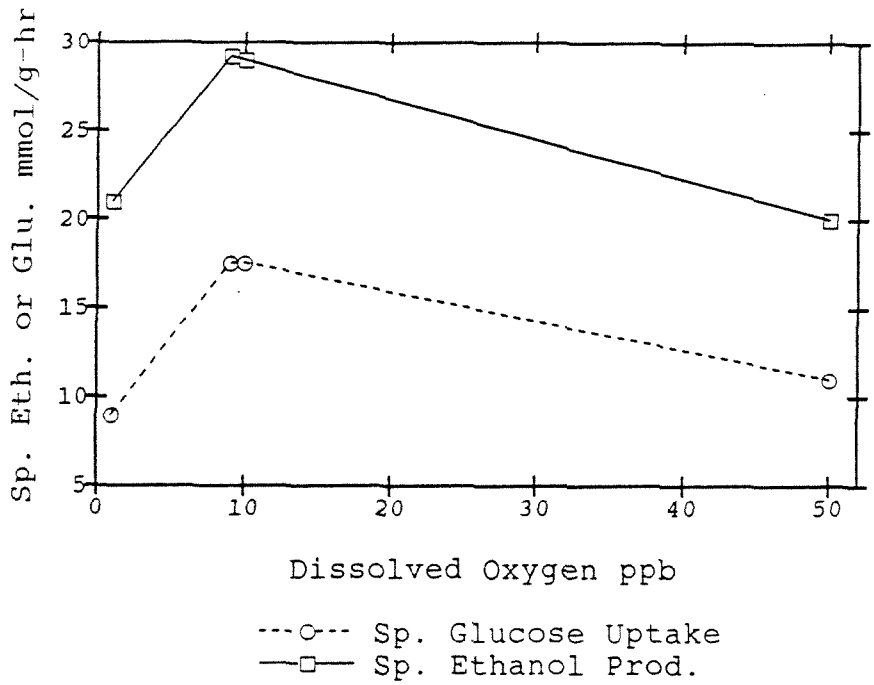

FIGURE 1.

Cysewski and Wilke(3)

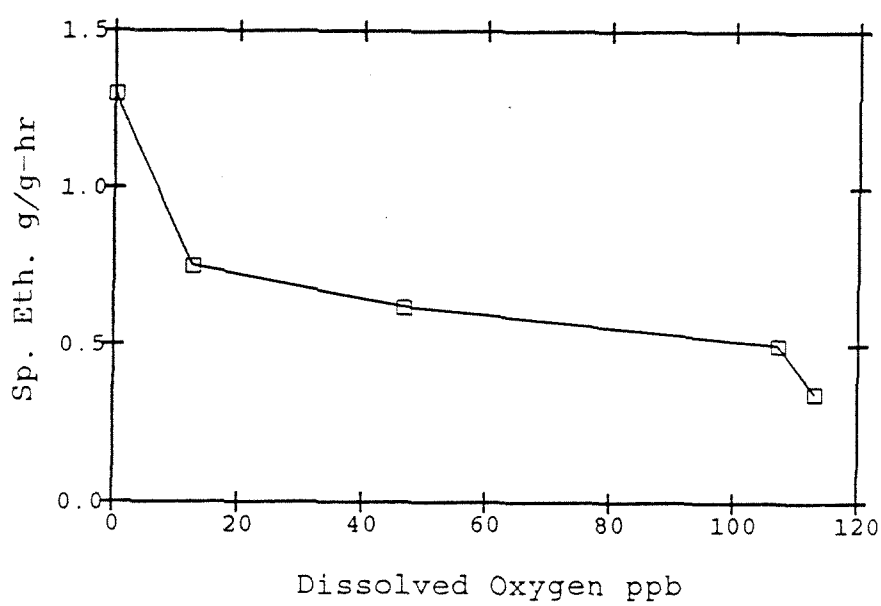

FIGURE 2.

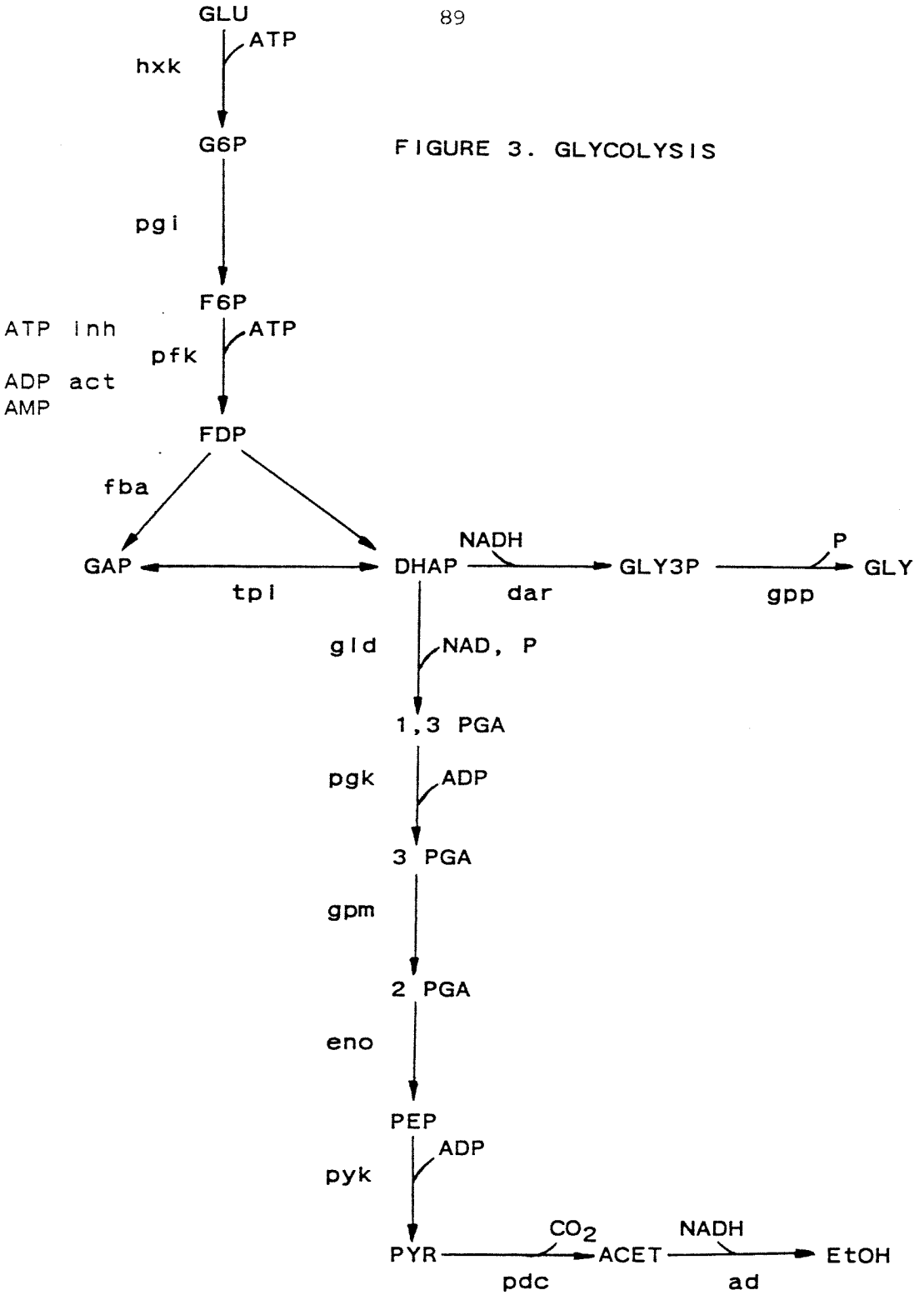

FIGURE 3. GLYCOLYSIS

FIGURE 4. ENZYMES and METABOLITES of GLYCOLYSIS

ENZYMES

AD	Alcohol Dehydrogenase
DAR	Dihydroxyacetone Phosphate Reductase
ENO	Enolase
FBA	Fructose Biphosphatase
GLD	Glyceraldehyde Phosphate Dehydrogenase
GPM	Phosphoglyceromutase
GPP	Glycerol 1-Phosphatase
HXK	Hexokinase
PDC	Pyruvate Decarboxylase
PFK	Phosphofructokinase
PGI	Glucose Phosphate Isomerase
PGK	Phosphoglycerate Kinase
PYK	Pyruvate Kinase
TPI	Triose Phosphate Isomerase

METABOLITES

ACET	Acetate
DHAP	Dihydroxyacetone Phosphate
EtOH	Ethanol
FDP	Fructose Diphosphate
F6P	Fructose 6-Phosphate
G6P	Glucose 6-Phosphate
GAP	Glyceraldehyde 3-Phosphate
GLU	Glucose
GLY	Glycerol
GLY3P	Glycerol 3-Phosphate
PEP	Phosphoenol Pyruvate
1,3 PGA	3-Phosphoglycerol Phosphate
2 PGA	2-Phosphoglycerate
3 PGA	3-Phosphoglycerate
PYR	Pyruvate

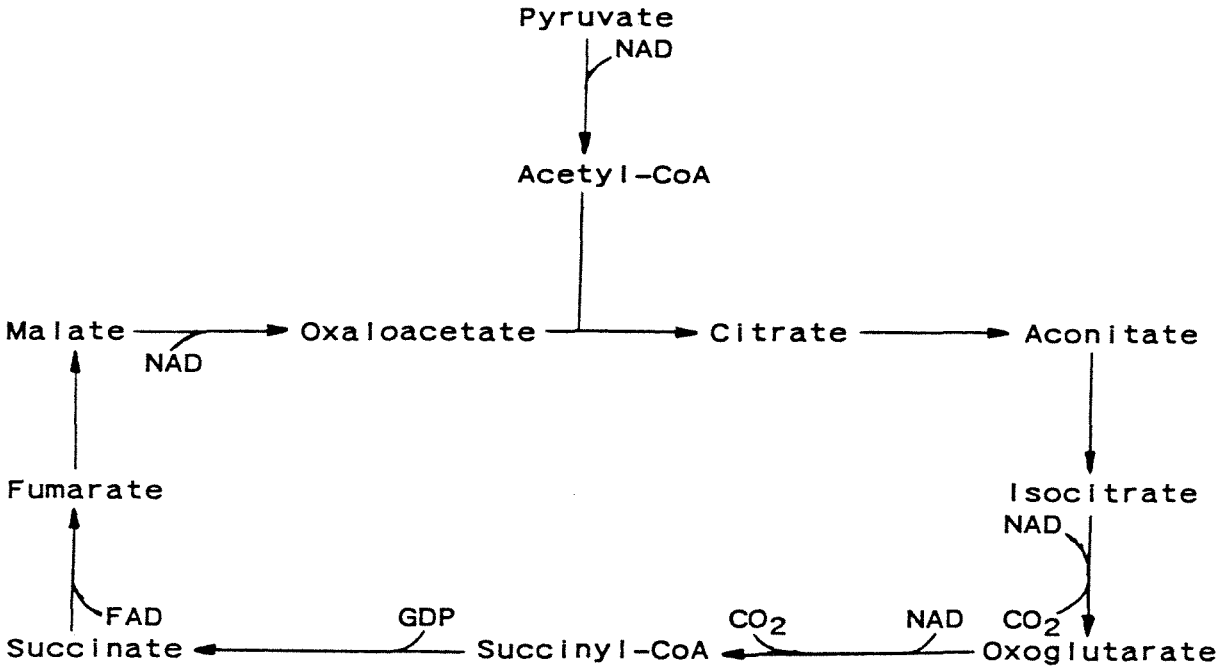

FIGURE 5. AEROBIC TCA CYCLE

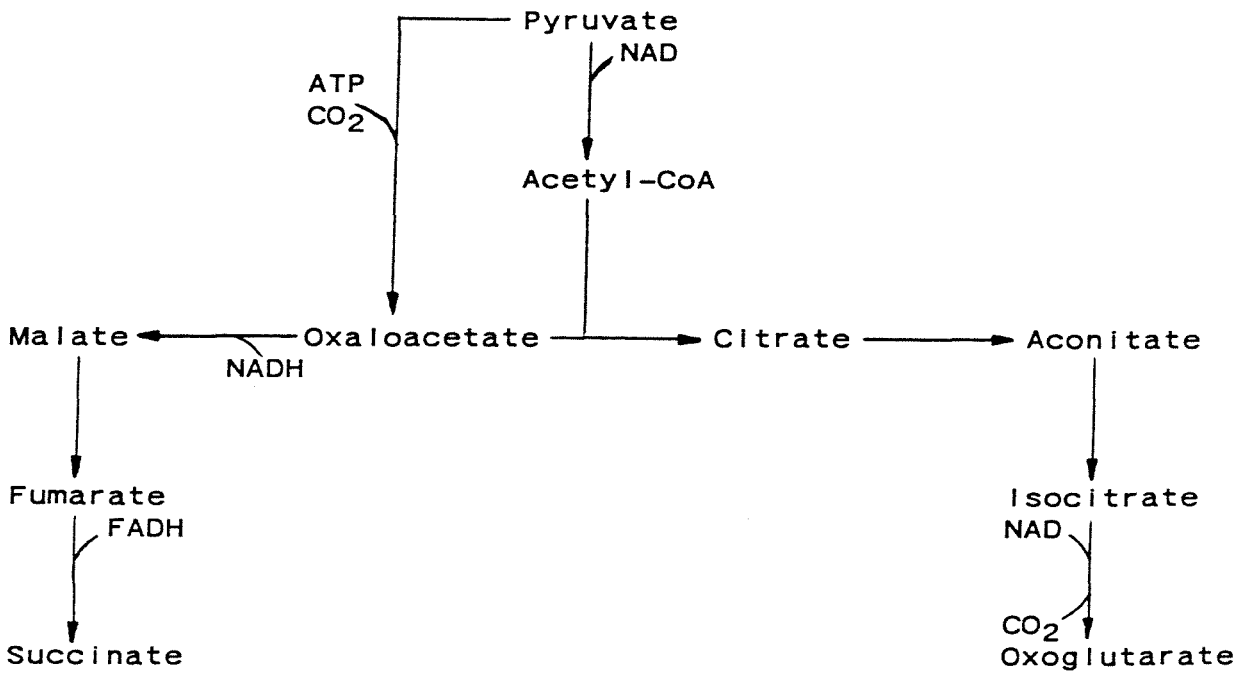

FIGURE 6. ANAEROBIC TCA CYCLE

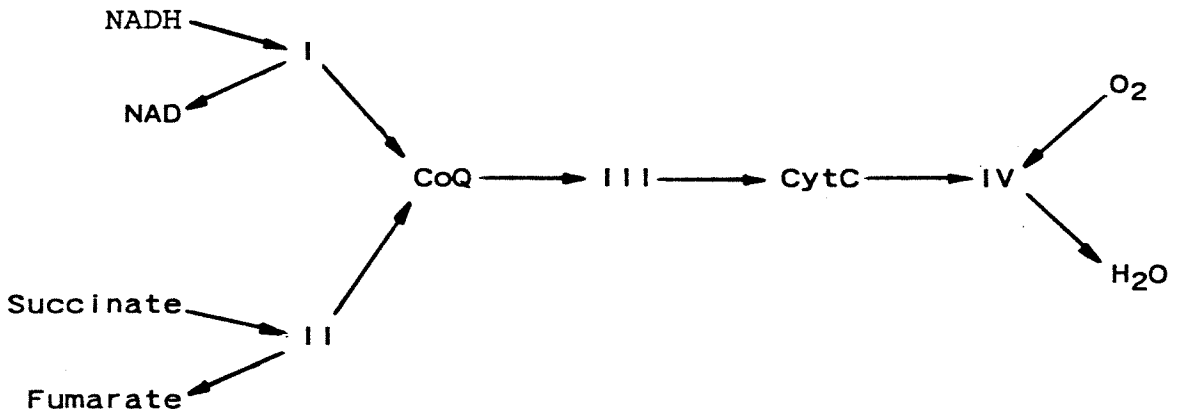

I. Succinate Coenzyme Q Reductase

II. NADH Coenzyme Q Reductase

III. Coenzyme Q Cytochrome C Reductase

IV. Cytochrome C Oxidase

FIGURE 7. RESPIRATORY CHAIN

FIGURE 8. POTENTIAL AND ACTUAL RESPIRATION

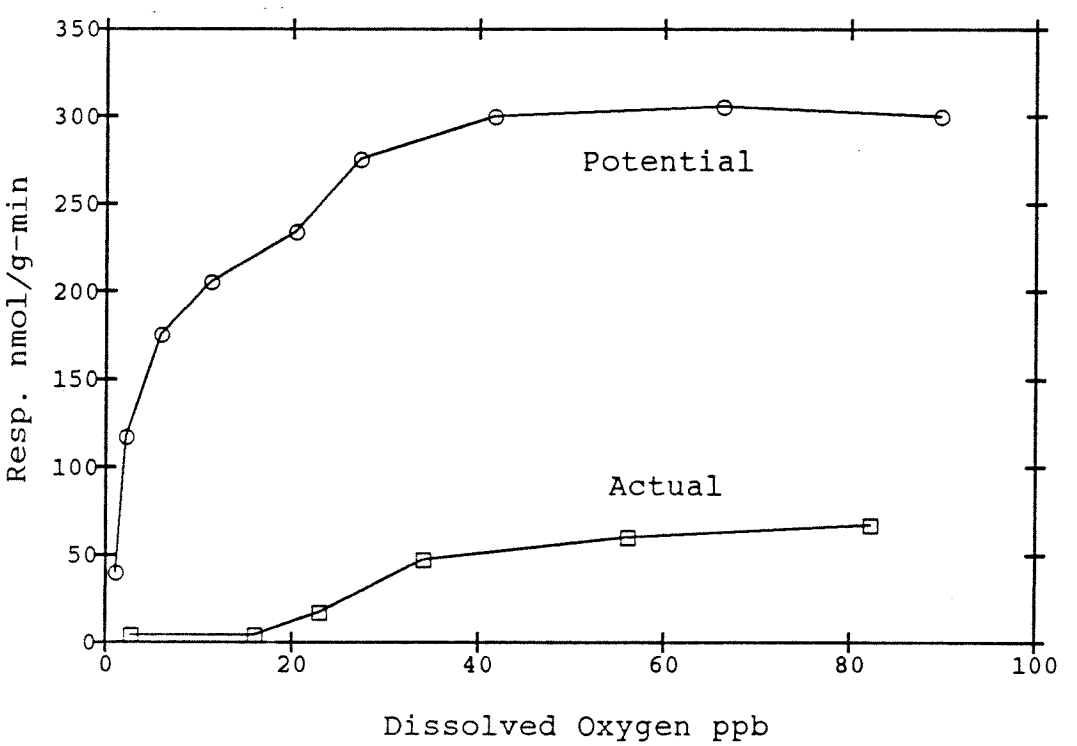

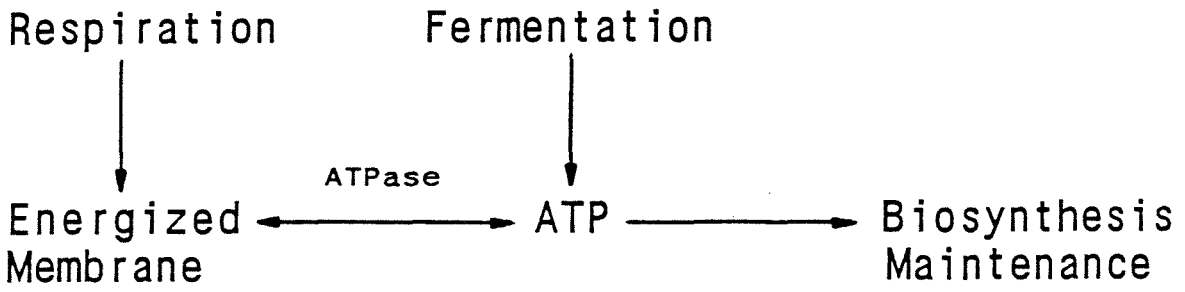

FIGURE 9. MEMBRANE ENERGIZATION

FIGURE 10. SIMULATED ACTIVITIES

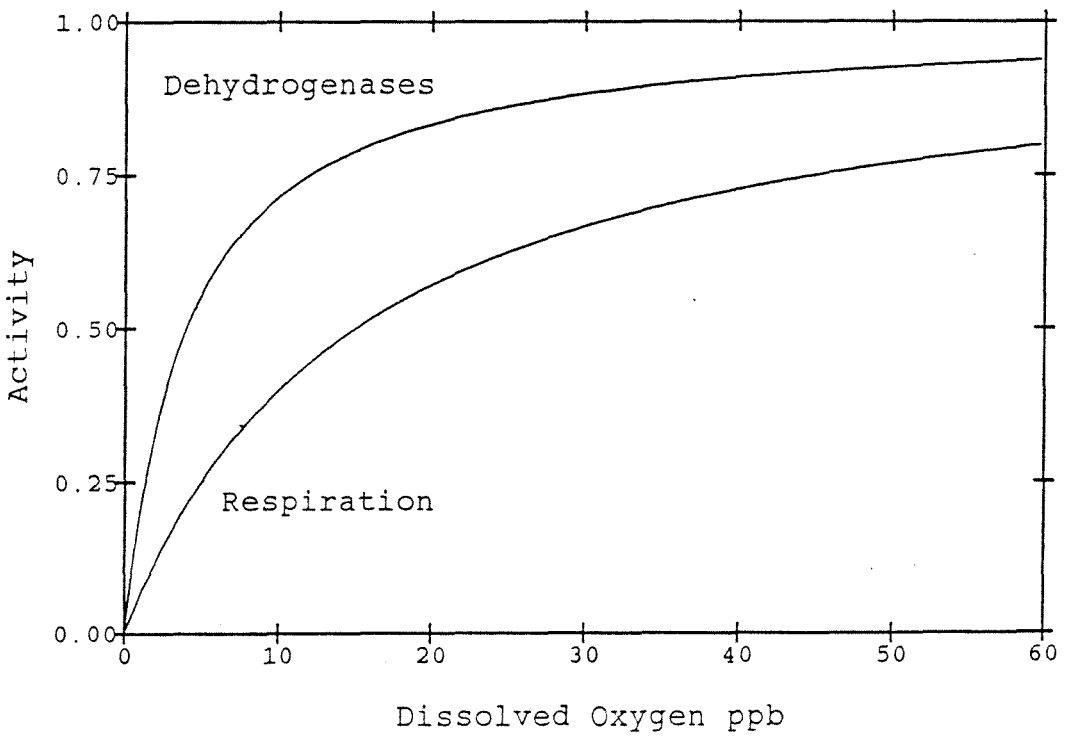

2.1 INTRODUCTION

In the introductory section of Chapter 1, the unusual behaviors of *Saccharomyces cerevisiae* in microaerobic chemostat culture found by Nishizawa et al. (1) and Cysewski and Wilke (2) were discussed. In addition, the importance of these observations and the elucidation of the underlying mechanisms to continuous ethanol production in an industrial setting have been argued. This chapter describes the microaerobic chemostat studies that were undertaken to confirm the results of the previous investigators and to explore potential mechanisms. Experiments were performed in a chemostat at varying degrees of aeration in the microaerobic range corresponding to a parts-per-billion dissolved oxygen concentration. The dilution rate, temperature and pH were held constant throughout the experiments.

In order to simplify the discussion, some of the unusual results of the previous investigators regarding the specific ethanol productivity are repeated here. Cysewski and Wilke (2) found that as the dissolved oxygen concentration was decreased, the steady-state specific ethanol productivity increased in two stages, one in the parts-per-million range and one in the parts-per-billion range of dissolved oxygen (Chapter 1, Fig. 2). However, as a plateau of relatively constant specific fermentation rate separated these two stages of increase, different mechanisms were likely. No obvious, known mechanism can explain the stimulation of fermentation in the parts-per-billion range.

Nishizawa et al. (1), working with the identical strain, dilution rate, medium, and culture conditions, found a different profile of specific

ethanol productivity (Chapter 1, Fig. 1). The parameter found a sharp maximum at 10 ppb D.O. with a 30% inhibition of fermentation at higher and lower dissolved oxygen concentrations. Again, as respiration is negligible in the ppb range and a plentiful 70 g/l of residual glucose saturated the glucose transporter, no obvious mechanism exists for these changes in the metabolic rate. The results of these investigators is also indicative of a plateau region of constant specific ethanol productivity at dissolved oxygen concentrations higher than those at which the maximum occurs.

In the experiments performed, the behavior found by Nishizawa et al. (1) was confirmed. In addition, new phenomena were discovered, such as a hysteresis type bifurcation diagram of biomass with the aeration rate as the bifurcation parameter. Characteristic of the hysteresis are the sudden ignition and extinction of biomass as the aeration is varied. In addition, a connection is made between the ability of the cells to undergo the sharp increase in ethanol productivity and the avoidance of the extinction of the biomass concentration. The involvement of ATP produced by fermentation in the sustenance of high biomass is conjectured. A new class of sustained oscillations of the bioreactor parameters as a function of time is reported. Finally, silicone polymer antifoam is found to affect metabolism by diverting metabolites away from ethanol production in favor of glycerol production and possibly by inhibiting glycolysis.

2.2 MATERIALS AND METHODS

All experiments were carried out in continuous culture at a dilution rate of 0.193/hr, at 30°C, and at pH 4.5, conditions that duplicate those employed by Nishizawa et al. (1). As did Nishizawa et al. and Cysewski and Wilke (2), the strain *Saccharomyces cerevisiae* ATCC #4126 was employed; the strain was selected more to reproduce the results of the previous investigators than for any other reason. Steady-states were attained in the chemostat at varying degrees of aeration in the oxygen-limited range. The latter was attained by the metering of air in the ccpm range, mixing it with 500 ccpm of N_2, and sending the mixture to the reactor. The medium employed and further details are presented below.

NUTRIENT

Some experiments were operated with a defined medium consisting of the carbon and nitrogen source and the vitamins and minerals listed in Table 1. The medium was patterned after the formulation of Oura (3). However, the latter could not support growth of this strain in continuous culture, but caused washout. When bolstered with a 7-fold increase in boric acid, a 60-fold increase in sodium molybdate, a 500-fold increase in zinc sulfate, a 5-fold increase in potassium iodide and the addition of 0.1 g/l EDTA, growth was supported. The components changed in concentration from the Oura medium are marked with an asterisk in Table 1. The glucose content of the medium was either 90 g/l or 40 g/l, depending on the experimental run. Also, 5 ml/l of Tween 80 were added in certain

experiments. When this was done, Tween 80 was mixed with water and heated and stirred to a uniform consistency before adding it to the medium. The specific medium variations for each run is specified in Table 2.

In some runs, a complex medium consisting of 8.5 g/l yeast extract (Difco), 3.25 g/l ammonium sulfate, 0.73 g/l magnesium chloride and 0.08 g/l calcium chloride was used. The glucose concentration was either 90 or 104.7 g/l, depending on the run. Also, 5 ml/l of Tween 80 were sometimes added. Again, the specific nutrient formulation for each run is specified in Table 2.

In the earlier experiments, General Electric antifoam AF60 was used, while later, Antifoam B from Sigma was used. Both are synthetic, silicone-based agents. In the earliest runs, antifoam mixed with water was pumped to the fermentor from a carboy separate from the nutrient in concentrations ranging from 67 to 470 mg/l.

In runs 1-5 of the discussion, the medium was sterilized by gravity filtration through Gelman capsule filters. The exceptions were the antifoam and the yeast extract, which were mixed with 1.5 liters of water and autoclaved with the nutrient carboy. In runs 6-10, the entire nutrient was autoclaved.

APPARATUS

A diagram of the apparatus is shown in Figure 1. The fermentor was a New Brunswick Scientific Bioflo with a 2 liter vessel and a working volume of 1.375 liters. Level control was maintained by pumping liquid from the surface at a more rapid rate than the nutrient input. The waste

was collected in a sterilized carboy and treated with bleach before disposal. In all but the last 2 runs, 3 equally spaced turbine impellers agitated the medium at 400 rpm. In those final runs, the top impeller was removed and the agitation speed increased to 450 rpm.

As the experiments were conducted at low dissolved oxygen, air or a 1% mixture of oxygen in nitrogen was mixed with a steady stream of pure nitrogen and sent to the fermentor. The pure nitrogen flow rate was maintained at 500 ccpm in all runs by a Tylan 0-1 liter-per-minute mass flow controller. Only the flow rate of the oxygen containing gas was altered from steady-state to steady-state and run to run. The highest aeration rate of 40 ccpm was metered by a 0-300 ccpm Tylan controller. Aerations of 1.5 to 30 ccpm were achieved with a 0-30 ccpm Tylan unit. Finally, aeration rates from 0.14 to 1.5 ccpm were accomplished by the 30 ccpm controller metering a Union Carbide Linde mixture of 1% oxygen in nitrogen. Results are reported in terms of the equivalent air flow. The nitrogen and oxygen containing streams were mixed and humidified in a bead and water containing flask, sterilized through 2 Balston filters in series, and sparged through the impeller shaft of the fermentor.

The nutrient was pumped from a 20 l carboy, through a breaker tube, and into the fermentor with a Masterflex peristaltic pump. Tygon tubing was used to minimize the diffusion of oxygen from the atmosphere into the nutrient line. In all but the first few experiments, the nutrient carboy was de-aerated by bubbling with pure nitrogen through a Balston filter while stirring with a magnetic stirrer. The deoxygenation was initiated at least 24 hours before placing the nutrient on-stream and continued thereafter.

The pH of the fermentor was maintained with a Chemtrix on-off pH controller activating a peristaltic pump sending 3N potassium hydroxide into the fermentor dropwise. The KOH was also de-aerated with the exhaust stream from the nutrient carboy. An Ingold steam sterilizable pH electrode was employed. Temperature was controlled with the manufacturer-supplied thermistor and heating element, and by circulating cooling water through a cooling finger immersed in the fermentor.

ON-LINE INSTRUMENTATION AND DATA ACQUISITION

The bioreactor variables measured continuously by a microcomputer were the gas phase oxygen and CO_2 concentrations and the time in seconds between consecutive activations of the pH control pump.

The gas stream leaving the reactor was dried with calcium sulfate desiccation material and distributed by a manifold to a Horiba CO_2 analyzer and either a Beckman or Rexnord oxygen analyzer. The CO_2 infrared analyzer had a flow cell appropriate for operation in the 0-19% CO_2 range. The instrument, whose output is nonlinear, was calibrated by mixing 19% CO_2 with pure nitrogen in varying ratios with the Tylan controller. Routinely, only the zero and the span were adjusted.

The Beckman paramagnetic O_2 analyzer was equipped with a circuit module allowing its operation in the 0-1% range of gas phase oxygen. The output of the instrument is linear, and calibration was performed with pure nitrogen and 1% oxygen in nitrogen span gas. For lower oxygen concentrations in the vicinity of 0.04%, a Rexnord parts-per-billion dissolved oxygen analyzer was used. The analyzer consisted of a galvanic dissolved oxygen probe with a lead anode, platinum cathode, potassium

iodide electrolyte, 1 mil Teflon membrane, and an amplifier. The amplifier allowed readings in the 0-20 ppb, 0-200 ppb, and 0-20 ppm ranges. Although specifically designed for dissolved oxygen measurements, accurate gas phase measurements were also obtained. Calibration of all ranges could be made with air.

The signal from these instruments and an on-off signal by the pH controller were conveyed to a Zenith or a Z80 based microcomputer through a California Data Systems, 12 bit analogue to digital converter. The details of the Z80 microcomputer are presented in the Ph.D. thesis of K.Y. San (4).

OFF-LINE MEASUREMENTS

Bioreactor parameters measured off-line were the optical density, the dry-weight biomass, and ethanol and glycerol concentrations in the supernatant. For optical density measurements, samples were drawn aseptically from the fermentor from dram vials and diluted by 1/11 or 1/26, as appropriate. The absorbance was measured at 660 nm with a Spectronic 21 spectrophotometer. Dilution was made so that the absorbance fell in the linear range of 0.050 to 0.250. However, these measurements were never used to determine the steady-state biomass concentration; only dry-weight measurements were used for that purpose. The optical density was used mainly to determine whether or not steady-state existed in the fermentor.

For dry-weight measurements 25 to 150 cc of fermentor fluid were withdrawn, filtered, washed twice with distilled water, and the filter with the yeast paste was dried for 6 hours at 100°C in a laboratory oven. The 0.45 micron pore-size filters were similarly dried and pre-

weighed before use. The dry-weight measurements were corrected for the non-negligible dry-weight of the nutrient, especially when high antifoam was added.

To measure the concentrations of components in the abiotic supernatant, 2-4 cc samples were withdrawn, placed into a syringe, and pushed through a 0.45 micron filter housed in a Millipore Swinnex filter unit. The clear supernatant was stored for a maximum of 1 month at -20°C, but was most often analyzed within a few days. In the earlier runs, glucose, glycerol, and ethanol concentrations were assayed enzymatically. The glucose and ethanol assay kits were obtained from Sigma, and the glycerol kit from Boehringer. All enzymatic reactions coupled the disappearance of the appropriate substrate with the appearance and disappearance of NAD(P)H, the concentration of which is measurable at 340 nm with the Spectronic 21. The exact procedure and operating principles are supplied in the instruction manuals of the kits.

In later runs, ethanol was measured using a Varian gas chromatograph with a Chromosorb 101 stainless steel column, flame ionization detector, and Shimadzu integrator. Injector temperatures were set to 230°C, the column temperature at 145°C, and the detector temperature at 300°C. Isopropanol was added as an internal standard.

With the final runs, all concentrations were measured with a Waters HPLC with a model 501 pump, 680 controller, R401 refractometer, wisp autoinjector, Shimadzu integrator, and a Biorad HPX-87H organic acid column. Analyses were isocratic, at 0.6 ml flow of the 0.01N H_2SO_4 mobil phase and a column temperature of 45°C. Injection volumes were set at 25 µl, and the refractive index detector positioned at 32X. Under these

conditions, glucose eluted at 9.4 minutes, glycerol at 13.5 minutes, and ethanol at 21.3 minutes. To maintain the glucose concentration within the linear range of the refractometer, samples were measured at full strength and in 1/9 dilutions.

BIOREACTOR STARTUP AND OPERATION

The stock culture was maintained on yeast extract, peptone, and glucose agar plates or slants. Inoculation cultures were initiated by transferring a colony from the plates to a flask containing the same nutrient employed in the fermentation, except for a lower glucose concentration of 10 g/l and the addition of 4 g/l phthalate buffer. After sufficient growth in the shaken flask, a portion of the medium was transferred to fresh nutrient in a new flask. At least one such transfer was made before using the culture for inoculation. Approximately 50 cc of the final culture were inoculated, and the fermentor maintained in batch mode until the optical density approached the final, steady-state value, whereupon dilution was started. Steady-state was acknowledged when the OD and the CO_2 concentration emanating from the fermentor remained constant for at least 24 hours.

2.3 RESULTS AND DISCUSSION

RUN 1

This run represented the first attempt to reproduce the data of Nishizawa et al. (1), which showed a maximum in the specific ethanol productivity in the parts-per-billion range of dissolved oxygen. In seeking to duplicate their results, the first temptation was to follow

their experimental procedure exactly, including the medium, strain, temperature, pH and dilution rate. All of these methods were indeed maintained, except for the medium, for two reasons. The first reason related to the remainder of more than 60 g/l of residual glucose out of 90 g/l in the feed at the point at which the maximum ethanol productivity occurred (1). If such high glucose concentrations are necessary to produce the maximum, then perhaps the entire phenomenon is irrelevant in an industrial setting, which seeks maximal glucose conversion. Thus, the first procedural change was to use only 40 g/l of glucose in the medium rather than 90 g/l. The second change regarded the addition of yeast extract to the medium in the previous studies (1,2). A complex, undefined medium seemed not optimally suited for the fundamental studies that were planned and which included detailed material balancing and enzyme and metabolite assays. In addition, since NADH was considered a candidate for a controlling metabolite influencing the metabolic pattern in the microaerobic range, the possibility of using on-line NADH culture fluorescence (5) was considered. However, the presence of yeast extract with its myriad of fluorogenic vitamins, flavine, and pigments would interfere with such a measurement. Thus, a defined medium outlined in the Materials and Methods section was employed. In this run, the medium was not deaerated, as previous investigators made no indication that this was necessary. General Electric AF60 antifoam mixed with water and pumped from a separate reservoir was used for foam control. In this and all other runs, the dilution rate was maintained at 0.193/hr, the temperature 30°C and the pH 4.5. The final decision concerned the level of aeration to be used during the initial steady-state and the magnitude of

the step changes for subsequent steady-states. Since the previous investigators reported the results in terms of the steady-state dissolved oxygen, no direct guidance was available for choosing the aeration. A safe starting point seemed to be anaerobiosis with only the 500 ccpm pure nitrogen stream flowing to the fermentor.

When dilution was started, steady-state was never attained. Rather, the gas phase CO_2 and OD measurements oscillated as a function of time for thirteen days. The time traces of the OD and CO_2 for the last 5 days of oscillation are shown in Figure 2. As can be seen, the period of oscillation is of the order of 10-15 hours. Both the CO_2 production rate and the optical density appear in phase, indicating that biomass and the total, but not specific, metabolic rates are oscillatory. The amplitudes of the oscillations amount to 20-30% of the mean values.

Such oscillations were not mentioned in either of the previous investigations, and are important phenomena by themselves, in addition to the unusual behaviors of the steady-state specific fermentation rate. However, oscillations were a hindrance to the investigations planned. Some further observations of oscillations and the conditions for their generation and avoidance are presented in the discussion of the other runs.

RUN 2

All procedures of the first run were followed with the exception of an initial aeration rate of 40 ccpm instead of zero. The aim was to establish the bioreactor parameters as a function of the aeration rate, starting from the highest aeration and decreasing it stepwise from steady-state to steady-state until anaerobiosis was reached. In proceeding in

this way, it was hoped to circumvent the oscillatory state encountered in run 1 by starting immediately with anaerobiosis. 40 ccpm were chosen as the highest aeration, because at this rate, the oxygen equilibrium would dictate a dissolved oxygen concentration of 750 ppb, far higher than the 10 ppb necessary to generate the peak in the specific ethanol production (1). Thus, the relevant region would not be missed.

The steady-state bioreactor parameters at different aeration rates are shown in Table 3. As planned, steady-states were attained as aeration was decremented from 40 to 0 ccpm, whereupon it was incremented through 5 ccpm. The best results would have been obtained if all steady-states were consecutive, without shutting down the fermentor and starting again. However, circumstances forced restarting at the aerations indicated by the asterisk in Table 3. The parameters as functions of the aeration rate are shown in Figures 3 and 4. It is mentioned for the last time that in this and all other runs the aeration indicated is actually mixed with 500 ccpm of pure nitrogen before entering the fermentor.

As shown by Table 3 and the graphs, the biomass concentration generally decreased as the aeration decreased. The one exceptional increase from 2.08 g/l to 2.62 g/l between the 1 ccpm and 0.5 ccpm aerations does not contradict the general trend, but indicates another process taking place, namely, the adaptation of the cells to the environment. Adaptation is clearly demonstrated in the transient of the downshift between those two aerations, during which the optical density decreased and only subsequently increased. Adaptation was also evident in the transient after the downshift in the aeration between the 0.5 ccpm and anaerobic levels. The trace of the gas phase CO_2 concentration and the time interval in

seconds between base additions during that transient are shown in Figures 5 and 6. The time between base additions is inversely related to the total growth rate, since cells take up ammonia in a stoichiometric proportion to the amount of biosynthesis and leave behind in the medium the proton from the ammonium ion (4). Clearly, the total CO_2 production and the total growth rate decrease immediately upon the aeration downshift, but after 170 hours, the total CO_2 production exceeds the initial level. Also remarkable about this trace is the onset of an oscillatory profile reminiscent of the first run, but which damps after a period of adaptation. This was the sole instance in which oscillations were observed during this run. Thus, the identical anaerobic conditions attained after a history of step decreases in aeration eliminated the oscillations that persisted with no such history. There is a clear connection between aerobic adaptation and the disappearance of oscillations.

By far, the most convincing case for adaptation is the result that all bioreactor parameters did not retrace their paths when increasing aerations followed the decreasing rates (Figures 3 and 4). After adaptation, the culture behaves identically to an unadapted culture at higher aerations. Cysewski and Wilke (2) also noted that after 3 weeks of cultivation, the optimal dissolved oxygen for total ethanol productivity decreased from 0.7 mm Hg initially to 0.07 mm Hg. Furukawa et al. (6) performed chemostat experiments under nearly identical conditions, only with 30 instead of 40 g/l of feed glucose. They, too, found that the culture parameters did not retrace their paths, and the culture at day 8 with a dissolved oxygen concentration of 2.4 mg/l behaved identically to the 21 day old culture with only 0.05 mg/l D.O. Adaptation affected not

only the macroscopic bioreactor parameters, but also the cell carbohydrate, protein, RNA, and cytochrome contents (6).

Despite the important occurrences of adaptation and oscillation, the overwhelming interest was placed upon the behavior of the specific ethanol productivity, as a sharp maximum in it was sought. However, this sharp maximum was not attained. Rather, the specific ethanol and glycerol production rates and glucose uptake rate monotonically increased with decreasing aeration rates. An exception was the decline in the specific ethanol productivity from 1.18 g/g-hr to 1.11 g/g-hr as the 1 ccpm aeration rate was taken away. However, this decrease does not rival the 30% inhibition of anaerobic fermentation found by Nishizawa et al. (1) and may be within experimental error. The 1.18 g/g-hr maximum also does not match the 1.30 g/g-hr found by the previous investigators. One result in keeping with observations of the previous investigators (1,2) was the plateau at about 1.00 g/g-hr in the specific ethanol productivity at an aeration higher than the sudden increase to 1.18 g/g-hr. A relatively narrow range of aerations spans this plateau compared to what was previously seen (1,2), but the decline in ethanol productivity towards the higher aerations is likely due to glucose limitation, which dropped to 0.023 g/l or less at these points, a level hardly high enough to saturate the glucose transporter. Since previous investigators used 90 g/l instead of 40 g/l of feed glucose here, the point of glucose limitation and the existence of the plateau region was extended to higher aerations.

As seen in Figure 2, the specific ethanol productivity also attained a maximum as the aeration was increased to 2.5 ccpm. The residual glucose was also higher there than at the surrounding points and may again reflect

glucose limitation when only 40 g/l of glucose is in the nutrient.

Although this experiment did not identically reproduce the results of prior investigators, it can hardly be considered a failure, since the outline of the literature results is discernible, with a plateau followed by a sharp jump, followed by a possible decline in the specific ethanol productivity, as aeration is decreased.

One final, important observation regards the energetics of growth throughout this region of aeration. At 40 ccpm aeration, the minimum specific ethanol productivity of 0.48 g/g-hr was found compared to the higher 1.18 g/g-hr at 1 ccpm aeration. Thus, fermentation supplied the more anaerobic cultures with 2.5 times more ATP. However, the specific growth rate and presumably the ATP demand are the same. The only means for the cell to generate the difference in ATP production is by respiration. Respiration was not measured in this run, but a rough calculation can be made. Assuming that half of the 40 ccpm air feed is respired and assuming an efficiency of oxidative phosphorylation of 1 ATP per oxygen atom (8-10), an additional 30% of oxidatively generated ATP can supplement the fermentative production. However, this is not nearly enough to account for the much larger difference in glycolytic ATP production at those two aerations. The situation is even more exaggerated when considering the very final steady-state at only 5 ccpm aeration and with specific ethanol productivity of only 0.62. Thus, there is a fundamental change in the energetic efficiency of growth, which will be a reoccurring theme throughout the upcoming discussions.

RUN 3

This run was performed identically to the previous one except for a 90 g/l concentration of glucose in the feed medium. Also, the respiration rate at the higher aerations was measured. The steady-state bioreactor parameters are shown in Figure 7 and Table 4. The initial aeration was again 40 ccpm, and steady-states were attained after decreasing the aeration rate through 5 ccpm. However, a further decrease to 2.5 ccpm did not produce a steady-state, but rather, the customary oscillations. It appeared that the bifurcation of periodic states was a hindrance to all runs, and if nothing was done, to all future runs. As a result, an effort was made to find an agent that permanently stabilized the system.

One possible explanation of the oscillations would be ethanol inhibition. One might envision a scenario, whereby during the oscillatory cycle, ethanol and biomass accumulate to a point in which both growth and fermentation are inhibited. At this point, both biomass and ethanol washout from the chemostat, and upon reaching sufficiently low levels, the metabolic processes reactivate and the cycle repeats itself. Ethanol inhibition was supported because oscillations bifurcated at the lower aeration rates, where unsaturated fatty acid and sterol synthesis needed for ethanol tolerance is hindered (10). Furthermore, adaptation possibly entailing an increased ethanol tolerance conferred stability upon the system. The approach to stabilizing the oscillations was to add unsaturated fatty acids in the form of Tween 80 directly into the medium.

At and below the oscillatory aeration of 2.5 ccpm, Tween 80, consisting primarily of the 18 carbon, singly unsaturated oleic acid, was added. The steady-states with this supplementation are marked with an asterisk in Table 4. Tween 80 boosted the biomass concentration from 5.65 g/l of

the even higher aeration rate to 10.5 g/l. This stimulation indicates that growth is limited by the unavailability of unsaturated fatty acids for new cell biosynthesis or for the development of ethanol tolerance (11). Also, no signs of oscillation were observed.

Among the steady-states in which no Tween 80 was added, the specific ethanol productivity increased very gradually with decreasing aeration, as is typical of the plateau region. Addition of Tween 80 caused a sharp drop in this parameter as biomass was able to accumulate to a level that consumed all feed glucose and caused glucose limitation. A decrease of aeration to anaerobiosis caused a sharp increase in the metabolic rate, partially because glucose limitation was alleviated and partially because of the characteristic jump in ethanol productivity past the plateau region. One unsatisfactory result was that even with pure nitrogen gasifying the fermentor, a high biomass concentration of 6.44 g/l and a relatively low residual glucose of 18.6 g/l were recorded. Cysewski and Wilke (2) saw only 2 g/l of biomass anaerobically, while Nishizawa et al. (1) found more than 70 of the 90 g/l feed left in the fermentor. For this reason, and because the major transitions in ethanol productivity occur below 5 ccpm aeration with Tween 80 in the medium, the nutrient was de-aerated with nitrogen bubbling in all subsequent experiments.

Finally, the respiration rate as a function of the aeration for the four highest aeration steady-states is shown in Table 5. Also shown are the calculated fractions of ATP production by respiration relative to fermentation, assuming an efficiency of oxidative phosphorylation of 1.0 moles of ATP per gram-atom of oxygen (7-9). Obviously, only a negligible

fraction of the ATP energy comes from respiration, indicating that changes in the specific ethanol productivity necessarily require changes in the energetic efficiency of growth.

RUN 4

As in the latter steady-states of the previous run, a defined medium with 90 g/l glucose and Tween 80 supplementation was used. What differed from the previous run was the continuous bubbling of pure nitrogen through the nutrient carboy to de-aerate the feed medium. In addition, as it was sought to eliminate all entrance of oxygen dissolved in incoming liquids, the GE AF60 antifoam was added directly to the medium, rather than separately pumped from its own carboy. The nitrogen emanating from the nutrient was channeled to the KOH solution used for pH control to strip dissolved oxygen from that liquid, also. All feed lines were changed to tygon to minimize the diffusive encroachment of atmospheric oxygen.

Bioreactor steady-states were attained starting with the highest aeration of 4 ccpm. The lower starting aeration was utilized, since run 3 demonstrated that the relevant action with Tween 80 in the medium occurs under 5 ccpm. The chronological order of the steady-states as well as the associated parameters are shown in Table 6. Also shown in this table are the ATP yields of growth expressed as the number of grams of biomass synthesized per mole of ATP generated by catabolism. This is easily calculated, since respiration contributes negligibly to ATP synthesis; one molecule of ADP is phosphorylated for each mole of ethanol produced and one mole of ATP dephosphorylated for each mole of glycerol produced (11). Also shown in Table 6 is the carbon recovery of the

consumed glucose in the products ethanol, glycerol, biomass, and the associated CO_2 production. The mass per carbon-mole of biomass is assumed to be 23.5 g (4). Negligible Tween 80 metabolism is assumed. Bioreactor parameters as functions of the aeration rate are shown graphically in Figures 8-11.

As seen from Figure 8, the general trend of decreasing biomass with decreasing aeration is repeated. The deaeration of the medium had a strong affect on the biomass pattern, since biomass concentrations as low as 0.5 g/l are observed at not quite anaerobic conditions, while in run 3, 6.44 g/l biomass remained even with pure nitrogen purging the fermentor.

Some very special phenomena were observed in this run, not previously observed. As the aeration decreased from 4.0 ccpm, the stability of the system decreased. At the steady-states near 1.6 ccpm marked "1" in Figure 7, the damped oscillations shown in Figure 12 characterized the transients of the system. The CO_2 in this figure is reported in terms of the voltage output from the infrared analyzer. Since this output is nonlinear with the CO_2 concentration, the amplitude of the oscillation is larger than it appears in the figure. At 45 hours, the percentage of CO_2 is 65% higher than at 20 hours. When the aeration rate is further decreased to the points marked "2" in Figure 7, the oscillations grew and were sustained, as shown by the trace of the CO_2 voltage in Figure 13. The last 40 hours of the trace indicate the possibility of a final damping, but may just be a lull before the onset of the next cycle. The data point in Table 6 at this aeration was obtained from this relatively steady region, and may approximate a steady-state value. The oscillation

shows some elements of periodicity and some elements of randomness. The period of the two large amplitude cycles are between 40 and 60 hours, as is also the case with damped oscillations. These oscillations were of longer periods and more chaotic than were observed in Figures 1, 2, 5 and 6.

When the aeration rate was decreased even further to 0.9 ccpm a catastrophic event occurred in that the biomass concentration washed out with atypical sharpness to 0.56 g/l, or less than one sixth the level in the oscillatory state with only a 30% decrease in the aeration (Figure 8). Nonetheless, stability was restored to the system. As the sudden drop in biomass is reminiscent of an extinction phenomenon encountered in chemical reactor theory (12), it was of interest to reverse the aeration and determine whether a different path of steady-state solutions was followed. Thus, the aeration was increased to 1.3 ccpm, at which the oscillatory state existed. The oscillatory state was not restored in doing this, but rather, a stable steady-state of only 1.22 g/l of biomass, far less than was present in the oscillatory state, was generated. Clearly, steady-state multiplicity exists at this aeration, and the one arrived at depends on the past history of the culture. The high biomass concentrations of the upper branch of solutions were restored with a further increase in the aeration to 1.65 ccpm. This hysteresis with the bifurcation of periodic states is not new to chemical reactor theory; Uppal, Ray and Poore (13) mathematically proved the existence of hysteresis and oscillations of the CSTR temperatures in response to residence time changes with an exothermic first-order reaction and external cooling. Obviously, the governing equations here are different, but are sufficiently

nonlinear to generate similar behaviors. An attempt to formulate growth equations producing hysteresis will be presented in Chapter 4.

As oscillations have repeatedly arisen in these runs, mention must be made of the relation of these oscillations to previous reports of instability in continuous yeast cultures. Borzani et al. (14) detected periodic oscillations in a moderately aerobic chemostat (1.3-1.6 v/v/m) as long as a nitrogen source other than the feed molasses was present. Oscillations were absent anaerobically, when the nitrogen source was missing, and when the aeration was increased to 3.3 v/v/m. Oscillations in the CO_2 production rate, the supernatant carbon and nitrogen content, out of phase with the biomass were also seen, but the total reducing sugar in the medium remained constant. Thus, it was assumed that the sugar was transformed to some other unmeasured compounds in the medium. The period of the cycles was around 20 hours.

Heinzle et al. (15) found oscillations at a 0.1/hr dilution rate during which the dissolved oxygen concentration varied between 600 and 20 ppb. During the cycle, extracellular glucose suddenly increased from 1 to 3 mg/l, followed by a sharp increase in the respiratory quotient and the onset of ethanol excretion. Afterwards, fermentation would subside, and the produced ethanol was respired with an associated decrease in the dissolved oxygen. The fact that glucose did not accumulate during this oxidative lull was interpreted as the production of polysaccharide storage material. When all of the ethanol was respired, polysaccharide synthesis stopped, glucose accumulated, and the cycle repeated itself. The sharp burst in the fermentation rate was assumed to be associated with the breakdown of the stored carbohydrates. Oscillations were arrested

at higher dilution rates and lower dissolved oxygen concentrations, indicating that oxidative metabolism was necessary for the unstable behavior. The biomass, substrate phase plane of the oscillation appeared different from the trajectories found by Borzani et al. with opposite directions of rotation. Possibly, this was indicative of different mechanisms. The oscillation period ranged from 1 to at most 10 hours.

Parulekar et al. (16) reported oscillations in the biomass and dissolved oxygen concentrations and the carbon dioxide evolution rate at a dilution rate of 0.2/hr and a dissolved oxygen of 50% of air saturation. Oscillations ceased at 20% and 67% of air saturation, indicating again, that moderately aerobic conditions were necessary. The period was typically 2.5 hours. Instability was also strongly correlated with low residual glucose in the medium.

Finally, Essajee and Tanner (17) and Agrawal et al. (18) derived conditions necessary and sufficient for the bifurcation of periodic states with substrate-limited and substrate-inhibition kinetics and variable yields of biomass on glucose.

It is argued that the oscillations observed in this run and the previous ones are generically different from these literature observations, especially those of Heinzle et al. (15) and Parulekar et al. (16) and represent perhaps the first report of oscillations of this kind. First, previous investigators found moderate aerations and dissolved oxygen concentrations necessary to maintain oscillations. Decreasing the dissolved oxygen to 20% of air saturation suppressed the oscillations (16) while aerations around 1.3 v/v/m were needed to maintain them. The oscillations in run 4 existed at an aeration of 0.0012 v/v/m and the

maximum dissolved oxygen that could possibly have existed was 0.25% of air saturation. Oscillations disappeared at higher aerations, but not nearly as high as in the literature studies. Previous investigations also associated oscillations with glucose concentrations as low as 1 to 3 mg/l (15). Oscillations were found to be induced by shutting off the nutrient feed to the fermentor and forcing temporary starvation (16). In this study residual glucose concentrations as high as 42 g/l coexisted with the oscillations. Previous reports found an oscillatory respiration rate to have an important role in the cycle (15, 16), while in the present study, respiration, of course, plays no part. Prior investigations yielded periods of oscillation of the order of 1-10 hrs. (15, 16) where here, 15-40 hour periods were recorded. Borzani (14) however, did observe a 20 hour period. Biomass and metabolic rates oscillated out of phase with one another in previous reports, whereas here, biomass appears in phase with the CO_2 production. Finally, the substrate limitation and inhibition models of Agrawal et al. (18) and Essajee and Tanner (17) are irrelevant because substrate is plentiful but not over the 100 g/l of sugar necessary for the onset of substrate inhibition (19). Oxygen limitation and ethanol inhibition are more likely candidates for participation in growth kinetics.

Shown in Figure 9 are the associated hysteresis behavior of the ethanol, glycerol, and residual glucose concentrations. Despite the very interesting behaviors of hysteresis and oscillations, attention was again focused upon the specific ethanol productivity, shown in Figure 10. There was a general increasing trend of the specific ethanol production rate as the aeration decreased. The ascent was uniform, with no

discernible plateau or jump characteristic of the previous runs. Also, no maximum was evident. A considerable scattering occurs at an aeration of 1.3 ccpm, but this is not surprising, since the hysteresis loop with multiple steady-states existed at this point. Thus, points close together in terms of aeration may exist on different solution branches of the hysteresis loop and may be widely separated in terms of physiological state. As the aeration is an input to the system, it does not respond to changes in the physiological state and may therefore not be the optimally chosen abscissa variable. On the other hand, the residual glucose is an output of the system tracking physiological changes of the microbe. Consequently, out of curiosity, the specific ethanol production rate is plotted against the residual glucose concentration in Figure 11.

The scatter is considerably reduced, since points on either side of the hysteresis loop are widely separated. A gap exists in the region of 45 to 72 g/l of residual glucose. Although there is no sought-after peak in the specific ethanol productivity, such a possibility cannot be excluded unless data is obtained in the gap region. However, no data is available there because this gap corresponds precisely to the unstable portion of the hysteresis loop. The entire phenomenon would be made much more interesting if this hysteresis were associated with the maximum in ethanol productivity. Thus, in the next run, methods were sought to eliminate hysteresis in order that data might be gained in this potentially critical region. It was conjectured that ethanol inhibition and the nonlinear kinetics associated with it may have caused these behaviors. It was also thought that the addition of yeast extract to the medium might alleviate the inhibition. If ethanol inhibits the biosynthesis of

certain monomers such as amino acids and nucleotides, then the addition of the monomers of yeast extract might bypass the inhibition altogether. Additionally, the previous investigators (1, 2) used yeast extract in the medium and found no hysteresis or oscillations. Thus, run 5 was carried out with yeast extract in addition to Tween 80 in the medium.

In Table 6 (still run 4), the ATP yield does indeed change from a minimum of 9.3 to a maximum of 11.6 grams of biomass per mole of ATP. This is a necessary result, since the specific ethanol production and associated substrate level phosphorylations change, but the specific growth rate stays the same. These yields are similar in magnitude to those found in the literature (7-9). Finally, the carbon recovery is in order with all but the steady-states at 0.9 and 1.32 ccpm aerations. At these points, 73 and 88 g/l out of 90 fed remained in the supernatant, making the glucose uptake rate calculation susceptible to error.

RUN 5

As mentioned, the defined medium with 90 g/l of glucose, Tween 80 and yeast extract added was employed in this run. The steady-state bioreactor parameters, ATP yields, and carbon recovery are shown in Table 7. Graphical results are presented in Figures 14-16. The carbon recovery is now an approximation, since glucose and ammonia were no longer the sole carbon and nitrogen sources.

In Figure 14, the steady-state biomass concentrations as a function of the aeration rate are juxtaposed with those of the previous run. In this case, the aeration was begun at a somewhat lower 1.8 ccpm level, at which the biomass concentration was somewhat, but not much, higher than

in the last run. As the aeration rate was decreased, the biomass concentration decreased in progressively greater increments but in a more orderly fashion than when no yeast extract was in the medium. The one point at 0.33 ccpm aeration slightly out of line with the others occurred chronologically after the minimum aeration was attained and after a subsequent aeration increase. The higher biomass concentration reflected adaptation, as a result of which such parameters do not retrace their paths. There were no signs of hysteresis or oscillations, indicating that the strategy to use complex medium worked. The most significant result from Figure 14 is that the precipitous drop in biomass is avoided when yeast extract is present.

Even more interesting are the behaviors of the specific metabolic rates shown in Figure 15. As aeration decreased, the specific ethanol production rate increased gradually and remained near a value of 1.0 g/g-hr down through an aeration rate of 0.22 ccpm. This gradual increase around this flux has been observed in the previous runs and has been referred to as the plateau. However, a further decrease in the aeration rate caused a sharp jump in the specific ethanol productivity from 1.0 to 1.3 g/g-hr, consistent with such sudden increases found by Nishizawa et al. and Cysewski and Wilke (1, 2). Furthermore, the 30% magnitude of the jump, and the flux levels before and after it, agree with those investigators. Assuming equilibrium, the dissolved oxygen concentration at .22 ccpm is 5 ppb, similar in magnitude to the 10 ppb level at which Nishizawa et al. (1) observed the maximum metabolic flux. To demonstrate consistency of this metabolic stimulation, the specific glycerol production rate and specific glucose uptake rate undergo similar magnitude increases

parallel to the specific ethanol productivity (Figure 15).

What is missing from Figure 15 is any observation of a decrease in the specific ethanol productivity at the very lowest aeration rate, negating the increase as observed by Nishizawa et al. (1). In other words, a simple increase rather than a peak in this parameter exists. However, this does not preclude the possibility that a physiological state exists with the inhibition of fermentation at even lower aeration rates and biomass concentrations than even at the lowest aeration tested in this run. 0.04 ccpm of air were introduced at the minimum rate, and the nitrogen used for the 500 ccpm steady gasification stream was only 99.996% pure. In addition, some diffusion of oxygen through the tygon tubing carrying the medium was inevitable. With the very rich medium supplemented with both Tween 80 and yeast extract, this trace introduction of oxygen yielded a biomass concentration of 1.05 g/l, nearly double that occurring in the lower solution branch of the hysteresis loop in the previous run (Figure 14). Therefore, there is no doubt that physiological states exist, producing more rarefied biomass concentrations. Such states are possibly necessary to demonstrate that inhibition of fermentation at aerations below the peak level exists.

However, the attainment of these states by decreasing the aeration below 0.04 ccpm is impractical and unrealistic, because the limitations of the apparatus such as diffusion through the tubing become important. Another approach would be to take advantage of the fact that in run 3, Tween 80 was found to increase the biomass concentrations and to shift the biomass vs. aeration curve to lower aeration rates. Thus, if Tween 80 is eliminated from the medium, the sought-after rarefied state might occur

at higher aerations, within the capabilities of the instrumentation. Yeast extract would be retained to avoid hysteresis and instability. As a result, run 6 was performed with yeast extract, but no Tween 80 in the medium.

As respiration contributes negligibly to the ATP production in this region, a Pasteur-type mechanism for the sudden increase in specific ethanol productivity in run 5 is excluded. Even if all air fed to the fermentor were respired, this would account for less than 1% of the ATP production by fermentation and could not be traded for the 30% increase in fermentation. Another tempting explanation for the jump would be a higher residual glucose level saturating the glucose transporter to a greater extent and boosting the transport flux and ethanol productivity. However, this would contradict the plateau for which a relatively constant ethanol productivity existed from 12 to 53 g/l of glucose. It is hard to imagine that an increase from 12 to 53 g/l residual glucose increases the metabolic flux only by less than 1%, while an increase from 53 to 70 g/l produces a 30% jump. In addition, in run 2, a 1.00 g/g-hr specific ethanol production rate characteristic of the plateau region was possible with less than 1 g/l of residual glucose. Therefore, this jump must occur by some other, previously undocumented, stimulation of the glycolysis pathway. The elucidation of this mechanism occupies most of the remaining experimentation and modeling.

Corresponding to increases in the specific ethanol productivity are decreases in the ATP yield as shown in Table 7. A 26% decrease in this yield from 10.47 to 8.8 grams biomass per mole ATP accompanies the shift in ethanol productivity. Sudden changes in the metabolic flux have

ramifications not only for the regulation of the glycolysis pathway, but also for the energetics of growth. The cell may be indifferent to the increased metabolic flux, using only the ATP that it needs and wasting the rest, or else the higher flux may have value to the cell. The research described hereafter is also aimed at this question.

It is of interest to juxtapose the specific ethanol production rates of this and the previous run, as has been done in Figure 17. Residual glucose is chosen as the abscissa, as it is a common denominator that must always lie between 0 and 90 g/l as long as 90 g/l are fed; the location along this 0-90 scale provides a unique measure for the state of the culture. This graph enhances the likelihood that a peak in the specific ethanol productivity does exist, not just a monotonic increase. If the fact that 2 runs are represented in one graph is ignored, then a peak is seen. In addition, the maximum in the ethanol productivity in run 5 occurs at a residual glucose excluded by the unstable portion of the hysteresis loop in run 4. Thus, the maximum ethanol productivity may, after all, be linked with the existence of hysteresis. To speculate further, perhaps the increased ATP production from the enhanced metabolic flux is useful to the cell in preventing the characteristic extinction of the biomass in the hysteresis loop. In Figure 18, the specific glycerol production and glucose uptake of the two runs are also compared.

RUNS 6 AND 8

These runs were performed with undefined medium outlined in the Methods section, consisting primarily of yeast extract and 90 g/l of glucose. This medium differed from the one used in run 5 by the elimi-

nation of Tween 80, the reason for which has already been discussed. Also, in run 5, the vitamin and mineral supplementation of the defined medium was retained despite the addition of yeast extract. In this run, those supplementations were eliminated to conform to the formulations of the previous investigators (1, 2). Antifoam B from Sigma rather than General Electric AF60 was used for the first time, with a 0.1 cc/l concentration similar to the amount employed by Nishizawa et al. (1). The steady-state parameters of these runs are shown in Tables 8 and 10. Graphical results are shown in Figures 19-21.

The steady-state biomass and ethanol concentrations as functions of the aeration rate are shown in Figure 29. As mentioned, the aim of removing the Tween 80 from the medium was to shift the biomass vs. aeration curve to higher aeration rates because of the less favorable conditions of the new medium towards growth. It was hoped that this shift would enable the attainment of lower level of biomass than was possible at the lowest aeration of the previous run, and thus to obtain a more complete range of the data. The desired shift to higher aerations was indeed accomplished, as seen by the comparison of Figures 19 and 14. Also, the decline of the biomass concentration is uniformly graded, with no sign of hysteresis, indicating the stabilizing influences of the yeast extract in the medium. However, the system was not completely stable, as oscillations resulted in the region of 1 ccpm aeration and below the minimum aeration, precluding the attainment of steady-states at the low levels of biomass desired. The low biomass concentrations of the washed-out branch of the hysteresis loop in run 4 were again not attained. The oscillations that prevailed here, especially at the 1 ccpm aeration

range, appeared different from those recorded previously, because of a vastly different time period of 5 hours or less and the appearance and disappearance of foam during the cycle, for the first time. A time trace of the oscillatory CO_2 voltage at around 1 ccpm aeration is shown in Figure 21. During the peak of the CO_2 cycle, foam would start to build and result in the sudden drop of both the CO_2 concentration and the optical density. At the minimum of the CO_2 trace, the foam would have already disappeared and both the OD and the CO_2 would again begin to build. The possible cause of both CO_2 and OD changes is the floatation of biomass above the liquid during foaming, removing cells from the liquid phase and their carbon source. This could also explain why the liquid phase ethanol and glucose concentration remained relatively constant. It must be emphasized that the foaming did not occur during the higher aeration rate, but existed in a narrow range of aeration around 1.0 ccpm and below the lowest aeration. The only point in Figure 19 affected by oscillations occurs at around 1 ccpm of run 6, so that steady-state values at this point are estimated from numerous measurements.

A remarkable feature revealed in Figure 19 is that the two cultivations performed with the identical methods and following nearly identical histories produced different results. The cultivation of run 6 had consistently lower biomass concentrations at all aeration rates than run 8, but the two had indistinguishable ethanol profiles. Thus, as shown in Figure 20, the specific ethanol production in run 6 is also consistently higher. Implied by these results are random elements controlling the adjustment of cells to their environment, producing cultures that are less or more successfully adapted in different instances. Run 8 produced

cells that could maintain the same specific growth rate and a higher biomass concentration with a lower specific ethanol productivity and associated ATP production. This not only shows that run 8 became randomly better adapted, but that ATP may be an important growth-limiting factor in this region.

As is also seen in Figure 20, the specific ethanol production in run 8 did find a peak. The magnitude of this maximum matches the value found by the previous investigators and in the prior runs. However, the magnitude of the drop at lower aerations is less than was observed by Nishizawa et al. (1). In addition, foaming and oscillations prevent the operation at yet lower aerations. Therefore, in run 7, a higher antifoam concentration of 0.7 cc/l was used.

RUN 7

The results of this run, with the higher antifoam concentrations, are shown in Table 9 and in Figures 22-24. A comparison of the biomass and ethanol concentrations of this run and runs 6 and 8 are shown in Figure 21. At around 2 ccpm, a very sharp, precipitous drop in the biomass and ethanol concentrations occurs as the aeration is decreased when high antifoam is present in the medium. If one inspects the chronology of the steady-states attained in Table 9, a small hysteresis loop exists with a lower biomass concentration recorded upon the approach of the 1.8 ccpm from lower aerations than upon reaching this state from higher aerations. This contrasts with the more orderly and gradual decline when only low antifoam is present. The transition from a gradual to catastrophic decline mediated by antifoam is analogous to the transition from the

hysteresis loop to the monotonic profile conferred upon the system by yeast extract in runs 4 and 5. In both cases, sharp drops are replaced by orderly, uniform profiles. It is very likely that the same mechanisms are involved. Definite clues as to the cause of these shifts are discernible from Figure 23. In the top portion of the Figure is shown an expanded version of the ethanol concentrations in the important region. Below it is a comparison of the specific ethanol productivity of run 6, which had a gradual profile, and run 7, which had the drop. Run 6 clearly possesses the higher specific ethanol productivity. It is possible that the higher concomitant ATP production maintained a higher biomass concentration without the need for a drastic washout of biomass. Conversely, with high antifoam, the specific ethanol productivity was prevented from attaining the same high value. Consequently, the cells may have suffered from an ATP deficiency, which had to be compensated by a drop in the biomass concentration. A lower biomass also would mean a lower extracellular ethanol, with the beneficial reduction of ethanol inhibition maintaining the specific growth rate despite the detrimental lack of ATP. A trade-off between ATP activation of growth and ethanol inhibition of growth is surmised.

Very similar events may have been motivated by the addition of yeast extract in run 5 to prevent the extinction of biomass in run 4. In the absence of yeast extract, additional ATP is expended in the biosynthesis of monomers such as amino acids and nucleotides. When the critical aeration was reached, a sudden demand of ATP overwhelmed the cells and caused the catastrophic drop in biomass. However, with yeast extract present, ATP required for monomer synthesis could be diverted to

the cause of maintaining the high biomass concentration.

Comparison of the specific ethanol productivities in the presence and absence of high antifoam (Tables 8 and 9) may be instructive in determining why sudden jumps in the specific ethanol productivities have been repeatedly observed in these investigations and by previous investigators. With low antifoam, the specific ethanol productivity begins near 1.00 g/g-hr at the highest aeration rate, a typical plateau value, and then jumps to 1.2 to 1.3 g/g-hr as the aeration is lowered. When high antifoam is present, a specific ethanol production of 1.0 g/g-hr is maintained at all aerations, and the jump is prevented. Since the jump occurs in the same vicinity of the aeration as the fall in biomass, and the absence of the jump causes the fall in biomass, the metabolic intensification may be a built-in mechanism possessed by the cell to respond to a sudden demand of ATP when this certain region is entered.

In Figure 24 is shown a comparison of the specific glycerol productivities and the specific glucose uptake rates in the high and low antifoam runs. The specific glycerol production graph is essentially a mirror image of the ethanol and biomass vs. aeration profiles. Thus, high antifoam stimulates glycerol production to a similar extent as its depression of biomass. Since glycerol production consumes ATP (11), it represents a further burden to the cell. The glucose uptake rate, although more scattered than the other parameters, is roughly equal among the three runs. Apparently, antifoam does not inhibit the overall transport rate, but rather short-circuits metabolism by diverting carbon skeletons away from ethanol and towards glycerol production. The possibility that antifoam alleviates the bottleneck in the glycerol production pathway in

the diffusion of the product through the cell membrane is considered further in the next chapter.

A very important observation is that antifoam is not an inert ingredient but is an influence upon cell metabolism. This observation is not unique in that silicone polymer antifoams have been reported to affect respiratory activity, transport through the cell walls, and oxygen transport (20). Silicone antifoam has a similar effect on *Brevibacterium flavum* upon cell morphology as oxygen limitation (20).

RUNS 9 AND 10

These runs represent the last attempt to find the inhibition of fermentation at the very lowest aeration rates and also to explore the influence of antifoam on culture parameters. The difference between these and the previous runs lies in the removal of one of the three turbine impellers closest to the gas-liquid-surface in this run. It was thought that the top impeller contributed mainly to the foaming problems at certain aeration rates in runs 6 and 8. Also, the impeller speed was increased from 400 to 450 rpm to partially compensate for the diminished agitation and gas to liquid mass transfer. In run 9, a low antifoam concentration of 0.067 g/l was used, while in run 10, 0.47 g/l was used. The glucose concentration in the feed medium was 104.7 g/l in run 9, while in run 10, it was 90g/l. In all other respects, the medium was the same as in the 3 previous runs. Chronologically, run 10 was performed directly after run 9, without shutting off and restarting the fermentor. Also, the aeration rates were not manipulated in a monotonic way, but were changed in different directions and with different magnitudes from steady-

state to steady-state.

The steady-state bioreactor parameters in the correct chronology are shown in Tables 11 and 12. The only exception to the chronology was that the last point in run 9 actually occurred after run 10 and was the very last point attained. Graphical results are presented in Figures 25 and 26.

The biomass versus aeration for both runs is shown in Figure 25. Obviously, the cells did not experience the drastic decline at around 2 ccpm aeration with the high antifoam in the medium. In fact, at some aerations, the high antifoam culture was able to attain higher biomass concentrations than the low antifoam case at the corresponding aerations. This result is obviously due to adaptation. Run 10 was performed immediately after run 9 without restarting the fermentation. In the one and one-half months during which run 9 occurred, the cells adapted to the environment to the extent that they were able to avoid the events that disfavored growth in the high antifoam, unadapted culture.

The specific ethanol productivities for both cultures are also shown in Figure 25. With low antifoam, as the aeration rate changes from 9.0 ccpm to 0.6 ccpm, the specific ethanol productivity increases from 0.84 to 1.32 g/g-hr. This very significant 57% increase is another example of the general stimulation of fermentation that has been mentioned repeatedly. This time, the magnitude of the stimulation exceeded the 30% increases registered by the previous investigators and in the previous runs. More interestingly, when the aeration rate is lowered further to 0.143 ccpm, the stimulation is reversed, with a decline of the productivity to 0.77 g/g-hr. The long sought-after peak in the specific ethanol

productivity originally found by Nishizawa et al. was finally, unequivocally, reproduced. The fear that this data point at the lowest aeration is a mistake is unfounded, because both biomass and supernatant metabolite concentrations were measured on two consecutive days, giving the same results. Also, as will be discussed in the next chapter, numerous intracellular metabolite assays, including ATP, NADH, pyruvate, glucose-6-phosphate and a variety of others showed very special events to occur at this point. The low biomass concentration of around 0.5 g/l attained at this point has eluded the previous runs, with the exception of the washed-out branch of the hysteresis loop in run 4. The difficulty in finding this point is attributable to either oscillations, or a medium too supportive of growth. In this run, the elimination of the third impeller and the Tween 80 from the medium provided the correct combination of environmental factors for success.

The sudden inhibition of fermentation at the lower aeration is, by definition, a negative Pasteur effect, which has been observed in *Saccharomyces* resting cell suspension and cell-free extracts in succinate buffer (21) and in growing respiratory-deficient mutants (22). Some mechanisms for this phenomenon have been proposed (21). In addition, some alternate mechanisms were considered in Chapter 1, Section 3, providing motivation for the entire course of research. Based on the bioreactor studies, it seems eminently reasonable that this inhibition of fermentation is the reversal of the very mechanism that caused the increased fermentation rates at the higher aeration. It was suggested earlier that the stimulated fermentation represents a built-in mechanism possessed by the cell to boost the ATP level in a narrow region in which

a sudden demand exists. This demand manifests itself as a sudden extinction of biomass in the hysteresis loop and other sharp drops in biomass experienced in the previous runs. The fact that fermentation is restored to a more normal level may indicate that the higher ATP demand no longer exists at the lowest aeration. The mechanism is also tuned to the cell's needs in this instance. As mentioned, some speculation about the nature of this mechanism has been presented in the previous chapter and is the subject of research in the upcoming chapters.

When high antifoam was present, the specific ethanol productivity was again inhibited from increasing at the point at which it normally does. This parameter was generally lower than in the low antifoam case. This is precisely what happened in run 7. The notable exception is the sharp jump in the parameter that occurred at the lowest aeration rate, corresponding to the drop when only low antifoam was present. The magnitude of the jump was the usual 30%. Therefore, antifoam does not stamp out completely the ability of the cell to stimulate fermentation, but rather, disrupts the regulation so that the stimulation occurs at the wrong point.

In Figure 26, the specific glycerol productivity and glucose uptake rates of the two cultures are compared. In agreement with prior observations, the specific glycerol production rate of the high antifoam culture is greater, meaning that antifoam diverts carbon skeletons away from ethanol and towards glycerol production. In disagreement with the previous result is that the specific glucose uptake rate is also inhibited by the high antifoam, except at the lowest aeration. Antifoam may also inhibit glucose transport or glycolysis.

Finally, mention must be made of some discrepancies in the carbon recoveries of the two runs. At the lowest aeration with low antifoam, only 70% of the calculated glucose uptake is accounted for in the measured products. However, 97 g/l of residual glucose out of 105 g/l fed remained unused. A combined 3% error in the residual glucose measurement and in the formulation of the medium would result in more than 30% error in the calculated glucose uptake; the latter measurement is unreliable here. Also, in run 10, only 80-95% of the glucose carbon taken up was recovered in the products ethanol, glycerol, biomass, and associated CO_2. Typically, the recovery is 90-95%. The presence of antifoam may have resulted in the generation of other compounds. No special peak was observed in the HPLC traces, meaning that a sum total of about 2 g/l of spectrum or other compounds such as acetate, succinate, acetaldehyde, pyruvate, and others (23) was excreted. Possibly, antifoam increases the membrane permeability of these compounds.

2.4 CONCLUSIONS

The experiments undertaken have verified some poorly documented phenomena in the literature regarding microaerobic yeast fermentation and have uncovered new ones. The bifurcation of sustained oscillations was found possible towards the lower end of aerations studied. These oscillations had distinctly different characteristics than those previously reported in the literature. Not the least of these differences was that previous reports required strictly oxidative conditions for their sustenance, while here, the opposite was true. Oscillations were alleviated after a period of adaptation, by a previous history of higher aeration,

and by the addition of Tween 80 and yeast extract. These all pointed to ethanol inhibition as a potential cause of the oscillations as all of these agents could in some way act to diminish ethanol inhibition.

Hysteresis characterized by steady-state multiplicity and the sudden extinction and ignition of biomass with aeration as a bifurcation parameter was for the first time reported. Addition of yeast extract eliminated the hysteresis and replaced it with a monotonic bifurcation diagram. Sudden drops in biomass with high antifoam, but not low antifoam, present were completely analogous.

The specific ethanol productivity was found to increase sharply as the aeration rate was decreased, and was restored to the normal level from this maximum when the aeration was further decreased. This peak in the specific ethanol productivity corroborated the observations of Nishizawa et al. (1). These changes in ethanol productivity could not be attributed to respiration or a Pasteur-type mechanism, nor to an incompletely saturated sugar transporter. Rather, a more subtle stimulation of the glycolytic pathway with some undocumented mechanism must have occurred.

More interesting was the connection between the high specific ethanol productivity and the ability of the culture to maintain high biomass concentrations. Conditions that prevented the attainment of increased ethanol productivity resulted in sudden drops in the biomass concentration. When fermentation was stimulated, these drops never occurred. These facts pointed strongly to the necessity of a greater ATP flux to sustain growth processes in the lower aeration rates. Without the increased fermentation, cells were starved for ATP, washed out, and reduced the

inhibition of extracellular ethanol to compensate for the ATP deficiency. The changes in ethanol productivity may be a built-in mechanism in response to the cell's needs.

Finally, silicone polymer antifoam has been found not to be an inert substance, but affects the cell's ability to increase the fermentation rate as it does normally. The antifoam apparently diverts carbon skeletons away from ethanol production and towards glycerol production and may additionally inhibit some part of the glycolytic pathway.^Z

REFERENCES

1. Nishizawa, Y., Dunn, I.J., and Bourne, J.R., "The Influence of Oxygen and Glucose on Anaerobic Ethanol Production," in Continuous Cultivation of Microorganisms, Proc. 7th Symp., Prague, 1980, p. 605.

2. Cysewski, G.R. and Wilke, C.R., "Utilization of Cellulosic Materials through Enzymatic Hydrolysis. I. Fermentation of Hydrolysate to Ethanol and Single Cell Protein," *Biotechnol. Bioeng.*, 18, 1297, 1976.

3. Oura, E., "Effect of Aeration Intensity on the Biochemical Composition of Baker's Yeast. I. Factors Affecting the Type of Metabolism," *Biotechnol. Bioeng.*, 16, 1197, 1974.

4. San, K.Y., "Studies on the On-Line Identification and Optimal Control of Bioreactors," Ph.D. Thesis, California Institute of Technology, 1983.

5. Zabriskie, D.W., "Use of Culture Fluorescence for Monitoring of Fermentation Systems," *Biotechnol. Bioeng. Symp.*, 9, 117, 1979.

6. Furukawa, K., Heinzle, E., and Dunn, I.J., "Influence of Oxygen on the Growth of *Saccharomyces cerevisiae* Continuous Culture," *Biotechnol. Bioeng.*, 25, 2293, 1983.

7. Meyenburg, H.K. von, "Energetics of the Budding Cycle of *Saccharomyces cerevisiae* during Glucose-Limited Aerobic Growth," *Arch. Mikrobiol.*, 66, 289, 1969.

8. Rogers, P.J. and Stewart, P.R., "Energetic Efficiency and Main-

tenance Energy Characteristics of *Saccharomyces cerevisiae* (Wild and Petite) and *Candida parapsilosis* Grown Aerobically or Micro-Aerobically in Continuous Culture," *Arch. Microbiol.*, 99, 25, 1974.

9. Dekkers, J.G.J., Kok, H.E. de, and Roels, J.A., "Energetics of *Saccharomyces cerevisiae* CBS426: Comparison of Anaerobic and Aerobic Glucose Limitation," *Biotechnol. Bioeng.*, 23, 1023, 1981.

10. Thomas, S.D., Hassack, J.A., and Rose, A.H., "Plasma Membrane Lipid Composition and Ethanol Tolerance in *Saccharomyces cerevisiae*," *Arch. Microbiol.*, 117, 239, 1978.

11. Sols, A., Gancedo, C., and De La Fuente, G., "Energy-Yielding Metabolism in Yeasts," in *The Yeasts*, vol. 2, Rose, A.H. and Harrison, J.S. eds., Academic: New York, 1971, p. 271.

12. Poore, A.B., "A Model Arising from Chemical Reactor Theory," *Arch. Rat. Mech. Anal.*, 52, 358, 1973.

13. Uppal, A., Ray, A.H., and Poore, A.B., "The Classification of the Dynamics Behavior of Continuous Stirred Tank Reactors - Influence of Reactor Residence Time," *Chem. Eng. Sci.*, 31, 205, 1976.

14. Borzani, W., Gregori, R.E., Vairo, M.L.R., "Some Observations on Oscillatory Changes in the Growth Rate of *Saccharomyces cerevisiae* in Aerobic Continuous Undisturbed Culture," *Biotechnol Bioeng.*, 19, 1363, 1977.

15. Heinzle, E., Dunn, I.J., Furukawa, K., and Tanner, R.D., "Modeling of Sustained Oscillations in Continuous Culture of *Saccharomyces cerevisiae*," in IFAC Modelling and Control of Biotechnical Processes, Helsinki, 1982, p. 57.

16. Parulekar, S.J., Semones, G.B., Rolf, M.J., Lievense, J.C. and Lim, H.C., "Induction and Elimination of Oscillations in Continuous Cultures of *Saccharomyces cerevisiae*," *Biotechnol. Bioeng.*, 28, 700, 1986.

17. Essajee, C.K. and Tanner, R.D., "The Effect of Extracellular Variables on the Stability of the Continuous Baker's Yeast-Ethanol Fermentation Process," *Process Biochem.*, 14, 16, 1979.

18. Agrawal, P., Lee, C., Lim, H.C., and Ramakrishna, D., "Theoretical Investigations of Dynamic Behavior of Isothermal Continuous Stirred Tank Biological Reactors," *Chem. Eng. Sci.*, 37, 543, 1982.

19. Jones, R.P., Pamment, N., and Greenfield, P.F., "Alcohol Fermentation by Yeasts - the Effect of Environmental and Other Variables," *Process Biochem.*, 16, 43, 1981.

20. Viesturs, V.E., Kristapsons, M.Z., and Levitans, E.S., "Foam in Microbiological Processes," in *Advances in Biochemical Engineering*, vol. 21, Fiechter, A. ed., Springer Verlag: New York, 1982, p. 170.

21. Wiken, T.O., "On 'Negative Pasteur Effects' in Yeast," in *Aspects of Yeast Metabolism*, Mills, A.K. and Krebs, H. eds., Blackwell: Oxford, 1967, p. 133.

22. Silhankova, L., Mostek, J., and Pizingerova, A., "Metabolic Quotients of Respiratory-Deficient Mutants in Brewer's Yeast and the Appearance of a Negative Pasteur Effect," *J. Inst. Brew.*, 81, 218, 1975.

23. Oura, E., "Reaction Products of Yeast Fermentations," *Process Biochem.*, 14, 19, 1977.

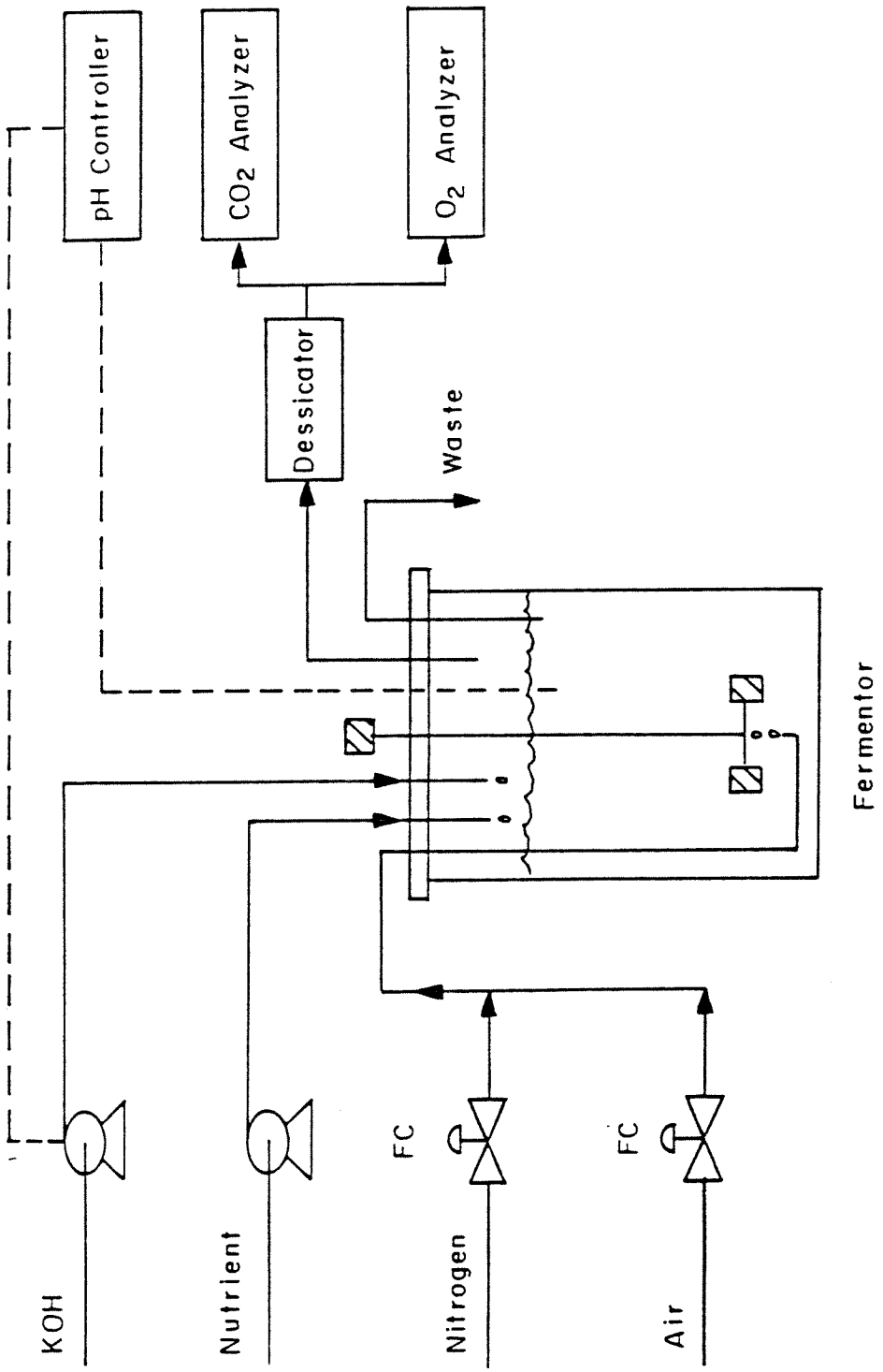
pH Controller
CO_2 Analyzer
O_2 Analyzer
Dessicator
Waste
Fermentor
KOH
Nutrient
FC
Nitrogen
FC
Air

FIGURE 1.

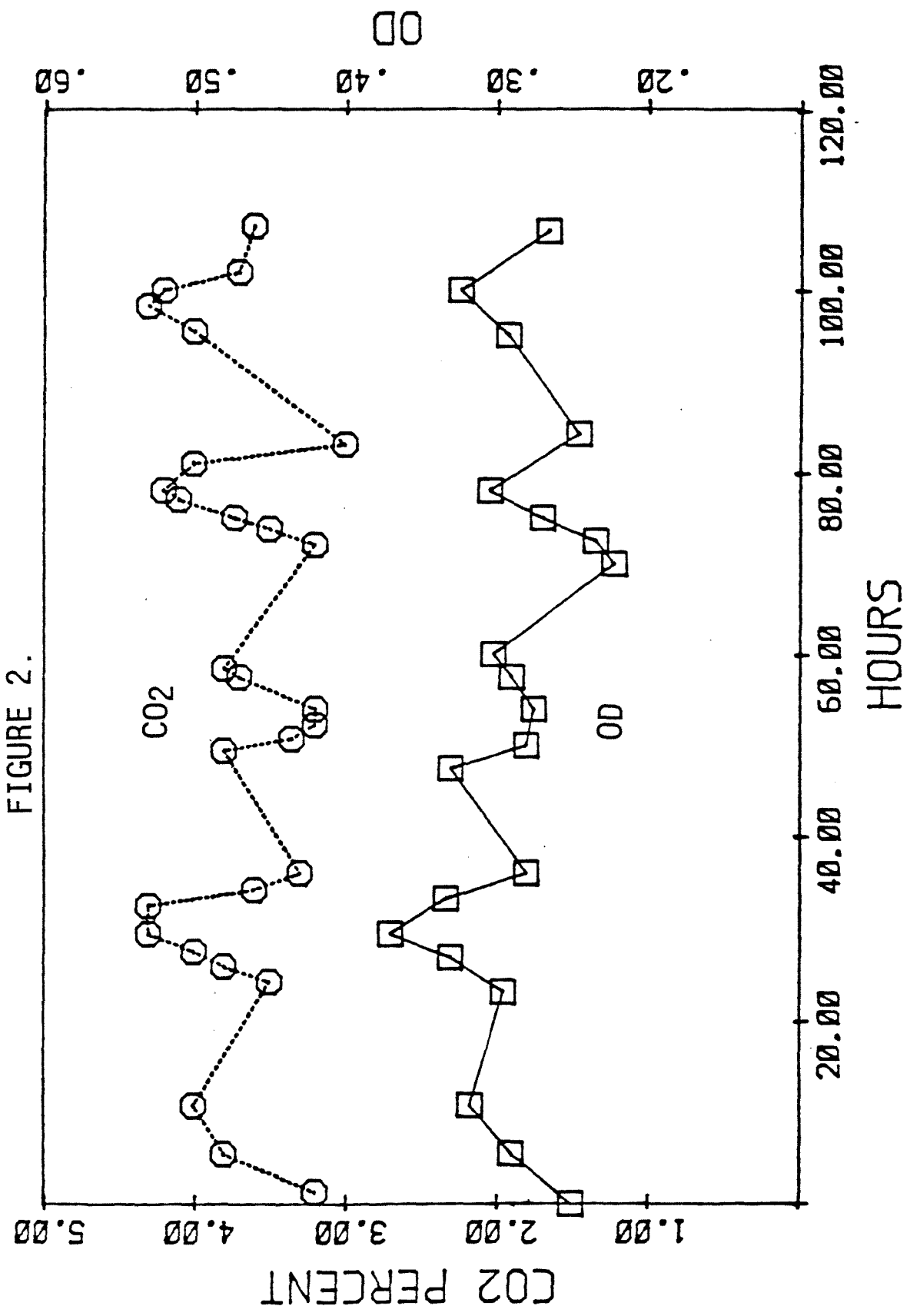
OD
.60
.50
.40
.30
.20
120.00
100.00
80.00
60.00
40.00
20.00
HOURS
CO_2
OD
CO2 PERCENT
5.00
4.00
3.00
2.00
1.00

FIGURE 2.

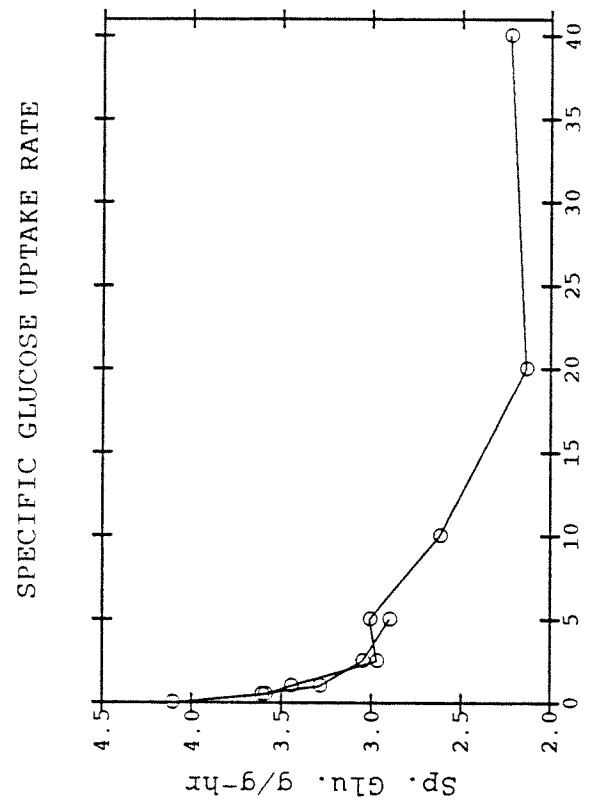
SPECIFIC GLUCOSE UPTAKE RATE
Sp. Glu. g/g-hr
Aeration ccpm

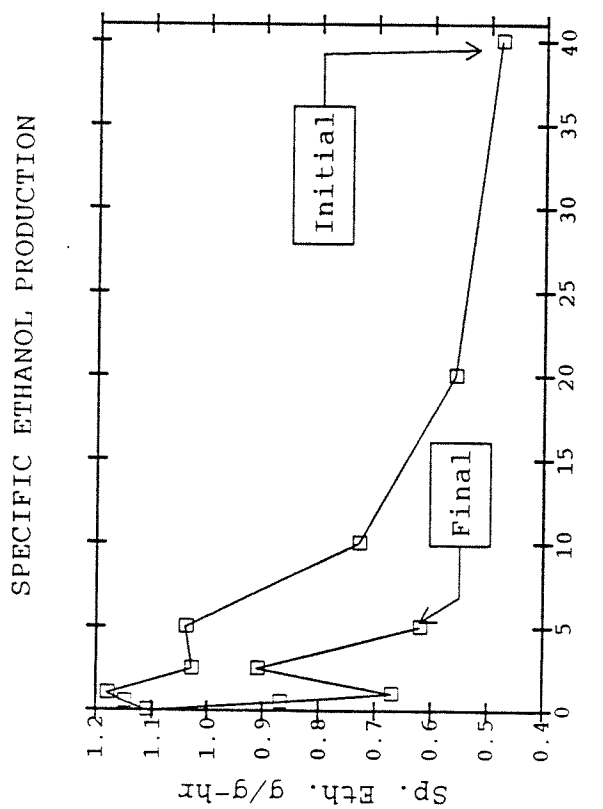
SPECIFIC ETHANOL PRODUCTION
Sp. Eth. g/g-hr
Initial
Final
Aeration ccpm

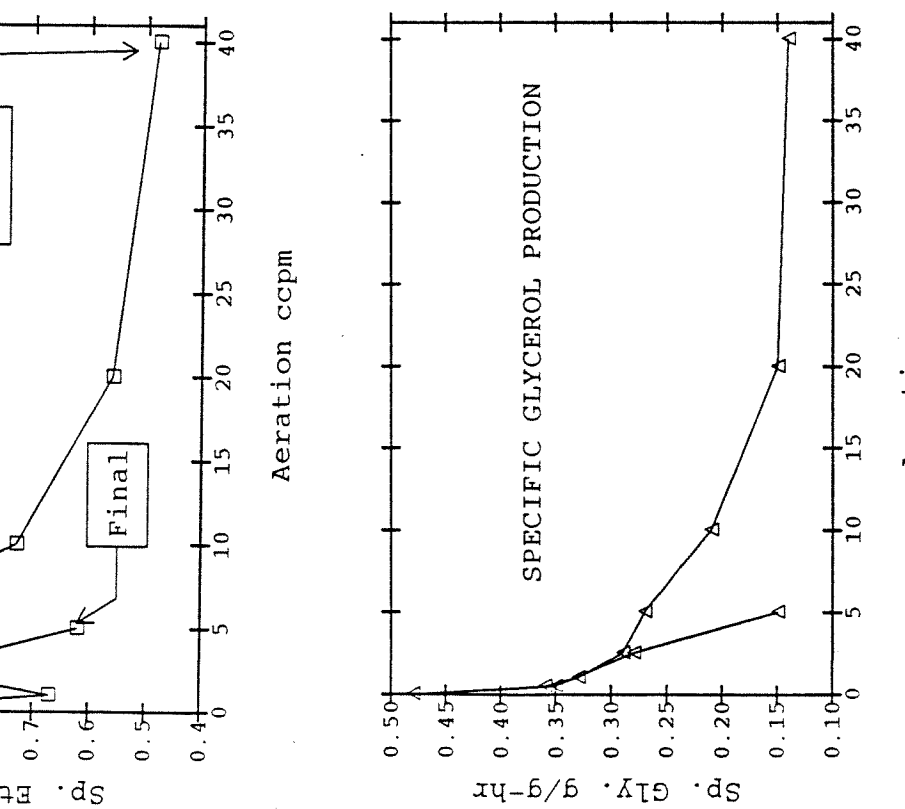
SPECIFIC GLYCEROL PRODUCTION
Sp. Gly. g/g-hr
Aeration ccpm

FIGURE 3.

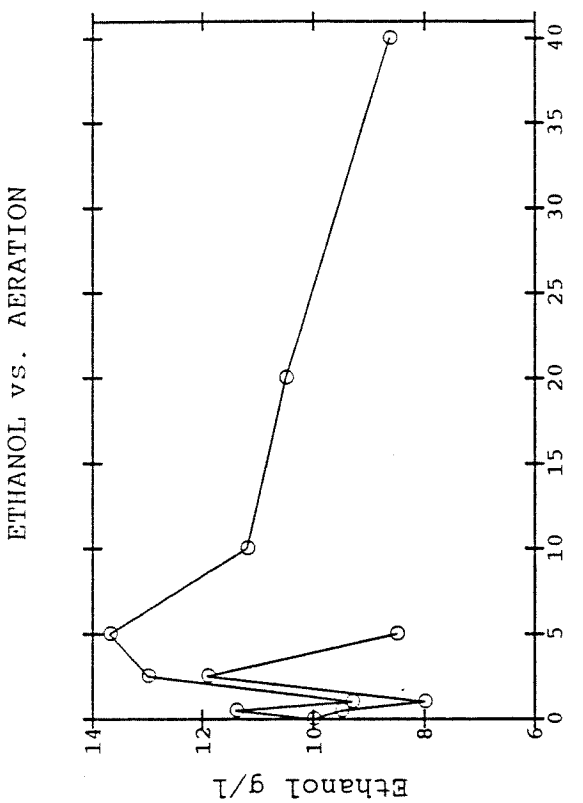
ETHANOL vs. AERATION
Ethanol g/l
Aeration ccpm

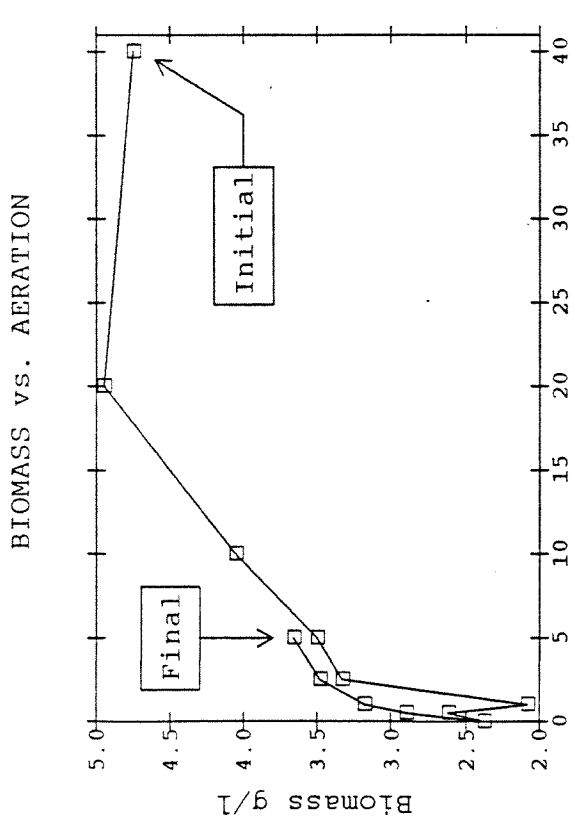
BIOMASS vs. AERATION
Final
Initial
Biomass g/l
Aeration ccpm

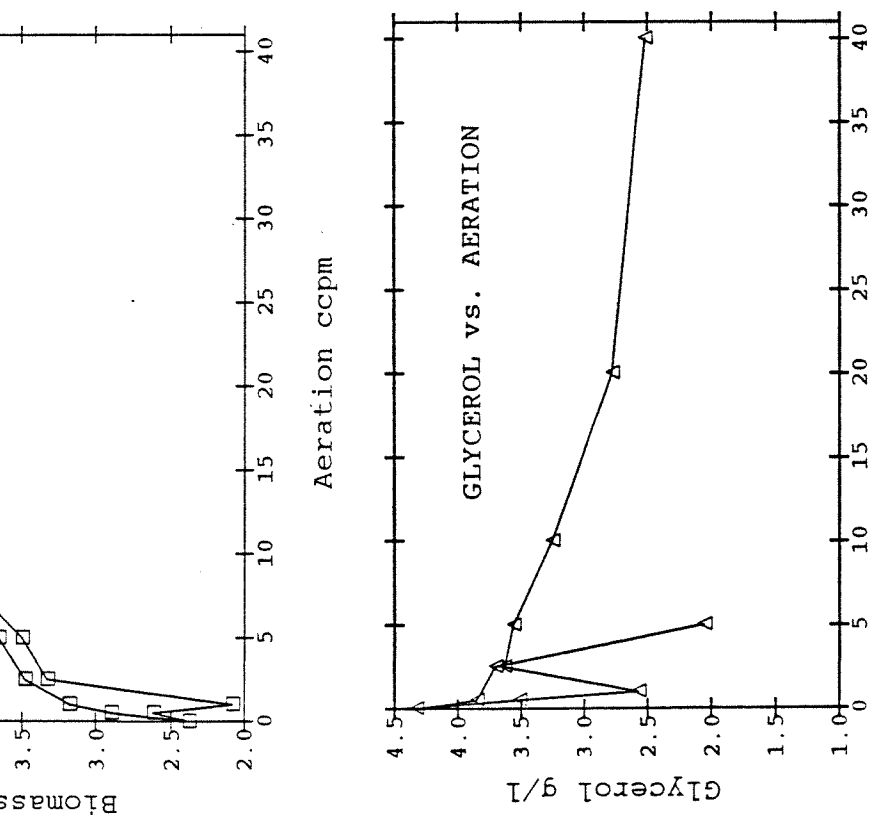
GLYCEROL vs. AERATION
Glycerol g/l
Aeration ccpm

FIGURE 4.

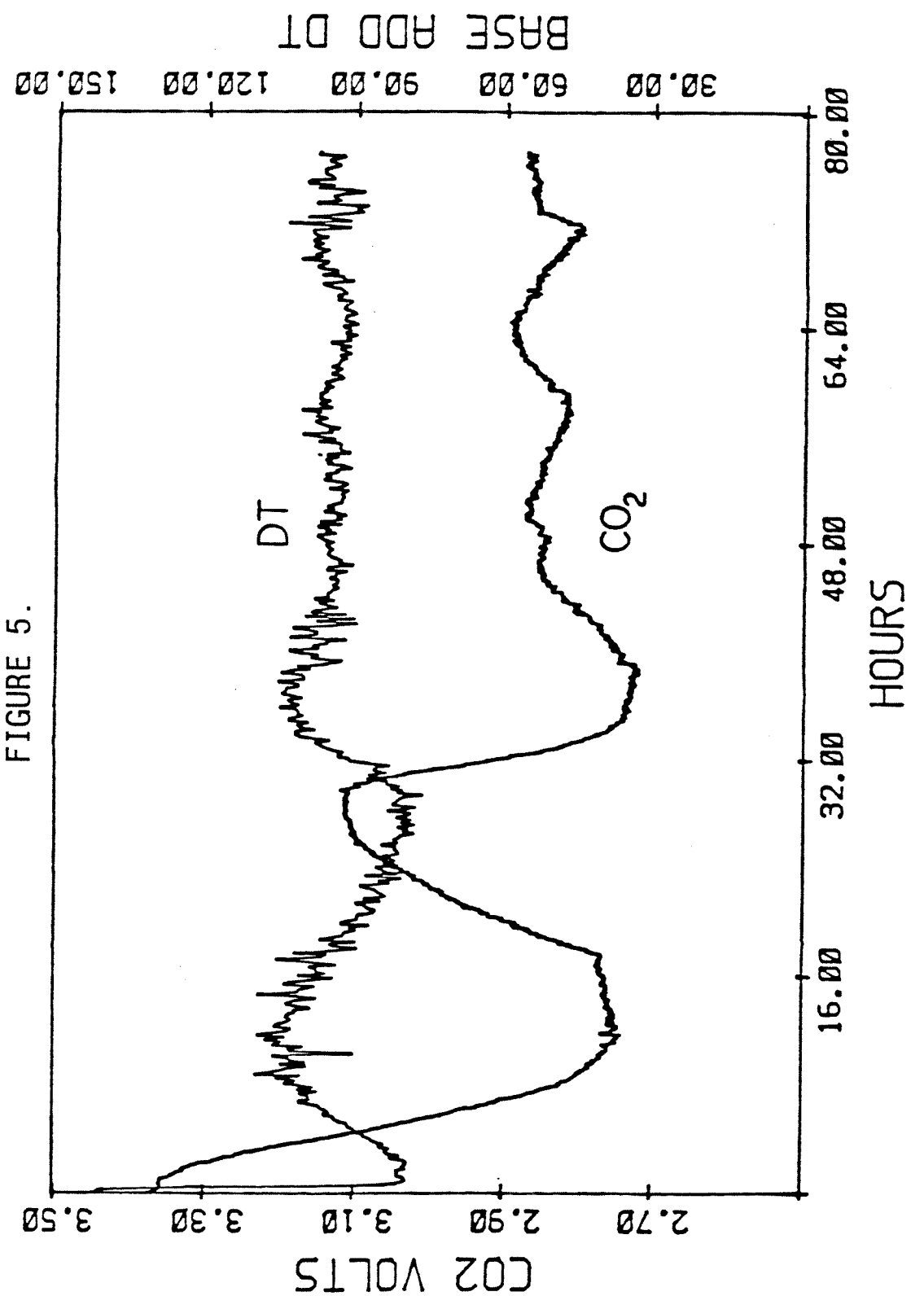
BASE ADD DT
30.00
60.00
90.00
120.00
150.00
80.00
64.00
48.00
32.00
16.00
HOURS
DT
CO_2
CO2 VOLTS
2.70
2.90
3.10
3.30
3.50

FIGURE 5.

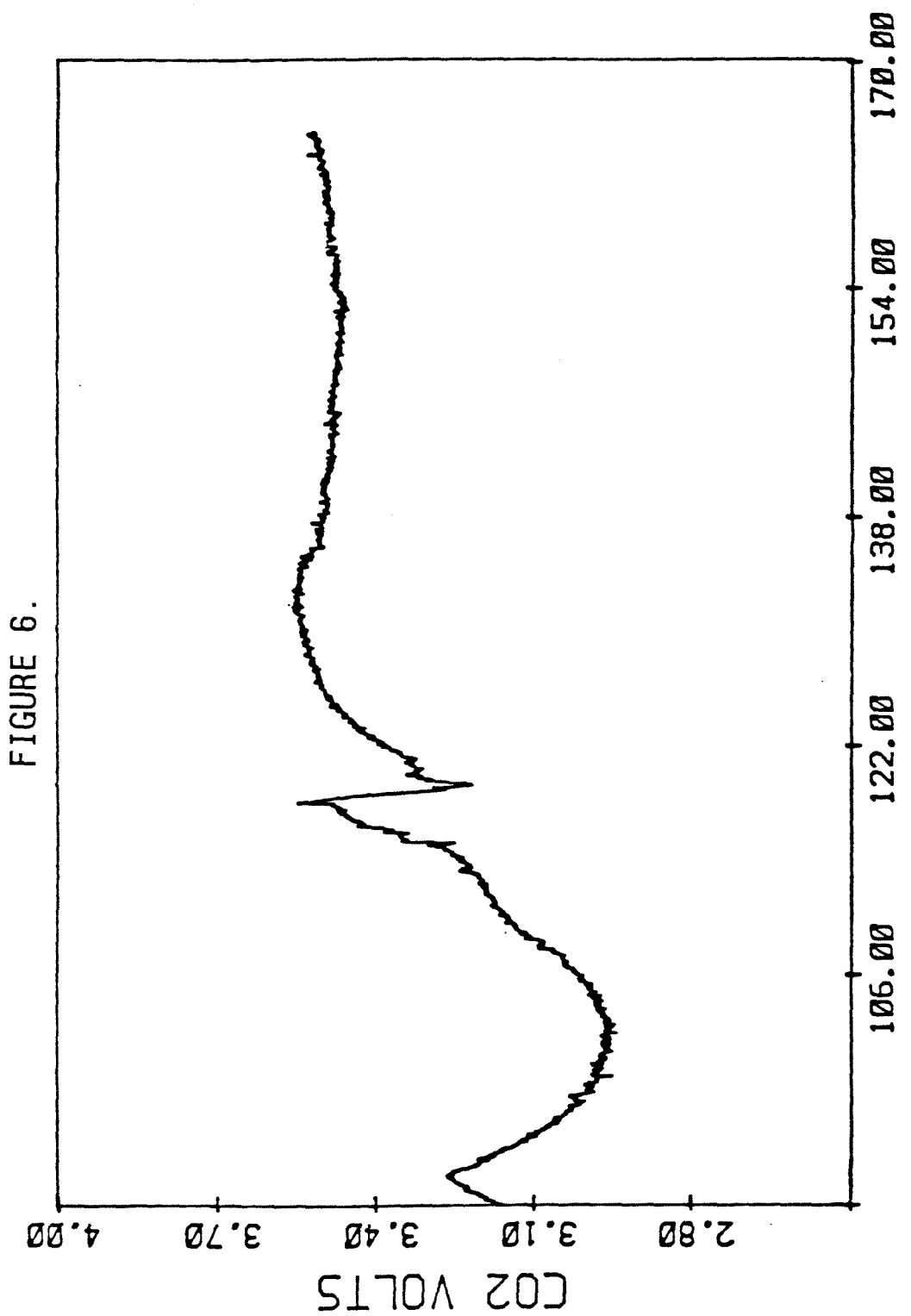
CO2 VOLTS
2.80
3.10
3.40
3.70
4.00
HOURS
106.00
122.00
138.00
154.00
170.00

FIGURE 6.

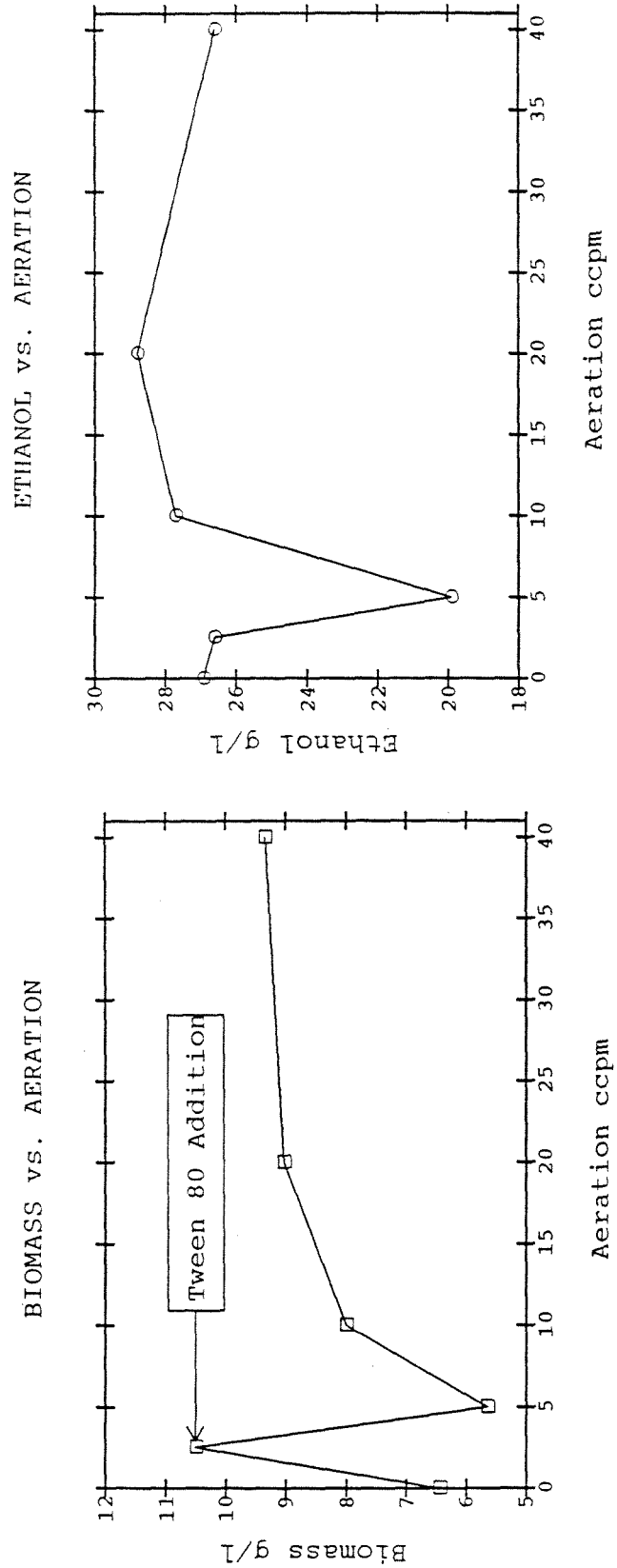
ETHANOL vs. AERATION
Ethanol g/l
Aeration ccpm
BIOMASS vs. AERATION
Tween 80 Addition
Biomass g/l
Aeration ccpm
SPECIFIC ETHANOL PRODUCTION
Sp. Eth. g/g-hr
Aeration ccpm

FIGURE 7.

FIGURE 8. BIOMASS vs. AERATION

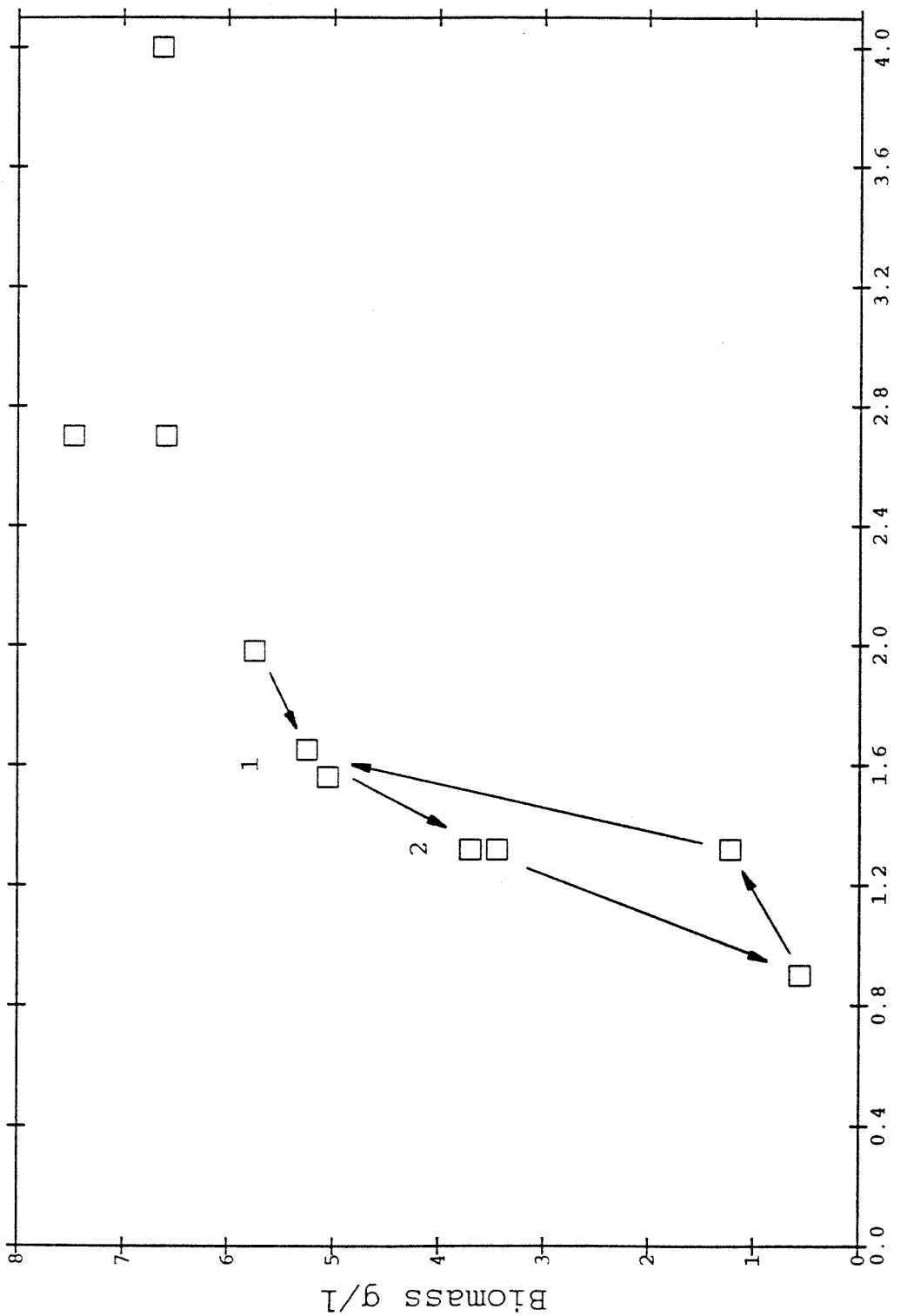

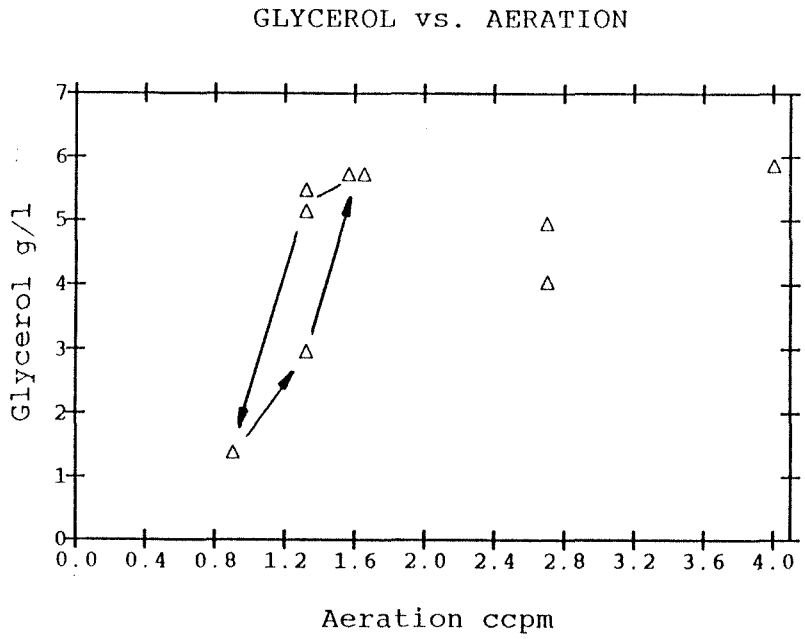
GLYCEROL vs. AERATION
Glycerol g/l
0
1
2
3
4
5
6
7
0.0 0.4 0.8 1.2 1.6 2.0 2.4 2.8 3.2 3.6 4.0
Aeration ccpm

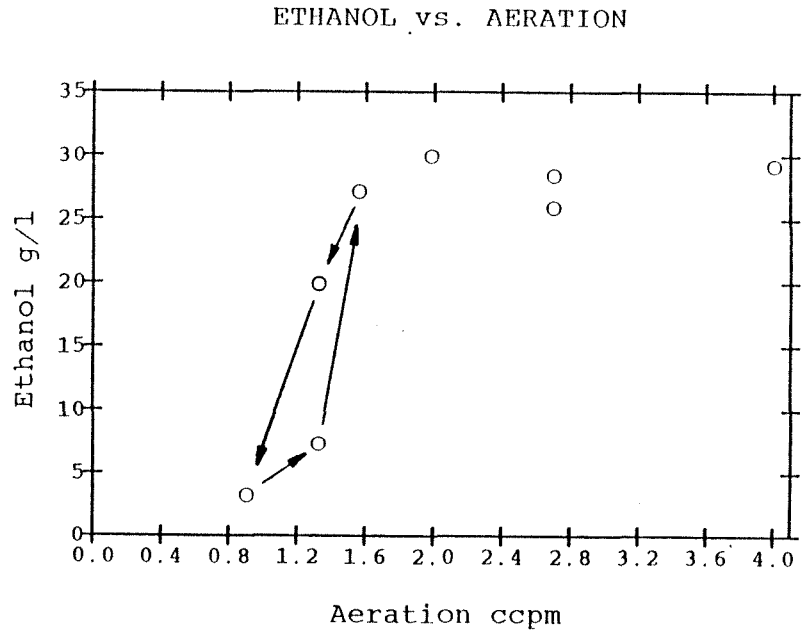
ETHANOL vs. AERATION
Ethanol g/l
0
5
10
15
20
25
30
35
0.0 0.4 0.8 1.2 1.6 2.0 2.4 2.8 3.2 3.6 4.0
Aeration ccpm

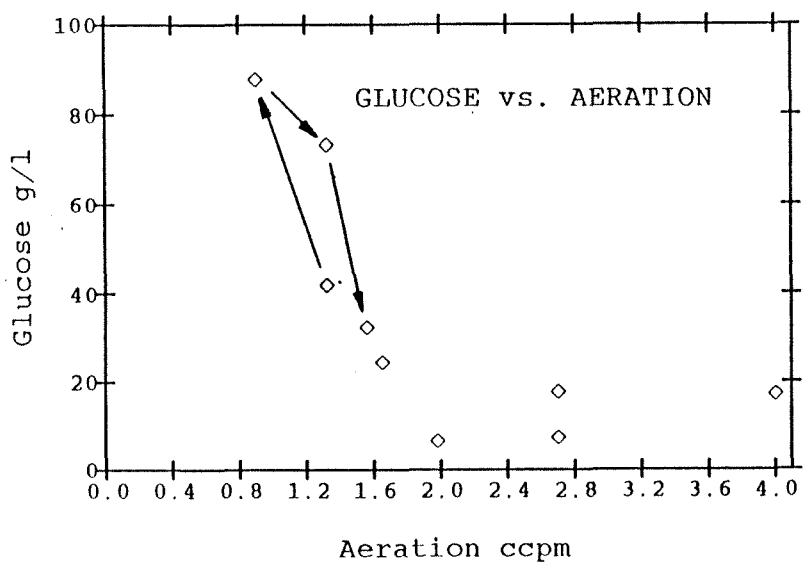
GLUCOSE vs. AERATION
Glucose g/l
0
20
40
60
80
100
0.0 0.4 0.8 1.2 1.6 2.0 2.4 2.8 3.2 3.6 4.0
Aeration ccpm

FIGURE 9.

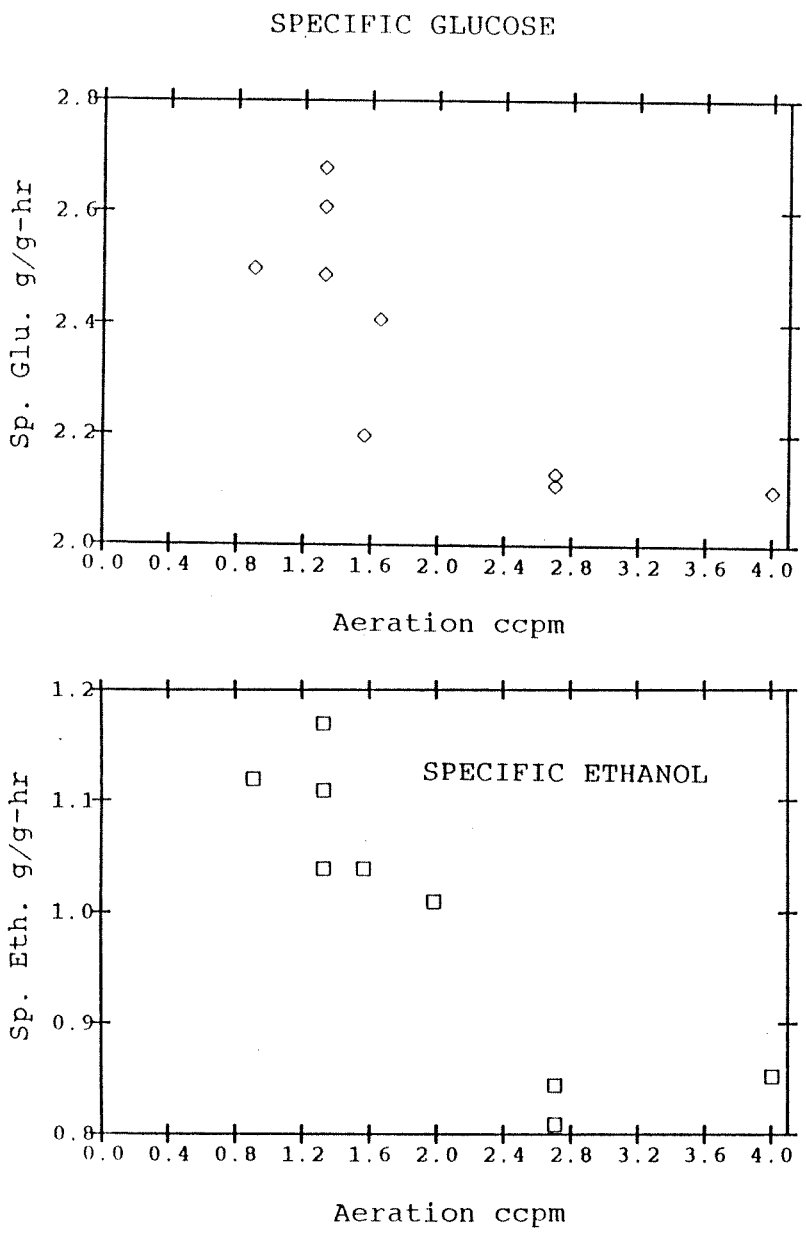
SPECIFIC GLUCOSE
Sp. Glu. g/g-hr
2.8
2.6
2.4
2.2
2.0
0.0 0.4 0.8 1.2 1.6 2.0 2.4 2.8 3.2 3.6 4.0
Aeration ccpm
SPECIFIC GLYCEROL PROD
Sp. Gly. g/g-hr
0.5
0.4
0.3
0.2
0.1
0.0 0.4 0.8 1.2 1.6 2.0 2.4 2.8 3.2 3.6 4.0
Aeration ccpm
SPECIFIC ETHANOL
Sp. Eth. g/g-hr
1.2
1.1
1.0
0.9
0.8
0.0 0.4 0.8 1.2 1.6 2.0 2.4 2.8 3.2 3.6 4.0
Aeration ccpm

FIGURE 10.

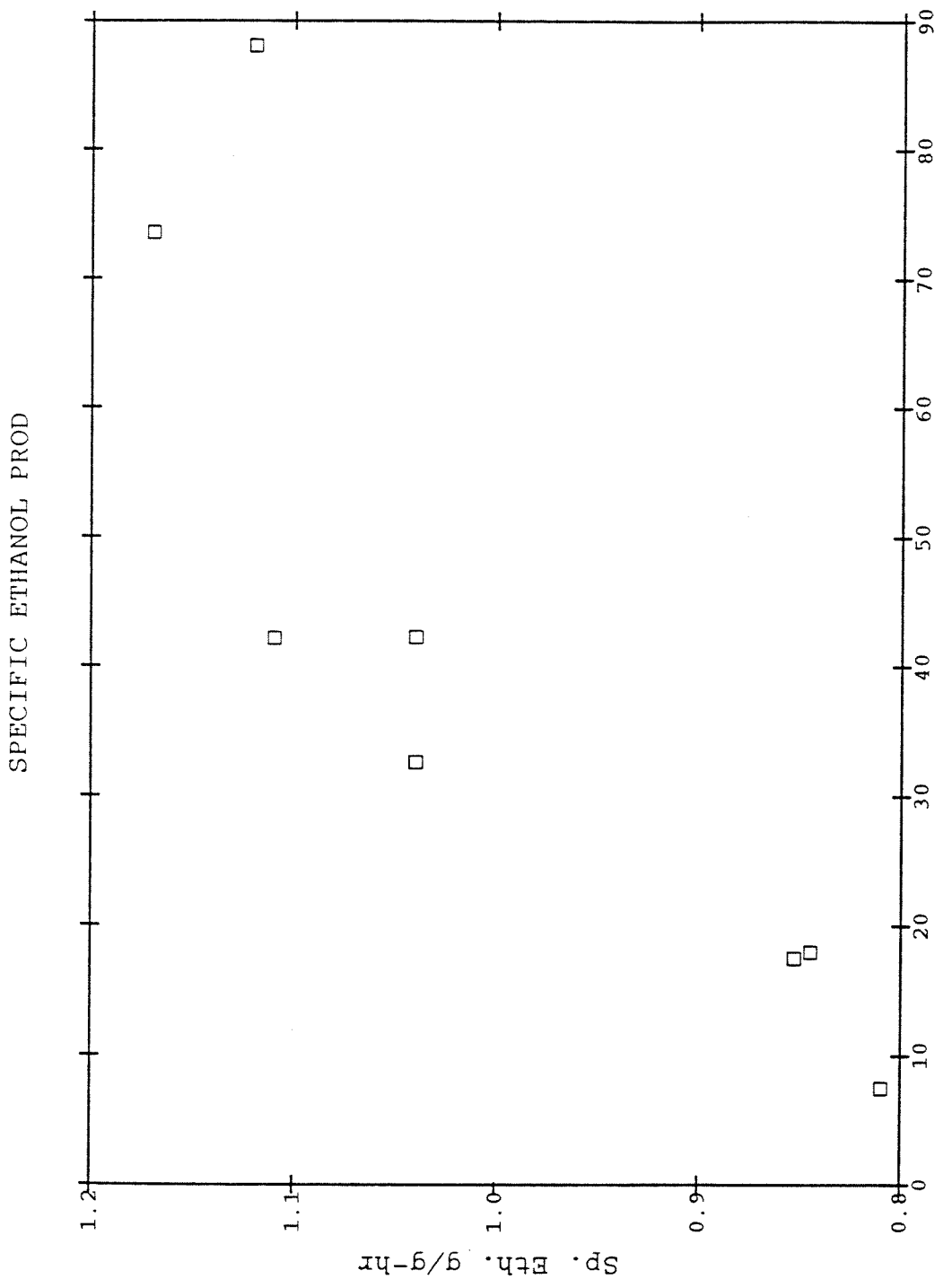
SPECIFIC ETHANOL PROD
Sp. Eth. g/g-hr
1.2
1.1
1.0
0.9
0.8
0
10
20
30
40
50
60
70
80
90
Glucose g/l

FIGURE 11.

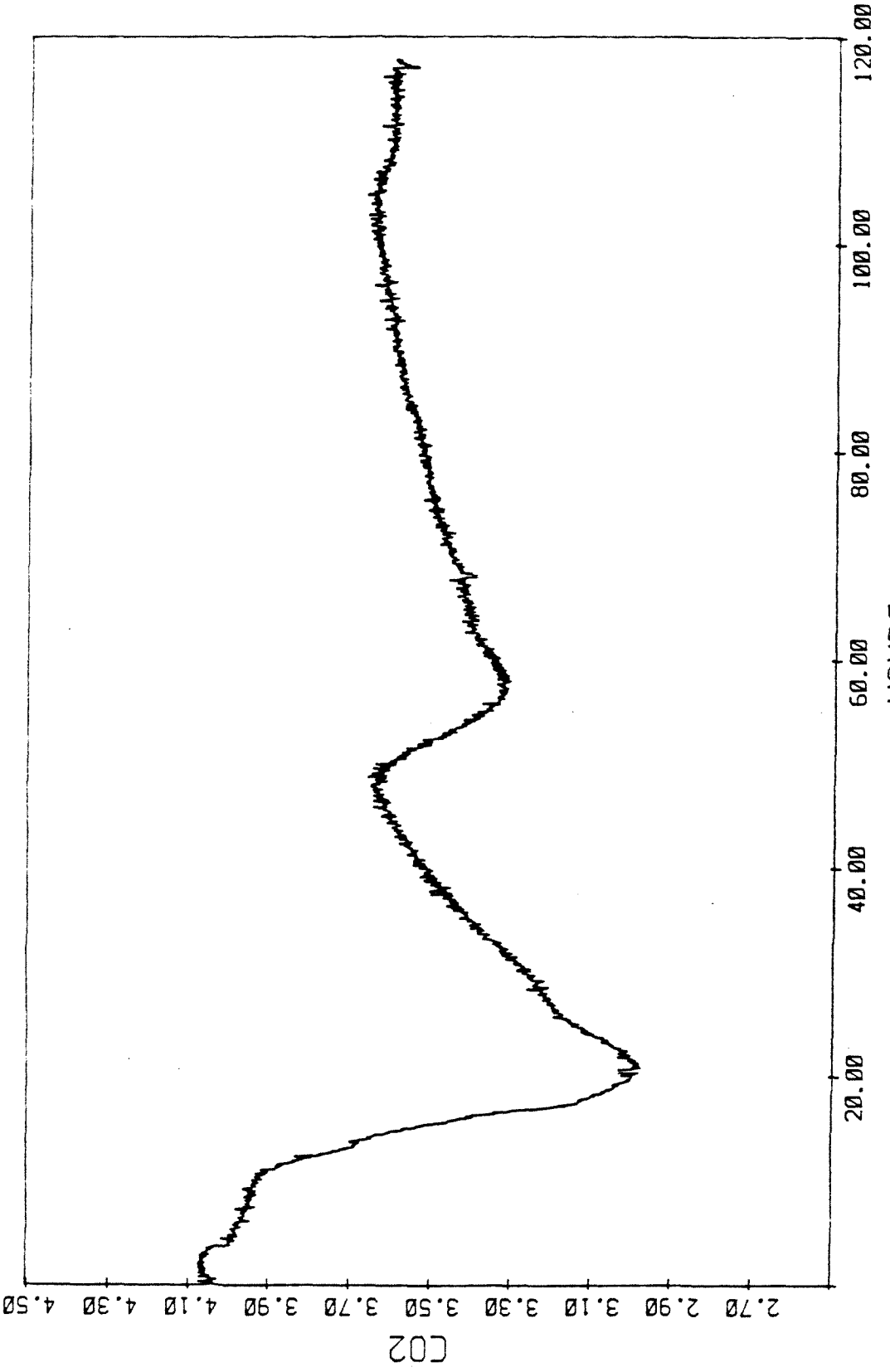

FIGURE 12. DAMPED OSCILLATIONS

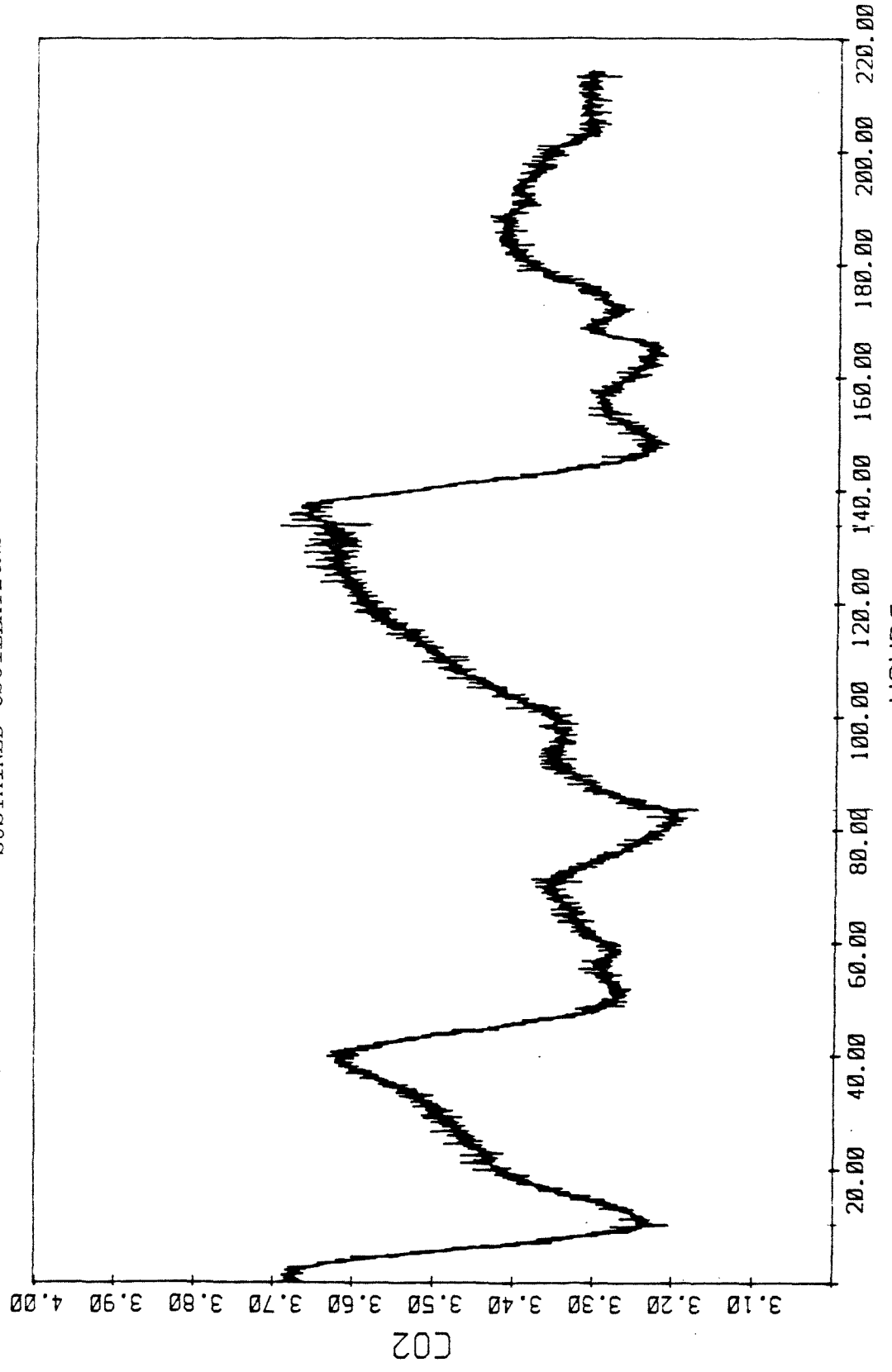

FIGURE 13. SUSTAINED OSCILLATIONS

FIGURE 14. BIOMASS vs. AERATION

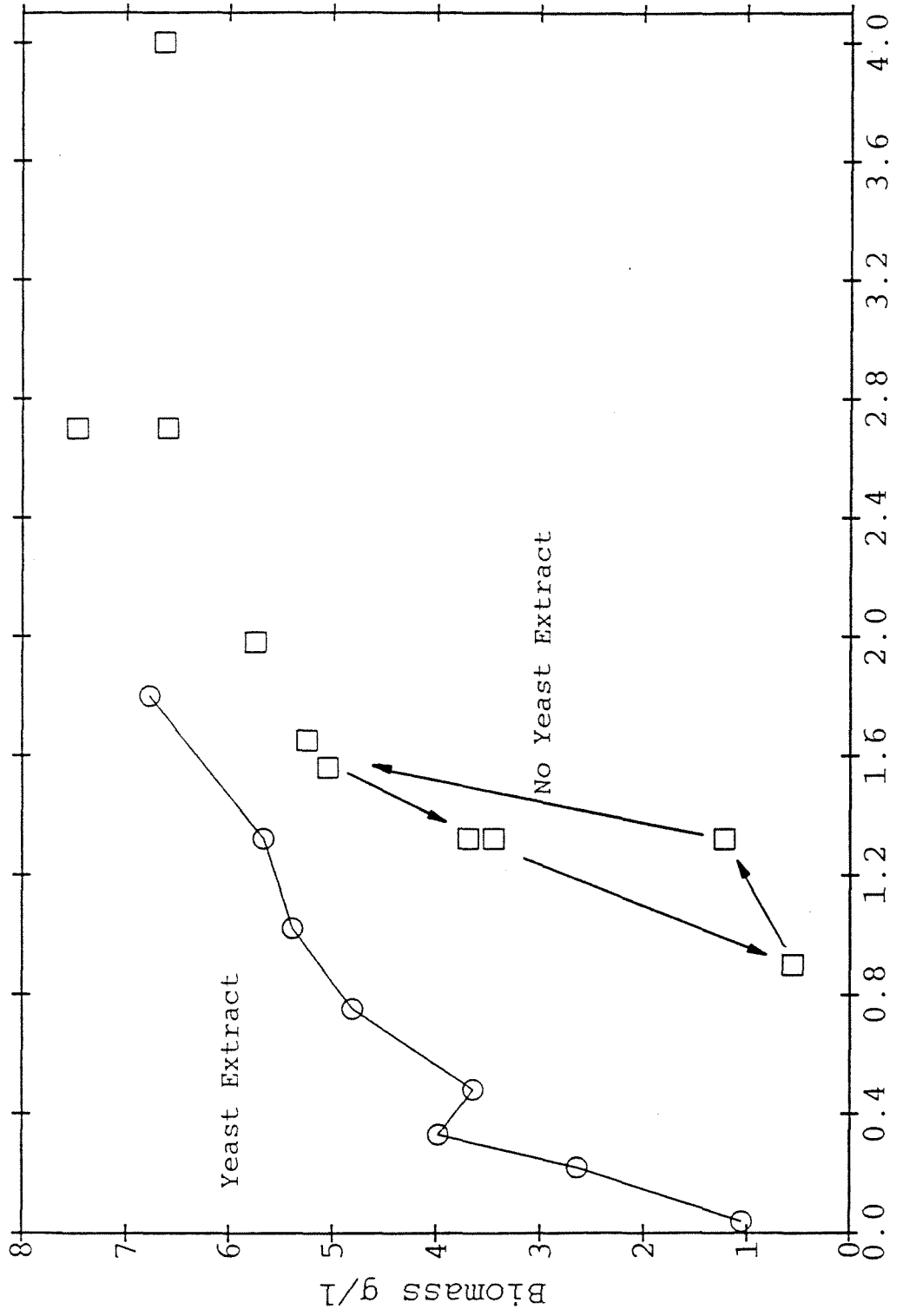

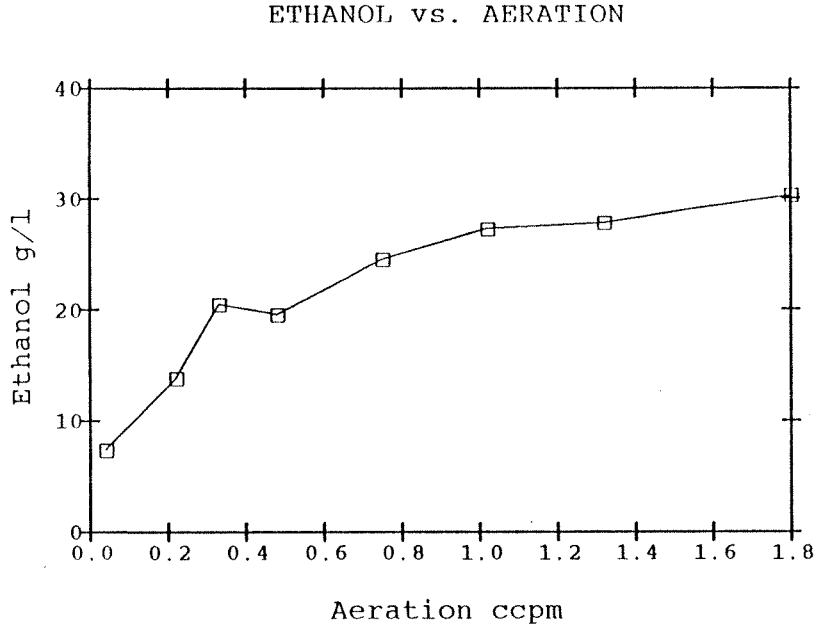
ETHANOL vs. AERATION
Ethanol g/l
0
10
20
30
40
0.0
0.2
0.4
0.6
0.8
1.0
1.2
1.4
1.6
1.8
Aeration ccpm

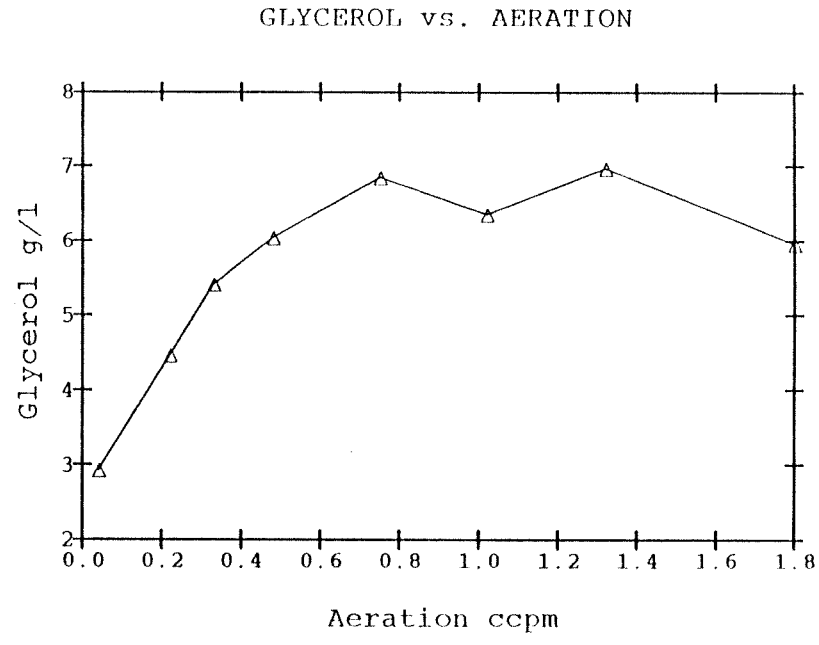
GLYCEROL vs. AERATION
Glycerol g/l
2
3
4
5
6
7
8
0.0
0.2
0.4
0.6
0.8
1.0
1.2
1.4
1.6
1.8
Aeration ccpm

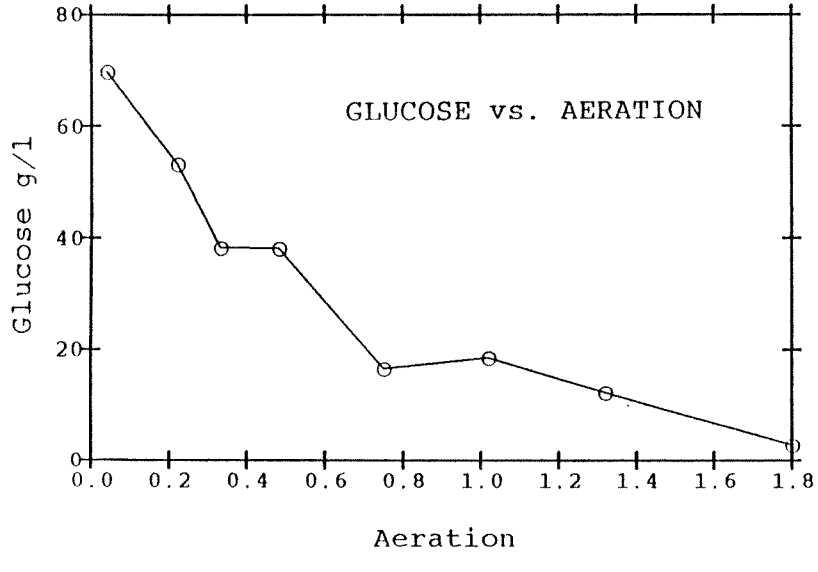
GLUCOSE vs. AERATION
Glucose g/l
0
20
40
60
80
0.0
0.2
0.4
0.6
0.8
1.0
1.2
1.4
1.6
1.8
Aeration

FIGURE 15.

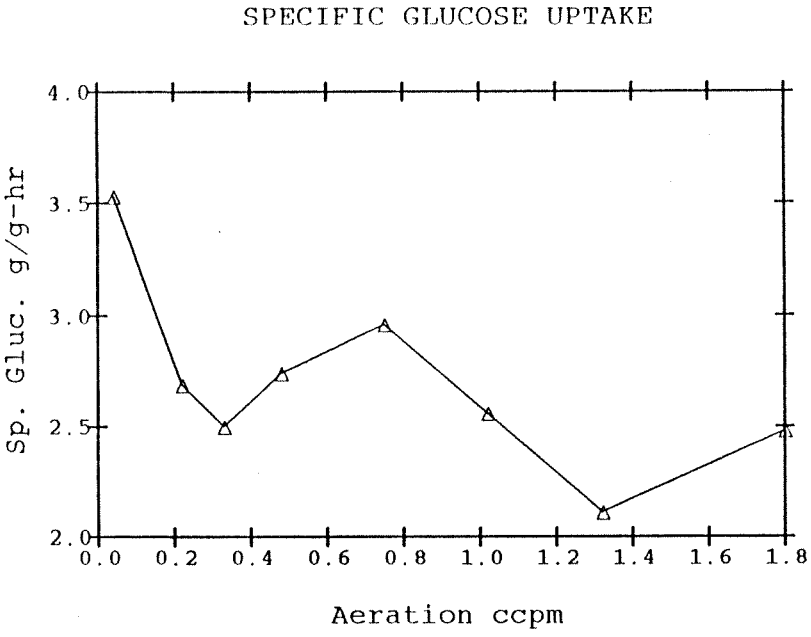
SPECIFIC GLUCOSE UPTAKE
Sp. Gluc. g/g-hr
4.0
3.5
3.0
2.5
2.0
0.0 0.2 0.4 0.6 0.8 1.0 1.2 1.4 1.6 1.8
Aeration ccpm

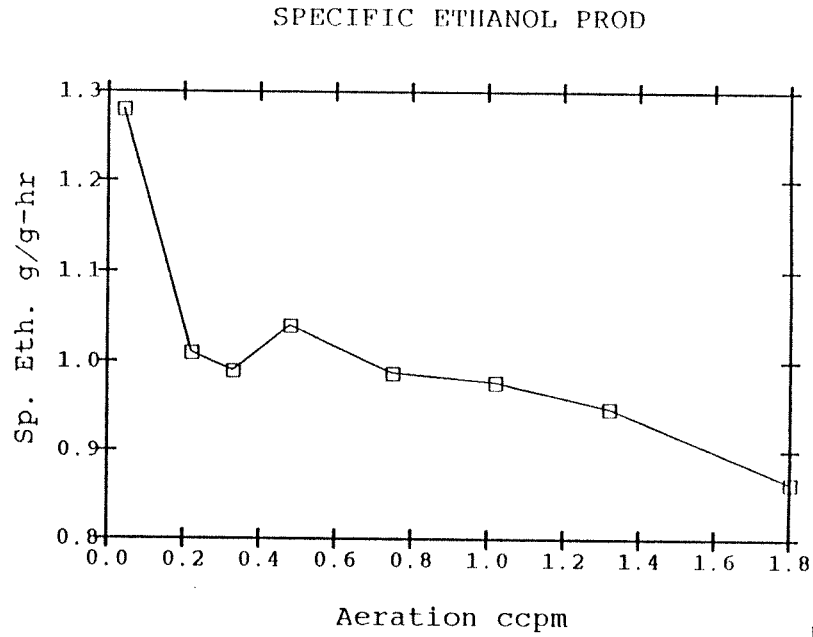
SPECIFIC ETHANOL PROD
Sp. Eth. g/g-hr
1.3
1.2
1.1
1.0
0.9
0.8
0.0 0.2 0.4 0.6 0.8 1.0 1.2 1.4 1.6 1.8
Aeration ccpm

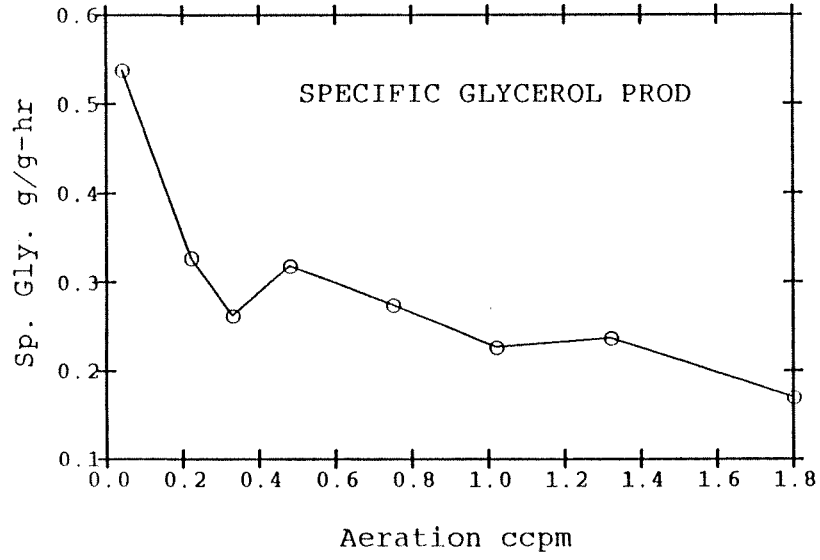
SPECIFIC GLYCEROL PROD
Sp. Gly. g/g-hr
0.6
0.5
0.4
0.3
0.2
0.1
0.0 0.2 0.4 0.6 0.8 1.0 1.2 1.4 1.6 1.8
Aeration ccpm

FIGURE 16.

FIGURE 17. SPECIFIC ETHANOL PROD

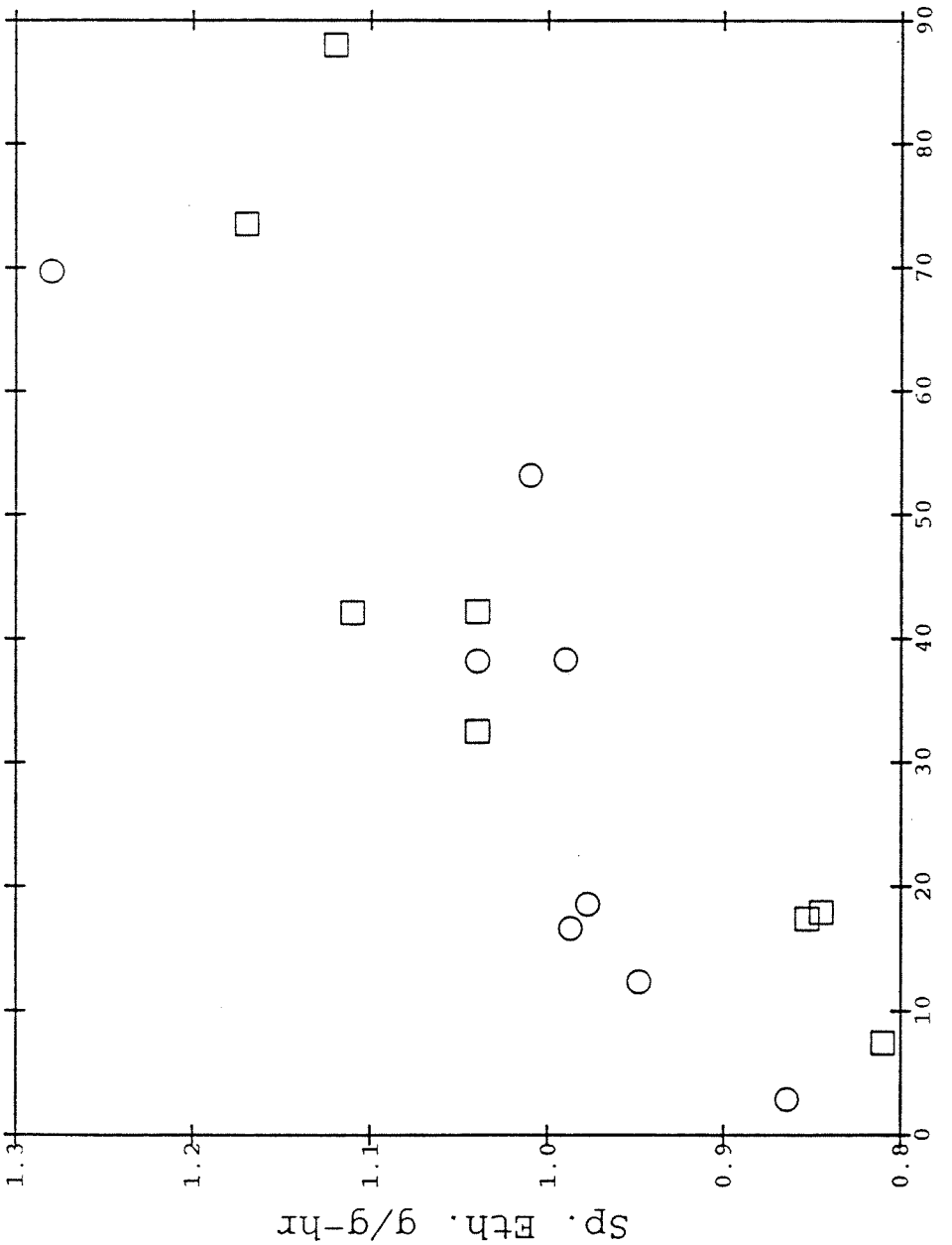

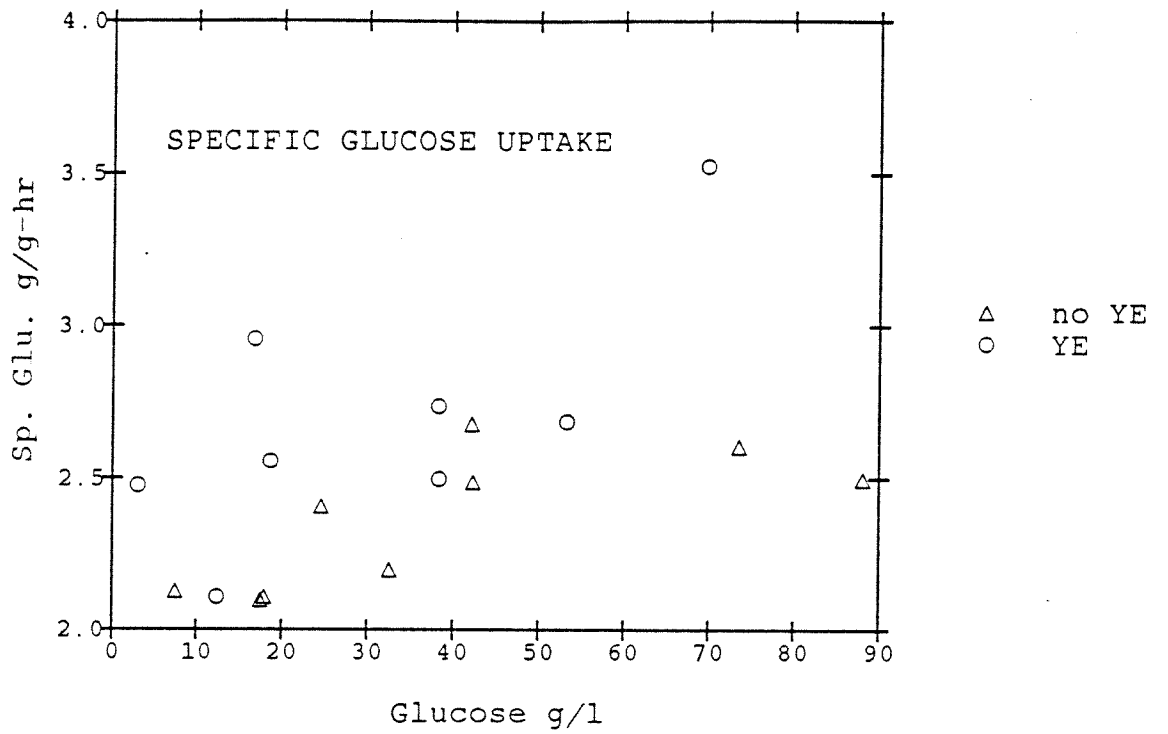
SPECIFIC GLUCOSE UPTAKE
Sp. Glu. g/g-hr
4.0
3.5
3.0
2.5
2.0
0
10
20
30
40
50
60
70
80
90
Glucose g/l
no YE
YE

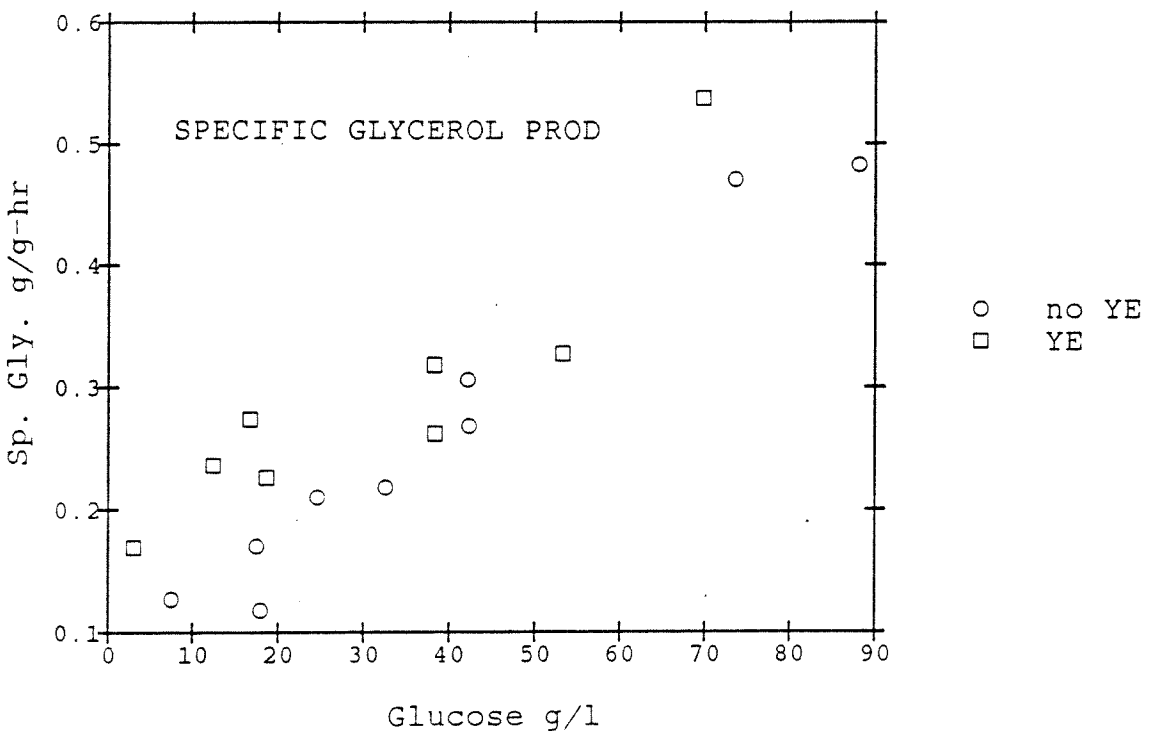
SPECIFIC GLYCEROL PROD
Sp. Gly. g/g-hr
0.6
0.5
0.4
0.3
0.2
0.1
0
10
20
30
40
50
60
70
80
90
Glucose g/l
no YE
YE

FIGURE 18.

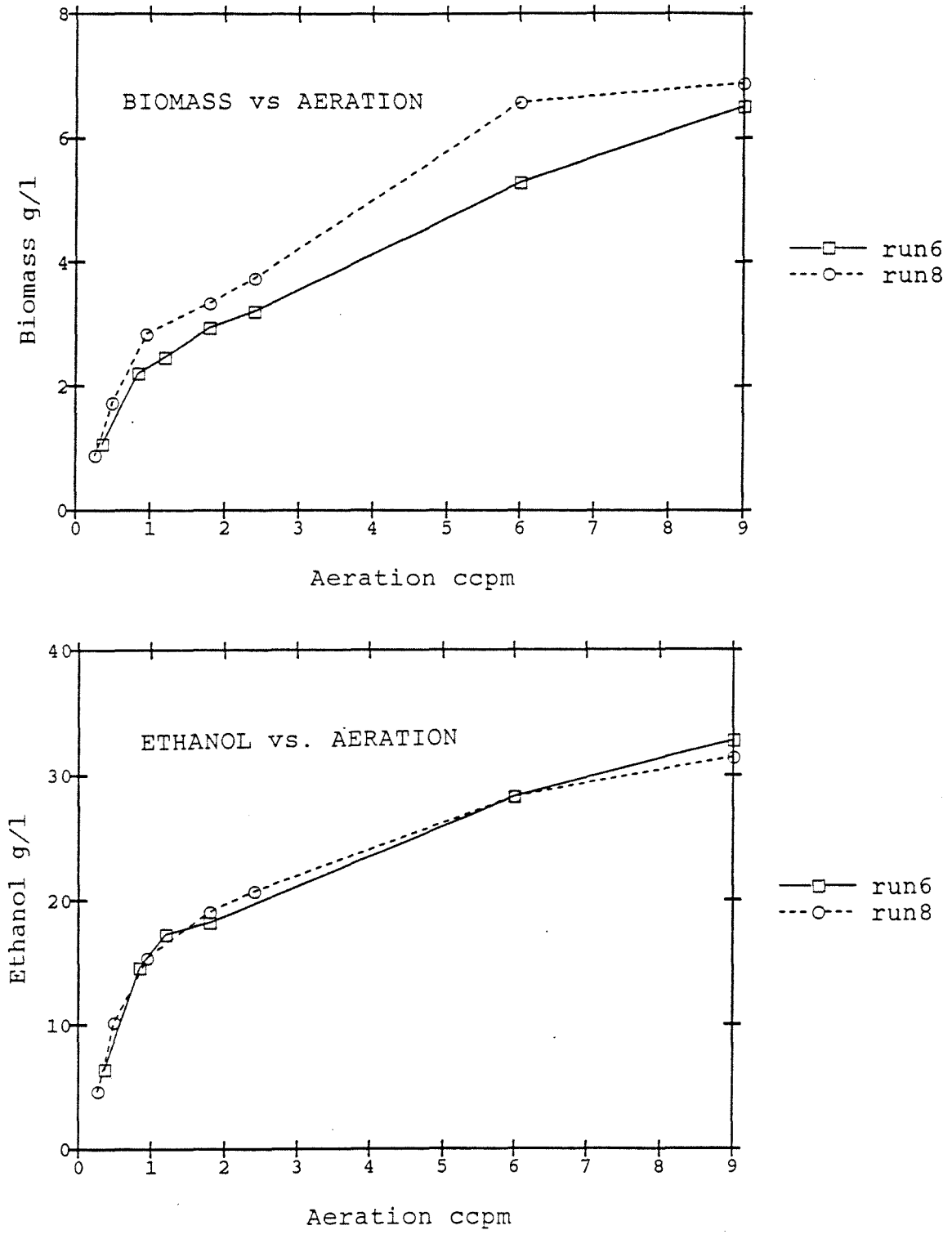
BIOMASS vs AERATION
Biomass g/l
Aeration ccpm
run6
run8
ETHANOL vs. AERATION
Ethanol g/l
Aeration ccpm
run6
run8

FIGURE 19.

FIGURE 20. SPECIFIC ETHANOL PROD

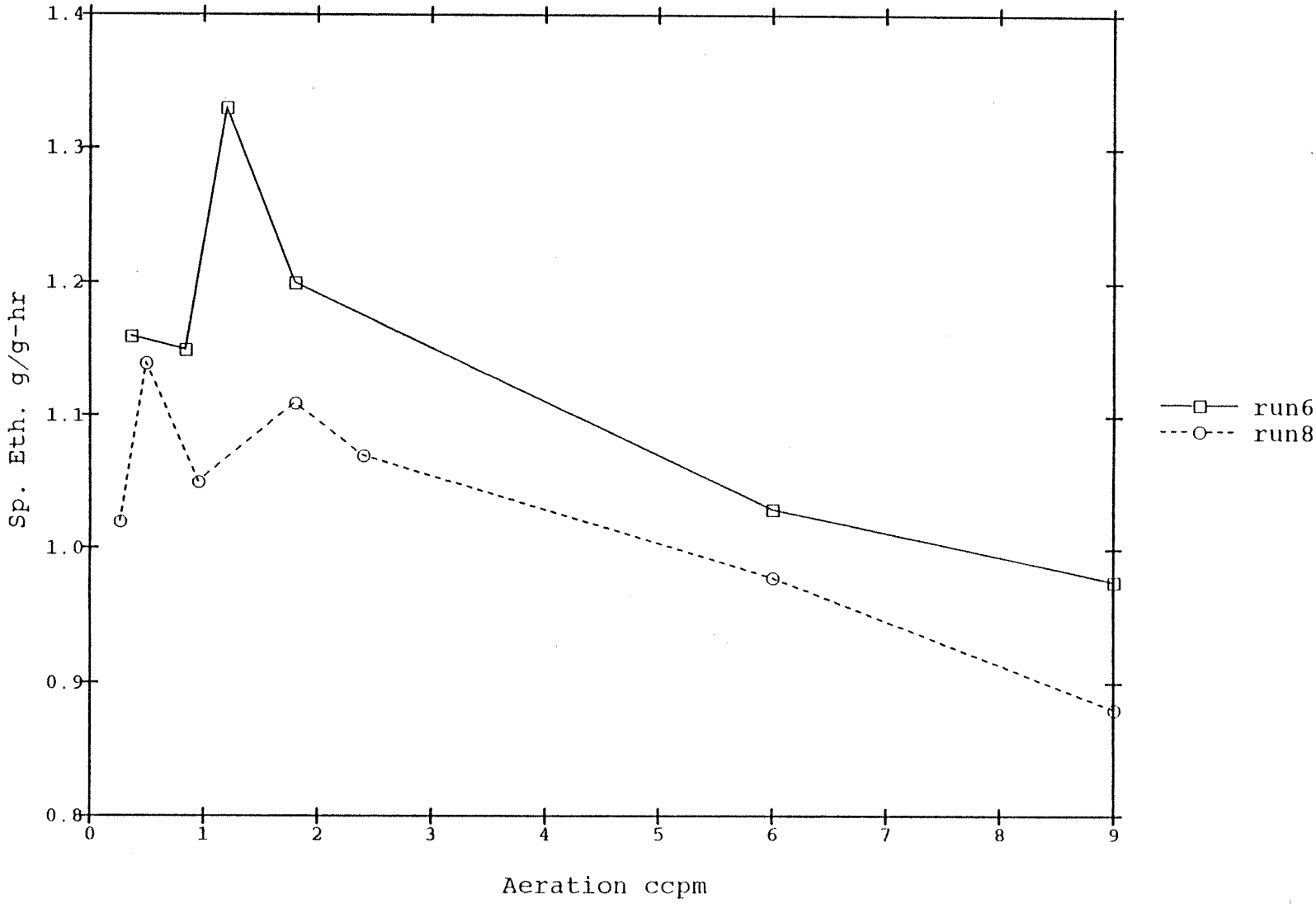

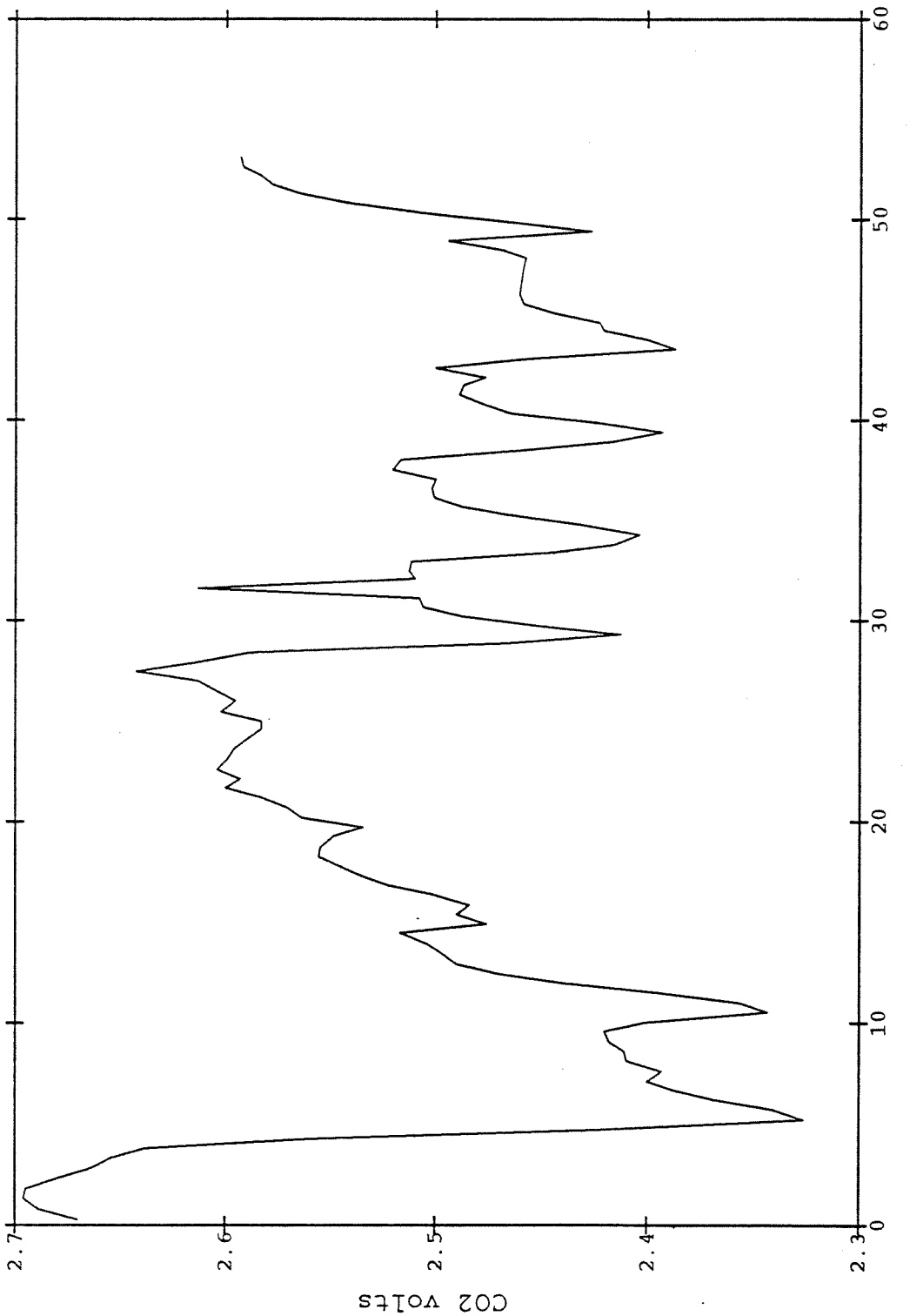

FIGURE 21. OSCILLATIONS

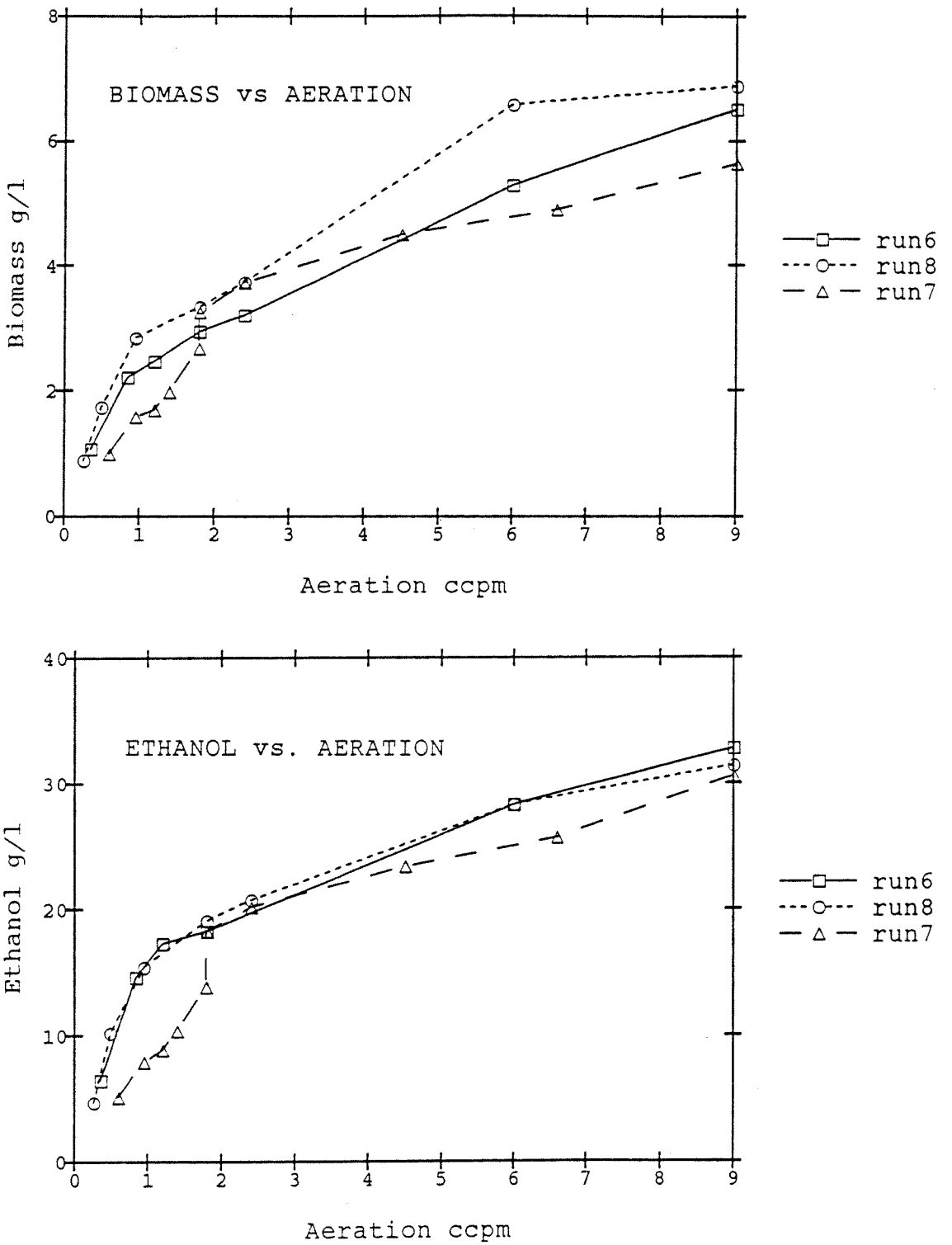
BIOMASS vs AERATION
Biomass g/l
Aeration ccpm
run6
run8
run7
ETHANOL vs. AERATION
Ethanol g/l
Aeration ccpm
run6
run8
run7

FIGURE 22.

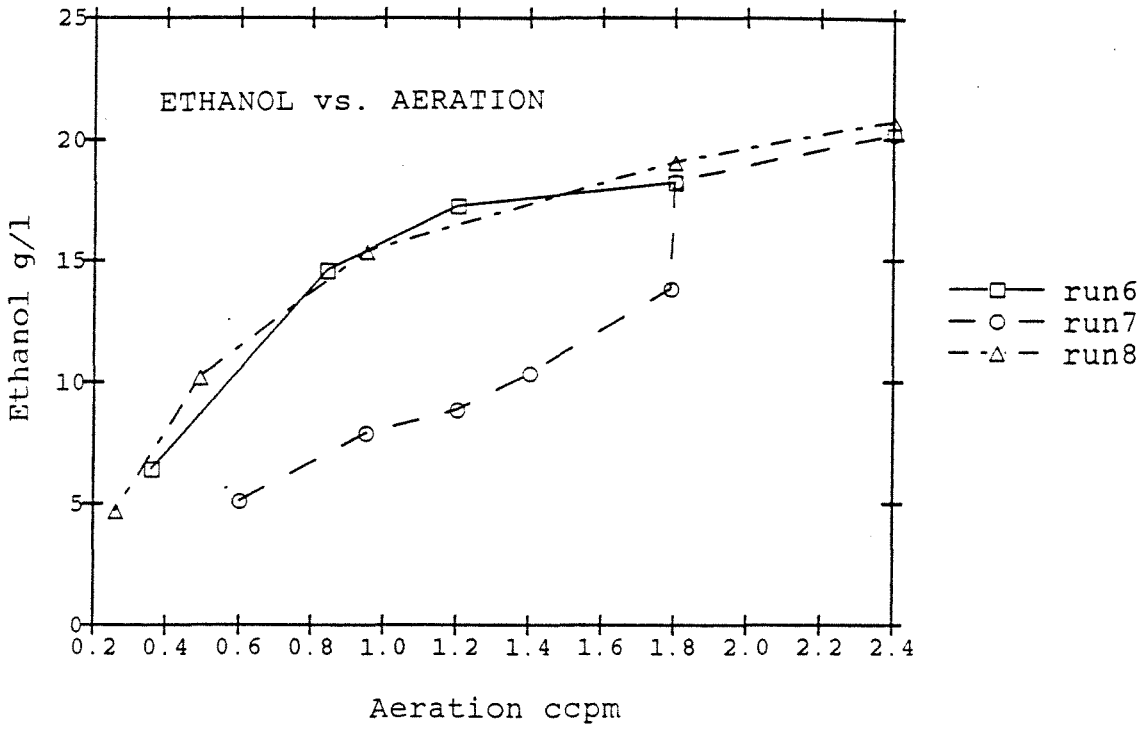
ETHANOL vs. AERATION
Ethanol g/l
25
20
15
10
5
0
0.2 0.4 0.6 0.8 1.0 1.2 1.4 1.6 1.8 2.0 2.2 2.4
Aeration ccpm
run6
run7
run8

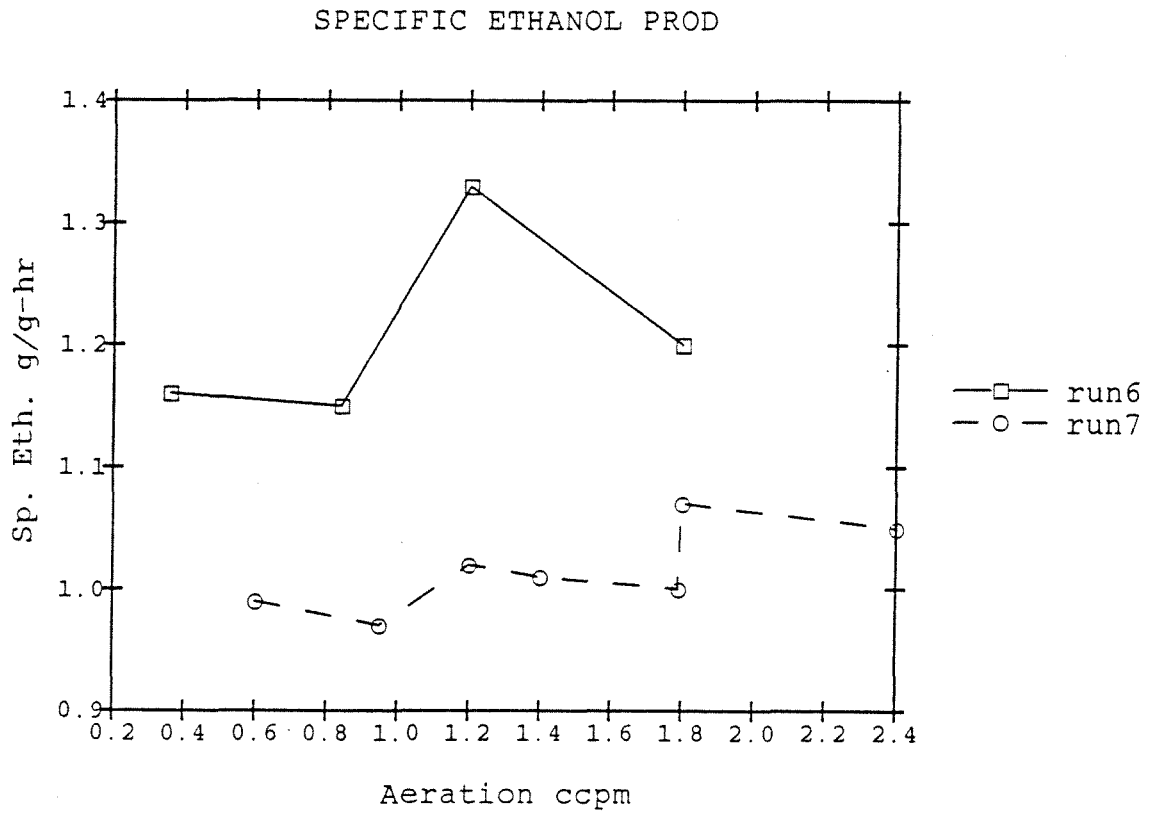
SPECIFIC ETHANOL PROD
Sp. Eth. g/g-hr
1.4
1.3
1.2
1.1
1.0
0.9
0.2 0.4 0.6 0.8 1.0 1.2 1.4 1.6 1.8 2.0 2.2 2.4
Aeration ccpm
run6
run7

FIGURE 23.

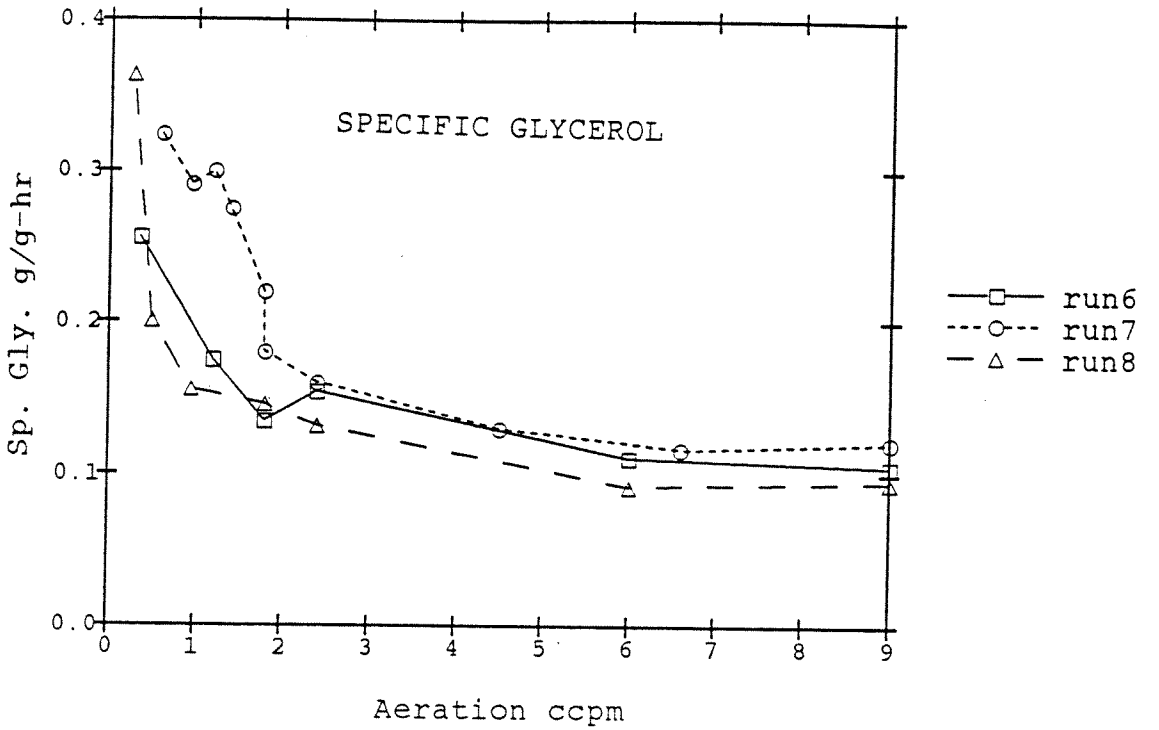
SPECIFIC GLYCEROL
Sp. Gly. g/g-hr
0.4
0.3
0.2
0.1
0.0
0
1
2
3
4
5
6
7
8
9
Aeration ccpm
run6
run7
run8

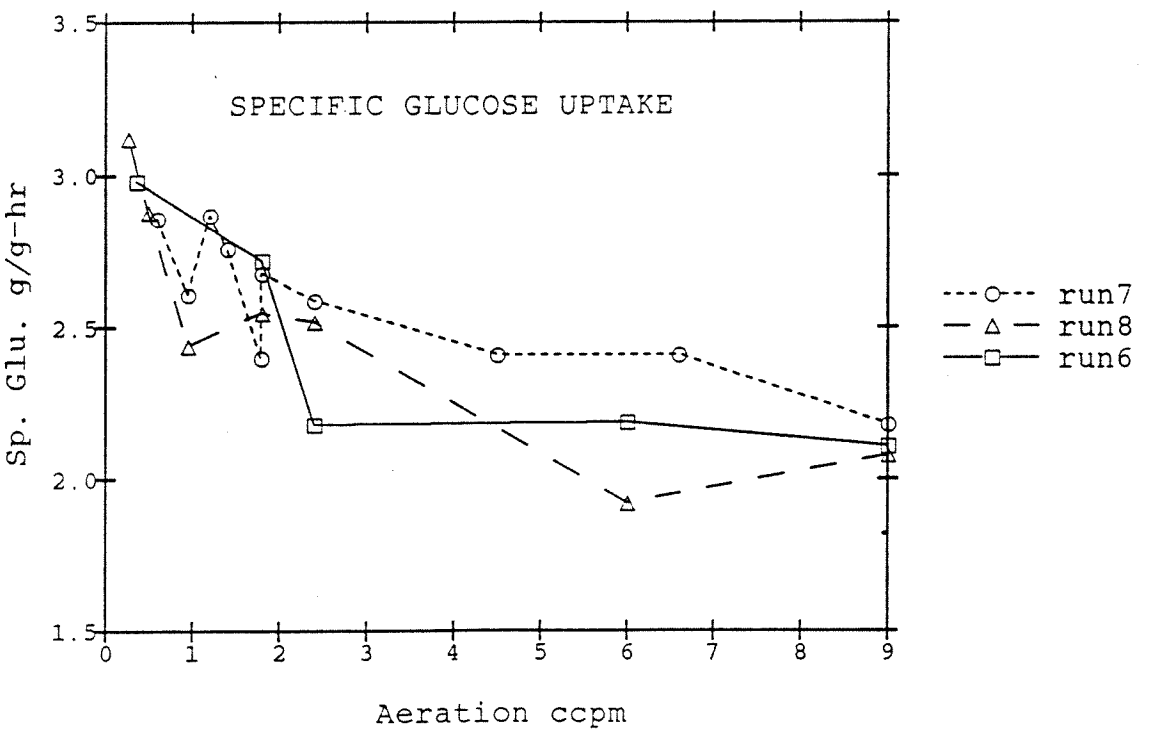
SPECIFIC GLUCOSE UPTAKE
Sp. Glu. g/g-hr
3.5
3.0
2.5
2.0
1.5
0
1
2
3
4
5
6
7
8
9
Aeration ccpm
run7
run8
run6

FIGURE 24.

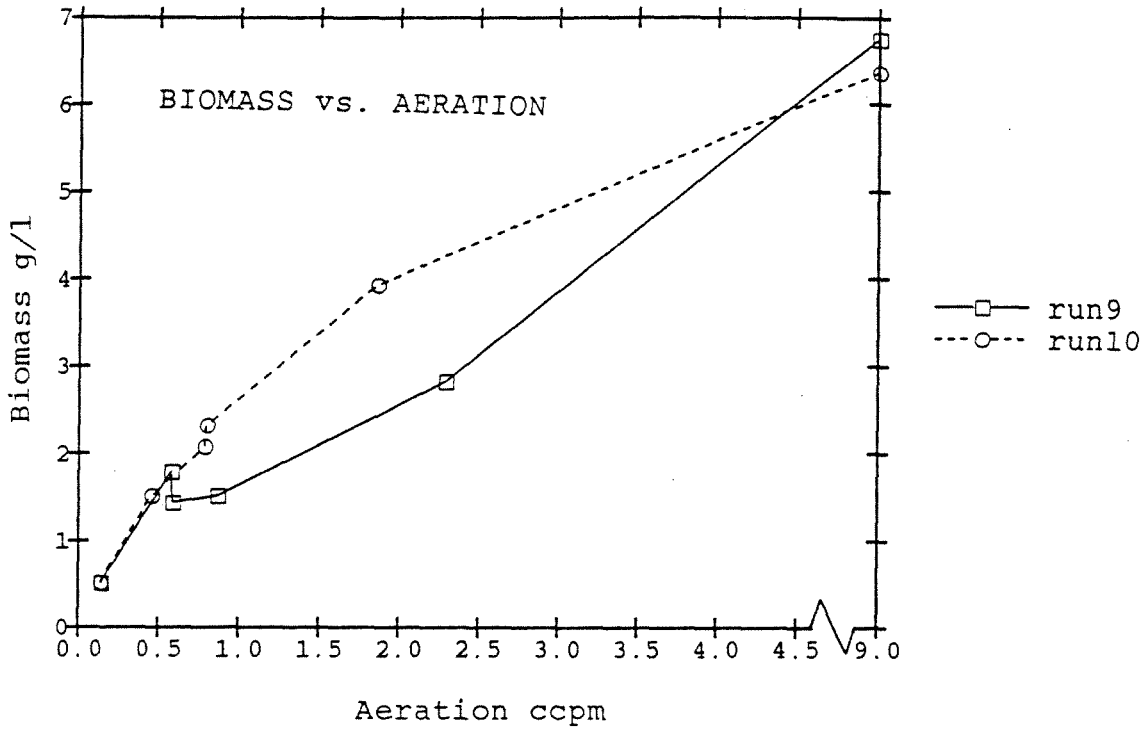
BIOMASS vs. AERATION
Biomass g/l
Aeration ccpm
run9
run10
0
1
2
3
4
5
6
7
0.0
0.5
1.0
1.5
2.0
2.5
3.0
3.5
4.0
4.5
9.0

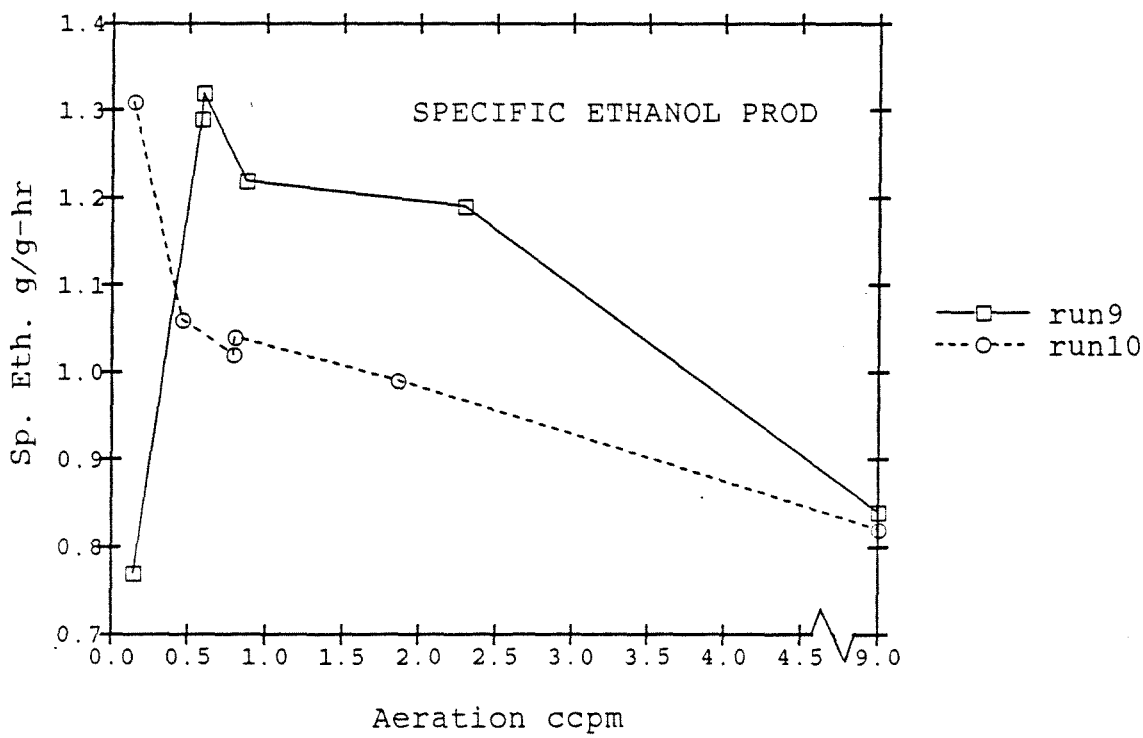
SPECIFIC ETHANOL PROD
Sp. Eth. g/g-hr
Aeration ccpm
run9
run10
0.7
0.8
0.9
1.0
1.1
1.2
1.3
1.4
0.0
0.5
1.0
1.5
2.0
2.5
3.0
3.5
4.0
4.5
9.0

FIGURE 25.

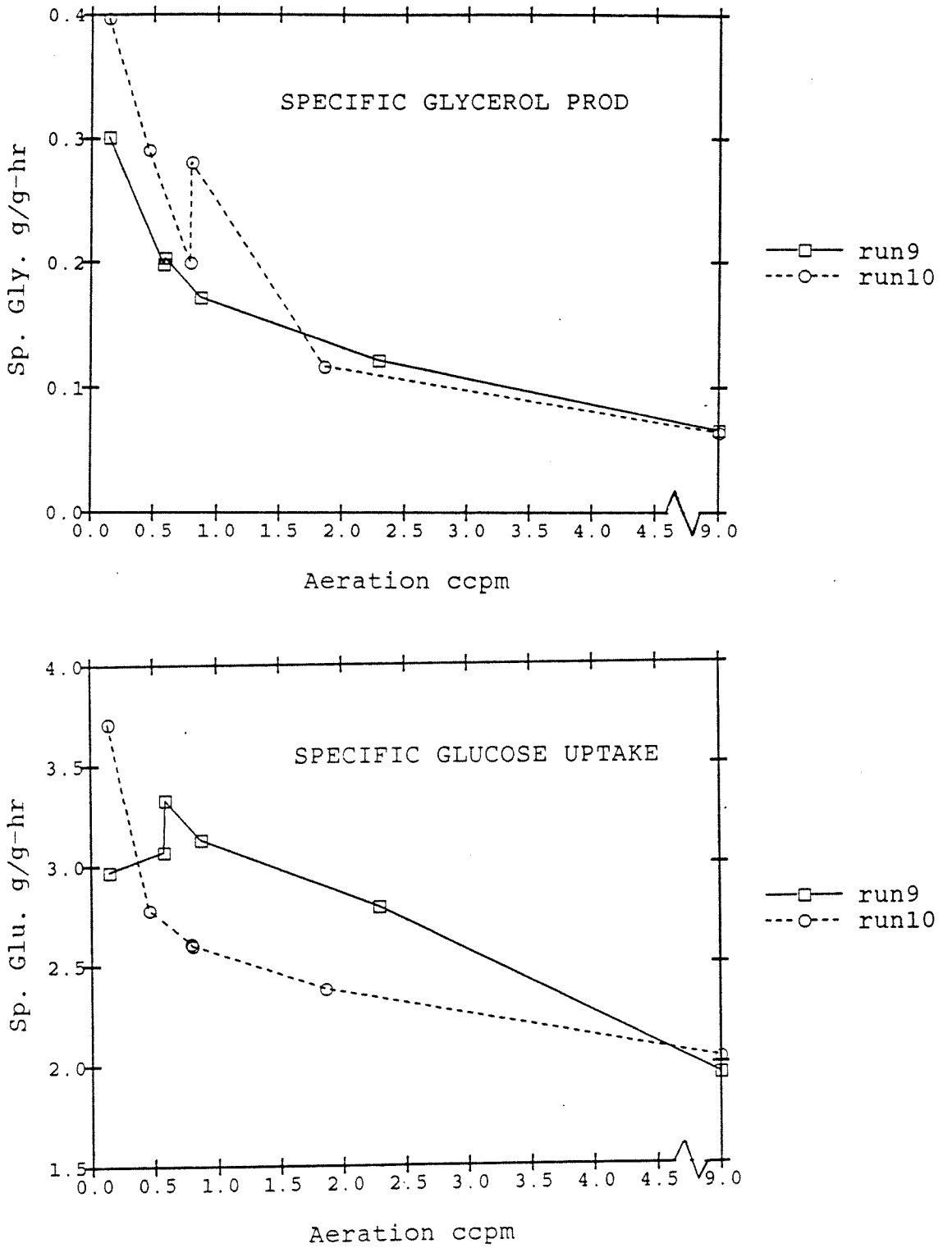
SPECIFIC GLYCEROL PROD
Sp. Gly. g/g-hr
0.4
0.3
0.2
0.1
0.0
0.0 0.5 1.0 1.5 2.0 2.5 3.0 3.5 4.0 4.5 9.0
Aeration ccpm
run9
run10
SPECIFIC GLUCOSE UPTAKE
Sp. Glu. g/g-hr
4.0
3.5
3.0
2.5
2.0
1.5
0.0 0.5 1.0 1.5 2.0 2.5 3.0 3.5 4.0 4.5 9.0
Aeration ccpm
run9
run10

FIGURE 26.

COMPONENT	AMOUNT(per l)
$MgCl_2 \times 6H_2O$	0.52 g
$(NH_4)_2SO_4$	12.0 g
H_3PO_4 85%	1.60 ml
KCl	0.12 g
$CaCl_2 \times 2H_2O$*	0.20 g
NaCl	0.06 g
$MnSO_4 \times H_2O$*	24.0 mg
$CuSO_4 \times 5H_2O$	0.50 mg
H_3BO_3*	0.50 mg
$Na_2MoO_4 \times 2H_2O$*	20.0 mg
NiCl	2.50 ug
$ZnSO_4 \times 7H_2O$*	12.0 mg
$CoSO_4 \times 7H_2O$	2.30 ug
KI	0.10 mg
$FeSO_4(NH_4)_2SO_4 \times 6H_2O$	35.0 mg
m-Inositol	0.125 g
Pyridoxine-HCl	6.25 mg
Ca Pantothenate	6.25 mg
Thiamine HCl	5.00 mg
Nicotinic Acid	5.00 mg
Biotin	0.125 mg
EDTA*	0.10 g
Glucose	40-100 g

TABLE I. DEFINED MEDIUM

TABLE 2. SUMMARY OF RUNS

1.) RUN 1 : Defined Medium, 40 g/l Glucose, AF60 antifoam as needed.

2.) RUN 2 : Defined Medium, 40 g/l Glucose, AF60 as needed

3.) RUN 3 : Defined Medium, 90 g/l Glucose, Tween 80 added later steady states, AF60 as needed

4.) RUN 4 : Defined Medium + Tween 80, 90 g/l Glucose, medium de-aeration, AF60 as needed

5.) RUN 5 : Defined Medium + Tween 80 + Yeast Extract 8.5g/l, Glucose 90 g/l, medium de-aeration, AF60 as needed

6.) RUN 6 : Yeast Extract Medium, 90 g/l Glucose, Antifoam B 0.1 cc/l, medium de-aeration

7.) RUN 7 : Yeast Extract Medium, 90 g/l Glucose, Antifoam B 0.7 cc/l, medium de-aeration

8.) RUN 8 : Yeast Extract Medium, 90 g/l Glucose, Antifoam B 0.1 cc/l, medium de-aeration

9.) RUN 9 : Yeast Extract Medium, 104.7 g/l Glucose, Antifoam B
0.1g/l, medium de-aeration

10.) RUN 10: Yeast Extract Medium, 90 g/l Glucose, Antifoam B 0.7g/l, medium de-aeration

TABLE 3. RUN 2 STEADY-STATE PARAMETERS

aer ccpm	biomass dw g/l	ethanol g/l	glucose g/l	glycerol g/l
40.0*	4.75	8.63	0.015	2.52
20.0	4.95	10.50	0.021	2.78
10.0	4.05	11.20	0.023	3.25
5.0*	3.50	13.70	0.180	3.56
2.5	3.33	13.00	0.272	3.63
1.0*	2.08	9.30	12.90	2.57
0.5	2.62	11.40	4.50	3.51
0.0	2.38	10.00	3.07	4.33
0.5	2.90	9.50	0.45	3.85
1.0	3.18	8.00	0.45	-
2.5	3.48	11.90	0.97	3.70
5.0	3.66	8.50	0.39	2.06

aer ccpm	spec. eth. g/g-hr	sp. gly. g/g-hr	sp. glu. g/g-hr
40.0*	0.48	0.14	2.23
20.0	0.56	0.15	2.14
10.0	0.73	0.21	2.62
5.0*	1.04	0.27	3.01
2.5	1.03	0.29	2.97
1.0*	1.18	0.33	3.45
0.5	1.15	0.36	3.59
0.0	1.11	0.48	4.11
0.5	0.87	0.35	3.61
1.0	0.67	-	3.29
2.5	0.91	0.28	3.05
5.0	0.62	0.15	2.90

* New Reactor Startup

TABLE 4. RUN 3 STEADY-STATE PARAMETERS

aer ccpm	biomass dw g/l	ethanol g/l	glucose g/l	glycerol g/l
40.0	9.33	26.6	6.33	0.14
20.0	9.03	28.8	7.03	0.17
10.0	8.00	27.7	6.60	3.26
5.0	5.65	19.6	5.60	19.60
2.5*	10.50	26.4	5.81	0.18
0.0*	6.44	26.9	5.21	18.60

aer ccpm	spec. eth. g/g-hr	sp. gly. g/g-hr	sp. glu. g/g-hr
40.0	0.76	2.56	0.18
20.0	0.85	2.64	0.21
10.0	0.92	2.87	0.22
5.0	0.93	3.30	0.26
2.5*	0.67	2.27	0.14
0.0*	1.10	2.94	0.21

* Tween 80 Addition

TABLE 5. OXIDATIVE ATP PRODUCTION: PERCENTAGE OF FERMENTATIVE PRODUCTION

aer ccpm	oxidative ATP prod percent
40.0	3.15
20.0	1.33
10.0	0.91
5.0	0.98

TABLE 6. RUN 4 STEADY-STATE PARAMETERS

aer ccpm	biomass dw g/l	ethanol g/l	glucose g/l	glycerol g/l	Y_{ATP} g/mol
4.00	6.63	17.42	5.88	29.30	11.6
2.70	6.59	17.90	4.06	28.50	11.4
1.56	5.05	32.50	5.74	27.20	9.5
1.32	3.70	42.20	5.16	20.00	9.8
0.90	0.56	88.00	1.41	3.27	10.1
1.32	1.22	73.50	2.98	7.42	9.5
1.65	5.25	24.50	5.74	-	-
1.98	5.75	6.67	-	30.00	-
2.70	7.47	7.40	4.97	26.00	11.9
1.32	3.45	42.10	5.49	19.90	9.3

aer ccpm	sp. glu g/g-hr	sp. gly. g/g-hr	sp. eth. g/g-hr	C-recovery %
4.00	2.11	0.17	0.85	98.5
2.70	2.11	0.11	0.84	94.8
1.56	2.20	0.22	1.04	113.4
1.32	2.49	0.27	1.04	102.2
0.90	2.50	0.48	1.12	116.0
1.32	2.61	0.47	1.17	114.0
1.65	2.41	0.21	-	-
1.98	2.79	-	1.01	-
2.70	2.13	0.13	0.81	91.9
1.32	2.68	0.31	1.10	101.0

TABLE 7. RUN 5 STEADY-STATE PARAMETERS

aer ccpm	biomass dw g/l	ethanol g/l	glycerol g/l	glucose g/l	Y_{ATP} g/mol
1.80	6.77	30.3	5.96	2.86	11.39
1.32	5.67	27.85	6.97	12.32	10.71
1.02	5.39	27.30	6.35	18.57	10.30
0.75	4.81	24.60	6.84	16.63	10.43
0.48	3.65	19.60	6.04	38.20	10.10
0.22	2.64	13.90	4.47	53.20	10.47
0.04	1.05	7.39	2.93	69.70	8.79
0.33	3.98	20.50	5.42	38.30	10.35

aer ccpm	sp. eth. g/g-hr	sp. gly. g/g-hr	sp. glu. g/g-hr	C-recovery %
1.80	0.86	0.17	2.48	84.6
1.32	0.95	0.24	2.11	90.3
1.02	0.98	0.23	2.56	92.8
0.75	0.99	0.28	2.96	82.9
0.48	1.04	0.32	2.74	94.6
0.22	1.01	0.33	2.69	94.8
0.04	1.28	0.54	3.53	92.7
0.33	0.99	0.26	2.50	97.3

TABLE 8. RUN 6 STEADY-STATE PARAMETERS

aer ccpm	biomass g/l	glycerol g/l	ethanol g/l	glucose g/l	Y_{ATP} g/mol
9.00	6.51	3.53	32.8	18.7	9.6
6.00	5.29	3.03	28.0	29.8	9.1
2.40	3.20	2.56	-	53.8	-
1.80	2.94	2.05	18.25	48.6	7.8
1.20	2.46	2.23	17.29	65.8	7.2
0.84		-	14.6	-	-
0.36	1.07	1.42	6.43	73.5	8.6

aer ccpm	sp. eth. g/g-hr	sp. gly. g/g-hr	sp. glu. g/g-hr	C-recovery %
9.00	0.976	0.105	2.11	107
6.00	1.03	0.111	2.19	108
2.40	0.972	0.154	2.18	-
1.80	1.20	0.135	2.72	100
1.20	1.33	0.175	1.89	159
0.84	1.15	-	-	-
0.36	1.16	0.25	2.98	92.4

TABLE 9. RUN 7 STEADY-STATE PARAMETERS

aer ccpm	biomass g/l	glucose g/l	ethanol g/l	glycerol g/l	Y_{ATP} g/mol
9.00	5.64	26.7	30.6	3.53	9.00
6.60	4.90	28.5	25.7	2.97	9.31
4.50	4.51	33.0	23.4	3.02	9.51
2.40	3.73	40.0	20.2	3.09	9.16
1.80	3.25	45.1	18.3	2.99	9.08
1.20	1.69	64.9	8.9	2.60	10.20
1.80	2.67	56.8	13.87	3.07	9.99
1.40	1.98	61.7	10.40	2.82	10.15
0.95	1.58	68.6	7.93	2.38	10.76
0.60	1.00	75.2	5.13	1.68	10.73

aer ccpm	sp. eth. g/g-hr	sp. gly. g/g-hr	sp. glu. g/g-hr	C-recovery %
9.00	1.05	0.121	2.18	111
6.60	1.01	0.117	2.41	97
4.50	1.00	0.130	2.41	96
2.40	1.05	0.160	2.59	95
1.80	1.07	0.180	2.68	94
1.20	1.02	0.300	2.87	89
1.80	1.00	0.220	2.40	100
1.40	1.01	0.275	2.76	88
0.95	0.97	0.291	2.61	93
0.60	0.99	0.324	2.86	87

TABLE 10. RUN 8 STEADY-STATE PARAMETERS

aer ccpm	biomass g/l	glucose g/l	glycerol g/l	ethanol g/l	Y_{ATP} g/mol
9.00	6.88	16.0	3.38	31.4	10.74
6.00	6.58	24.7	3.14	28.3	9.51
2.40	3.74	41.1	2.55	20.7	8.82
1.80	3.33	46.0	2.51	19.1	8.57
0.95	2.84	54.1	2.30	15.4	9.15
0.49	1.73	64.2	1.80	10.2	8.53
0.26	0.89	75.6	1.68	4.7	10.6

aer ccpm	sp. eth. g/g-hr	sp. gly. g/g-hr	sp. glu. g/g-hr	C-recovery %
9.00	0.881	0.095	2.08	98
6.00	0.979	0.092	1.92	117
2.40	1.07	0.132	2.52	98
1.80	1.11	0.146	2.55	100
0.95	1.05	0.156	2.44	100
0.49	1.14	0.201	2.88	93
0.26	1.02	0.364	3.12	83

TABLE 12. RUN 9 STEADY-STATE PARAMETERS

aer ccpm	biomass g/l	ethanol g/l	glycerol g/l	glucose g/l	Y_{ATP} g/mol
0.59	1.44	9.90	1.60	79.8	7.28
0.87	1.52	9.75	1.31	80.0	7.84
2.29	2.82	17.3	1.84	63.9	7.86
9.00	6.76	29.0	2.31	36.3	10.98
0.14	0.51	2.04	0.93	96.8	14.37
0.58	1.79	11.95	1.85	76.2	7.47

aer ccpm	sp. glu. g/g-hr	sp. eth. g/g-hr	sp. gly. g/g-hr	C-recovery %
0.59	3.33	1.32	0.204	90.8
0.87	3.13	1.22	0.172	89.3
2.29	2.79	1.19	0.122	96.5
9.00	1.95	0.84	0.066	100.5
0.14	2.97	0.77	0.301	68.6
0.58	3.07	1.29	0.199	96.1

TABLE 12. RUN 10 STEADY-STATE PARAMETERS

aer ccpm	biomass g/l	glucose g/l	glycerol g/l	ethanol g/l	Y_{ATP} g/mol
9.00	6.37	22.9	2.10	27.4	11.28
1.86	3.93	41.5	2.08	19.9	11.82
0.80	2.32	58.7	3.39	12.6	12.49
0.46	1.52	68.1	2.30	8.4	12.26
0.80	2.08	61.9	2.16	11.0	12.04
0.14	0.52	80.0	1.07	3.54	10.11

aer ccpm	sp. eth. g/g-hr	sp. gly. g/g-hr	sp. glu. g/g-hr	C-recovery %
9.00	0.82	0.064	2.03	93.8
1.86	0.99	0.117	2.38	96.6
0.80	1.04	0.281	2.60	98.6
0.46	1.06	0.291	2.78	93.8
0.80	1.02	0.200	2.61	93.4
0.14	1.31	0.397	3.71	86.0

3.1 INTRODUCTION

In the second chapter, some unusual behaviors of the steady-state bioreactor parameters in the microaerobic baker's yeast culture were noted, some of which confirmed literature reports, and some of which were new. The specific ethanol productivity and glucose uptake rates were found to attain sharp maxima at aeration rates low enough that the respiration rate was negligible. The maximum was characterized by a 30 to 50% intensification of the specific fermentation rate as the aeration rate was reduced to the optimal level, followed by a reversal of the intensification as the aeration was further decreased. These changes in the metabolic rate could not be explained by a Pasteur mechanism because of the absence of respiration. In addition, changes in the glycolytic rate occurred even as the residual glucose concentration in the fermentor saturated the glucose transporter. Therefore, it was concluded that some previously undocumented mechanism was responsible for the metabolic changes.

In this chapter, assays of intracellular metabolite and cofactor levels and enzyme activities are described, through which the causes of the metabolic rate changes were sought. These assays included the intracellular concentrations of ethanol, glycerol, glucose 6-phosphate, pyruvate, NADH, ATP, the activities of hexokinase, alcohol dehydrogenase, fumarase, and isocitrate dehydrogenase, and the cell viability. These assays were performed during the steady-states of run 9 with low feed antifoam, and run 10, with high antifoam. The effects of antifoam upon cell metabolism were instrumental in determining the operative mechanisms under all operating conditions. The metabolite assays aided in the

identification of crossover points or rate-limiting steps in the glycolytic pathway that controlled the observed changes in the metabolic rate. Glycolytic intensification resulted in the depletion of metabolites upstream of the crossover points and the depletion of those downstream, while glycolytic slowdown produced the opposite pattern. Assays of enzyme activities and cofactor concentrations revealed possible causes of the rate limitations, as the overall reaction rate is dependent on the enzyme activity and its modulation by the cofactors.

The crossover points revealed that the rate limiting step during the metabolic acceleration with decreasing aeration was caused by an increase in the glucose transporter activity. The possibility is explored that ATP, the concentration of which paralleled the transporter activity, was the activator of the transporter. The limiting reactions during the metabolic slowdown resulting from a further reduction in the aeration rate appeared to be either phosphoglycerate kinase or pyruvate kinase. The cause of the limitation was surmised to be the further accumulation of ATP at this point to a level that made conditions suboptimal for these kinases.

The ATP yield of the cell passes through a minimum, as the specific fermentation rate passes through a maximum, but the chemostat dilution rate and specific growth rate remain constant. Changes in energetic efficiencies of growth also manifest themselves in changes in the intracellular ATP concentration. The patterns of both the ATP yield and the ATP concentrations are predicted by assuming ATP hydrolyzing reactions that become stronger with higher ATP concentrations and are further activated by dissolved oxygen.

It was also seen in Chapter 2 that high antifoam in the medium prevented the attainment of the high specific ethanol productivity of the low antifoam culture and possibly caused the rapid drop in the biomass concentration as the aeration decreased. It was seen that the ethanol productivity was diminished as a result of the diversion, by antifoam, of metabolites away from ethanol production and towards glycerol production, and possibly because of a direct inhibition of glucose uptake by the silicone polymer. It was conjectured that the sharp decline in the biomass concentration was caused by a diminished ATP supply from the forgone ethanol production. In this chapter, The intracellular to extracellular glycerol driving force was measured, to explore whether antifoam enhanced glycerol production by decreasing the resistance to its efflux, and this hypothesis was partially confirmed. In addition, intracellular ATP measurements demonstrated that the high antifoam culture was not able to attain the same, high ATP concentrations as the low antifoam culture, supporting the presumed cause of the sharp decline in the biomass concentration.

Dasari et al.(23) reported that there exists no resistance to the diffusion of ethanol across the cell membrane, condemning previous reports of the accumulation of up to 300g/l of intracellular ethanol as faulty. The difficulty arose in the centrifugation of the cell sample prior to ethanol analysis, during which large amounts of ethanol, incorrectly attributed to intracellular ethanol, accumulated. In this chapter, a novel method of the estimation of intracellular ethanol avoiding this pitfall is introduced, and the conclusions of Dasari et al. are supported.

NADH oxidation in glycerol production could not be matched by NADH

generation from the other measured products, indicating the excretion of a spectrum of unmeasured, relatively oxidized products to close both the redox and carbon recovery balances. The role of the TCA cycle dehydrogenases in the supply of a portion of the NADH oxidized in glycerol production is explored.

3.2 MATERIALS AND METHODS

PREPARATION OF CELL-FREE EXTRACTS FOR ENZYME ASSAYS

A variety of chemical and mechanical methods exist for the disruption of intact cells and the release of intracellular enzymes into the supernatant(2,3). From among those the method employed in these studies is the wet bead mill disintegration in a Braun MSK homogenizer. Several reasons lie behind this choice. First, several investigations of the enzymatic pattern in *Saccharomyces cerevisiae* used bead disintegration (4-7). In particular, Rogers and Stewart(3) used the Braun MSK in their study of the oxygen induction of the respiratory enzymes. The mechanisms described in Chapter 1, Section 3 make heavy use of these investigators' findings. Since the participation of the respiratory enzymes in the changes of the fermentation pattern in this study was originally suspected, the enzyme assays were patterned after those of Rogers and Stewart. The bead disintegration technique is also rapid, effective, and procedurally simple. The manufacturer claimed 99.7% disruption within 60 seconds, with no denaturing of the released enzymes. Temperature control is made easy in the MSK through the circulation of liquefied CO_2 to the rotating chamber.

The MSK homogenizer consists of an electric motor that rotates the

sample containing chamber at 2000 or 4000 RPM, depending on the pulley to which the belt is attached. In these studies, 4000 rpm was used. The rotating chamber possessed a fitting through which the a stainless steel tube conveying liquid CO_2 can be attached. This tube is connected at the other end to a liquefied CO_2 cylinder with a simple, manual valve. An adapter was used so that 12 ml culture tubes, rather than the 75 ml usual gas container could hold the sample. The culture tubes were partially filled with 4cc Of 0.45-0.5 mm glass beads and 5cc of sample to be homogenized. With these volumes, the culture tube was between 1/2 to 2/3 full, as recommended by the manufacturer. Air, and variable quantities of air have been found to play an important role in the disruption(3), so that exact reproduction of these volumes for all samples was essential. The mechanism for cell wall breakage is thought to be the high liquid shear produced as the fluid rapidly passes through the interstitial spaces between the beads.

Temperature control in this instrument ia a delicate, manual task, which must be mastered through trial and error and experience. The aim of the temperature control is to maintain the sample temperature at 0-5 degrees to maintain the stability of the released enzymes. Uncontrolled, the temperature of the rotating chambers would attain a destructively high level. The necessary cooling action is accomplished by supplying liquid CO_2 to the chamber. However, the valve must not be open continuously, since the sample would rapidly freeze. The optimal cooling strategy was to supply a 10 second burst of cooling before the initiation of shaking and 10 second bursts after each minute of shaking. During the bursts, the coolant valve was opened 1/8 turn.

The procedural aspect of prime importance was the amount of time necessary for breakup. This time should be sufficient so that at least 95% of the cells are broken, but not too long, since enzymes and subcellular particles as mitochondria are rapidly degraded. The degree of disruption is measured by three means, the amount of protein released from the cells, the broken-to-unbroken cell population measured with a coulter counter, and the activity of fumarase released from the cells. Thus, a breakup time would be chosen such that no unbroken cells would be detected, and no further increase in protein release or fumarase activity would be noticed with an increased breakup time.

A coulter counter coupled to a multichannel analyzer is useful in determining the cell size distribution in a population and to distinguish two different populations based on size difference. The details of the instrument, procedures, and principles are presented elsewhere(8). Since broken cell debris appears smaller to the coulter counter than intact cells, the instrument can be applied to the assessment of the fraction of the intact population broken. Figure 1 shows the two different population size distributions for broken and intact cells. The ordinate represents the number of counts that were grouped into 128 channels shown on the abscissa as a 5 microliter sample passed through the instrument's orifice. The channel number follows the particle volume in a slightly nonlinear way. Obviously, breaking had the desired effect of reducing the particle volumes so that they could be distinguished from the unbroken cells. As shown in Figure 2, partially broken samples show a bimodal distribution. Thus, the optimal breaking time would be the shortest time for which the unbroken population would disappear. Figure

3a-d show the population distributions for samples broken for 20 sec, 1 min., 3 min, and 5 min. The unbroken population shrinks with increasing breakup time and virtually disappears by 3 minutes. No real gain is realized by breaking the cell for 2 additional minutes. Microscopic examination of the broken samples confirms this finding. After 3 minutes of breakup, more than 90% of the cells appear hollow and empty.

On this basis, 3 minutes seems to be the appropriate duration. The manufacturer claims more than 99% breakup within 1 minute, but is not supported in these results. A possible cause for the disagreement is the lower cell density in the sample in these studies. Braun recommends a 50% cell suspension, which is vastly too concentrated for the sample sizes and bioreactor cell densities relevant in these studies. Suspension concentrations of the order of 2.5% were actually used.

A second criterion for the success of the breakup is the amount of protein released to the supernatant. The Bio-Rad total protein assay based on the absorbance shift from 465 to 595 nm in the protein binding of Coomassie Blue dye was employed. This method is superior to the standard Lowry(8) method because of the fewer reagents, shorter reaction times, enhanced protein-dye complex stability, and better linearity and reproducibility of the results. The procedure outline in the instruction manual was followed exactly. Absorbance at 595nm was measured in a Spectronic 21 spectrophotometer. Shown in Figure 4 is the change in absorbance at 595 nm as a function of breakup time. After 2 minutes 15 seconds, approximately 95 % of the protein is released compared to the 3 minute sample. Again, a 3 minute breakup seems optimal.

The final assessment of the breakup is the measurement of the activity

of fumarase released to the supernatant. The method of enzyme activity assay is presented later. Shown in Figure 5 is the fumarase activity as a function of the homogenization time, the former being in arbitrary absorbance-related units. 93% of the activity of fumarase released after 5 minutes appeared after 3 minutes.

Although numerous measurements indicated 3 minutes to be a sensible breakup time, this duration was deemed too long considering the sensitivity of subcellular particles and other enzymes. The manufacturer claims release of intact mitochondria after 20 seconds of breakup, implying that damage already occurs with the usual 1 minute breakup time. Damage to mitochondria may affect the activities of the respiratory enzymes measured. The increase in the activity of released fumarase with increasing breakup time may have been partially due to the destruction of the transport barrier of the mitochondrial membrane. A compromise was struck in the choice of a 2 min 15 second breakup time, after which the majority of the breakup was already accomplished. Consistency of the procedure would assure comparability of enzyme activity measurements from different samples, despite the fact that perhaps 85-90% of the true activity is actually represented.

The procedure for sampling and breakup is now provided. 5-25 cc of the fermentor fluid, depending on the biomass concentration, was sampled over crushed ice, centrifuged at 12000 rpm(22000g) for 10 minutes at 2 degrees, washed with 10cc of ice cold 1M tris buffer PH 7.5, and recentrifuged. Crushed ice and the low-temperature treatment minimized the synthesis and degradation of enzymes, especially the respiratory enzymes after the exposure to atmospheric oxygen and glucose limitation after

washing. The yeast pellet was resuspended in 5cc of the tris buffer, added to 4cc of 0.45-0.5 micron beads glass beads in a culture tube, and broken for 2 min, 15 sec. The homogenate was separated from the beads by filtration through a coarse fritted Buchner funnel. The beads were washed twice with 2cc of ice cold tris buffer and combined with the filtrate. The homogenate was centrifuged at 3600 rpm (1000g) for 10 minutes, and the debris-free extract decanted. The centrifuge speed was chosen at 1000g to prevent the sedimentation of mitochondria(4).

PREPARATION OF EXTRACT FOR METABOLITE ASSAYS

In this section, the method used for sample preparation in the assays of intracellular ATP, glucose 6-phosphate, pyruvate, and glycerol are described. The metabolites excluded from this method are the NADH and intracellular ethanol, extracted by the procedure in the next section.

The turnover rate of the pools of several intracellular metabolites is extremely rapid, in the order of 1 second(10,11). For ATP, for example, the turnover rate is easily calculated from the rate of phosphorylation by glycolysis compared to the intracellular concentration of the nucleotide. To accurately assay the intracellular metabolite concentration, it is imperative to rapidly sample the fermentor contents and instantly inactivate all enzymes involved in the turnover of the metabolites. Obviously, no sampling and extraction scheme can possibly be accomplished in less than 1 second. However, the assay is likely to be accurate as long as environmental conditions such as the glucose and dissolved oxygen concentration are not significantly changed from those existent in the fermentor. This allows possibly for a few seconds for the procedure. Longer times necessary to centrifuge or filter the sample prior to ex-

traction may reduce the ATP concentration by 50%(10).

The first approach to the metabolite extraction followed the procedure of Weibel et al.(9), in which the sample withdrawn was immediately mixed in a 4:1 ration with 35% perchloric acid precooled to its freezing point in an ethanol, solid CO_2 bath. ATP was easily and accurately measured with this extraction method. However, problems arose with the other metabolites. It turned out that pyruvate is a significant extracellular product approaching the intracellular concentrations at around 0.1 g/l. As the supernatant was not separated from the cells in this procedure, mostly extracellular pyruvate was being measured. A problem also arose with the glucose 6-phosphate assay, even though it is exclusively an intracellular metabolite. The method of assay of G6P is the fluorometric determination of the NADPH produced in an enzymatic reaction having G6P as the substrate. However, the fermentation medium most often contained large concentrations of yeast extract, which had a high fluorescence at the same wavelength pair as NADPH. The change in fluorescence due to the changed NADPH concentration from the assay was completely masked by the background fluorescence. Any fluorometric assay would suffer from the same drawback as long as the yeast extract medium was processed together with the cells. Only ATP could be assayed through the bioluminescence method.

It would seem that, given the extracellular appearance of the desired metabolites and the high fluorescence of the medium, filtration of the sample to separate the cells from the medium prior to extraction was inevitable. However, time delays in such a separation and washing would likely change the concentration of the metabolites. The method of Franco

et al.(11) seemed an attractive alternative. As recommended by these authors, the sample from the fermentor was mixed with perchloric acid precooled to -20 degrees in a syringe. The initial concentration of the perchloric acid was sufficient to make the final perchloric acid content of the sample mixture 6%. This mixture was immediately pushed with the syringe plunger through a Teflon, 0.5 micron pore-size filter hosed in a Millipore Swinnex unit at the base of the syringe. The cells on the filter were washed once with ice-cold 6% perchloric acid before the filter and the cells on it were permanently placed in a 6% perchloric acid solution. It was assured that no metabolites would leak out of the cell in the first 180 seconds of contact between the cells and the acid during which the sampling process would proceed(12). In addition, contrary to ordinary filtration, the presence of perchloric acid during the filtration step would presumably arrest metabolism, causing the turnover of the metabolites. However, this approach failed. 73% of the ATP content of the cell leaked out during the sampling procedure, 22% during the initial filtration and the remainder during the perchloric acid washing. Recall that ATP could be assayed without filtration owing to the bioluminescence assay method that does not suffer from the presence of yeast extract. The disagreement with the results of the previous investigation may lie in that the cells in this study were harvested from a microaerobic chemostat, in contrast to the aerobically grown cells in the previous study. Perhaps the cell wall or membrane structures are more fragile in the absence of oxygen.

The final solution to the problem involved the immediate filtration of the sample through a Swinnex unit attached to the syringe and the

placement of the cells together with the filter into an ice-cold 6% perchloric acid solution. The cells on the filter were not washed, and the entire process was completed in approximately 15 seconds. It was reasoned that this 15 second delay could not significantly change the intracellular metabolite pattern under the existent conditions, even though filtration under other circumstances resulted in a significant decrease in the ATP concentration. In these studies, the residual glucose concentration was of the order of 25-90 grams per liter, high enough to significantly saturate the glucose transporter and also high enough that the percentage change in the 15 second sampling delay would be negligible. This contrasts to the residual glucose concentration of the order of milligrams per liter in glucose-limited chemostat culture, which would change significantly in a matter of seconds. The dissolved oxygen in the fermentor was very low, and would be expected to undergo a large percentage change during the 15 second procedure. However, it is argued that the effects of oxygen are of a slow time scale compared to the filtration, given the respiratory incompetence of the glucose-repressed, microaerobically grown cells. Changing oxygen levels could not cause significant changes in the metabolites from respiration simply because respiration contributes a negligible percentage of the glycolytic metabolism, regardless of a transient increase or decrease of the dissolved oxygen. Oxygen could only initiate slow time scale processes such as respiratory enzyme induction and unsaturated fatty acid and sterol synthesis(4). Thus, it is reasoned that filtration did not alter the environment of the cells and was not detrimental to the assays. The technique was carried out to determine whether the resulting ATP concentration was

identical to the direct extraction procedure without filtration, with conclusively positive results. The method was also used for the other metabolites.

One unresolved issue is the measurement of those metabolites that also were present extracellularly. Since the samples were filtered but not washed, the extracellular metabolite would still be present in the interstitial space in the filtered cell paste occupied by medium. The high residual glucose was again of advantage. Intracellular glucose attains a negligibly low concentration under a variety of culture conditions, even when the transporter has surplus activity above and beyond the glycolytic activity(13,14). This is probably due to the rapid phosphorylation of glucose by hexokinase and the regulation of glucose uptake by glucose 6-phosphate or some related compound. In any case, this fact enabled the calculation of the volume of interstitial fluid, knowing the residual glucose concentration in the fermentation medium and measuring the carryover of glucose from the filtered sample into the extract. A correction factor could be included, accounting for the glucose utilization during the 15 seconds, assuming an unchanged specific glucose uptake rate. In this way, the intracellular metabolites could be distinguished from the extracellular contribution. More details of the methods and calculations are presented in the discussion of the procedures of the individual assays.

The exact procedure for the assays is as follows. 5-25 cc of the fermentor fluid were sampled, loaded into a syringe, and pushed through a 0.45 micron pore size filter housed in a Swinnex unit. The Swinnex housing was rapidly opened, and the filter with the yeast paste on it

was carefully placed with forceps into 5cc of a 6% perchloric acid solution chilled in an ice bath. One-half to one hour in an ice bath was allowed for the complete extraction of the metabolites from the sample before neutralization with 3M potassium bicarbonate. The usual cell homogenization or repeated freeze-thaw cycling prior to neutralization to enhance breakage and extraction was deemed unnecessary, since 73% of the ATP was found to leak from the cell in a matter of minutes. Freeze-thaw cycling was found actually to reduce the ATP concentration, presumably through degradation. Neutralization proceeded slowly in an ice bath to minimize the frothing of the produced CO_2. The final PH was around 7.0. The cell debris and the precipitated potassium perchlorate were sedimented by centrifugation at 12000 rpm for 10 minutes at 2 degrees. The supernatant was decanted as the extract.

EXTRACTION METHOD FOR NADH AND INTRACELLULAR ETHANOL

NADH is rapidly destroyed by acid(14), prohibiting the use of the perchloric acid extraction for this metabolite. Bartley and Polakis(15) tested 10 alkaline extraction methods, of which only one produced acceptable results. In this method, the sample was extracted in 0.1N NaOH, 10mM mercaptoethanol, and 10mM EDTA at 60 degrees for 1 minute. This was the only combination tested by these authors that prevented the interconversion of the nicotinamide nucleotides, NAD, NADP, NADPH, and NADH. When the mercaptoethanol was replaced by cysteine, another reducing agent, or omitted altogether, either too little or too much NADH was recovered from a synthetic mixture of the four nucleotides added to the the cell suspension prior to extraction. This implies that the mercaptoethanol was necessary in the inactivation of dehydrogenases or oxidases

liberated from the cells during extraction.

The method of Bartley and Polakis(15) was attempted in the present study, but failed. NADH added to the cell suspension prior to extraction was quantitatively recovered, but added NAD was invariably converted to NADH, implying that some dehydrogenase had not been inactivated in the procedure, but apparently, oxidases were. As a result, a search was undertaken for an agent eliminating this dehydrogenase activity. Cysteine was used in place of mercaptoethanol, in vain. The base concentration was boosted to 0.5 to 1.0 and finally to 2.4N, with no result. The extraction temperature was raised to 100 degrees. A nonacidic extraction procedure proposed by Ludin and Thore(16) involving chloroform was attempted without success. As suggested in Bergmeyer(1), the base was dissolved in 50% ethanol rather than water, but still failed. Success finally came when copper, an inhibitor of the glycolytic enzyme glyceraldehyde phosphate dehydrogenase was added to the alkaline extraction medium. For the first time, NAD added to the cell suspension was not converted into NADH. Addition of NADP and NADPH also did not interfere with the NADH recovery. Finally, added NADH was recovered to an extent of 90% or more. Thus, all aspects of the extraction were successful.

The details of the extraction procedure are now outlined. 2cc of 1N NaOH were placed into a beaker in a 60 degree water bath. Immediately afterwards, 5-15 cc of the fermentor fluid was sampled and filtered through a Swinnex unit as with the perchloric acid procedure. The filtration was necessary because the fluorescence assay of the NADH suffered from the high fluorescence of the complex medium. The filter with the cell paste was placed into the alkaline in the 60 degree water bath, and

without delay, 2cc of 0.3g/l copper sulfate solution was pipetted into the beaker. This was done last since copper hydroxide precipitates in the base. Heating at 60 degrees continued for one minute, after which the beaker was plunged into an ice bath. The pH of the extract was reduced to 8.5-9, using a 3% by volume acetic acid solution. Neutralization was carried out dropwise with shaking to prevent the local buildup of acid and the destruction of the NADH. Also, since the solution was relatively unbuffered, just the correct amount of acetic acid had to be added, as a few extra drops could send the PH to destructive levels below 7.0. The neutralized extract was centrifuged at 12000 rpm for 10 minutes and the supernatant filtered again through a Swinnex unit. This last step was necessary, since the sedimented debris would very easily resuspend itself when the samples were decanted from the centrifuge tubes. Fluorescence assays require an absolutely clear liquid free of any particulate debris.

Extraction for the intracellular ethanol assays was carried out with the identical procedure. This, rather than the perchloric acid extraction was used, because the action of the latter upon the cell mass produced HPLC peaks, which interfered with the ethanol peak.

THE ATP ASSAY

The intracellular ATP from the perchloric acid extract was assayed through the bioluminescence reaction governed by the following equation(20):

$$\text{ATP} + \text{Luciferin} + O_2 \xrightarrow[\text{Mg}]{\text{Luciferase}} \text{Oxyluciferin} + \text{AMP} + CO_2 + \text{Light} \ .$$

The mediating enzyme, luciferase, is derived from the firefly, which produces its glow base on this reaction. The quantum yield of the reaction is nearly 100%(20), meaning that one mole of ATP reacting generates nearly one mole of light quanta. The kinetics of the reaction is easily followed by measuring the light emission. It remains only to connect the kinetics with the ATP concentration.

The instrument used to measure the light emission was a Perkin Elmer LS-5 fluorescence spectrophotometer. A fluorimeter ordinarily measures the light emission from a sample at a precise wavelength resulting from its illumination at a precise excitation wavelength. In this reaction, no excitation is required, as the light is autonomously generated. Therefore, the excitation shutter of the instrument was close, isolating the light source from the sample. In addition, there was no interest in filtering the emitted light to any particular wavelength, since all emitted light was of interest. Thus, the emission grating was set to zero order, permitting all wavelengths to pass, and the emission slits were opened to the maximum width of 30 nm. The instrument was also equipped with a total emission accessory, which places a mirror into the path of the emitted light, capturing a greater fraction of it for amplification in the photomultiplier. This accessory allowed for a 20 fold increase in the strength of the signal, without which the measurement may not have been possible. The instrument also possessed a bioluminescence accessory consisting of a more light-tight sample compartment and a septum above the cuvette holder through which the sample could be injected to initiate the reaction. As the reaction is rapid, direct injection is essential.

The measurement was carried out in the phosphorescence mode of the instrument, for reasons clearly explained in the instruction manual. Three modes of signal amplification are available, the photomultiplier gating time, the voltage supplied to the photomultiplier, and the numerical amplification of the display scale. The voltage supply to the photomultiplier was always maintained at the level that exists when the parameter "20" is used in entering the phosphorescence mode. The gating time was maintained at the highest allowable value of 9 milliseconds. The numerical expansion of the "fixed scale" was varied from 10 to 200, depending on the concentration of the sample. The photomultiplier delay time was irrelevant and was left at the default value.

The temperature of the reaction was maintained at 26 degrees by circulating water from a thermostatted bath through the jacket of the cuvette holder. A 20 degree temperature is optimal(20) and should be used if a refrigerated water bath is available. The signal from the instrument was recorded by a Perkin Elmer R100 strip chart recorder.

It was attempted to use the Boehringer ATP bioluminescence assay kit consisting of luciferin, luciferase, and other essential buffers, cofactors, stabilizing ingredients, and components. It was soon learned that the assay kit was designed for more sensitive instruments such as luminometers and scintillation counters, and only a weak signal could be discerned in the desired ATP concentration range. To obtain a measurable signal, the luciferase concentration was raised from 1.6 ug/ml in the kit to 6.7 ug/ml, and the luciferin concentration from 19.6 ug/ml to 75 ug/ml. The Boehringer kit also has the luciferase inhibitor AMP purposely added to produce a slower and more uniform reaction rate. The inhibitor

was eliminated in the formulation of the reaction mixture. The separate purchase of the luciferin and luciferase reagents also provided for greater flexibility, since only as much of the reagents could be used as was necessary on the days during which the assays were undertaken. The kit, once activated, was stable for only several days. The inconvenience and inaccuracy resulting from the freezing and storage of a large number of samples on a single occasion were avoided.

The solutions used and the quantities pipetted into the cuvette for each assay are shown in Table 1. Synthetic crystalline luciferin was purchased from Sigma in 1 milligram vials, and were stored at -20 degrees in the freezer. Luciferase was purchased from Boehringer in 1 mg quantities. The enzyme was dissolved in 1 ml of 0.5 M Tris buffer, PH 7.4, subdivided into 10 equal parts, and each part stored frozen in its own vial. Only one of these vials had to be diluted and used on each day of ATP assaying. The handling and storage of the reagents were based on the manufacturer recommendations and the published documentation of their stabilities(20,21). Bovine serum albumin, fraction 5 powder was obtained from Sigma. The PH of the tris buffer solution was adjusted on each day of use.

Once pipetted into the cuvettes, the mixture was gently agitated and placed into the cuvette holder for 5 minutes to allow for temperature equilibration. During this wait, the ATP sample was removed from the ice bath and submerged in the temperature-controlled bath servicing the fluorimeter, so that it, too, could attain the reaction temperature. After the 5 minutes, 1cc of the ATP sample was withdrawn from sample into a plastic syringe and rapidly injected through the septum into the

cuvette to initiate the reaction.

The time course of the luminescence reaction after injection is recreated from strip chart recordings in Figure 6. The luminescence signal is unique to the instrument and amplification settings and is therefore expressed in the arbitrary units of the display. Upon injection, there is a rapid rise in the luminescence signal. The signal then decays before attaining a more constant level. The extent of the decay is greater with higher ATP concentrations as shown in Figure 6, and as has been observed previously(22). Possible causes for the decay are product inhibition and the utilization of ATP by luciferase itself or ATPase contaminants, all of which are amplified at high ATP concentrations(22).

The luminescence profile can be interpreted in many ways to obtain a calibration curve. The $\overline{ATP}$ concentration has been related to the steepness of the initial rise of the signal, the maximum value, the average luminescence over several minutes, and the instantaneous signal after several minutes of reaction(22). The last two are accurate only when a relatively constant signal is produced as with low ATP concentrations and highly purified enzyme preparations. The first two are used when a sharp peak in the signal is attained, as was indeed demonstrated in Figure 6. Of these, the maximum signal is the easiest to measure and is immediately seen from the strip chart recording.

A calibration curve spanning two orders of magnitude of ATP concentrations in synthetic mixtures, from 2×10^{-6} to 2.5×10^{-8} M was constructed and is shown in Figures 7 a-c. In these figures, the maximum signal and 20 second integrations of the signal beginning at 1 minute and 3 minutes after injection are shown. The instrument provided these

integrations simply by pushing the integration button. In Figure 7a, the x axis scale is relevant only to the higher ATP concentrations. In Figure 7c, the two highest concentration points are eliminated so that the scale could be expanded to show more clearly the behavior at the lower ATP concentrations. In Figure 7b, a log-log plot encompassing all tested concentrations is provided. As is clearly seen, the maximum luminescence signal is linear with the ATP concentration over two orders of magnitude. The only point out of line with the others is the one at 1×10^{-6} M, but is most likely due to an isolated incidence of experimental error. The 1 and 3 minute integrations are also linear with the concentrations in the lower ranges, but become nonlinear at concentrations higher than 0.5 uM. This is expected, since the luminescence decay becomes more pronounced with the higher ATP concentrations and affect the longer time measurements to a greater extent.

The single ATP calibration curve is not sufficient for the subsequent determination of the concentration in real samples. Obviously, the activity of the luciferin and luciferase varies with different lots and decays with extended storage. Also, materials present in the medium and introduced during perchloric acid extraction inhibit the reaction, as indicated by the lower signal obtained from standards added to real samples. The degree of inhibition introduced in the extraction is not necessarily reproducible from sample to sample. Also, the neutralization of the extract is not exactly reproducible, and the PH of the samples may change as CO_2 from the bicarbonate buffer bubbles out over time. The reaction is critically dependent on the PH(21). Therefore, variation in the enzyme activity and the sample preparation had to be corrected by

introducing an internal standard of a known concentration of a synthetic ATP solution to each and every sample analyzed. The luminescence of the sample alone would be measured. Immediately afterwards, 50 to 200 microliters of a 0.31 mM ATP solution would be added to 1.25 cc of the sample, and the luminescence of the mixture assayed. The concentration of the ATP in the sample could then be calculated, given the linear response of the bioluminescence signal. Linearity of the calibration curve with varying amounts of an internal standard added to a real sample is shown in Figure 8. The span of concentrations represented in this calibration curve is not as great as shown with the synthetic samples, but encompasses the entire range of concentrations encountered during the performance of the real assays.

In the measurements of the ATP concentrations in the fermentation extracts, 2-3 extracts were prepared and measured on the same day. One or two measurements were performed on each of the extracts, with a total of no less than four measurements. Internal standard measurements accompanied each and every sample measurement. The precision of the measurement, based on the typical variation among repeat measurements, is conservatively plus or minus 10%.

GLUCOSE 6-PHOSPHATE ASSAY

The assay of glucose 6 phosphate is based on the following reaction(10):

$$\text{Glucose 6-P} + \text{NADP} \xrightarrow[\text{Mg}]{\text{G6P Dehydrogenase}} \text{NADPH} + \text{6-P Gluconate} .$$

The glucose 6-phosphate oxidation results in the reduction of NADP to

NADPH, the latter of which can be measured fluorometrically with a 340 nm excitation and 460 nm emission wavelength(10).

The Perkin Elmer LS5 was used for the measurements at these wavelengths. Unlike the bioluminescence measurement, the instrument was placed into the fluorescence mode. The excitation and emission slits were set at 5.0 nm. The response factor, which is essentially a noise-damping factor, was set to the maximum value of 4. The temperature of the reaction cuvette was maintained at 26 degrees by circulating thermostatted water through the jacket of the cuvette holder. The expansion factor of the display scale was typically 50, but was adjusted as needed. The time trace of the reaction was monitored with the R100 strip chart recorder.

The solutions prepared for the assay and the amounts of each pipetted into the cuvette for each assay are shown in Table 2. The glucose 6-phosphate dehydrogenase in ammonium sulfate suspension was obtained from Sigma or Boehringer and stored according to the manufacturer recommendations. Glucose 6-phosphate was obtained from Sigma as was NADP, in 10 mg vials. Dilute HCl was the solvent of the NADP as the nucleotide is most stable under mildly acidic conditions(14).

The cuvette with the reagents was placed into the holder and left for several minutes for temperature equilibration. The reaction was initiated by withdrawing the cuvette, pipetting the enzyme suspension into it, inverting it gently for mixing, and replacing the cuvette into the holder.

A typical time trace of the reaction is shown in Figure 9. The reaction is mostly over after 10 minutes, but a gradual increase in

NADPH fluorescence continues for an additional 15 minutes, as shown in the Figure, but actually continues indefinitely. It was found that this drift is due to a contaminating hexokinase activity in the glucose 6-phosphate dehydrogenase preparation of both manufacturers. Synthetic samples with only glucose and the enzyme and no glucose 6-phosphate were found to generate the same gradual increase in fluorescence. Thus, the residual glucose is slowly converted into glucose 6-phosphate by the contaminating activity and is incorrectly registered as native G6P in the sample. The measurements were corrected for this drift by extrapolating the inclination at the later times back to zero time and using the resulting intersection with the ordinate as the true fluorescence change. The extrapolation is demonstrated in Figure 9.

A calibration curve of the final fluorescence change against the G6P concentration is shown in Figure 10, demonstrating no problem with the linearity of the measurement in the relevant concentration ranges.

The samples used for this assay were actually the same as the ATP samples, and were assayed on the same day that the extractions were made. Two or three assays were made altogether for each steady-state in the fermentation, owing to the relatively long time required for each assay. The variability of repeat measurements indicated a precision of plus or minus 10%, conservatively.

PYRUVATE ASSAY

The following reaction governs this assay(10):

$$\text{Pyruvate} + \text{NADH} \xrightarrow{\text{Lactate Dehydrogenase}} \text{Lactate} + \text{NAD}.$$

The disappearance of NADH fluorescence at the 340 nm excitation, 460 nm emission wavelength pair was used to quantify the pyruvate in the sample. The LS5 with the identical settings of the glucose 6-phosphate assay was employed. The solutions and the quantities of them added into the cuvette for this assay are shown in Table 3. The enzyme was obtained from both Sigma and Boehringer and the pyruvate from Boehringer. Special 1 mg vials of NADH obtained from Sigma were opened and completely used on the same day for both convenience and uninterrupted desiccation of the reagent, found to be absolutely necessary. Larger NADH preparations of 1 gram or more had to be continually opened and closed to withdraw the required amount of reagent for the given occasion. Water absorbed in this opening and closing destroyed the reagent. Improperly desiccated NADH was found to react upon lactate dehydrogenase in a proportion completely independent of the pyruvate concentration present!

In performing the assay, the reagents would first be allowed to equilibrate to the 26 degree reaction temperature before initiation. The fluorescence of the NADH in the uninitiated reagent would decrease as the temperature approached the equilibrium. Stabilization of the fluorescence also indicated stabilization of the temperature. The reaction was then initiated by withdrawing the cuvette and pipetting in the enzyme suspension. The reaction was complete almost instantly. A calibration curve for synthetic pyruvate samples in Figure 11 shows no problem with the linearity of the assay.

As mentioned in the previous section, the samples withdrawn from the fermentor were filtered, but not washed, before the filter and the yeast paste upon it were placed into the perchloric acid extraction

solution. Since pyruvate is found extracellularly in significant quantities, a correction would have to be made to account for the medium volume trapped in the interstitial spaces of the unwashed yeast paste to account for only the intracellular pyruvate. To do this, the extracellular pyruvate concentration in the bioreactor supernatant and the interstitial medium volume would have to be found. To calculate the latter, advantage was taken of the high residual glucose concentration in the medium in all assayed steady-states and the fact that intracellular glucose concentrations are negligible(13,14). The amount of glucose in the perchloric acid extract would reflect the volume of medium carried into the extract with the yeast paste.

The amount of medium carried into the extract is given by:

$$G_{sup}V_{int} - \nu_g X V_{sam} t$$

where	G_{sup}	= residual glucose conc. in supernatant	g/l
	V_{int}	= interstitial volume in yeast paste	l
	ν_g	= specific glucose uptake rate	g/g-hr
	X	= biomass concentration in fermentor	g/l
	V_{sam}	= sample volume from fermentor	l
	t	= time delay from sampling to extraction	hr.

The glucose concentration in the extract was measured by HPLC, only with a 200 µl sample injection volume instead of the usual 25 µl. In the above equation, a correction factor is applied to account for the glucose taken up by the cells in the time lag between filtration and the dumping of the paste into the extraction medium. An average of 15 seconds (0.0042 hours) was used for this lag. It is assumed that the specific glucose uptake rate in the yeast paste is the same as in the fermentor. The correction factor is typically 4% of the first term of the above equation.

The total glucose content of the extract is given by the following

equation:

$$G_{ext}[V_{per} + V_{neu} + V_{bio} + V_{int}]$$

where G_{ext} = glucose concentration in extract g/l
V_{per} = vol. of perchloric acid extr. soln. l
V_{neu} = vol. for extract neutralization l
V_{bio} = vol. of biomass in yeast paste l
V_{int} = interstitial volume in paste l.

The volume of the biomass in the paste can be calculated, based on 2cc of water per gram dry-weight of yeast(23,1) found from the equilibration of tritiated water into the cell water compared to the exclusion of ^{36}Cl from the intracellular volume(23). Therefore, the sought-after interstitial volume can be calculated by equating the above expressions:

$$V_{int} = \frac{G_{ext}[V_{per} + V_{neu} + V_{bio}] - \nu_g X V_{sam} t}{[G_{sup} - G_{ext}]} \quad (1)$$

The pyruvate concentration per gram of biomass can then be calculated by the formula:

$$C_{pyr} = \frac{C_{ext}[V_{per} + V_{neu} + V_{bio} + V_{int}] - \nu_{pyr} X V_{sam} t - C_{sup} V_{int}}{V_{sam} X} \quad (2)$$

where C_{pyr} = intracellular pyruvate g/gdw
C_{ext} = pyruvate conc. in extract g/l
ν_{pyr} = spec. pyruvate production g/g-hr
C_{sup} = pyruvate conc. in supernatant g/l.

Here, a correction factor also accounts for the pyruvate produced by the cells during the sampling period. The extracellular pyruvate brought into the sample by the interstitial fluid is deducted from the total pyruvate in the sample to give only the intracellular quantity.

The typical interstitial volume turned out to range from 80 to 150 microliters, depending on the sample size. The typical intracellular volume in a typical filtered sample is 50 microliters based on a 2cc per gram dry-weight intracellular volume. The extracellular pyruvate concentration varied from 30 to 100% of the intracellular concentration. Therefore, in the worst cases, 2/3 of the pyruvate in the sample originated from outside the cell. A combined error of 5% in the extract and supernatant pyruvate measurements and in the interstitial volume calculation could lead to a 15% error in the intracellular pyruvate measurement. For this reason, pyruvate and interstitial volume measurements were made for each of three extracts per steady-state, and the extracellular pyruvate concentration was measured at least three times. In a case in which the intra and extracellular pyruvate concentrations were nearly equal, the mean of three determinations of intracellular pyruvate would differ from the extremes by 15%. The measurements had some built-in inaccuracies, but it represents a superior procedure to one in which the filtered sample is thoroughly washed. Any such change in the cell's environment would likely lead to a drastic change in the intracellular pyruvate concentration, owing to the rapid turnover of the intracellular pyruvate pool. By not washing the filtered cells, it was hoped to preserve the environmental conditions existent in the fermentor for the 15 seconds from sampling to extraction. Large-scale changes in the intracellular pyruvate pool should be detectable by this method.

NADH ASSAY

The lactate dehydrogenase reaction used for the pyruvate assay is also applicable to the NADH assay, only this time, pyruvate is the added

reagent, and NADH is the unknown in the sample. The LS5 fluorometer with the identical settings as in the pyruvate assay was employed to measure the disappearance of NADH fluorescence at the 340nm, 460nm wavelength pair. The solutions prepared and the quantities pipetted into the cuvettes are shown in Table 4. A larger sample size was necessary, since the NADH concentration is generally lower than the pyruvate concentration. The pyruvate reagent concentration of 0.025 g/l is sufficient to drive the reaction to completion within the measurement resolution of the fluorometer; higher concentrations of pyruvate should be avoided, since it absorbs at either the excitation or emission wavelength and interferes with the assay. The procedure for temperature equilibration and reaction initiation is similar to the pyruvate assay, and the decrease in fluorescence with the reaction is equally straightforward. A calibration curve in the relevant concentration range is shown in Figure 12.

The extracts from the fermentor retained a blue color from the copper sulfate of the extraction solution. This color interfered with the assay by absorbing approximately 30% of either the exciting or emitted light. Also, the intensity of the color varied from sample to sample, because of slight differences in the pH. Consequently, an internal standard of a known concentration of NADH was added to each sample to correct for the light absorbance. The sample alone and the sample with the internal standard would be assayed. The concentration of the sample could then be calculated, given the linearity of the calibration curve. Reproducibility of repeated measurements indicated a precision of plus or minus 5%. At least three extracts from each steady-state were assayed on the same day as they were prepared.

INTRACELLULAR GLYCEROL ASSAY

Since glycerol is both intracellular and extracellular, the principles of the pyruvate assay were also applied here. The glycerol in the extract originating from the interstitial fluid in the filtered yeast paste was deducted from the total glycerol content to give only the intracellular contribution. Corrections were made for the glucose uptake and glycerol production during the 15 second interval between filtration and extraction. Equations 1 and 2 of the pyruvate section were applied in this case, only with the extract glycerol concentration, the extracellular glycerol concentration in the fermentor, and the specific glycerol production rate replacing the terms peculiar to the pyruvate assay. In most instances, the intracellular glycerol concentration exceeded the extracellular level by a factor of 10 or 20, so that the majority of the glycerol originated from inside the cell. The errors introduced in the pyruvate assay from the subtraction of a large extracellular contribution to the total level were avoided, and repeat measurements showed relatively little variance. The precision of this assay is plus or minus 5%. The glycerol concentration was measured with the HPLC with the maximum allowable 200 µl injection volume.

INTRACELLULAR ETHANOL

The same comments applying to the intracellular pyruvate and glycerol assays apply here. Equations 1 and 2 of the pyruvate section were used to separate the contributions of intra and extracellular ethanol to the extract ethanol concentration. Of course, ethanol concentrations and

the specific ethanol production rate replace the terms relevant to the pyruvate assay. The corrections for ethanol production and glucose uptake in the filtered paste in the delay before extraction were also made. The extract ethanol was measured in the HPLC with the maximum allowed 200 µl injection volume. To obtain the most accurate results, the peak integrations could not be blindly trusted, because of the relatively low ethanol concentration in the extracts ranging from 0.25 to 0.6 g/l. The attenuation of the integrator should be set so that the ethanol peak appears large. In this way, artifacts in the baseline that may alter the peak integrations may be detected. The best strategy was to impose a horizontal baseline at the base of the ethanol peak; the way this is done is described in the integrator manual. Peak area integrations from the samples were always compared manually to standards with a ruler.

It was found that the intracellular ethanol concentration does not differ significantly from the extracellular level. In such an instance, as discussed in the pyruvate section, approximately 2/3 of the ethanol in the extracted sample is contributed by extracellular ethanol. The usual assay errors are magnified by a factor of 3 in the final calculation of the intracellular ethanol. Adding to the errors in the ethanol measurements are the errors in calculating the interstitial volume in the yeast paste. Given these sources of error, 4 to 6 extracts were prepared for each steady-state in the fermentor. The deviation encountered in the assay is exemplified by the instance in which the mean of 6 extracts was 9.67 g/l of intracellular ethanol, and the maximum and minimum were 5.44 and 12.6 g/l. In another instance, the mean was 25.3, and the high and low were 26.8 and 24.2 g/l. In yet another instance, the mean was 23.2,

and the high and low were 25.3 and 20.4 g/l. From these numbers, one can see that a gram-per-liter resolution is not possible, but a prediction within 10 g/l is definite. Any large-scale changes in the intracellular ethanol from steady-state to steady-state in the fermentor can be seen.

Much controversy has surrounded the intracellular ethanol concentration measurements in the literature(1), stirred by reports of the accumulation of as much as 100-300g/l of intracellular ethanol in the early stages of batch growth(24,25). Dasari et al.(23) claim that these reports are all in error because of flaws in the sample preparation. Specifically, samples were centrifuged, and the yeast paste injected directly into a gas chromatograph. During the long time interval during the centrifugation, a large concentration of ethanol was newly produced in the dense yeast paste and incorrectly attributed to intracellular ethanol. Ethanol apparently continues despite refrigeration of the centrifuge. Compounding the problems of sample preparation is the fact that the yeast paste cannot be washed, because most of the intracellular ethanol diffuses out and is lost during the process(22).

Dasari et al.(23) devised a method based on a dense batch culture which eliminated the need to centrifuge the sample, avoiding the problematic step. They were able to show, contrary to previous claims, that intracellular ethanol never accumulates above extracellular levels, supporting the general knowledge that the cell membrane does not pose a transport barrier to ethanol.

This assay also avoids the accumulation of ethanol in the relatively short, 15 second filtration and extraction procedure. The correction factor to the intracellular ethanol concentration deriving from ethanol

produced during the extraction delay amounts to 8%, and this is included in the calculation. This method is certainly able to distinguish whether the claims of 300g/l intracellular ethanol concentrations or the challenges of Dasari et al. apply.

ENZYME ACTIVITY ASSAYS

The activities of all enzymes were assayed by following the rate of change of the absorbance of a reactant or product species of the enzymatic reaction in a Kontron Uvikon 810 spectrophotometer with a strip chart recorder and an RS232 interface connected to a printer. The wavelength of the absorbance measurements was adjusted to the properties of the particular species being measured and, differed among the different assays. Such details will be considered in the discussion of the individual assays. The instrument was equipped with enzyme kinetics software so that the rate of the reaction, given by the slope of the absorbance trace as a function of time, was printed out at the end of the reaction period. In addition, the absorbance as a function of time was graphically output to the strip chart recorder as the reaction proceeded. Three parameters specified to the kinetics software the needs of the particular assay, the cycle time, the dwell time, and the cycle number. The cycle time specifies the duration between two consecutive absorbance readings which are entered into the software to calculate the slope of the absorbance trace. A cycle time of 1 minute would imply that the machine obtains absorbance data points separated by 1 minute during the reaction. The cycle number is the total number of data points that the machine was programmed to take in the assay. The dwell time specified the length of

time that the absorbance was integrated in the registration of one data point. This parameter could range from 1 second to the cycle time minus 2 seconds. At the end of the assay period, the machine would print out the derivative of the absorbance change throughout the time course of the reaction. When several consecutive measurements gave the same derivative, the linear portion of the reaction had been reached, and the activity calculation was based on this derivative.

The temperature of all assays was maintained at 30 Celsius for all assays by circulating thermostatted water through the cuvette holder jacket.

For each bioreactor steady-state, at least 3 total activity determinations were made from 2 or 3 cell-free extracts. The typical variability of the results for all assays pointed to a precision of plus or minus 10% for all assays, owing primarily to variability between different extracts, and not repeated measurements of the same extracts.

HEXOKINASE ACTIVITY ASSAY

The hexokinase activity was measured by coupling its reaction to the production of NADPH, which has a strong absorbance at 340 nm(26) with an extinction coefficient of 6300 1/M-cm:

$$\text{Glucose} + \text{ATP} \xrightarrow{\text{Hexokinase}} \text{Glucose 6-phosphate} + \text{ADP}$$

$$\text{Glucose 6-P} + \text{NADP} \xrightarrow{\text{G6P Dehydrogenase}} \text{6P-Gluconate} + \text{NADPH}$$

An excess of glucose 6-phosphate dehydrogenase was provided in the assay so that the overall process was limited by the hexokinase activity.

The cycle time of the spectrophotometer was set to 30 seconds. The cycle number was 10 and the dwell time was 28 seconds, so that the duration

of the entire assay was 5 minutes. The time constant, or the damping of the recorder pen, was set to the minimum value of 0.2.

The solutions prepared for the assay, as well as the amounts of each pipetted into the cuvettes, are shown in Table 5. Originally, the assay method was based on the method presented by Maitra and Lobo(27). In particular, the tris buffer pH was chosen at a lower value of 7.4, and tris rather than citrate buffer was used to dissolve the ATP. With this procedure, the results were unsatisfactory in that the activities were 1/6 that required to match the rate of glycolysis. In searching for the cause of the anemic rate, it was found that trace quantities of aluminum present in commercial preparations of ATP can strongly inhibit the hexokinase activity, especially at low pH(28). The inhibition is reversed at higher pH values and by the chelating action of citrate and other buffers. Therefore, the reaction was carried out at PH 8.0, and the ATP was dissolved in citrate buffer. These changes boosted the activities to levels comparable to the glycolytic rate. Enzymes and metabolites were obtained from Sigma, and an additional glucose 6-phosphate dehydrogenase preparation was obtained from Boehringer. Sample sizes to introduce into the cuvette were chosen such that the resulting absorbance change was of the order of 0.04 units per minute, a rate at which the rate of the reaction is linear with the sample size.

The reaction was initiated by sample addition because the glucose 6-phosphate dehydrogenase preparations or both manufacturers had contaminating hexokinase activity. This activity was measured by following the trace of the absorbance increase before sample addition and subtracting this slope from that attained after sample addition. A typical trace of

the absorbance recreated from a strip chart recording is shown in Figure 13.

ALCOHOL DEHYDROGENASE

The reaction governing this assay is(29):

$$\text{Ethanol} + \text{NAD} \xrightarrow{\text{Alcohol Dehydrogenase}} \text{acetaldehyde} + \text{NADH} + H^+.$$

The product, NADH, absorbs at 340 nm with an extinction coefficient of 6300 1/M-cm(29). The settings of the spectrophotometer were identical to those of the hexokinase assay.

A list of all solutions and the quantities pipetted into the cuvette is shown in Table 6. Reagents were obtained from Sigma. The semicarbazide and the high PH of the buffer were necessary to drive the reaction forward. Semicarbazide is a trapping agent reacting with and removing the produced acetaldehyde, making the free energy change of the entire reaction more favorable. The buffer from the Sigma ethanol assay kit was used for convenience, since all components were present in the necessary concentrations. All other concentrations were based on the assay method of Maitra and Lobo(27). Sample sizes were chosen to maintain the rate of absorbance change at less than 0.07 absorbance units per minute to assure linearity of the measurement with the activity.

FUMARASE

The governing reaction is(30):

$$\text{Malate} \xrightarrow{\text{Fumarase}} \text{Fumarate} + H_2O \ .$$

The product, fumarate, strongly absorbs at 240 nm with an extinction coefficient of 2440 1/M-cm(30). The Uvikon was set identically to the hexokinase assay, with the exception of the wavelength. A list of the

reagents pipetted into the cuvette is shown in Table 7, and is based on the assay of Rogers and Stewart(31). Phosphate, rather than the tris buffer of the other assays, was used, as the reaction rate was found to decay with the latter but not the former.

Sample volumes were chosen to limit the reaction rate to 0.025 absorbance units per minute to assure linearity of the assay.

ISOCITRATE DEHYDROGENASE

The activity of the NAD linked isocitrate dehydrogenase was measured through the following reaction(32):

$$\text{Isocitrate} + NAD^+ \xrightarrow{\text{Isocitrate Dehydrogenase}} \text{Ketoglutarate} + CO_2 + NADH$$

The absorbance of the NADH was measured with the spectrophotometer with the identical settings as the hexokinase reaction. The reagents used are shown in Table 8 and are based on the assay of Polakis and Bartley(33). AMP is added as an activator of isocitrate dehydrogenase. Cysteine was present to maintain anaerobic conditions and thus to prevent the oxidation of the NADH produced by the reaction. A higher than usual sample volume was needed, since this activity was relatively low. The typical rate of absorbance change with the large sample was 0.010 units/min.

VIABILITY

The viability of the cells was assessed by a rapid methylene blue staining method devised by Lee et al.(34). Inviable cells are unable to exclude the blue dye from the cytoplasm. They can be distinguished from

viable cells by their attainment of a blue color visible under the microscope. The stain was prepared according to the formulation of Lee et al.(34), except that the glucose addition was eliminated, since the sample itself had plentiful glucose. The sample to dye was mixed in a ratio of 1:1 to 1:10, depending on the existing biomass concentration. This ratio was chosen to make the microscopic counting the most convenient.

3.3 RESULTS AND DISCUSSION

The results of all enzyme and metabolite assays is shown in Tables 9, 10, and 11. The assays were performed after steady-states had been established in the fermentor at the aeration rates indicated. Recall that this was actually the amount of air that was mixed with 500ccpm of pure nitrogen before entering the fermentor. The chronology of the steady-states is retained in the Tables. The assays correspond identically to runs 9 and 10 of the previous chapter with run 9 of a low feed antifoam concentration and run 10 of high antifoam.

As discussed in the previous chapter, the specific ethanol productivity and glucose uptake rate undergo sharp increases as the aeration rate is decreased in the parts-per-billion range of dissolved oxygen. It was concluded that the metabolic stimulation cannot occur as a result of a known mechanism. The Pasteur effect was excluded because several calculations and measurements showed that the contribution of respiration to the energy metabolism in this microaerobic range is negligible, with

less than 1% of the total ATP production being generated from oxidative phosphorylation. The Pasteur mechanism would require a significant reduction of ATP generation from respiration as the aeration is decreased, causing a drop in the energy charge of the cell and stimulating glycolysis at the allosterically regulated phosphofructokinase reaction(35). In addition, as the aeration rate was reduced, the biomass concentration in the fermentor also declined, leaving progressively greater concentrations of residual glucose in the medium. However, it was concluded that the metabolic stimulation could not be due to an increasing degree of saturation of the glucose transporter. Changes in the residual glucose from less than 1 g/l to near 50 g/l caused no visible change in the metabolic rate, but a sudden stimulation of metabolism occurred between 50 and 70 g/l of residual glucose. The two most obvious mechanisms for the glycolytic intensification were disproved. Some other stimulation of the glycolytic pathway of unknown origin was surmised. Such a stimulation could take the form of an increase in the activity of one or more of the enzymes of the glycolytic pathway or the glucose transporter. Also, it could take the form of the modulation of glycolytic enzyme activity by changing concentrations of regulatory metabolites such as the adenine and nicotinamide nucleotides.

Part of the aim of the enzyme and metabolite assays was to elucidate the cause of the metabolic stimulation. Intracellular metabolites at various stages of the glycolytic pathway spanning from the beginning to the end were assayed in search of a crossover point, i.e., a rate-limiting step. With a stimulation of fermentation, all metabolites upstream of the crossover point would be expected to be depleted, while those down-

stream would accumulate. The metabolites assayed, in order of their occurrence along the glycolytic pathway, were glucose 6-phosphate, intracellular glycerol, pyruvate, and intracellular ethanol. The glycerol production pathway branches from glycolysis in its reduction of dihydroxyacetone phosphate(35). Thus, the intracellular glycerol level is expected to be a reflection of the state of that portion of the glycolytic pathway. In addition to these metabolites, the role of the adenylate and nicotinamide nucleotides was investigated through the assay of the intracellular ATP and NADH levels. Finally, the activities of two representative glycolytic enzymes, alcohol dehydrogenase and hexokinase, were assayed.

The results of the assays, reported as the steady-state metabolite levels and enzyme activities as functions of the aeration rate are shown in Figure 14. Data only from the steady-states with low antifoam in the medium are included because the antifoam was found to interfere with the attainment of the higher metabolic fluxes. Also, the steady-state at the lowest aeration rate was excluded because of the reversal of the metabolic stimulation, to be discussed later, that occurred here. Glucose 6-phosphate, intracellular glycerol, and pyruvate all increased in concentration with the metabolic intensification. In addition, the specific glycerol and pyruvate production rates all increased in parallel with the specific ethanol production and glucose uptake rates. Every indication was that the limiting factor in glycolysis occurred before glucose 6-phosphate, and heightened fluxes emanating from all portions of the glycolytic pathway reflected a greater supply of metabolites from the source. The accelerated feeding of the glycolytic pathway was the responsibility of either the glucose transporter or the hexokinase reaction.

In Figure 14, the activity of hexokinase and alcohol dehydrogenase is also reported. It is evident that the glycolytic flux did not follow the hexokinase activity, as the latter decreased at the same time that the former increased. These hexokinase activities must be viewed with caution however. The quantities are approximately one- sixth the level necessary to support the glycolytic rate. It was later found that the origin of this discrepancy was most likely the presence of trace amounts of aluminum in the commercial ATP preparation, aluminum being a potent hexokinase inhibitor(28). The inhibition was later prevented by raising the pH of the assay buffer and dissolving the ATP in citrate buffer, a chelating agent. The sudden increase in the hexokinase activities reported in Table 10, after high antifoam was introduced, reflects the chronology with which the assay modifications were instituted. The higher activities were consistent with the glycolytic rate. It is hoped that, although the assays reported in Table 10 are not the true hexokinase activities, those values are in the same proportion to the true activities, with the enzyme's being inhibited to the same extent. The same pH, ATP source and buffers were used in all assays. Even if these assays are inaccurate, the modified assays also indicate that the glycolytic rate has no connection with the hexokinase activity. With the new assays, the hexokinase activity remained constant at 2.05×10^{-4} moles per gram dry-weight per minute, even as the specific glucose uptake rate changed from 2.03 to 2.38 to 2.60 g/g-hr.

Another possibility of the involvement of hexokinase in the metabolic intensification would be its activation by an increased concentration of ATP, one of the enzyme's substrates. Inspection of Figure 14 reveals

that the ATP concentration did increase simultaneously with the glycolytic flux. However, the lowest intracellular concentration of ATP measured, 1.75 mM, assuming 0.002 cc intracellular volume per gram dry-weight(23), is one order of magnitude greater than the half-saturation coefficient of this reaction with respect to ATP(35). It is doubtful that the modulation of the enzyme activity could have an effect when changes in the maximal activity had none.

The most likely possibility remaining is the glucose transporter itself as the activator of the metabolism. Changes in the transporter activity are not a new observation in *Saccharomyces cerevisiae*. Spoerl et al.(36) demonstrated that the glucose transporter is more active in the presence of a metabolizable sugar than in its absence, and that inhibitors of glycolysis as iodoacetate also decrease transporter activity. There is a clear connection between the transporter activity and the energetic state of the cell. In addition, amino acids activated, and inhibitors of protein synthesis deactivated, the solute transporter, indicating that the state of the protein-synthesizing machinery is also relevant to the transport activity. Finally, these authors observed a decay in the transporter activity when the enhancing factors were removed(36). It was theorized that the transporter is subject to continual synthesis and degradation, with synthesis requiring both ATP energy and an intact protein synthesis. The final activity attained strikes a balance between the two opposing processes, and is, therefore, dependent on the energy state of the cell. Serrano and De La Fuente(37) and Bisson and Fraenkel(38) also reported changes in the transporter properties in response to the metabolic state and the aerobic adaptation of the cells.

Some factor motivated by the decrease in the aeration rate caused the increased transporter activity in this study. Speculation about what this factor might have been is presented in Figure 15a. The activation of the transporter, as indicated by the specific glucose uptake rate is accompanied by an identical increase in the ATP concentration. Data from all steady-states in which the ATP concentration was measured, including data from the high antifoam run, are included in the figure. One can argue that the correlation between these two parameters arises simply because the ATP is a product of catabolism and would naturally respond in the identical manner as the catabolic rate. However, this argument is now reversed in the conjecture that the higher ATP concentration was the cause of the increased transporter activity. Such a claim is consistent with the findings of Spoerl et al.(36), if the ATP activates the transporter by enhancing its synthesis.

In Figure 15b, the specific glucose uptake rate is plotted against the residual glucose concentration to demonstrate the unlikelihood that kinetics of the transporter with respect to glucose is the sole cause of the increased transport activity. Both the high and low antifoam cultures have the same specific glucose uptake rate approximately 2.0 g/g-hr despite a 50% difference in the residual glucose concentration, 22.0 g/l for the high antifoam culture, and 36 g/l for the low antifoam culture. These points occurred at the highest aeration rate, where the ATP concentrations of the two cultures were nearly the same. In addition, a sharp inclination of the transport rate occurs above a 70 g/l residual glucose concentration in the high antifoam culture, reminiscent of the sharp increase that occurred after a relative lull at lower glucose concentra-

tions in run 5(Chapter 2). No ordinary saturation kinetics can explain such behavior.

A complication with the view that ATP activates the transporter is the presence of positive feedback. ATP would be both the cause and the result of the higher metabolic rate. As the ATP content increases, the transporter is activated, resulting in a higher glycolytic flux and the production of even more ATP. The process would perpetuate itself until the glycolytic rate climbed to a level at which the process became saturated. In one sense, the positive feedback mechanism is of the type necessary to cause the sudden changes in the metabolic rate actually observed. However, mechanism this must still operate together with another mechanism, because otherwise, glycolysis would always occur at the same maximal rate.

The above argument takes into account the production of ATP by glycolysis and its newly found regulatory mechanism, not the ATP utilizing processes of biosynthesis, maintenance, and ATP wastage by ATPases and futile cycling(39). The ATP requirement for biosynthesis should be stoichiometrically related to the amount of matter biosynthesized. Theoretical calculations(39) indicate that approximately 29 grams of biomass should be formed from 1 mole of ATP energy, based on the known stoichiometries and weighted sums of all biosynthetic pathways. However, in this and in other studies, The ATP yield was found to be of the order of 8-12 grams per mole. Lagunas(40) has remarked that this vast discrepancy between the theoretical and the actual yield in yeast indicates an unknown utilization of ATP for other than biosynthesis. This ATP utilization could not be accounted for by the cmaintenance requirements of the

cell. Stouthamer(39), noting the same discrepancy in bacteria, discovered that 50% of the catabolic ATP production in *E. coli* goes towards cell membrane energization, accounting for a large part of the missing utilization. The proton gradient across the cell membrane in *E. coli* has to be continually restored by ATP hydrolysis by membrane-bound ATPases, since the membrane is leaky to protons. Whether this leakiness is important to the cell or whether it is an outright waste of ATP is unknown(39). However, a precedent has been set for the significant hydrolysis of ATP by the subversion of energy-conserving processes.

ATP utilization by waste reactions may be of importance to the other mechanism described, especially since it represents negative feedback. ATP waste by the ATPases, for example, is expected to become stronger as the ATP concentration increases. If this negative feedback mechanism is added to the positive feedback mechanism previously described, then the previously discussed problems can be averted. If the ATP concentration increases, then as before, the glucose transporter is activated, leading to accelerated glycolysis and the further increase in the ATP concentration. However, unlike before, the process cannot activate itself perpetually because the increasing ATP concentration has a progressively stronger sink in the waste reactions. The steady-state ATP concentration, transport activity and degree of ATP wastage represents a balance among these processes. The fact that the steady-state levels all change with the aeration rate may mean that oxygen directly influences the transport or ATP utilizing activity. Later in the discussion, more evidence is presented that oxygen changes the activity of the forces, causing waste and destruction of ATP.

Attention is now turned to the very important phenomenon that occurs as the aeration rate is further decreased to the lowest levels supplied in these studies. The 30 to 50% metabolic intensification reverses itself and a glycolytic rate characteristic of the highest aeration rates is restored. The cause of this reversal is again investigated with a view towards a crossover point or a rate-limiting step. In this instance, the metabolic slowdown would result in the accumulation of metabolites upstream of the crossover point and the depletion of those downstream.

In Figure 16, the results of the intracellular metabolite and enzyme assay are shown together with the decline in the glycolytic rate. From among all steady-states studied, those towards the lowest aerations of the low antifoam run are represented in this Figure. The glucose 6-phosphate, intracellular glycerol(Table 9), specific glycerol production rate, ATP, and NADH increase in opposition to the decrease in the specific glucose uptake and specific ethanol production rates. In contrast, the specific pyruvate production rate and pyruvate concentration decrease. With the aid of the diagram in Figure 17, all of these tendencies can be explained if the rate-limiting step is either the pyruvate kinase or the phosphoglycerate kinase reaction. Furthermore, the explanation is most satisfactory if the cause of the rate limitation is the accumulation of ATP, the product of both reactions, or the associated decrease in ADP, the substrate of both reactions.

Assume that some event external to the glycolytic pathway causes an energetic surplus in the cell, resulting in an increase in the energy charge, or better, the ATP/ADP ratio of the cell as the aeration rate is

decreased to the lowest point. Such an event would account for the increase in the ATP concentration that was actually observed(Figure 17). The heightened ATP/ADP ratio could slow the glycolytic rate, as was actually observed, by making conditions for the phosphofructokinase, pyruvate kinase, or phosphoglycerate kinase reactions suboptimal. It is well known that phosphofructokinase is allosterically inhibited by ATP and activated by ADP and AMP. In addition, ADP is a substrate and ATP a product of the downstream kinases. The limitation of the glycolytic rate by one or more of these reactions would cause the accumulation of metabolites upstream and depletion of those downstream. The observed accumulation of glucose 6-phosphate would support all three candidates for rate limitation, since this is the first metabolite in glycolysis (Figure 17). However, the minor accumulation(Table 9) of intracellular glycerol and the significant increase in the specific glycerol production rate would argue against phosphofructokinase as the rate limiter, but support the pyruvate kinase and phosphoglycerate kinase reactions equally. The glycerol production pathway originates in the reduction of the glycolytic intermediate dihydroxyacetone phosphate(35), downstream of phosphofructokinase but upstream of the other kinases. The observed depletion of the intracellular pyruvate and diminution of the specific pyruvate production rate are also consistent with the crossover at the kinases. The 3-fold increase in the NADH concentration is also in accord with the crossover at one of the downstream kinases. NADH is a product of the 3-phosphoglycerate dehydrogenase reaction upstream of the kinases and a substrate of alcohol dehydrogenase, downstream(Figure 17). The NADH concentration, to an approximation, reflects a balance between the oxi-

dizing and reducing actions of these two glycolytic enzymes, likely the most active of the cell's oxireductases. A slowdown in glycolysis between these reactions would hinder NADH oxidation by alcohol dehydrogenase by limiting the supply of the substrate acetaldehyde. In contrast, the upstream dehydrogenase would be amply fed. Thus, a sudden rise in the NADH concentration may be a consequence of the transient inability of the downstream oxidation to keep pace with the upstream reduction. An increased NADH/NAD ratio would tune the upstream dehydrogenase activity to the overall rate of glycolysis.

In the Pasteur effect, the energetic surplus of the cell induced by the onset of respiration results in an increase of the energy charge (41,42). This process is quite analogous to the energy surplus attained by some other mechanism as the aeration rate was decreased in this study. However, most studies of the Pasteur effect point to phosphofructokinase as the target of the altered adenylate level. The findings of den Hollander et al.(41) might indicate that phosphofructokinase may yet have taken part in the glycolytic regulation in this study. Those investigators measured numerous intracellular metabolites by NMR spectroscopy to gauge the Pasteur response to the onset of respiration. The resulting change in the adenylate and phosphate levels and the kinetics of the PFK reaction with respect to these components strongly indicated PFK inhibition of glycolysis. Yet, despite PFK regulation, products downstream of the reaction as fructose diphosphate and 3-phosphoglycerate accumulated. The authors concluded that an additional downstream step, most likely pyruvate kinase, had to share in the regulation. Based on these results, it is possible that phosphofructokinase had a regulatory role in the

present study, despite NADH accumulation and enhanced glycerol production. However, as in the study of den Hollander et al., a downstream kinase shared in the regulation.

The event motivating the slowdown of glycolysis was an energetic surplus resulting in ATP accumulation. A surplus could result only if biosynthesis became energetically more efficient or ATP waste processes abated as the aeration was reduced. This is the second instance in which oxygen is implicated as an influencer of ATP utilization. At the high aeration rates, it was speculated that the ATP level found a balance between glycolytic production and the utilization by ATPases and other processes. Wastage was necessary to counterbalance the positive feedback mechanism by which ATP activated the glucose transporter. The fact that the ATP level, transport rate, and ATP waste changed with the aeration rate raised the possibility that oxygen also alters the ATP waste activity at the higher aeration rates. Therefore, there may be common elements to the two opposing processes, the stimulation of the glycolytic flux as the aeration was decreased, and the reversal of the entire process as the aeration further decreased. An attempt is now made to unify these dichotomous processes under a single mechanism involving the effect of oxygen on the ATP wasting of the cell.

A measure of the efficiency of biosynthesis is the ATP yield, Y_{atp}, or the number of grams of biomass synthesized per mole of ATP expended(39). This is easily calculated, knowing the specific growth and ethanol and glycerol production rates and the facts that 1 mole of ATP is generated for each mole of ethanol produced, and one mole of ATP is consumed for each mole of glycerol excreted(35). As the influence of oxygen on the

ATP utilizing is suspected, it is of interest to examine the ATP yield as a function of the aeration rate, as is done in Figure 18. The high and low antifoam runs are shown separately. With low antifoam in the medium, the parameter passes through a minimum at low aeration rates and resembles a mirror image of the specific ethanol production rate profile. It would be tempting to explain these changes in the ATP yield by simply stating that a decrease in the dissolved oxygen level decreases the ATP yield to a certain point, whereupon it suddenly increases the ATP yield. However, the known effects of oxygen upon the cell metabolism and physiology are all monotonic processes; these include the induction of respiratory enzymes and structures and the enhancement of the synthesis of unsaturated fatty acids and sterols(31,33,43). In addition, a decrease in the ATP yield, or the efficiency of growth as the aeration was reduced to all but the lowest levels, cannot explain the fact that the ATP concentration, and presumably the energy, is increasing.

The efficiency of ATP utilization is perhaps not best characterized by the ATP yield. Assume, for simplicity, that all ATP wasting is done by a single ATPase. As an enzyme, this ATPase has a monotonic kinetic rate with the ATP concentration. The total rate of ATP hydrolysis would be given by the activity of the ATPase and the degree of its saturation by the adenine nucleotide. With a simple model, this rate is:

$$R_w = R^{max} \frac{ATP}{K_{atp} + ATP} ,$$

where R_w = rate of ATP waste
R^{max} = activity of ATPase
K_{atp} = half saturation constant

$$ATP = \text{ATP concentration} \quad .$$

In the very simplest instance, the Michaelis Menten constant would be large compared to the ATP concentration, and the rate would be:

$$R_w = ATP\ R_{max} \quad .$$

Therefore, a fundamental study of ATP wastage would be concerned more with the activity of the ATPase than with the total rate of ATP hydrolysis.

If this analogy with a simple ATPase is extended to all ATP waste reactions, then the waste activity might be characterized by the total rate of waste divided by the ATP concentration. A suitable measure of the energy waste would be the inverse of the ATP yield, $1/(Y_{atp})$. Therefore, in Figure 19, $1/(Y_{atp} \times \underline{ATP})$ is plotted against the aeration rate, with all steady-states, including the high-antifoam ones, represented. As can be seen, this ratio behaves monotonically with the aeration rate and actually resembles a saturation-type profile. Therefore, the capricious changes in the ATP yield can be explained on the basis of component monotonic processes. With reference to Figure 18, reduction of the aeration rate in the low antifoam run lead to a decrease in the ATP yield, not because the activity of the ATP wasting enzymes increased, but because the ATP concentration was increasing; the activity of ATP utilizing enzymes were presumably decreasing monotonically with the decreasing aeration rate. It will be shown in Chapter 4 that the behaviors of the metabolic rate, ATP wastage, and ATP concentration can be explained with three monotonic processes:

1) ATP monotonically increasing the transport activity
2) Oxygen monotonically increases the activity of ATP waste
3) ATP waste increases monotonically with increasing ATP .

The saturation profile of $1/(Y_{atp} \times ATP)$ may be accidental, but is noteworthy. Rogers and Stewart(31) noted a very similar induction of respiratory enzyme activities by oxygen that became half-saturated in the parts-per-billion range of dissolved oxygen where respiration was negligible. It is possible that ATP utilizing enzymes such as ATPases are similarly induced by low levels of oxygen. Perlman and Mahler(43) observed that the mitochondrial ATPase activity closely followed the activities of numerous respiratory enzymes in response to glucose derepression. Rogers and Stewart(44) calculated a decrease in the ATP yield and increase in the ATP maintenance requirement under aerobic, compared to anaerobic, conditions. This, they concluded, was due to the biosynthesis of more complicated cellular structures during aerobic growth associated with respiration. It is possible that the increased ATP utilization with increasing aeration here is a manifestation of the induction of respiratory structures and mitochondrial ATPases, despite the minimal degree of respiration.

Another goal of the enzyme and metabolite assays was the elucidation of the effect of silicone polymer antifoam on the microbe's metabolism. In Chapter 2, antifoam was described as causing the diversion of carbon skeletons away from ethanol production and towards glycerol production, and possibly the inhibition of glucose uptake. As a result, cultures with high feed antifoam concentrations had lower specific glucose uptake and ethanol production rates, but higher specific glycerol productions. In Figure 20, the specific glycerol productivity is plotted against the driving force for glycerol efflux, which is the concentration difference between intracellular and extracellular glycerol. Clearly, efflux at a

given driving force is enhanced by the high antifoam, suggesting that high antifoam decreased the resistance to diffusion across the cell membrane. A change in the transport resistance is not an entirely satisfactory explanation. An experiment was carried out in which 20 g/l of glycerol was introduced into the feed medium containing high antifoam. The 20 g/l matched the existent intracellular glycerol concentration. As a result, the intracellular glycerol concentration increased to 40 g/l and preserved the 20 g/l driving force for transport. The specific glycerol production rate decreased by only 15% in this exercise. Nonetheless, it is clear that higher glycerol productivities are attained with high antifoam in the medium(Chapter 2).

The robbing of metabolites from ethanol production had a dire consequence for the cell in that the prevention of the attainment of high ethanol productivities resulted in the precipitous drop in the biomass concentration as the aeration rate was decreased. This drop was never seen under conditions in which the high specific ethanol productivity was attained. Based on these facts, it was concluded that the increased specific ethanol productivity was a built-in mechanism possessed by the cell to generate a sharp increase in the ATP production in response to a sudden need. Without the additional ATP, catastrophic events such as the extinction of the biomass concentration resulted. It has already been shown that with low feed antifoam, the metabolic intensification with decreasing aeration does indeed produce a greater ATP concentration. It is now shown in Figure 21a that high feed antifoam concentrations prevented the attainment of the same high ATP concentrations; the latter was lower at each aeration rate in the high antifoam case compared to

the low antifoam. Figure 21b indicates that the lower ATP concentration was the result of a more sluggish specific ethanol productivity, the supplier of ATP. Figure 21c shows the consequences of the lower ATP concentration, the sudden drop in the biomass and ethanol concentration that was otherwise prevented. Runs 6, 7 and 8 are represented in Figure 21c.

In Chapter 2, it was mentioned that the high antifoam cultures had a lower glucose transport rate than the equivalent low antifoam cultures. This lower transport rate can be accounted for by the lower ATP concentration in the high antifoam culture just discussed, assuming that the glucose transporter is activated by ATP. This observation provides more evidence for the proposed mechanism. The generally higher ATP yield in the high antifoam culture and the relative constancy of it(Figure 18) can also be explained on the basis of the ATP pattern. The lower ATP concentration provided for a lesser degree of wasting by the ATPases, improving the energetic efficiency of growth. This observation further supports the contention that ATP utilizing reactions are invigorated by higher ATP concentrations.

A raging controversy exists in the literature regarding the role of intracellular ethanol in ethanol-producing yeast cultures. Reports have been issued of the accumulation of 100-300 g/l of intracellular ethanol (24,25) in the early phases of batch culture. If these claims are valid, intracellular ethanol inhibition is likely to be the most dominant force in all kinetic processes. However, Dasari et al.(23) have disputed the claims of the accumulation of intracellular concentrations above extracellular levels, condemning the measurement methods of previous investi-

gators as faulty. The primary complaint was the long period of time required for the centrifugation of cell samples for the intracellular ethanol assay. During this time, the dense yeast pellet would accumulate high concentrations of newly produced ethanol in the small volume, and this would incorrectly be attributed to intracellular ethanol. Dasari et al. devised a method of assay in a dense yeast culture that circumvented the centrifugation step. They concluded that there is little or no difference between the intracellular and extracellular ethanol concentrations, even in early batch culture. This view is supported by the present data, shown in Figure 22, in which the extracellular ethanol is plotted against the intracellular level. As discussed in the Material and Methods section, the assay method was immune to the pitfalls mentioned by Dasari et al. The data do not permit the distinction between intra and extracellular ethanol levels, given the experimental error and the fact that a literature value of 2cc of intracellular volume occupied by 1 gram of dry weight of yeast(23) was entered into the calculation.

Rogers and Stewart(31) found a sharply increasing respiratory enzyme activities with increasing dissolved oxygen concentrations in the micro-aerobic range. It was of interest to see whether the same thing occurred in the present investigation. In Figure 23, the activities of fumarase and isocitrate dehydrogenase, two TCA cycle enzymes, are shown as a function of the aeration rate. In most cases, the isocitrate dehydrogenase activity decreases with increasing aeration in opposition to the literature result. The fumarase activity does not show a consistent pattern with the aeration. However, part of the difficulty in the seemingly chaotic behavior may be related to the discontinuous chronology with which the

steady-states at different aerations were attained. For example, the increase in the fumarase activity at the very lowest, compared to the second lowest aeration, may relate to the fact that the former was attained more than one month later than the latter. During the intervening time, adaptation of the cells to their environment may have enabled the cells to attain a higher fumarase activity at even a lower aeration rate. For the same reason, the observation that both TCA cycle enzymes are more active in the high antifoam cultures may arise from the introduction of high antifoam to the medium after the low antifoam steady-states were finished. An alternate explanation of the behavior of isocitrate dehydrogenase is provided shortly. In any event, the isocitrate dehydrogenase activity was two orders of magnitude, and the fumarase activity one order of magnitude lower than the typical glycolytic enzyme activity. Neither appeared to exert a profound influence on the overall metabolic rate of the cell.

The importance of glycerol production to the cell is questionable, since no ATP is generated, and no building blocks of biosynthesis are derived from the pathway(35). It has been speculated that under anaerobic conditions, where respiration is nonexistent, glycerol production oxidizes the surplus NAD(P)H produced in the biosynthetic reactions, maintaining the redox balance of the cell(45). Of course, the glycolytic pathway cannot participate in this task, since it is redox-balanced. Based on the elemental composition of biomass(46), it can be calculated that approximately 1 mole of NADH reducing power is generated in the biosynthesis of one carbon mole of biomass, which is enough to support the production of 0.08 g/g-hr of glycerol at the specific growth rate of

0.2g/g-hr. However, specific glycerol productivities ranging from 0.065 to 0.4 g/g-hr have coexisted with the specific growth rate of 0.2/hr. This means that the rate of NADH oxidation in this pathway far surpasses the need imposed by biosynthesis; additional NADH generation by other processes must now be accounted for.

Glycerol production in this study has been governed by factors other than redox considerations. The specific glycerol production rate increased with the general metabolic stimulation, as the aeration was reduced to all but the lowest rates(Figure 14). Presumably, the more active glucose transporter was able to increase the concentration of dihydroxyacetone phosphate, the first metabolite in the glycerol production pathway, as it was able to increase the concentration of all intracellular metabolites. When the lowest aeration was reached, a bottleneck downstream of dihydroxyacetone phosphate probably caused its accumulation and the further stimulation of glycerol production(Figure 17). When high antifoam was added to the medium, glycerol production was enhanced, possibly because of the decreased resistance to its transport across the cell membrane(Figure 20). Therefore, glycerol production seems to respond to the rate at which its pathway is fed glycolytic intermediates, and the rate at which the product is removed from the cell. The need to oxidize NAD(P)H from biosynthesis does not enter into consideration. Rather, glycerol production seems to place a burden on other cell processes to supply NADH.

If glycerol production actually responded to the need to oxidize NADH, then a correlation between the specific glycerol production rate and the NADH concentration would be expected. In Figure 24, the relation-

ship between these variables is shown. At intermediate NADH concentrations, an inverse of the expected behavior is seen, meaning that, in this region, the NADH level is a consequence, not a cause of the specific glycerol productivity.

As mentioned, there is a need for other processes to supply NADH. In Chapter 2, it was shown that typically 90-95% of the glucose carbon taken up by the cell is recovered in the products ethanol, glycerol, biomass, and the associated CO_2 production. The remaining 5-10% of the carbon must be excreted as products of a relatively low degree of reductance, to satisfy both the carbon and redox balances. No additional, significant peaks eluted in the HPLC analyses of the supernatants. Most likely, small amounts of an entire spectrum of compounds, such as acetate, succinate, pyruvate, acetaldehyde, and fusel oils(45) were discharged.

One possible source of NADH is the dehydrogenase activity of the TCA cycle. As is seen in Table 10, isocitrate has a small but nonzero activity. This allows for the complete oxidation of glucose by glycolysis and the TCA cycle in the reaction:

$$6\ H_2O + C_6H_{12}O_6 + 4\ ADP + 12\ NAD \longrightarrow 12\ NADH_2 + 4\ ATP + CO_2 .$$

Glycerol production from glucose occurs as(35):

$$6\ C_6H_{12}O_6 + 12\ NADH_2 + 12\ ATP \longrightarrow 12\ C_3H_8O_3 + 12\ NAD + 12\ ADP .$$

A partial coupling can occur between the two reactions, but with a net loss of 8/7 high energy phosphate bonds for each glucose molecule processed in this way. Assuming that isocitrate dehydrogenase is the rate-limiting enzyme in the TCA cycle, this coupling process can account for an addi-

tional specific glycerol productivity ranging from 0.065 to 0.16 g/g-hr, a substantial fraction of the actual productivity. However, oxoglutarate oxidase has been found to be less active than isocitrate dehydrogenase under conditions of respiratory incompetence(33).

In Figure 25, the relationship is shown between the specific glycerol productivity and the isocitrate dehydrogenase activity. There is a general correlation between these two variables, with the exception of the highest glycerol productivity. However, this point occurred at the lowest aeration rate, at which the specific glycerol productivity was stimulated by a downstream bottleneck. It is argued that the specific glycerol productivity does not respond to the higher NADH supply of the more active isocitrate dehydrogenase. To the contrary, the isocitrate dehydrogenase activity is deployed to contribute to the general NADH demand placed on the cell by glycerol production.

Because of the low activity of oxoglutarate oxidase under anaerobic conditions, it has been proposed that the TCA cycle separates into two branches, with oxoglutarate being produced oxidatively and succinate reductively(45)(Chapter 1, Figure 6). Redox considerations in this study disfavor reductive succinate production, and thus the entire concept of branching.

Recorded in Table 11 is the viability of the cell population at the various aeration rates of runs 9 and 10. In all cases, the viability exceeded 95%. Inviability does not enter into consideration of the metabolic phenomena observed.

3.4 CONCLUSIONS

The utility of enzyme and intracellular metabolite assays in the elucidation of new metabolic phenomena has been demonstrated. Where metabolic phenomena can be attributed to one or to a few pathways, the assays provide a means to assess rate limiting steps in the phenomenon and the causes of rate limitation.

In this study, the metabolic phenomenon was an acceleration of the metabolic rate with decreasing aeration and the reversal of the intensification with further aeration reduction. Assays of intracellular metabolites spanning the glycolytic pathway implicated the glucose transporter as the rate-limiting step in the metabolic acceleration, and the downstream kinases were the rate-limiting steps in the reversal.

The enzyme and cofactor assays were also instrumental in determining the causes of the metabolic changes, as the rate of enzymatic reactions must follow the maximum enzyme activity and its modulation by cofactors as ATP, NAD, etc. The transporter activity was best correlated with the intracellular ATP concentration, which led to the conclusion that ATP is a likely activator of glucose transport. The accumulation of ATP at the lowest aeration rate made conditions suboptimal for the downstream kinases, as ADP is reactant and ATP a product of these reactions.

The assays also exposed important metabolic regulations external to the immediate glycolytic pathway. The accumulation of ATP at the lowest aeration rate indicated that the energetic efficiency of growth must change, and that oxygen is a likely cause of the energetic changes. Also, the energetic efficiency was inversely correlated to the ATP concentration, indicating that ATPases and other ATP waste reactions partially governed the growth efficiency. This conclusion would have been impossible

without the ATP concentration measurements to compare to the growth efficiency. In addition, stimulation of glycerol production by antifoam was traced to a possible enhancement of glycerol transport across the cell membrane. To obtain this information, it was necessary to measure the intracellular glycerol concentration, and thus, the driving force for glycerol export. Finally, the ATP measurement fostered speculation that the sudden extinction of the biomass concentration in the fermentor with small environmental changes was caused by a shortage of ATP energy.

REFERENCES

1. Bergmeyer, H.A., *Methods of Enzymatic Analysis*, vol. II, 3rd ed., Verlag Chemie: Deerfield Beach, FL, 1983, p. 66.

2. Hughes, D.E., Wimpenny, J.W.T., and Lloyd, D., "Disintegration of Microorganisms," in *Methods of Microbiology*, vol. 5B, eds. Norris, J.R. and Ribbons, D.W., Academic: NY, 1971, p. 1.

3. Rogers, P.J. and Stewart, P.R., "Mitochandrial and Peroxisomal Contribution to the Energy Metabolism of *Saccharomyces cerevisiae* in Continuous Culture," *J. Gen. Microbiol.*, 79, 205, 1973.

4. Gorts, C.P.M., "Effect of Different Carbon Sources on the Regulation of Carbohydrate Metabolism in *Saccharomyces cerevisiae*," *Antonie van Leeuwenhoek*, 33, 451, 1967.

5. Oura, E., "Effect of Aeration Intensity on the Biochemical Composition of Baker's Yeast. II. Activities of Oxidative Enzymes," *Biotechnol. Bioeng.*, 16, 1213, 1974.

6. Beck, C. and Meyenburg, H.K. von, "Enzymatic Pattern of Aerobic Growth of *Saccharomyces cerevisiae* under Various Degrees of Glucose Limitation," *J. Bact.*, 96, 479, 1968.

7. Davison, B.H., Dynamics and Coexistance of Microbial Mixed Cultures, Doctoral Dissertation, Calif. Inst. Tech., Pasadena, CA, 1985.

8. Lowry, O., Rosebrough, N., Farr, A., and Randall, R., "Protein Measurement with the Folin Phenol Reagant," *J. Biol. Chem.*, 193, 265, 1951.

9. Weibel, K.E., Mor, J.R., and Fiechter, A., "Rapid Sampling of Yeast Cells and Automated Assays of Adenylate, Citrate, Pyruvate, and Glucose 6-Phosphate Pools," *Anal. Biochem.*, 58, 208, 1974.

10. Chapman, A.G. and Atkinson, D.E., "Adenine Nucleotide Concentrations and Turnover Rates. Their Correlation with Biological Activity in Bacteria and Yeast," *Adv. Microb. Physiol.*, 15, 253, 1977.

11. Franco, C.M.M., Smith, J.E., and Berry, D.R., "Effect of Nitrogen and Phosphate on the Levels of Intermediates in Baker's Yeast Grown in Continuous Culture," *J. Gen. Microbiol.*, 130, 2465, 1984.

12. Kleinzeller, A. and Kotyk, A., "Transport of Monosaccharides in Yeast Cells and its Relationship to Cell Metabolism," in *Aspects of Yeast Metabolism*, eds. Mills, A.K. and Krebs, H., Blackwell: Oxford, 1968, p. 33.

13. Serrano, R. and De La Fuente, G., "Regulatory Properties of the Constitutive Hexose Transport in *Saccharomyces cerevisiae*," *Molec. Cell. Biochem.*, 5, 161, 1974.

14. Lowry, O.H., Passanneau, J.V., and Rock, M.K., "The Stability of Pyridine Nucleotides," *J. Biol. Chem.*, 236, 2756, 1961.

15. Bartley, W. and Polakis, E.S., "Changes in the Intracellular Concentrations of Adenosine Phosphate and Nicotinamide Nucleotides during the Aerobic Growth Cycle of Yeast on Different Carbon Sources," *Biochem. J.*, 99, 521, 1966.

16. Ludin, A. and Thore, A., "Comparison of Methods for Extraction of Bacterial Adenine Nucleotides Determined by Firefly Assay," *Appl. Microbiol.*, 30, 713, 1975.

17. Bergmeyer, H.A., loc. cit., vol. III, p. 261.

18. Lehninger, A.L., *Biochemistry*, Worth: New York, 1975. p. 427.

19. Bergmeyer, H.A., loc. cit., vol. III, p. 358.

20. Webster, J.J. and Leach, F.R., "Optimization of the Firefly Luciferase Assay for ATP," *J. Appl. Biochem.*, 2, 469, 1980.

21. Ludin, A. and Thore, A., "Analytical Information Obtainable by Evaluation of the Time Course of Firefly Bioluminescence in the Assay of ATP," *Anal. Biochem.*, 66, 47, 1975.

22. Beaven, M.J., Charpentier, C., and Rose, A.H., "Production and Tolerance of Ethanol in Relation to Phospholipid Fatty-Acyl Composition in *Saccharomyces cerevisiae* NCYC 431," *J. Gen. Microbiol.*, 128, 1447, 1982.

23. Dasari, G., Keshavarz, E., Connor, M.A., and Pamment, N.B., "A Reliable Method for Detecting the Intracellular Accumulation of Fermentation Products: Application to Intracellular Ethanol Analysis," *Biotechnol. Lett.*, 7, 541, 1985.

24. Navarro, J.M. and Durand, G., "Fermentation Alcoolique: Influence de la Temperature Sur l'Accumulation d'Alcool dans les Cellules de Levure," *Ann. Microbiol. (Inst. Pasteur)*, 129B, 215, 1978.

25. Novak, M., Strehaiano, P., Moreno, M. and Goma, G., "Alcoholic Fermentation: on the Inhibitory Effect of Ethanol," *Biotechnol. Bioeng.*, 23, 201, 1981.

26. Bergmeyer, A.H., loc. cit., vol. II, p. 222.

27. Maitra, P.K. and Lobo, Z., "A Kinetic Study of Glycolytic Enzyme

Synthesis in Yeast," *J. Biol. Chem.*, 246, 475, 1971.

28. Womack, F.C. and Colowick, S.P., "Proton-Dependent Inhibition of Yeast and Brain Hexokinases by Aluminum in ATP Preparations," *Proc. Nat. Acad. Sci.*,76, 5080, 1979.

29. Bergmeyer, A.H., loc. cit., vol. II, p. 139.

30. Ibid., p. 189.

31. Rogers, P.J. and Stewart, P.R., "Respiratory Development in *Saccharomyces cerevisiae* Grown at Controlled Oxygen Tension," *J. Bact.*, 115, 88, 1973.

32. Bergmeyer, A.H., loc. cit., vol. II, p. 230.

33. Polakis, E.S. and Bartley, W., "Changes in the Enzyme Activities of *Saccharomyces cerevisiae* during Aerobic Growth on Different Carbon Sources," *Biochem. J.*, 97, 284, 1965.

34. Lee, S.S., Robinson, F.M., and Wang, H.Y., "Rapid Determination of Yeast Viability," Bio*technol. Bioeng. Symp.*, 11, 649, 1981.

35. Sols, A., "Regulation of Carbohydrate Transport and Metabolism in Yeast," in *Aspects of Yeast Metabolism*, eds. Mills, A.K. and Krebs, H., Blackwell: Oxford, 1967, p. 47.

36. Spoerl, E., Williams, J.P. and Benedict, S.H., "Increased Rates of Sugar Transport in *Saccharomyces cerevisiae* a Result of Sugar Metabolism," *Biochem. Biophys. Acta*, 298, 956, 1973.

37. Serrano, R. and De La Fuente, G., "Regulatory Properties of the Constitutive Hexose Transport in *Saccharomyces cerevisiae*," *Mol. Cell. Biochem.*, 5, 161, 1974.

38. Bisson, L.F. and Fraenkel, D.G., "Expression of Kinase Dependent Glucose Uptake in *Saccharomyces cerevisiae*," *J. Bact.*, 159, 1013, 1984.

39. Stouthamer, A.H., "The Search for Correlation Between Theoretical and Experimental Growth Yields," in *Microbial Biochemistry*, ed. Quayle, J.R., University Park: Baltimore, 1979, p. 1.

40. Lagunas, R., "Energy Metabolism of *Saccharomyces cerevisiae*. Discrepancy Between ATP Balance and Known Metabolic Functions," *Biochem. Biophys. Acta*, 440, 661, 1976.

41. Den Hollander, J.A., Ugurbil, K., and Shulman, R.G., "^{31}P and ^{13}C NMR Studies of Intermediates of Aerobic and Anaerobic Glycolysis in *Saccharomyces cerevisiae*," *Biochemistry*, 25, 212, 1986.

42. Fiechter, A., "Chemostat Studies of Glycolysis in Yeasts," in Continuous Cultivation of Microorganisms, Proceedings 7th International Symp, Prague, 1980. p. 81.

43. Perlman, P.S. and Mahler, H.R., "Derepression of Mitochandria and their Enzymes in Yeast: Regulatory Aspects," *Arch. Biochem. Biophys.*, 162, 248, 1974.

44. Rogers, P.J. and Stewart, P.R., "Energetic Efficiency and Maintenance Energy Characteristics of *Saccharomyces cerevisiae* (Wild Type and Petite) and *Candida parapsilosis* Grown Anaerobically and Microaerobically in Continuous Culture," *Arch. Microbiol.*, 99, 25, 1974.

45. Oura, E., "Reaction Products of Yeast Fermentations," *Process*

Biochem., 13, 19, 1977.

46. San, K.Y., Studies on the On-Line Identification and Optimal Control of Bioreactors, Doctoral Dissertation, Cal. Inst. of Tech., Pasadena, CA, 1983.

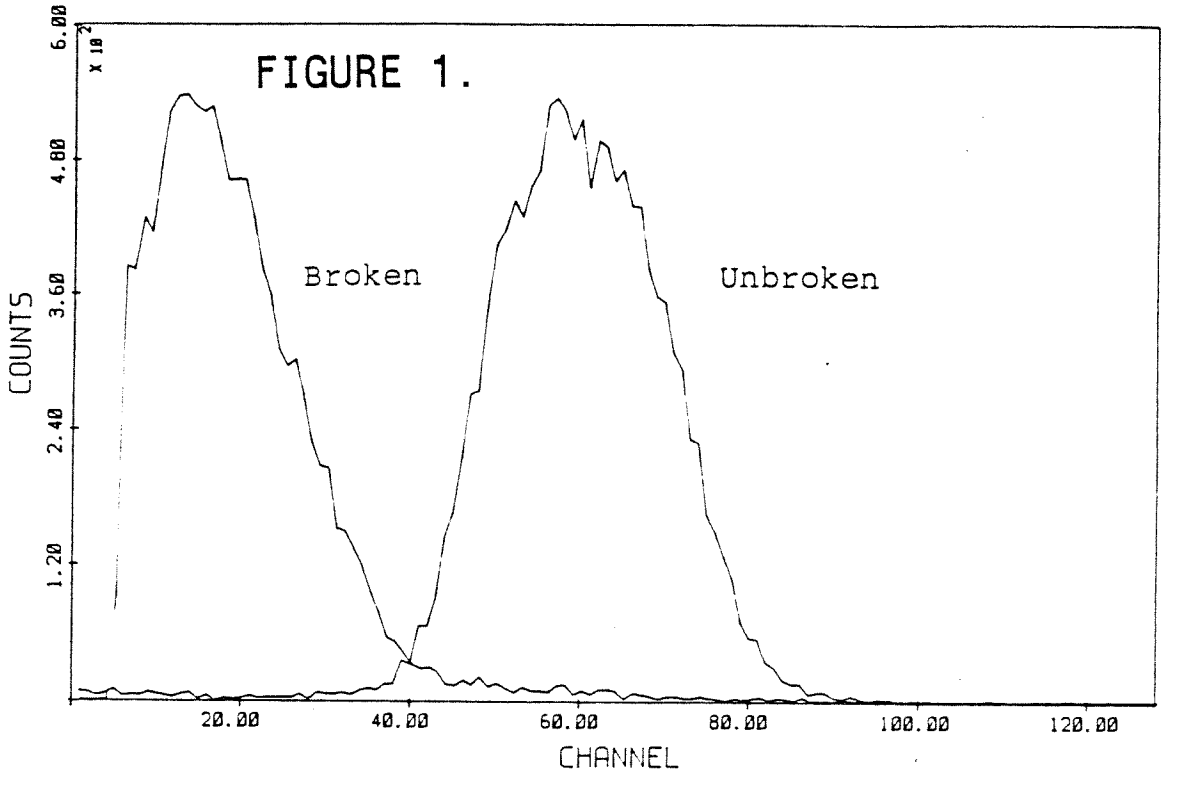
FIGURE 1.
X 10 2
6.00
4.80
3.60
2.40
1.20
COUNTS
Broken
Unbroken
20.00
40.00
60.00
80.00
100.00
120.00
CHANNEL

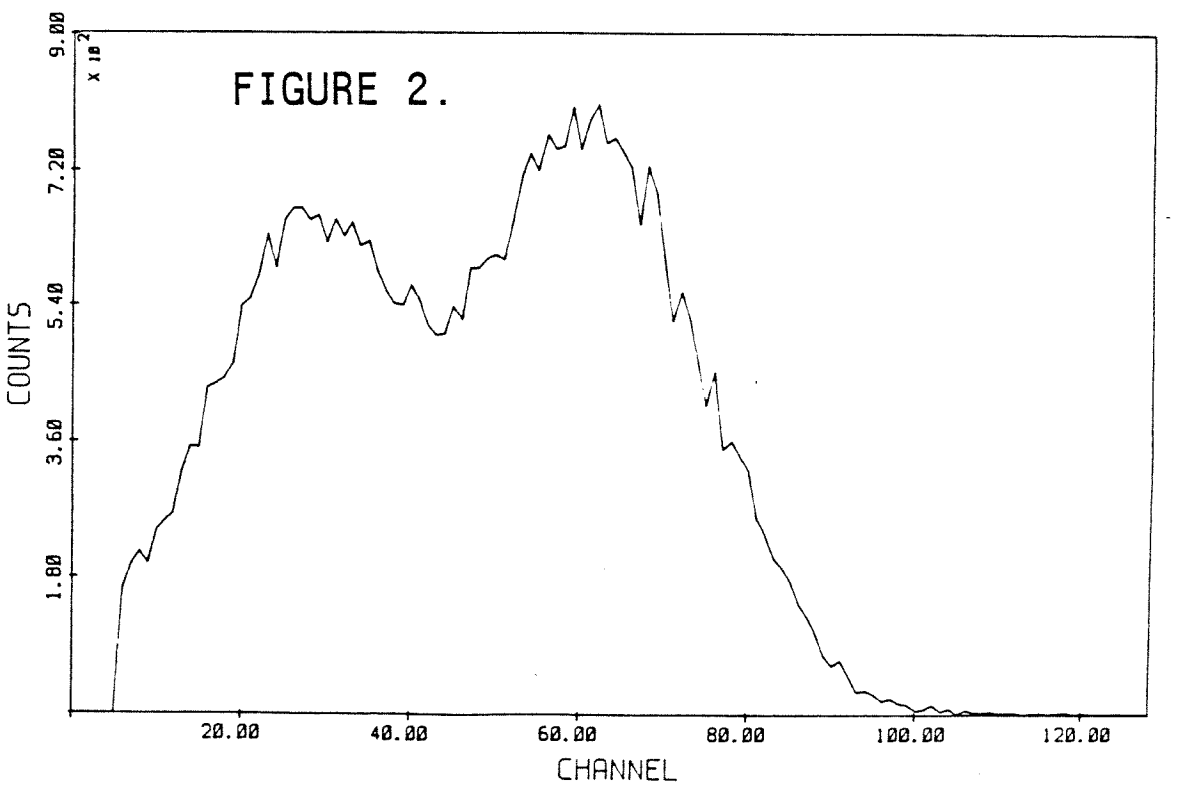
FIGURE 2.
X 10 2
9.00
7.20
5.40
3.60
1.80
COUNTS
20.00
40.00
60.00
80.00
100.00
120.00
CHANNEL

FIG. 3A 20 SEC. BREAKUP

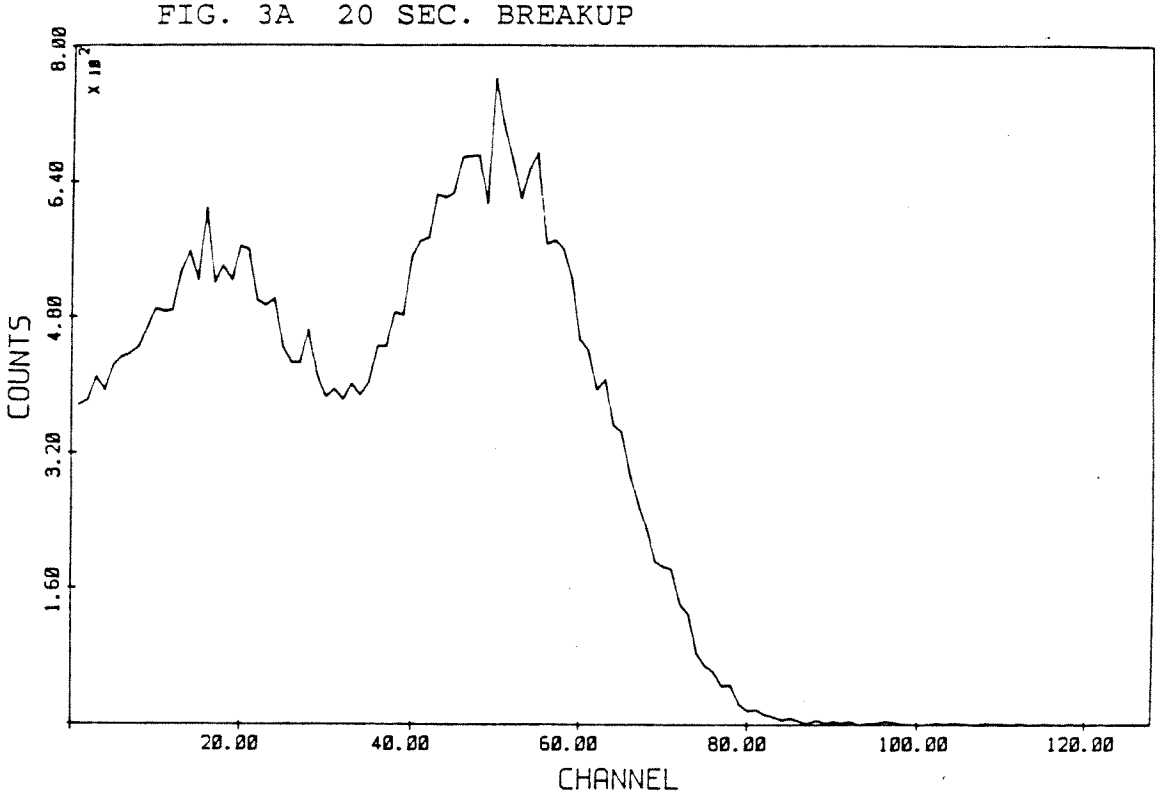

3B. 1 MIN. BREAKUP

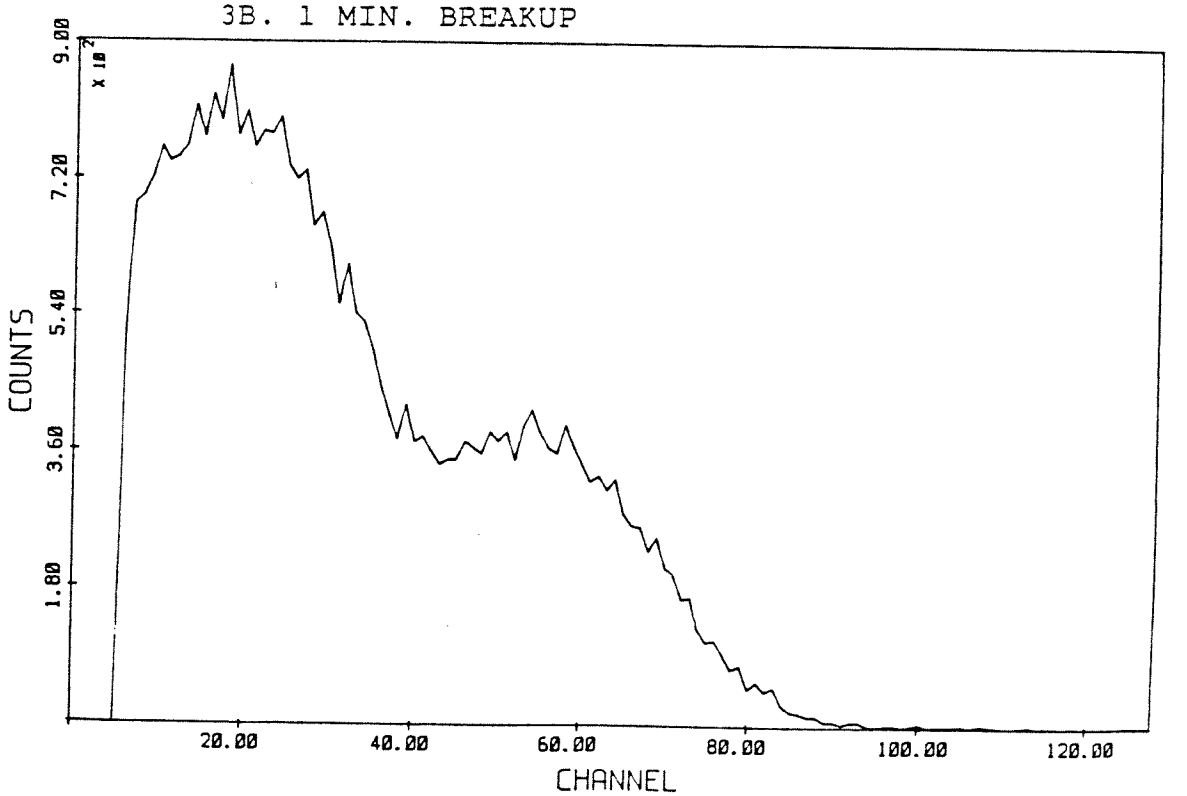

FIGURE 3C. 3 MIN. BREAKUP

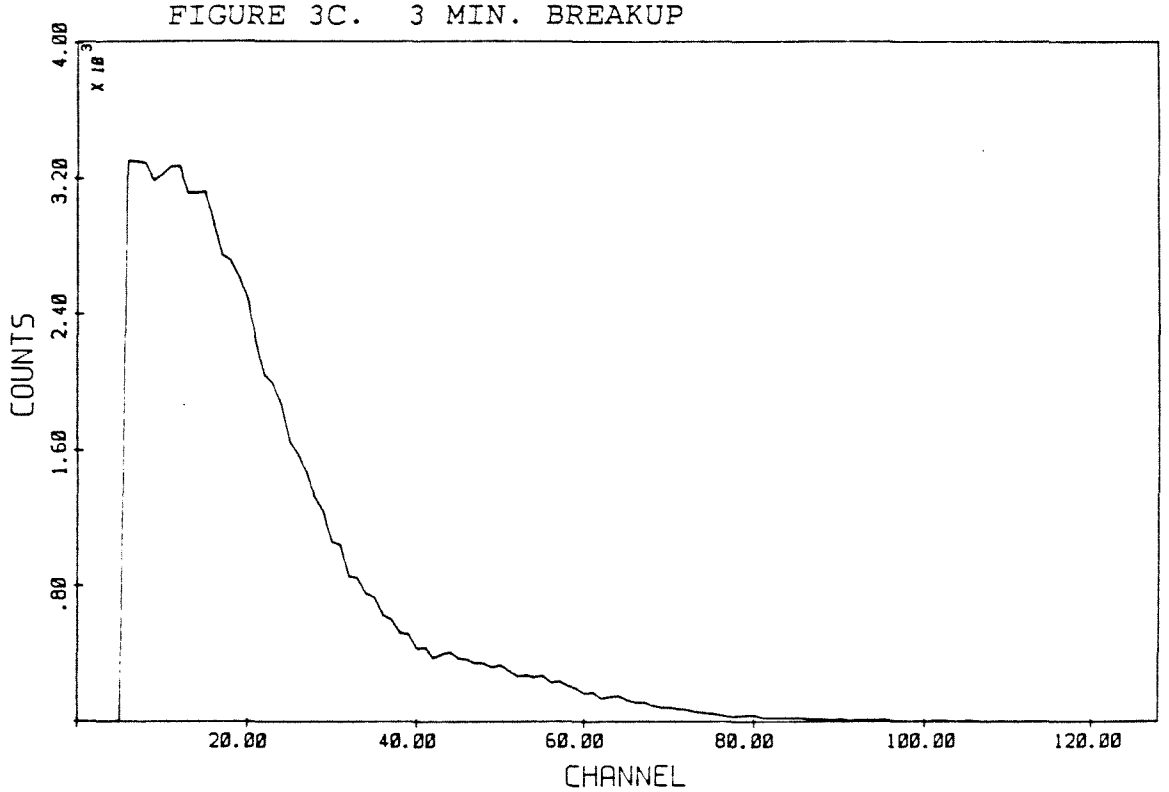

5 MIN. BREAKUP

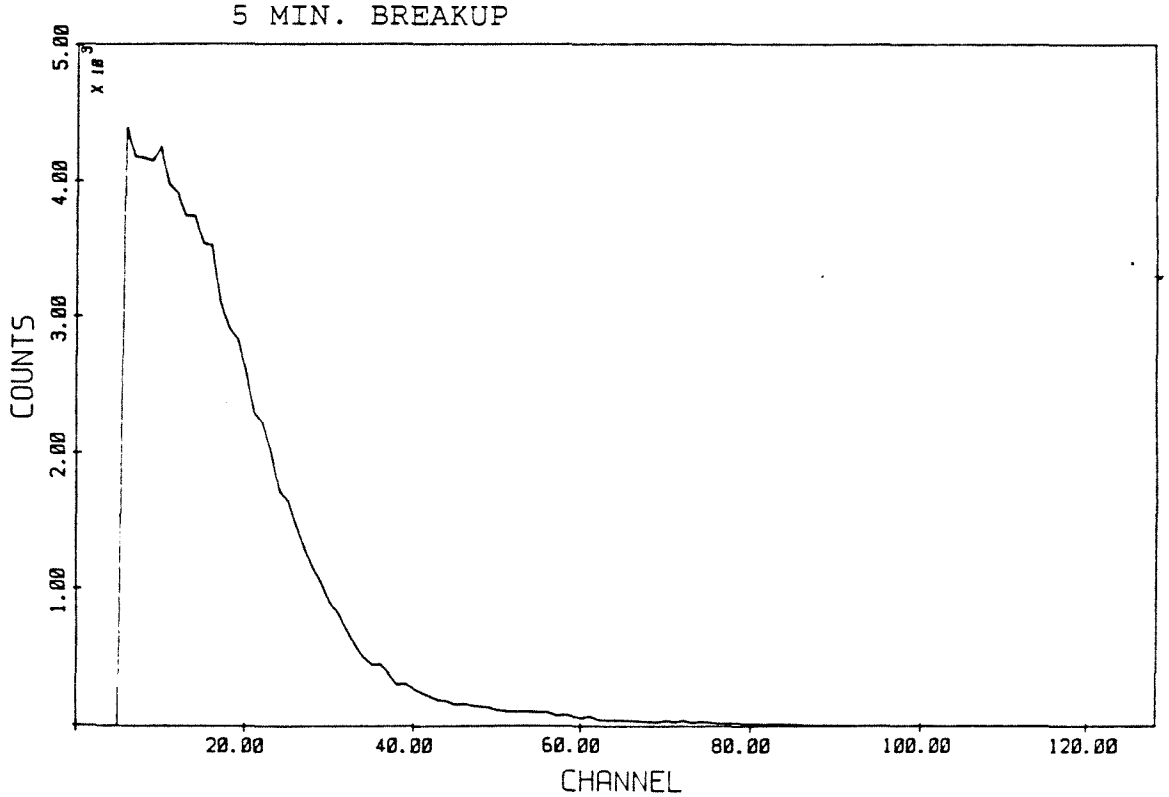

FIGURE 4. PROTEIN RELEASE vs. BREAKUP TIME

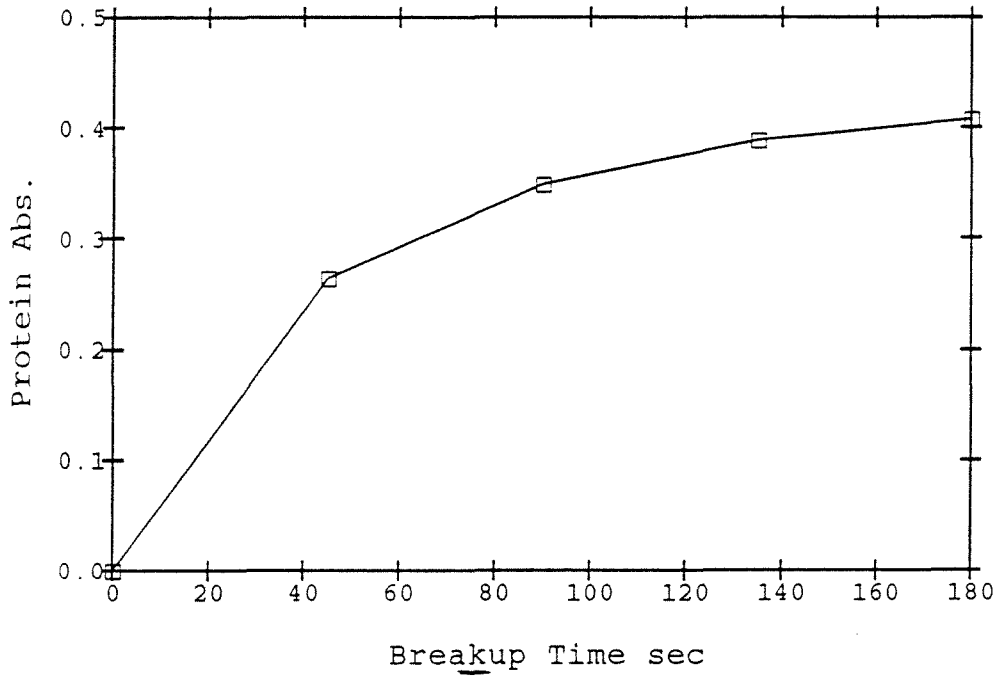

FIGURE 5. FUMARASE ACT. vs. BREAKUP TIME

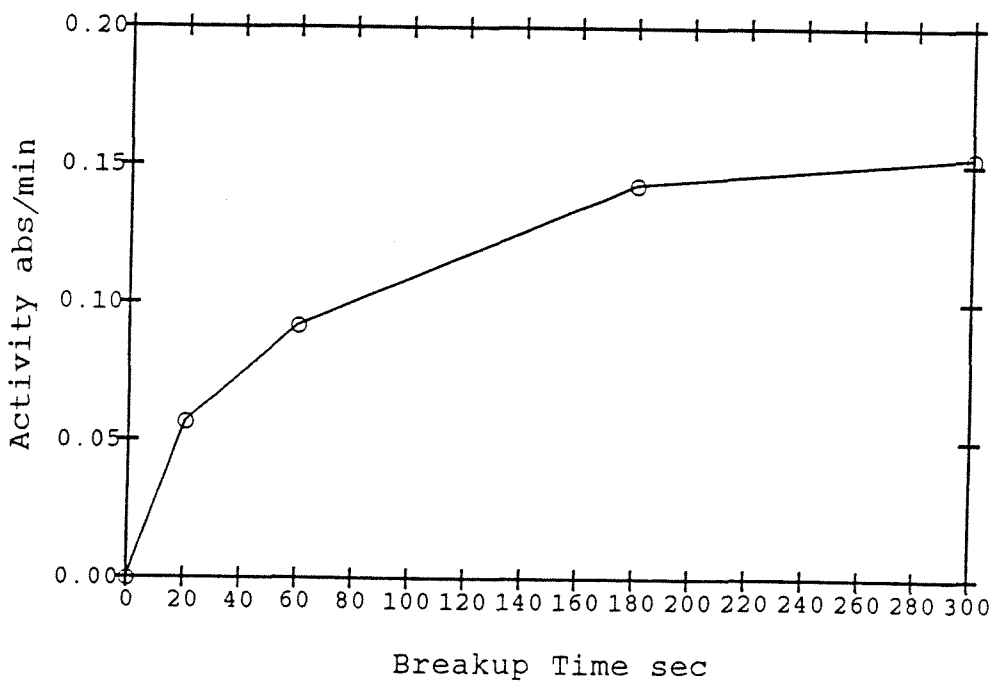

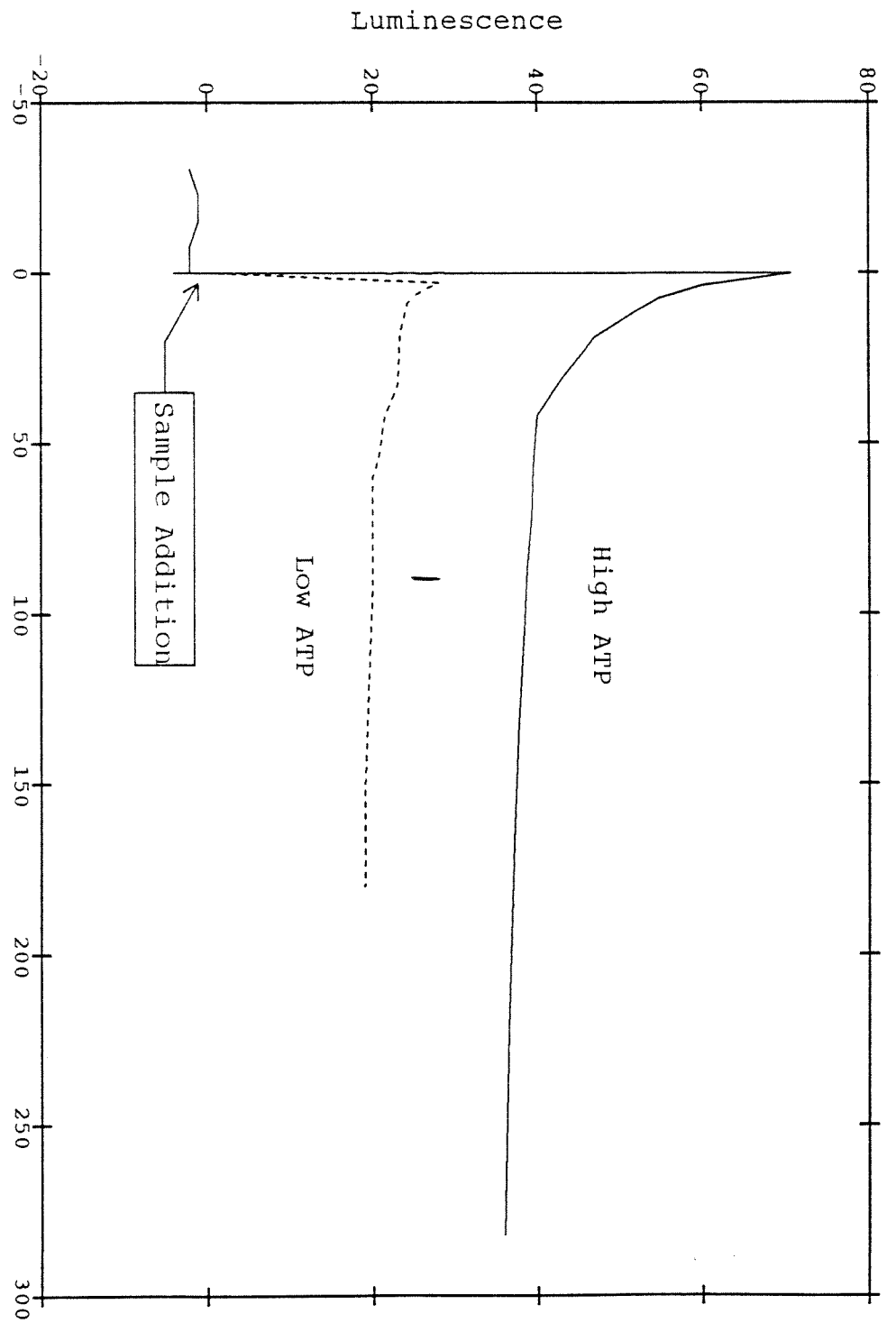

FIGURE 6. LUMINESCENCE vs. TIME

FIGURE 7A. ATP CALIBRATION

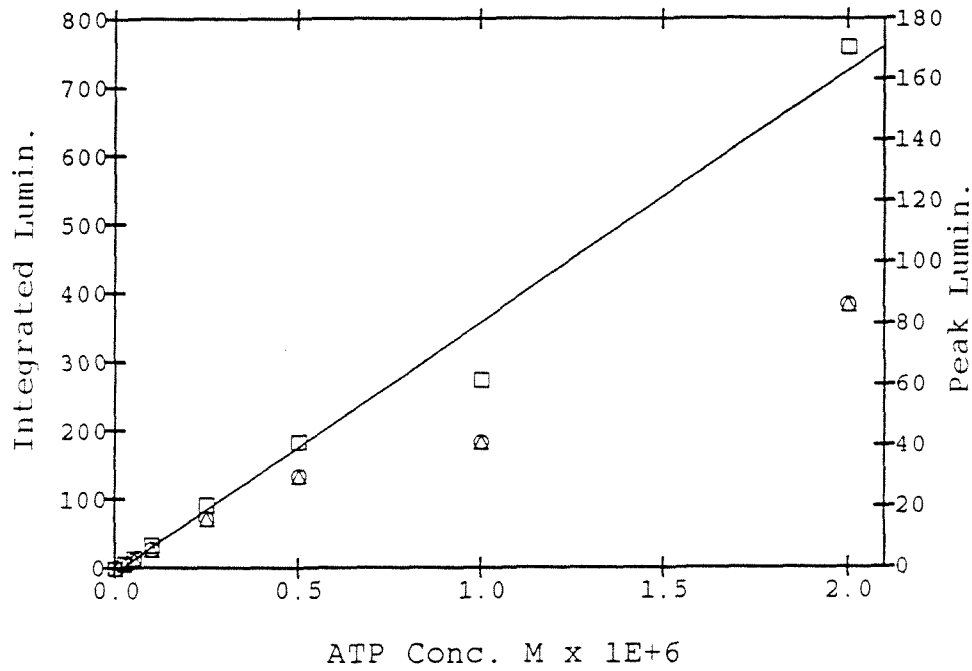

□ Peak
○ Int. after 1 min
△ Int. after 3 min

B. ATP CALIBRATION

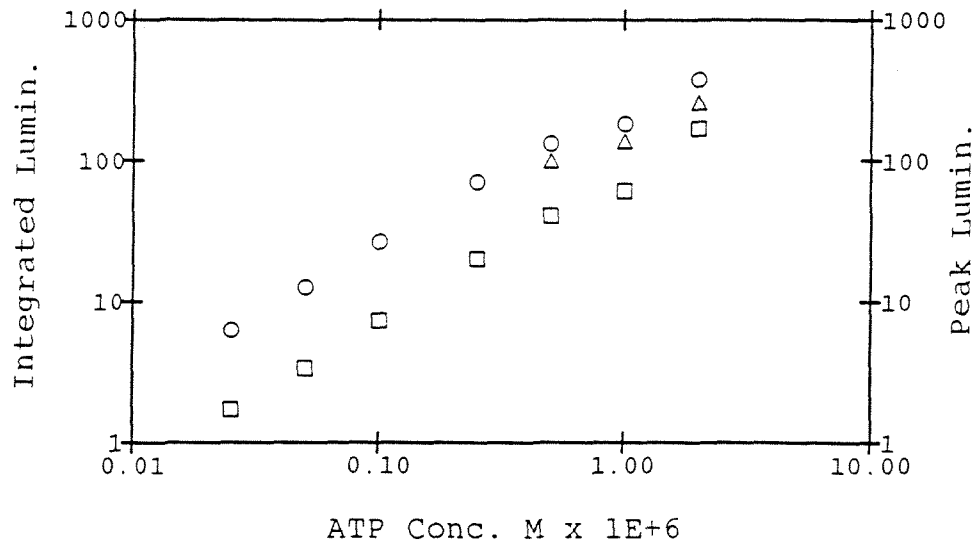

C. ATP CALIBRATION

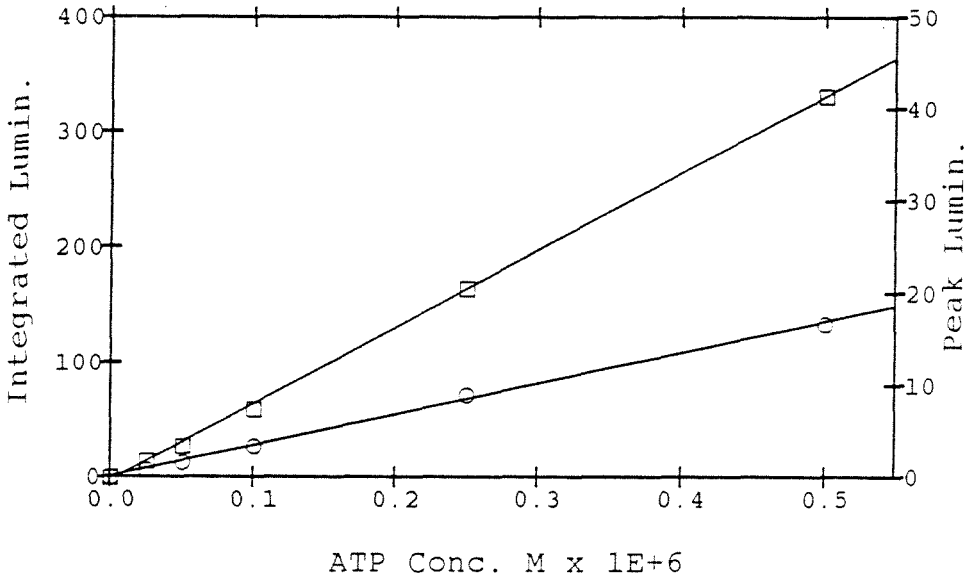

FIGURE 8. ATP INTERNAL STAND. CAL.

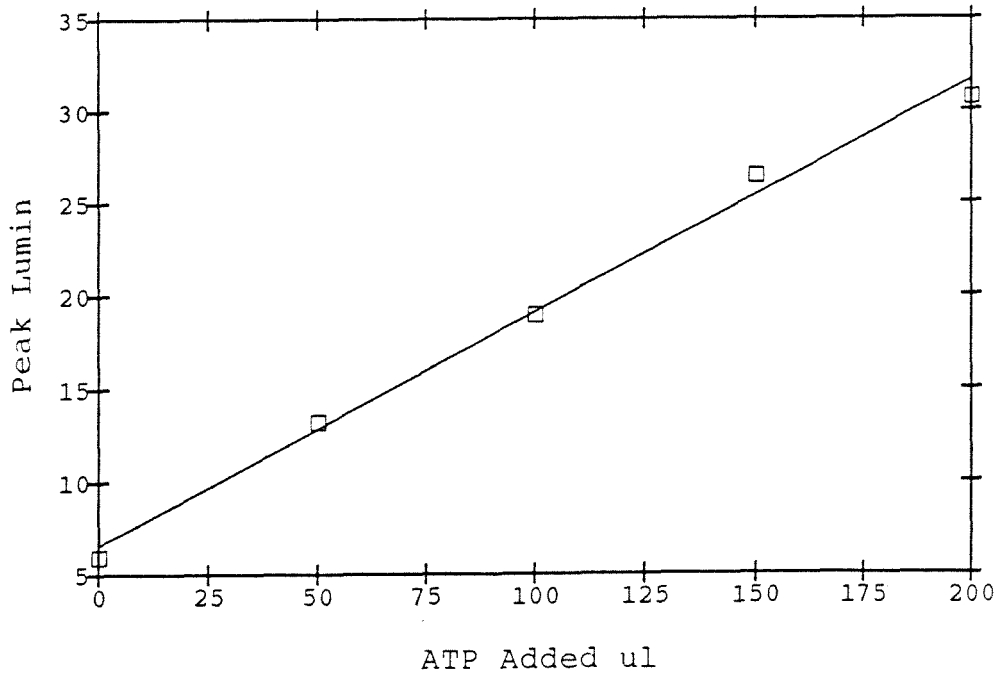

FIGURE 9. G6P ASSAY REACTION

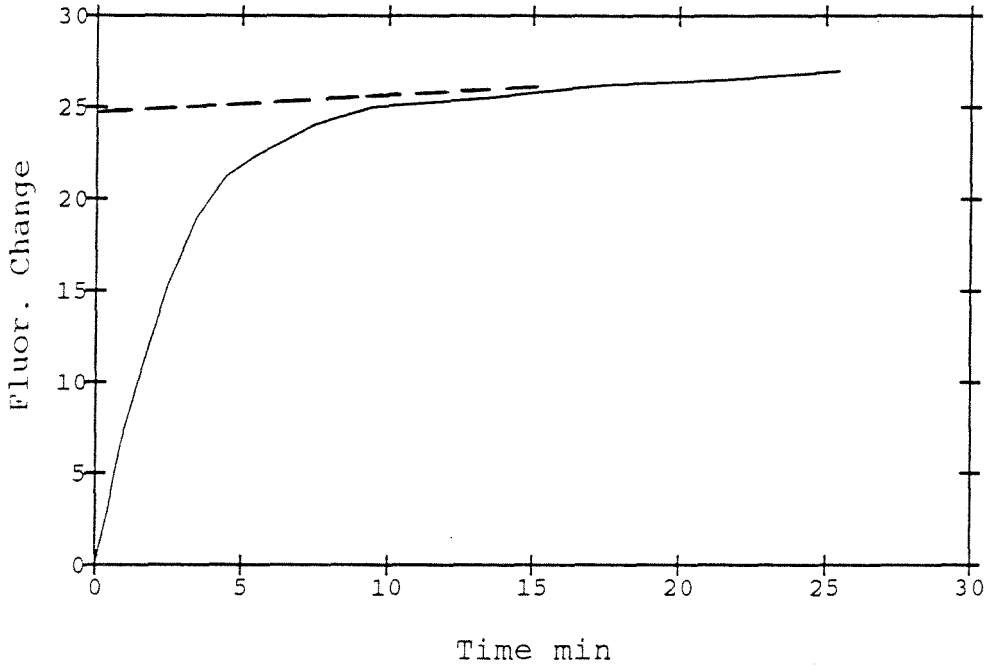

FIGURE 10. CALIBRATION G6P

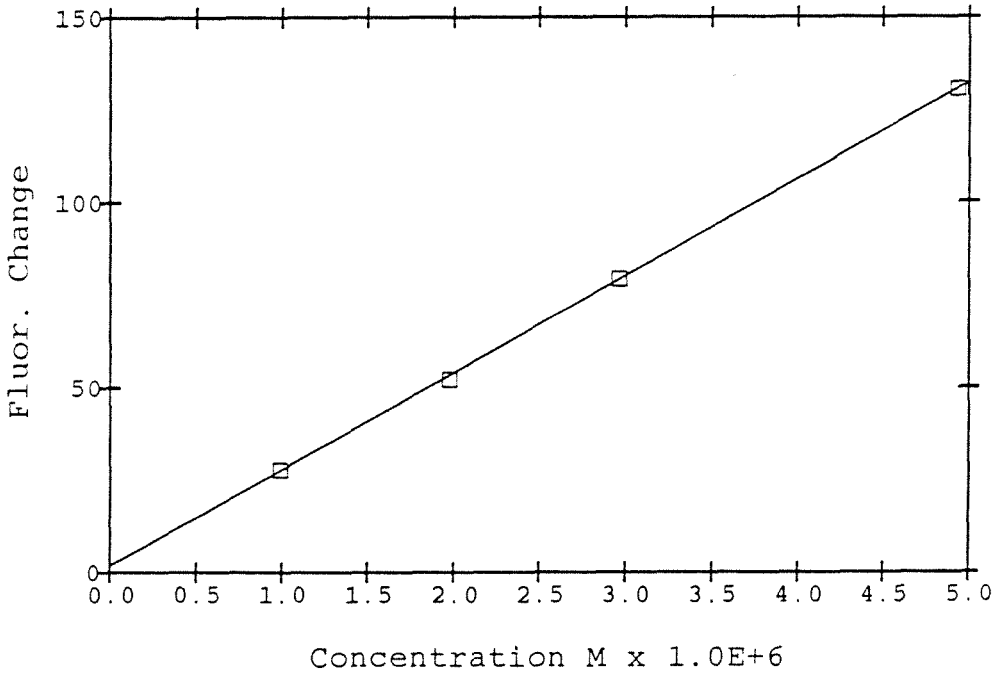

FIGURE 12. NADH CALIBRATION

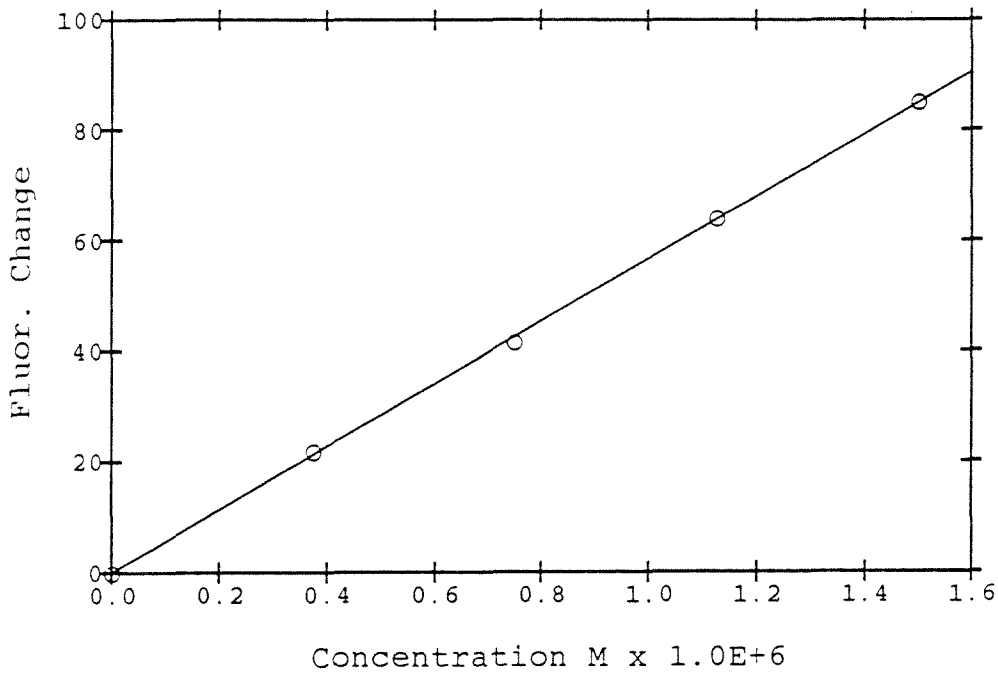

FIGURE 11. PYRUVATE CAL

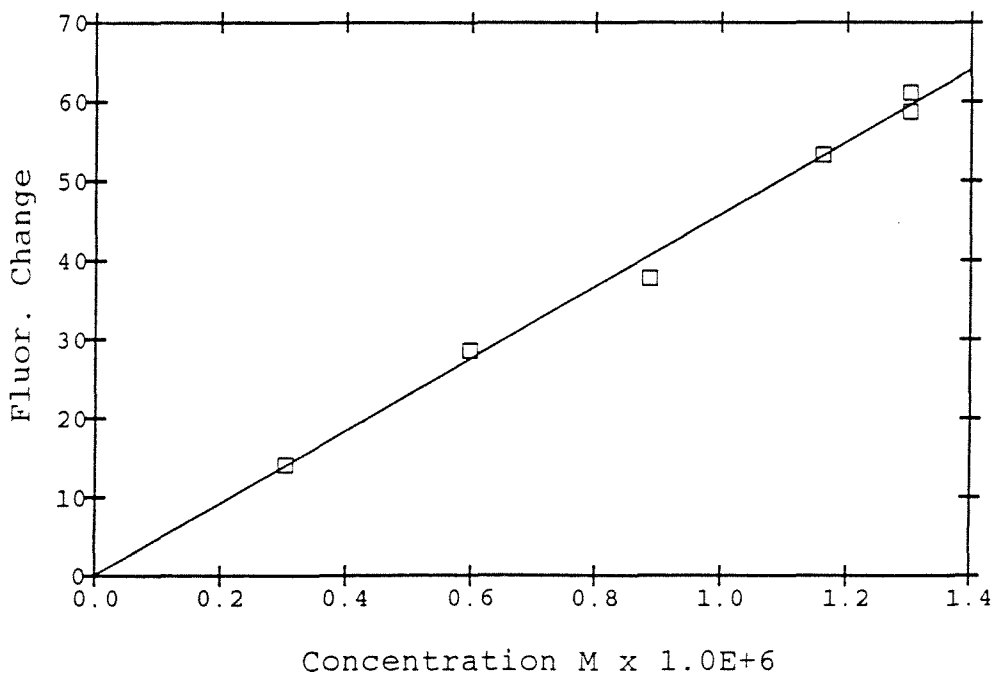

FIGURE 13. HEXOKINASE ASSAY

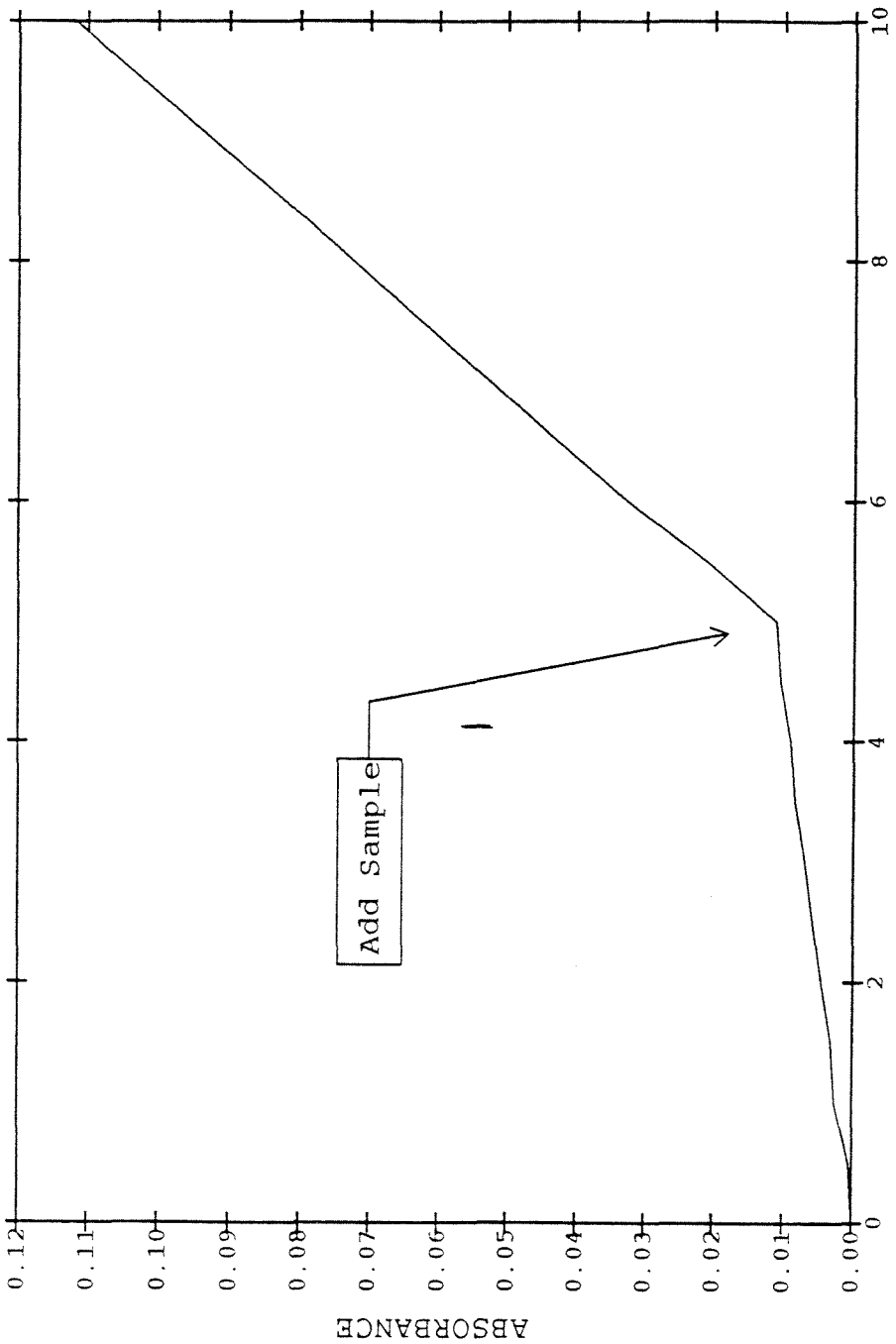

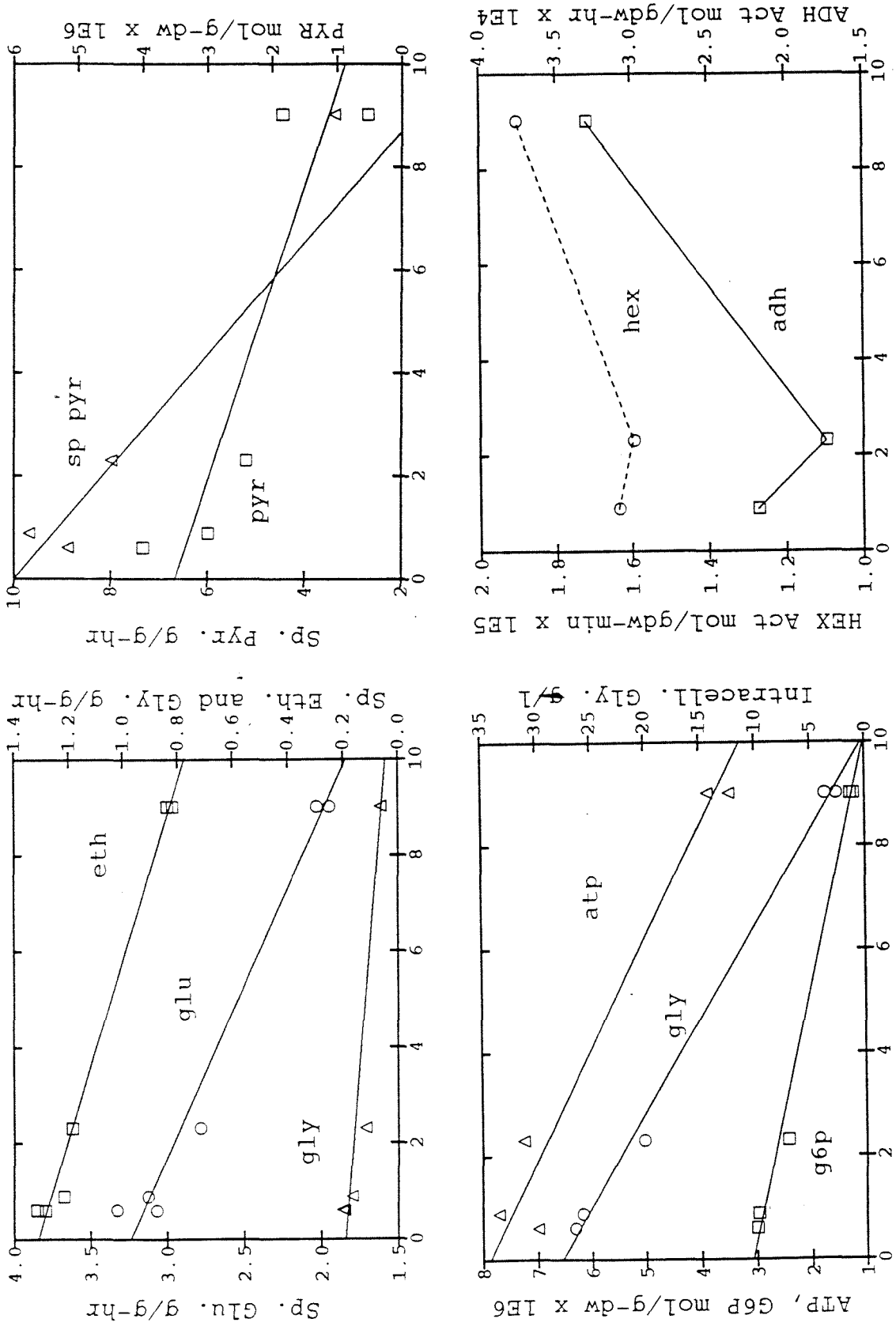
Sp. Glu. g/g-hr
Sp. Eth. and Gly. g/g-hr
eth
glu
gly
ATP, G6P mol/g-dw x 1E6
Intracell. Gly. g/l
atp
gly
g6p
Aeration ccpm
HEX Act mol/gdw-min x 1E5
ADH Act mol/gdw-hr x 1E4
hex
adh
Aeration ccpm
Sp. Pyr. g/g-hr
PYR mol/g-dw x 1E6
sp pyr
pyr

FIGURE 14.

FIGURE 15A. TRANSPORT vs. ATP

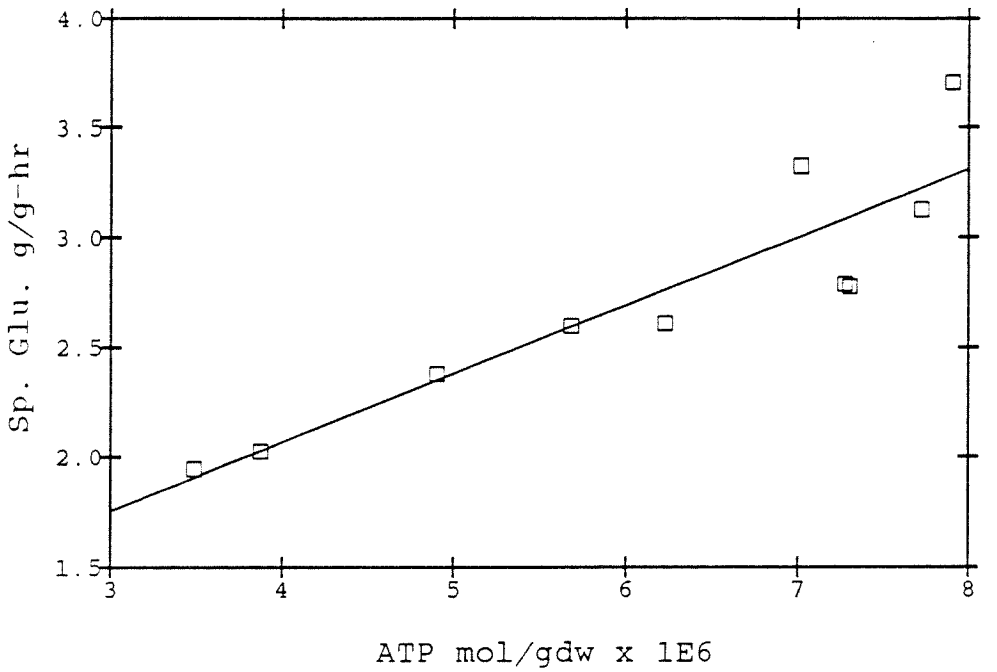

B. TRANSPORT vs. RESIDUAL GLUCOSE

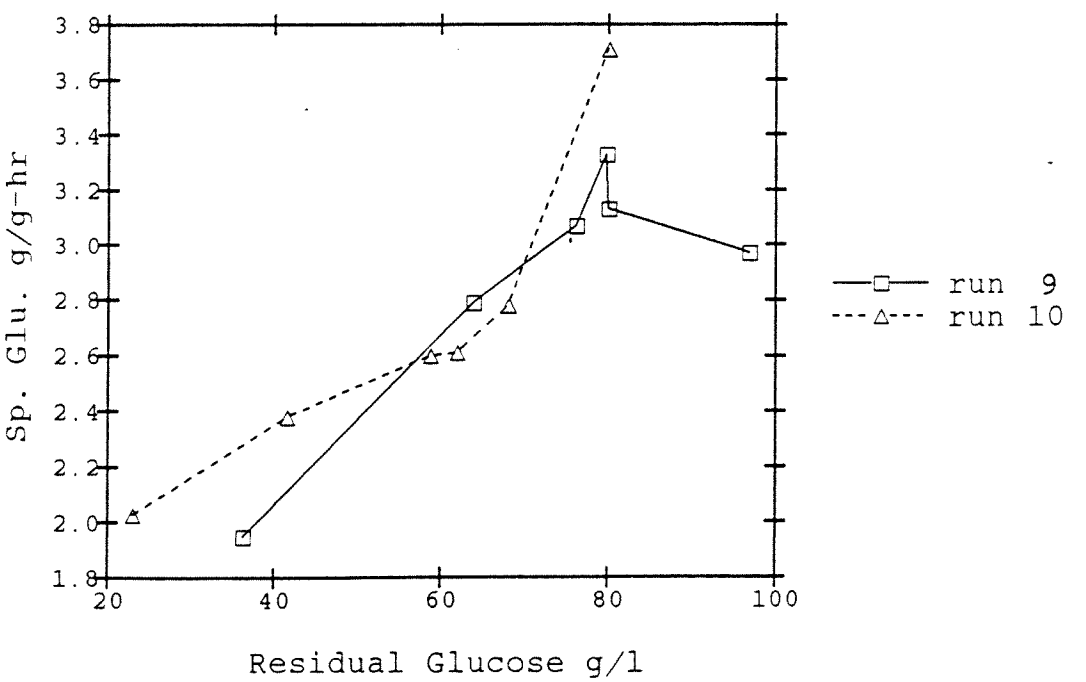

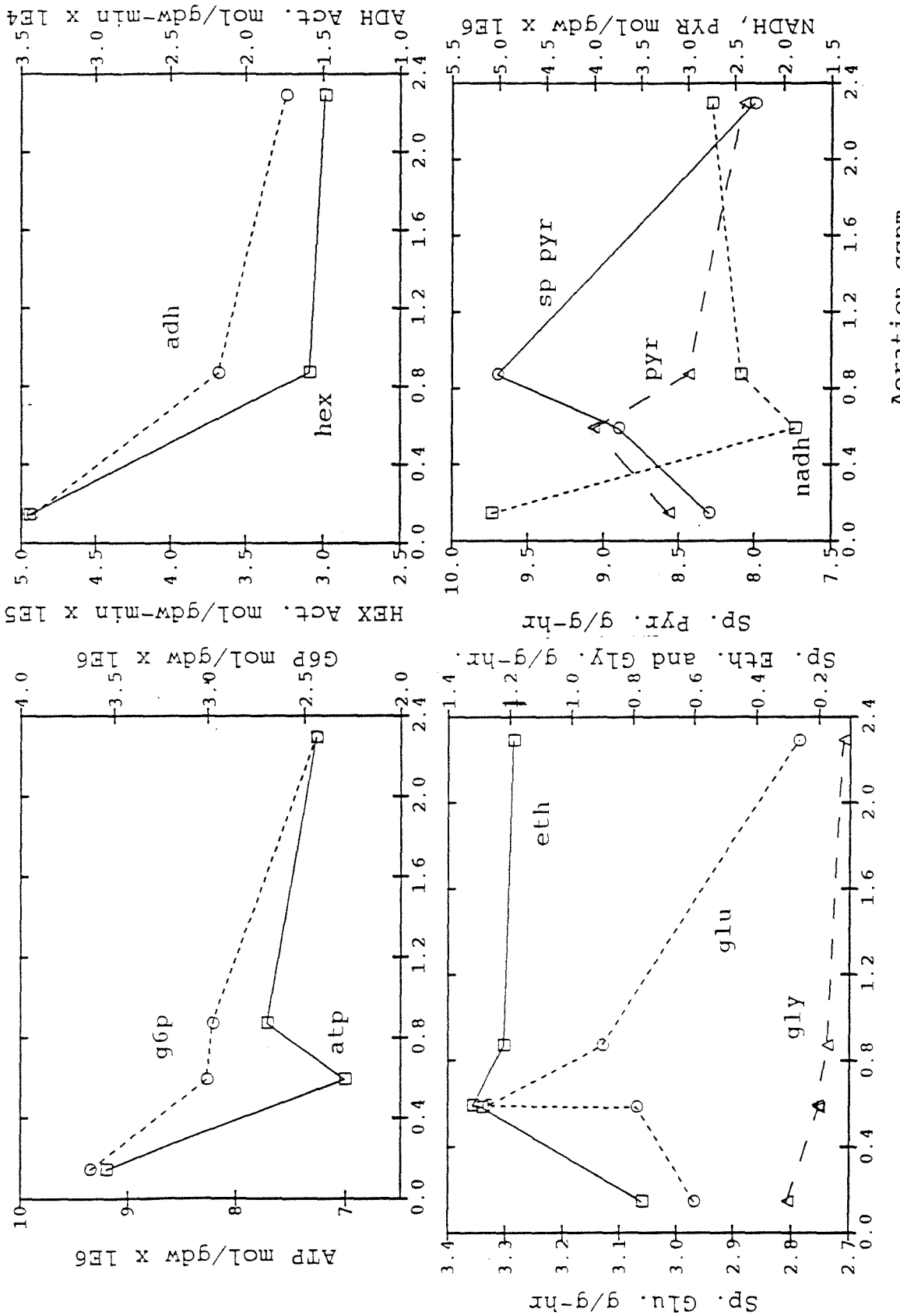
ATP mol/gdw x 1E6
G6P mol/gdw x 1E6
HEX Act. mol/gdw-min x 1E5
ADH Act. mol/gdw-min x 1E4
Sp. Glu. g/g-hr
Sp. Eth. and Gly. g/g-hr.
Sp. Pyr. g/g-hr
NADH, PYR mol/gdw x 1E6
Aeration ccpm
Aeration ccpm
atp
g6p
hex
adh
gly
glu
eth
pyr
sp pyr
nadh

FIGURE 16.

FIGURE 17.

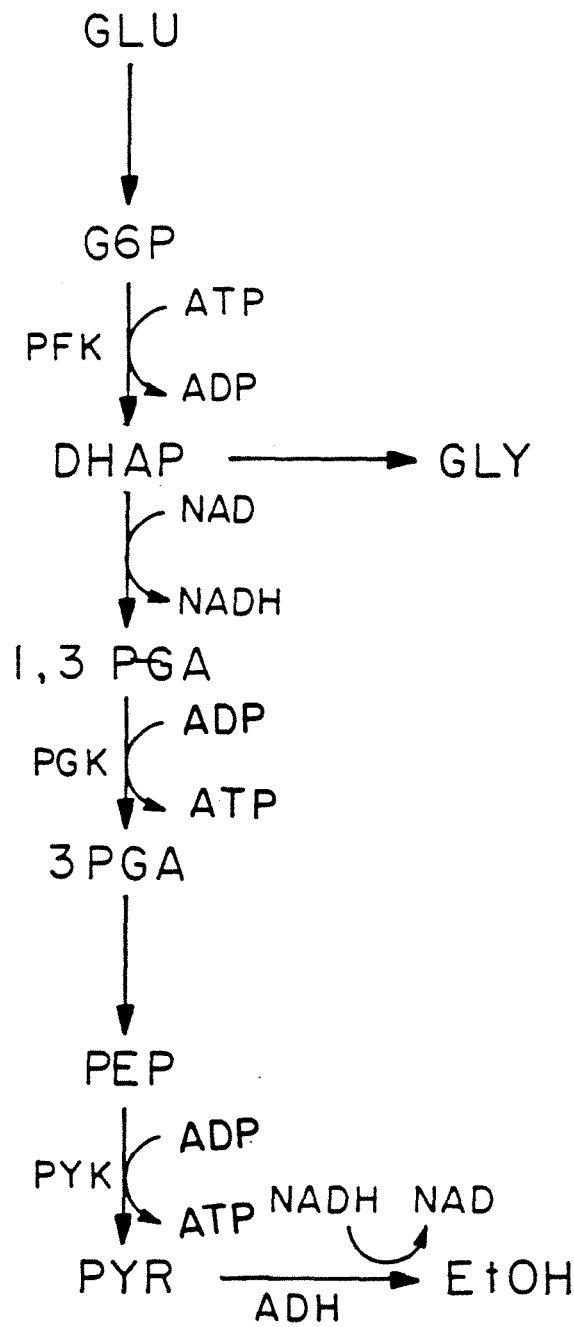
GLU
G6P
ATP
PFK
ADP
DHAP
GLY
NAD
NADH
1,3 PGA
ADP
PGK
ATP
3PGA
PEP
ADP
PYK
ATP
NADH
NAD
PYR
EtOH
ADH

FIGURE 18. ATP YIELD

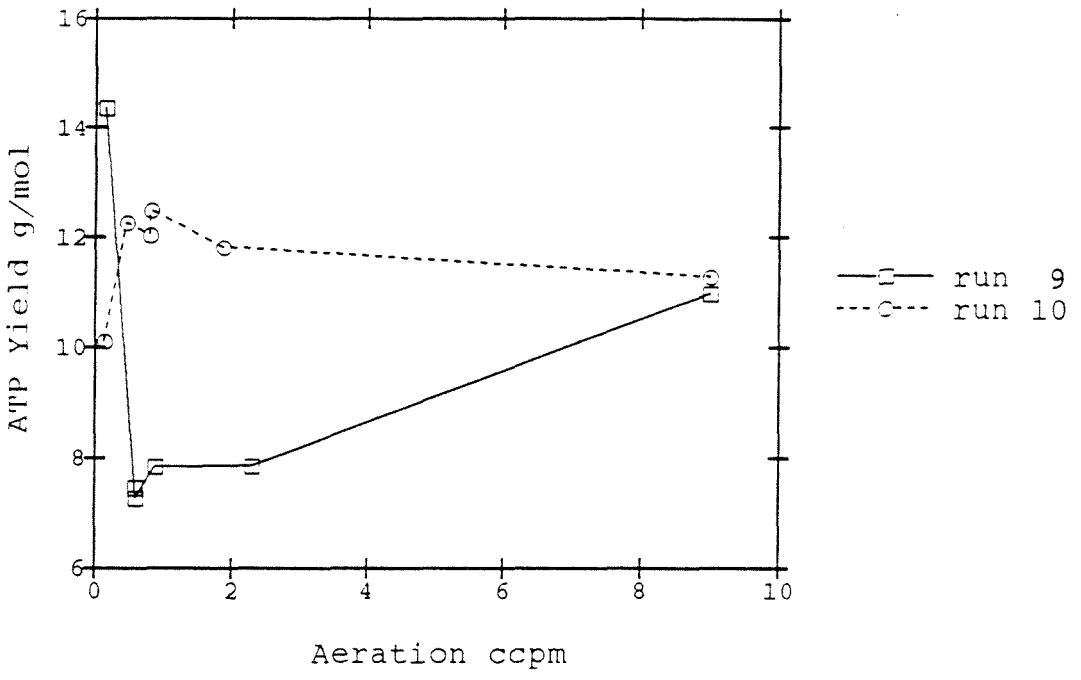

FIGURE 19. ATP WASTE ACTIVITY

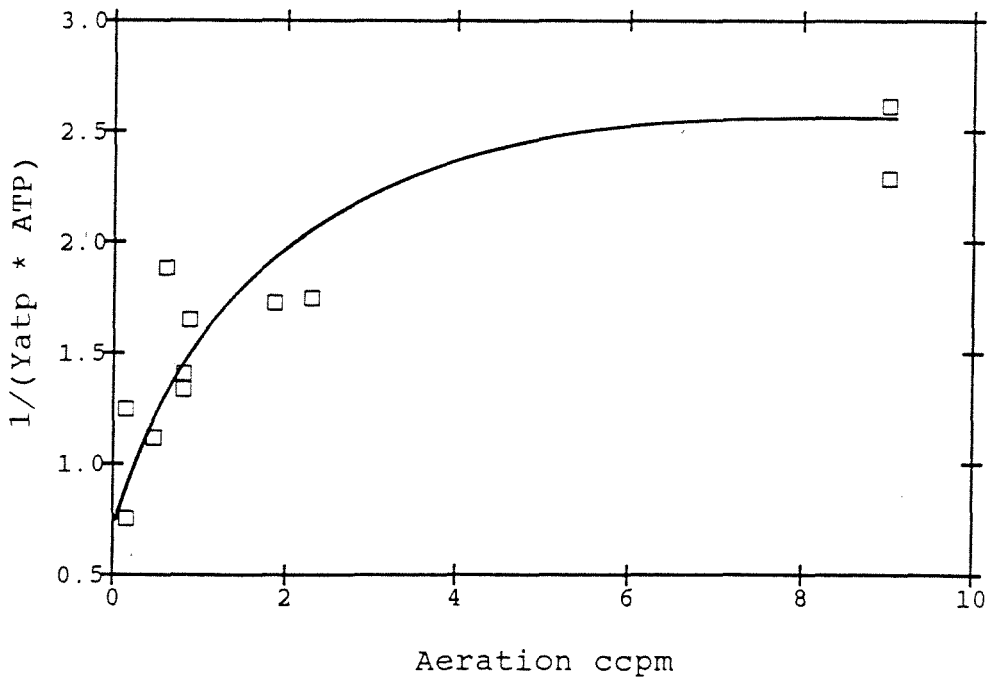

FIGURE 20. SP. GLY. VS. DRIVING FORCE

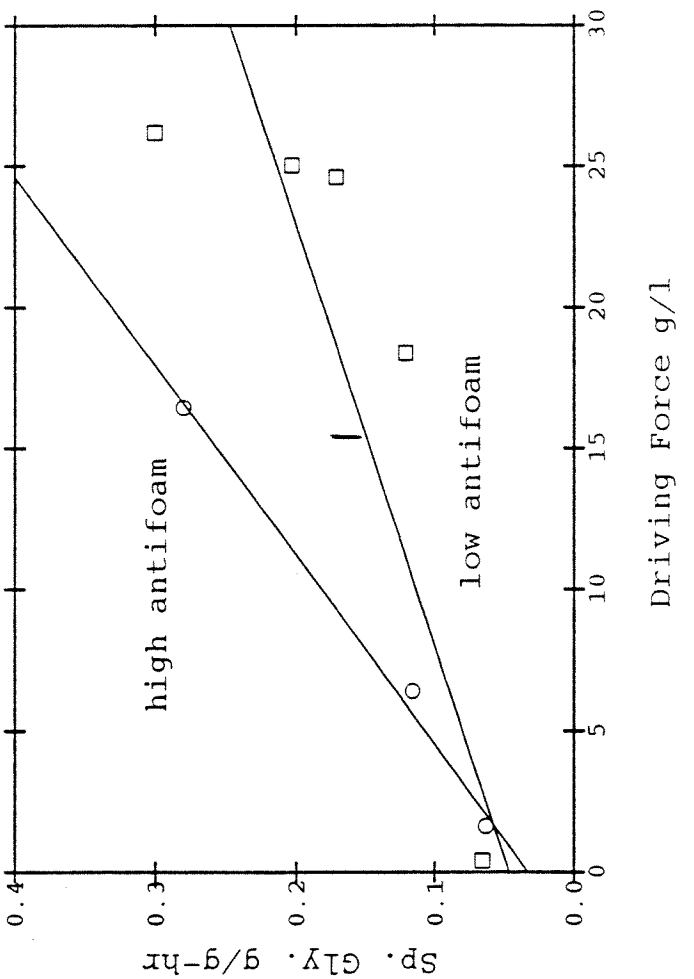

FIGURE 21A. ATP vs. AERATION

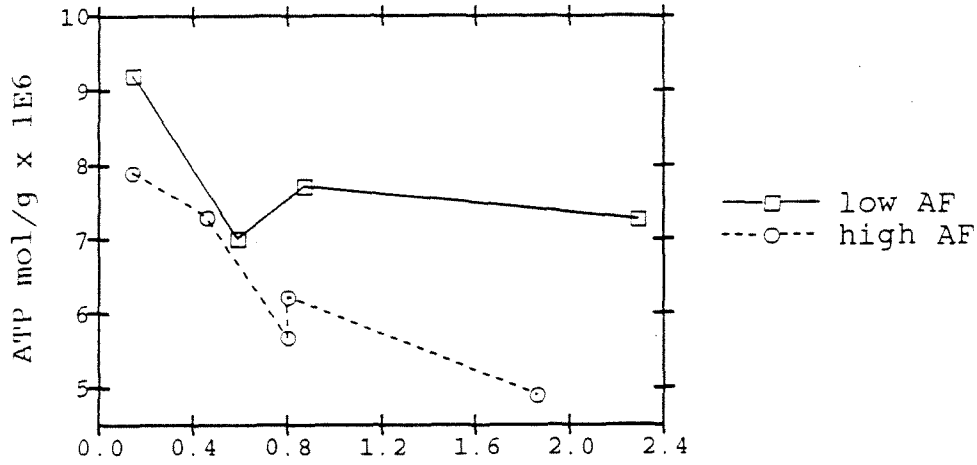

B. SPECIFIC ETHANOL PROD

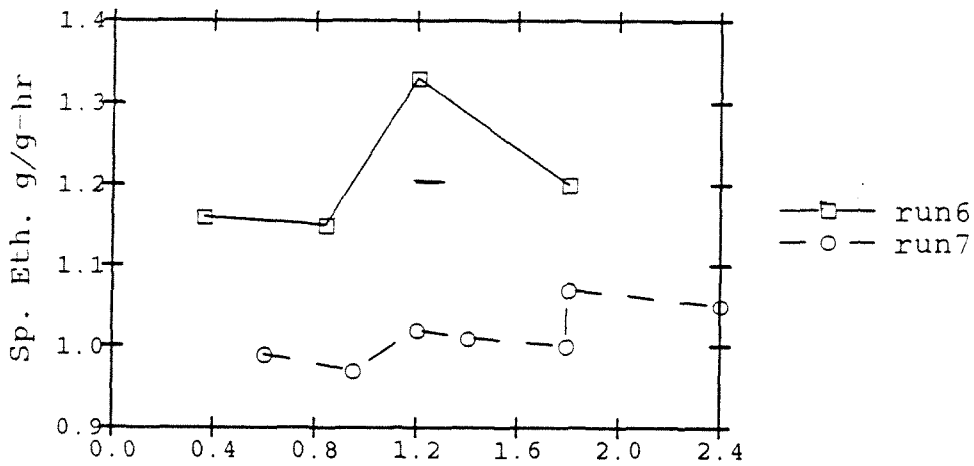

C. ETHANOL vs. AERATION

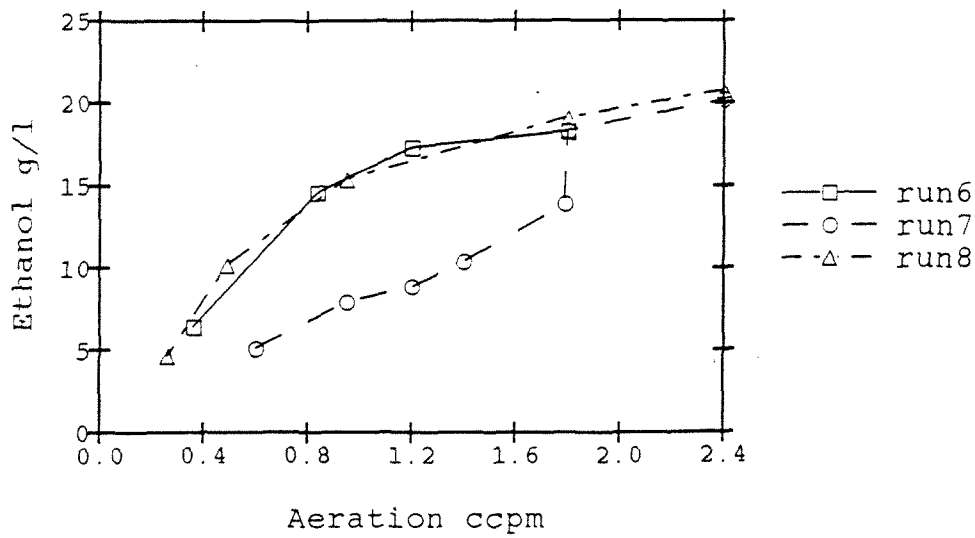

FIGURE 22. INTRA. and EXTRACELL. ETH.

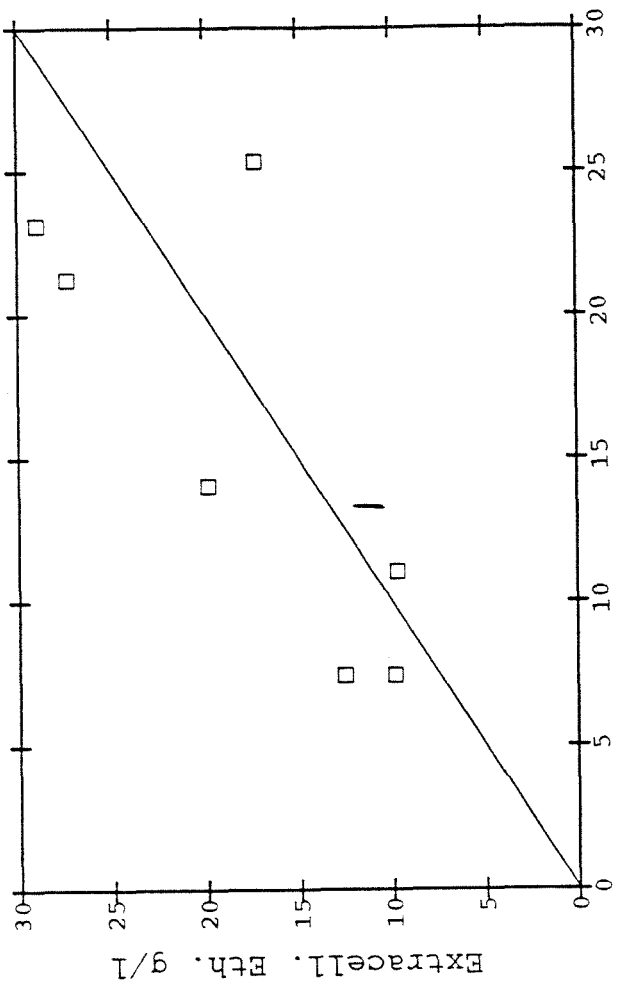

FIGURE 23A. ISOCITR. DEHYDR. ACT.

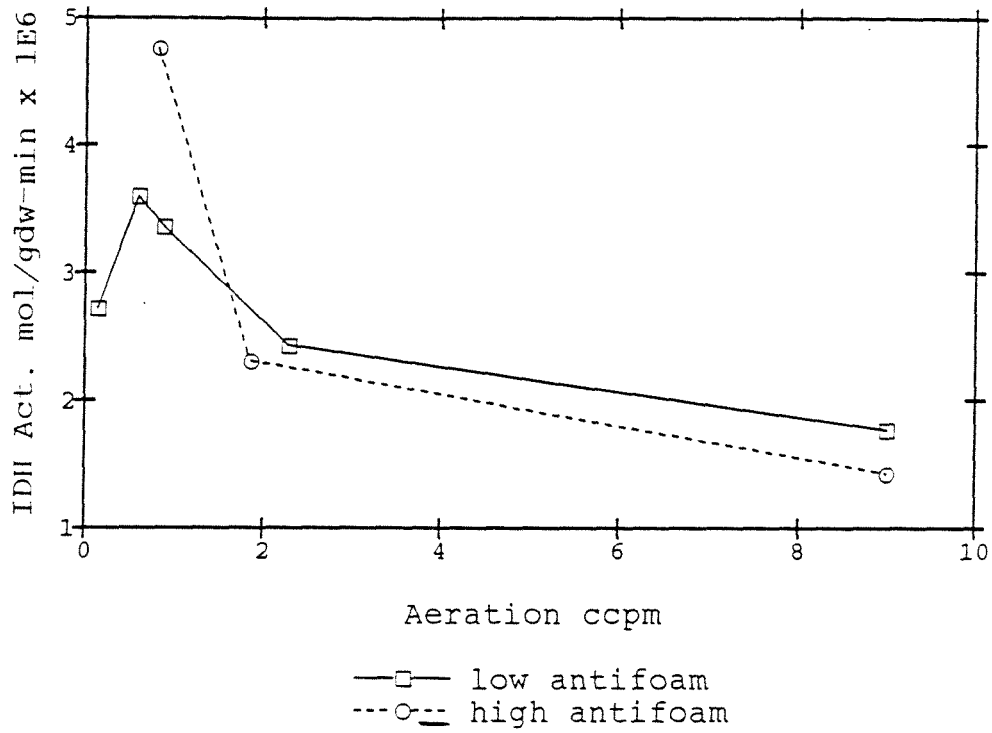

B. FUMARASE vs. AERATION

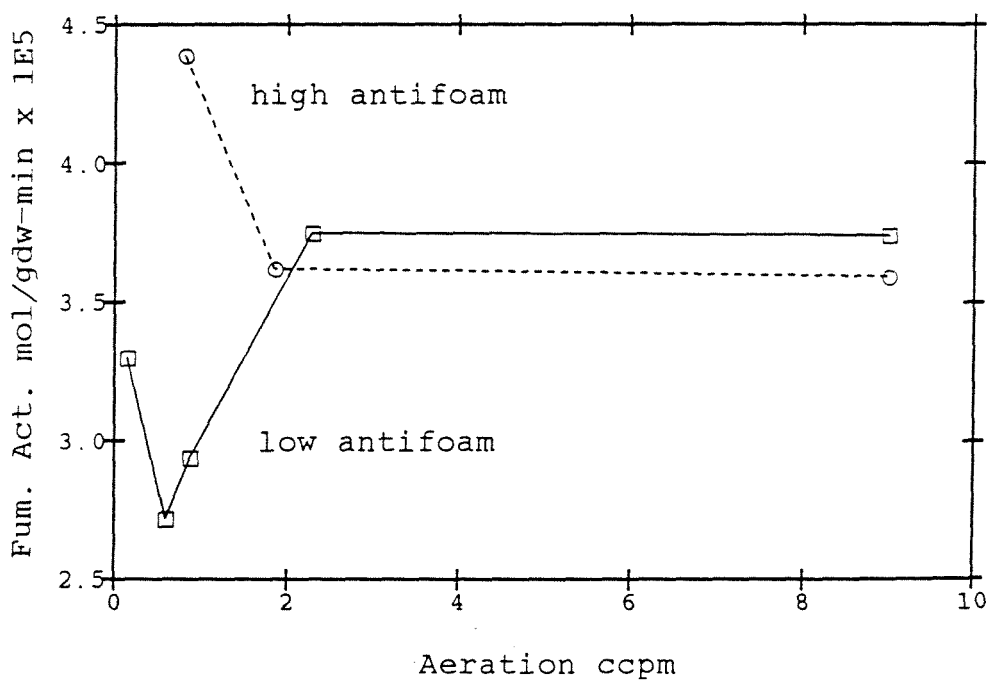

FIGURE 24. SP. GLY. vs. NADH

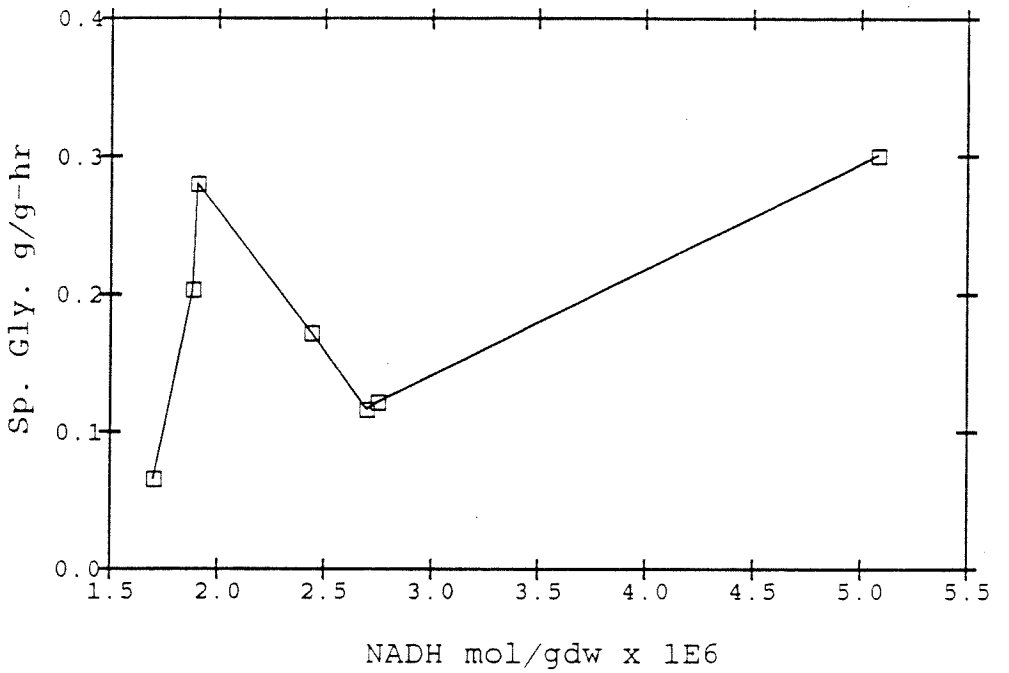

FIGURE 25. SP. GLY. vs. ISOC. DEHYDR.

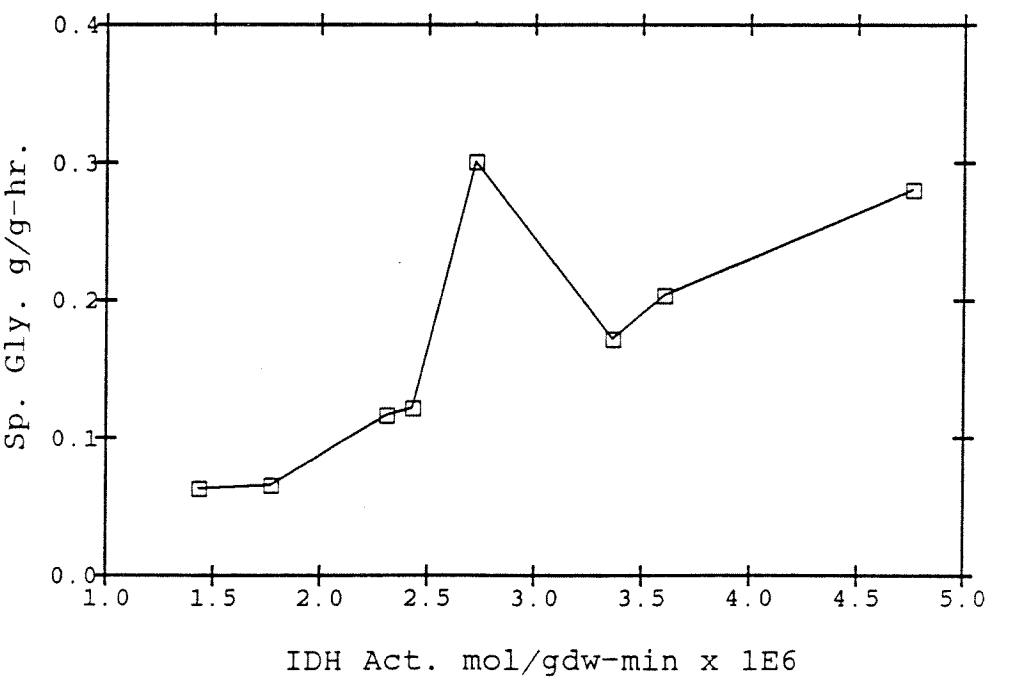

TABLE 1. ATP ASSAY

A. Solutions

1. Tris buffer, 0.5 M, pH 7.4 w/H_2SO_4.
2. Tris Buffer, 0.1 M, pH 7.4 w/H_2SO_4.
3. Tris buffer, 8.48 g/l, EDTA 0.744 g/l, pH 7.7 w/H_2SO_4.
4. Bovine Serum Albumin, 150 mg/50 cc.
5. Magnesium acetate, 0.129 g/100 cc.
6. Luciferase, 0.1 mg in 600 µl of 1.
7. Luciferin, 1 mg in 1 ml of 2.
8. ATP, 15 mg/100 cc.

B. Pipette Into Cuvette

1. Solution 3, 500 µl
2. Solution 4, 200 µl
3. Solution 5, 200 µl
4. Solution 6, 40 µl
5. Solution 7, 75 µl

C. Initiate By Injection of 1 cc Sample

TABLE 2. GLUCOSE 6-PHOSPHATE ASSAY

A. Solutions

1. Tris Buffer, 0.1 M, pH 7.5.
2. HCl, 0.22 cc of 35% HCl in 100 cc water.
3. NADP, 10 mg in 10 cc 2.
4. $MgCl_2$, 3 g/100 cc.
5. Glucose 6-Phosphate Dehydrogenase - commerical preparation.
6. Glucose 6-Phosphate, 1 mg/100 cc of 1.

B. Pipette into Cuvette

1. 2.3 cc Solution 1.
2. 100 µl Solution 2.
3. 100 µl Solution 3.
4. 500 µl Sample

C. Initiate with 1 µl Solution 6

TABLE 3. PYRUVATE ASSAY

A. Solutions

1. Tris Buffer, 0.1 M, pH 9.5.
2. Tris Buffer, 0.1 M, pH 7.5.
3. Lactate dehydrogenase - commerical preparation.
4. NADH, 1 mg in 10 cc of solution 1.
5. Pyruvate, 0.33 mg/100 cc solution 2.

B. Pipette into Cuvette

1. 2.9 cc solution 2.
2. 60 µl solution 3.
3. 20-100 µl sample.

C. Initiate With 1 µl Solution 3

TABLE 4. NADH ASSAY

A. Solutions

1. Tris buffer, 0.1 M, pH 9.5.
2. Tris buffer, 0.1 M, pH 7.5.
3. Lactate Dehydrogenase - commercial preparation.
4. NADH, 1 mg/10 cc of 1.
5. Pyruvate, 0.025 g/100 cc.

B. Pipette into Cuvette

1. 2.4 cc solution 2.
2. 100 µl solution 5.
3. 500 µl sample.

C. Initiate with 1 µl enzyme.

TABLE 5. HEXOKINASE ASSAY

A. Solutions

1. Tris buffer, 0.1 M, pH 8.0.
2. Citrate buffer, 0.1 M, pH 8.0
3. Glucose 10 g in 100 cc of 1.
4. $MgCl_2$, 3 g/100 cc.
5. NADP, 10 mg/ml.
6. ATP, 10 mg/ml solution 2.
7. Glucose 6-phosphate dehydrogenase - commerical preparation.

B. Pipette into Cuvette

1. Solution 1, 1.5 cc.
2. Solution 3, 1 cc.
3. Solution 4, 200 µl.
4. Solution 5, 200 µl.
5. Solution 6, 100 µl.
6. Solution 7, 2 µl.

C. Initiate with 20 µl sample.

TABLE 6. ALCOHOL DEHYDROGENASE ASSAY

A. Solutions

1. Sigma glycine, semicarbazide buffer, pH 9.
2. NAD, 10 mg in 1 cc of water, pH 2.0.
3. $MgCl_2$, 3 g/100 cc.
4. EtOH, 13 cc in 100 cc water.

B. Pipette into Curvette

1. 2.3 cc solution 1.
2. 200 µl solution 2.
3. 200 µl solution 3.
4. Circa. 20 µl sample.

C. Initiate with 200 µl solution 4.

TABLE 7. FUMARASE

A. Solutions

1. $KHPO_4$, 0.1 M, pH 7.4.
2. Cysteine, 0.383 g/100 cc.
3. Malate, 1.4 g/100 cc.

B. Pipette into Cuvette

1. Solution 1, 2.2 cc.
2. Solution 2, 500 µl.
3. Sample, circa. 300 µl.

C. Initiate with 500 µl solution 3.

TABLE 8. ISOCITRATE DEHYDROGENASE ASSAY

A. Solutions

1. Tris buffer, 0.1 M, pH 7.4.
2. Isocitrate, 0.065 g/100 cc.
3. AMP, 13 mg/10 cc.
4. NAD, 17.5 mg/5 cc.
5. Cysteine, 0.363 g/100 cc.
6. $MgCl_2$, 3 g/100 cc.

B. Pipette into Cuvette

1. Solution 1, 1.8 cc.
2. Sample 300 µl.
3. Solution 3, 200 µl.
4. Solution 4, 200 µl.
5. Solution 5, 200 µl.
6. Solution 6, 75 µl.

TABLE 9. METABOLITE ASSAY RESULTS

aer ccpm	ATP µmol/g	G6P µmol/g	NADH µmol/g	GLY* g/l	ETH* g/l
0.59	7.01	3.01	1.88	26.6	7.4
0.87	7.72	2.98	2.44	25.9	11.0
2.29	7.27	2.44	2.75	20.2	25.3
9.00	3.48	1.28	1.70	2.67	23.1
0.14	9.20	3.63	5.08	27.1	-
9.00+	3.87	1.22	1.99	3.70	21.2
1.86+	4.90	1.66	2.70	8.46	14.0
0.80+	5.68	3.03	1.90	19.8	7.4
0.46+	7.30	3.07			
0.80+	6.22	2.90			
0.14+	7.90	2.44			

* Intracellular
\+ High Antifoam

TABLE 10. ENZYME ASSAY RESULTS

aer ccpm	ADH mol/g-min x10^{4}	HEX mol/g-min x10^{4}	FUM mol/g-min x10^{5}	ISDH mol/g-min x10^{6}
.59	-	-	2.72	3.60
.87	2.18	0.309	2.94	3.36
2.29	1.74	0.299	3.75	2.43
9.00	2.12	0.376	3.74	1.77
0.14	3.43	0.495	3.30	2.72
9.00^{+}	3.30	2.08	3.59	1.43
1.86^{+}	4.19	2.05	3.62	2.31
0.80^{+}	2.22	2.05	4.39	4.76

$^{+}$ High Antifoam

TABLE 11. MISCELLANEOUS ASSAY RESULTS

aer ccpm	PYR extracellular g/l	Sp.PYR g/g-hr x10³	viability %
0.59	0.066	8.9	100
0.87	0.078	9.7	100
2.29	0.117	8.0	100
9.00	0.118	3.4	100
0.14	0.028	8.3	95
9.00+	0.133	4.0	96
1.86+	0.075	4.0	99
0.80+	0.044	3.7	98

+ High Antifoam

4.1 INTRODUCTION

This chapter presents mathematical models of the metabolism of yeast which are aimed at explaining the unusual phenomena that were observed in the macroscopic bioreactor parameters and in the assays of the intracellular components. Interesting phenomena were exposed in three interdependent aspects of the cell metabolism, the catabolic rate, the efficiency of energy utilization, and the underlying rate processes of cell growth reflected in the biomass concentration attained in the fermentor.

The mathematical modeling is subdivided into three categories corresponding to the processes just mentioned. Nonetheless, the three submodels can be combined into one grand model which can qualitatively predict all aspects of intra and extracellular behaviors and quantitatively describe most aspects.

The first division models the factors governing the catabolic rate, including the specific ethanol and glycerol production rates and the specific glucose uptake rate. The model recognizes the vital role played by the intracellular ATP concentration in determining the catabolic rate. It was suggested in the previous chapter that ATP is a potential activator of the glucose transporter, since no other factor can explain the increase in transporter activity that was observed with decreasing aeration rates. High ATP concentrations were also implicated as the cause of the metabolic slowdown at the lowest aeration rates, with the downstream glycolytic kinases being the most likely targets of action. In short, the fact that the specific ethanol productivity and specific glucose uptake rates pass through maxima as the aeration is reduced can be

predicted by incorporating the two targets of action of ATP, the glucose transporter and the downstream kinases. High concentrations of antifoam were also seen to alter catabolism by stimulating glycerol production at the expense of ethanol production. All aspects of the influence of antifoam are well modeled by making transport coefficient for the export of glycerol across the cell membrane a function of the presence of high antifoam in the medium. This division of the modeling also predicts the intracellular glucose 6-phosphate concentrations.

The second modeling division describes the energetic efficiency of ATP utilization in the cell. As the specific ethanol productivity finds a maximum with decreasing aeration rates, the energetic efficiency of growth, Y_{ATP}, passes a minimum, since ethanol production generates ATP and the specific growth rate in the fermentor was always constant. This observation, in addition to the higher ATP yields and lower ATP concentrations of the high antifoam culture and the ATP versus aeration rate profiles of both cultures are all explained by the model. The model postulates two monotonic processes, an increase in the ATP utilization with increasing ATP concentrations, as would be the case with energy wasting ATPases, and an increase in the activity of the waste reactions with increasing dissolved oxygen concentrations.

The final aspect of the modeling addresses the hysteresis and the extinctions and ignitions of the biomass concentration in the fermentor when the aeration rate changes. Specifically in run 4, with no yeast extract in the medium, these sudden events were seen, whereas, they were prevented in run 5 with yeast extract added to the medium of run 4. Also, in run 7, with the high antifoam medium, the hysteresis reappeared.

In runs 6 and 8 with low antifoam, hysteresis was replaced by monotonic, uniformly descending biomass versus aeration profiles. The model focuses on the kinetics of the specific growth rate to explain these phenomena. The model admits all processes which are thought to influence growth kinetics under the experimental conditions. These processes are dissolved oxygen induction of biosynthetic intermediates in the parts per billion concentration, ethanol inhibition, and ATP growth rate enhancement. In addition, another unknown process mediated by oxygen is necessary to generate the hysteresis behavior. Higher ATP concentrations in the low antifoam runs and the biosynthetic intermediates supplied by yeast extract are modeled to influence this unknown process in such a way that the biomass versus aeration profile changes from one exhibiting hysteresis to one exhibiting monotonicity. The convenient tools of singularity theory are applied to this problem.

4.2 MODELING OF THE CATABOLIC RATE

The importance of the intracellular ATP concentration in controlling the rates of the catabolic pathways was demonstrated in the previous chapter. The increase in the steady state specific glucose uptake rate and specific ethanol, glycerol, and pyruvate production rates as the aeration was decreased was traced to an increase in the activity of the glucose transporter, the originator of all of these pathways. ATP posed as the most likely activator of the transporter. Enhanced transporter activity could not be solely due to a progressively increasing degree of saturation by the climbing residual glucose concentration. The specific ethanol productivity remained in the vicinity of 1.00 g/g-hr as the

residual glucose varied from less than 1 g/l to 50 g/l in the fermentor. A sudden increase of 30% in the specific ethanol productivity occurred in the transition between 50 and 70 g/l of residual glucose in runs 5 and 10. No saturation type kinetics with respect to glucose can account for the sudden increase after a relative lull.

Another explanation of transporter activation was supplied by the rising ATP concentration which paralleled the transporter activity. It was proposed that this increase in ATP was the cause and not only the result of accelerated transport. Such a mechanisms would not be unique in *Saccharomyces cerevisiae*, as Spoerl et al. (1) discovered that ATP energy expended in the synthesis of the transport protein governed the final activity attained by it.

The ATP concentration was also implicated as the cause of the glycolytic slowdown seen as the aeration rate of the chemostat was decreased from the optimally stimulating level. The continued accumulation of ATP in this transition resembled the energetic surplus experienced by the cell in the Pasteur mechanism (2) and in the same manner inhibited glycolysis at one of the downstream kinase reactions and possibly phosphofructokinase.

Therefore, ATP was the prime regulator in two of the most important catabolic phenomena seen. The other changes in the metabolic pattern were instigated by the presence of high silicone polymer antifoam concentrations in the medium. High antifoam concentrations spurred glycerol production at the expense of ethanol production, possibly by decreasing the resistance to glycerol diffusion across the cell membrane, thereby, increasing the overall attractiveness of this pathway to the cell. The

specific glucose uptake rates were also hindered by high antifoam, implying that antifoam may be a direct inhibitor of glucose uptake.

In this portion of the modeling, the entire catabolic pattern, including the specific glucose uptake and glycerol and ethanol production rates will be determined as functions only of the intracellular ATP concentration and additional interferences of antifoam. The ATP concentration is an input in this portion of the modeling. The level it attains is determined by energetic balancing to be discussed in the next section.

The catabolic processes in the cell are represented in Figure 1. The specific rate of transport of glucose into the cell is represented by R_1. Several metabolic intermediates in the upper portion of the glycolysis pathway are lumped into a single metabolite I. Represented by I are all metabolites upstream of the rate limiting step in the ethanol production pathway. From the observed crossover in the metabolite levels described in the previous chapter, the limiting reaction is either pyruvate kinase or phosphoglycerate kinase. Therefore, I spans metabolites from glucose 6-phosphate, the first in the pathway, to as far along the pathway as phosphoenolpyruvate. It includes dehydroxyacetone phosphate, the origin of the glycerol production pathway (3). The lumped intermediate, taking the identity of phosphoenol pyruvate or diphosphoglycerate, is converted to ethanol at a specific rate R_3 and with the phosphorylation of ADP. I, posing as dehydroxyacetone phosphate is reduced in its investment, at a rate R_2, in the production of glycerol. Other unmeasured products required to close the carbon and degree of reluctance balances are generated from the intermediates I at a rate R_4. On the average, these products must be oxidized relative to I to support the reducing power

demand in glycerol production. Finally, not shown in Figure 1 is the utilization of I and all other intermediates in biosynthesis.

The residual glucose concentrations of the order of 30 to 90 g/l are sufficient to saturate the glucose transporter, so there is no need to include the glucose concentration in the rate equation of R_1. However, activation by ATP is important, as has been discussed. Another important regulation is the inhibition of glucose uptake by glucose 6-phosphate. Some inhibition of glucose uptake is necessary as downstream bottlenecks in the ethanol pathway have been seen to slow glucose uptake. As the aeration rate was decreased to the lowest supplied in the experimentation, the specific ethanol productivity declined by 40%, and the specific glucose uptake rate was measured to decline by 10%. However, the residual glucose concentration approached the feed glucose level at this point, making the glucose uptake measurement inaccurate. Only 70% of the carbon taken up was recovered in the measured products, with 90-95% being more usual. Therefore, the specific glucose uptake rate probably decreased by more than 10% in response to the downstream bottleneck.

Inhibition of glucose uptake, although not as strong as the decay of ethanol production, also accompanies the Pasteur effect. Den Hollander et al. (4) reported a 40% reduction in glucose uptake simultaneous to a 46% aerobic inhibition of ethanol production in glucose grown cells. The glucose and ethanol rate decreases in acetate grown cells were 45% and 66% respectively. Fiechter (5) noted a 48% drop in the specific ethanol productivity and a 25% drop in glucose uptake in resting cells undergoing Pasteur regulation. It has been proposed that in the Pasteur effect, the blockage of glycolysis at phosphofructokinase results in the

accumulation of the upstream metabolite glucose 6-phosphate, an inhibitor of glucose uptake. Evidences exist both for and against glucose 6-phosphate being a transport regulator (2,6,7). Nonetheless, there must be some regulation of glucose uptake, and in this study, G6P is a candidate as it accumulates to 120% of the preexisting level in response to downstream glycolytic inhibition.

The final modeled effect upon the glucose transporter is the interference by silicone antifoam. The specific glucose uptake rate was generally lower at all aerations when high antifoam was present. It was unknown whether this represented a real inhibition or whether this resulted from the inability of the high antifoam culture to attain the high intracellular ATP concentrations, ATP being the transport activator. Direct inhibition is included in the model, and parameter estimation may partially answer these questions.

The rate of uptake, therefore, is modeled as:

$$R_1 = \frac{K_1}{K_{11}} \left[\frac{ATP}{I + K_2}\right] \qquad (1)$$

where R_1 = sp. transport rate, mmol/g-hr

ATP = ATP concentration, mol/g

I = intermediate concentration, mol/g

K_1 = kinetic constant, mmol/g-hr

K_{11} = inhibition constant of silicone

K_2 = inhibition constant of glucose 6-phosphate

Modeled in Equation 1 are all of the effects discussed. The proportionality with respect to ATP reflects the activation of the transporter. Inhibition kinetics with respect to the intermediate I simulates inhibition

of uptake by glucose 6-phosphate. Finally, K_{11} represent the inhibition of uptake by silicone antifoam. With low silicone present, it assumes a value of 1.0, while with high antifoam, the value is greater than or equal to 1.0.

Expression (1) was modified so that analytic solutions could be attained at this stage of the modeling. The necessity of numerical solutions at this stage would present a severe hindrance to the later stages of modeling. After modification, the equation became:

$$R_1 = \frac{1}{K_{11}} [K_1 \, ATP - K_2 \, I^2] \qquad (2)$$

Naturally, the true activation and inhibition kinetics are distorted and the parameters no longer reflect the strengths of real interactions. However, the essential concepts of ATP activation and glucose 6-phosphate inhibition are retained. In addition, a quadratic dependence was imposed upon the intracellular G6P concentration, because otherwise, an unduly high intracellular G6P content would be predicted. This result is expected as a demand of 40% inhibition is placed upon an observed 20% increase in G6P.

The expression describing the specific ethanol productivity is:

$$R_3 = K_6 \, I \, [K_7 - ATP] \qquad (3)$$

where R_3 = specific ethanol productivity, mmol/g-hr

K_6 = limiting kinase activity

I = metabolite level, mol/g

K_7 = pool of ATP and ADP, mol/g

ATP = intracellular ATP, mol/g

This expression simulates the activity of the limiting kinase reaction. I represents the substrate of the reaction, possibly diphosphoglycerate or phosphoenol pyruvate. Linear kinetics with respect to the substrate is assumed for simplicity. The other substrate for the kinase is ADP, the concentration of which is modeled by the difference between the multiply phosphorylated adenylate pool and the ATP concentration. Of course, interconversion among these cofactors and AMP, and changes in the total adenylate level are neglected. This expression, through the participation of the intermediate I is designed to describe the increase in specific ethanol production resulting in a greater degree of feeding of the metabolism, as a whole as the glucose transporter is activated. It is also designed, through the participation of ADP, to account for the drop in glycolysis arising from the energetic surplus attained at the lowest aeration.

Entry into the glycerol production pathway is modeled as:

$$R_2 = K_3 \, I - K_4 \, GLY_I \qquad (4)$$

where R_2 = sp. glycerol production, mmol/g-hr

K_3 = dehydroxyacetone-P dehydrogenase activity

K_4 = inhibition parameter, or glycerol kinase activity

GLY_I = intracellular glycerol, g/l

The participation of I in this way assures that glycerol production responds to the increased feeding by the glucose transporter, as has been the observed trend. Inhibition, or reversal of this reaction by intracellular glycerol is assumed, if glycerol transport out of the cell in any way limits the overall pathway. A heightened tendency to produce

glycerol was conferred by high antifoam concentrations, possibly through its decrease of the transport resistance of this metabolite across the cell membrane.

Transport of glycerol across the membrane is represented by:

$$R_2 = K_5 [GLY_I - GLY] \sim K_5 GLY_I \qquad (5)$$

where K_5 = transport coefficient

GLY = extracellular glycerol, g/l

In most cases, the intracellular glycerol concentration was more than four times larger than the extracellular levels, so that the driving force for transport is approximated by the intracellular level. In the previous chapter, the ratio between the glycerol production rate and driving force was greater with the high antifoam, possibly identifying the source of stimulation of glycerol production by antifoam. Therefore, the parameter K_5 takes on different values, depending on whether high antifoam is present. Equating the intracellular glycerol production to its excretion gives:

$$R_3 = \frac{K_3 K_5}{K_4 + K_5} I = K_9 I \qquad (6)$$

Since the combination of parameters involving K_3, K_4, and K_5 never appears differently, they are lumped into a new parameter K_9, which has a different value with high or low antifoam.

It was mentioned in the previous chapter that although one mole of glycerol production oxidizes 1 mole of NADH, its production rate is indifferent to the redox considerations of the cell. Rather, as modeled, it responds to the rate of feeding of the pathway by the glucose trans-

porter and the rate of removal of the product by diffusion through the membrane. Nonetheless, the redox balance of the cell must be maintained. Based on the elemental composition of baker's yeast (8), one carbon mole of biomass generates 0.1 mole of NADH, supplying enough reducing power for a specific glycerol production rate of approximately 0.07 g/g-hr at the specific growth rate of 0.2/hr maintained in all experiments. Glycolysis ending in ethanol production neither supplies nor consumes reducing equivalents. Therefore, the additional 0.0 to 0.3 g/g-hr of observed glycerol productivity must be fueled with reducing equivalents generated by the excretion of products oxidized with respect to glucose. These products would account for 5-15% of the feed glucose carbon not recovered in the products ethanol, glycerol, biomass, and associated CO_2 production. In Chapter 3, one possible source of reducing power was recognized in the oxidation of glucose to CO_2 and $NADH_2$ by glycolysis and the TCA cycle. The TCA cycle had a residual activity in this microaerobic range despite the absence of respiration.

Therefore, excretion of other products is made proportional to the glycerol production rate above the 0.07 g/g-hr supported by biosynthesis:

$$R_4 = K_8 [R_2 - 0.6] \qquad (7)$$

where R_4 = sp. glucose util. in other prod., mmol/g-hr

K_8 = relative reductance of product

R_2 = sp. glycerol prod., mmol/g-hr

As the identities of the other products are not known, the correct value for K_8 cannot be chosen, but will be computed based on parameter optimization.

The sum totality of all equations in this section are shown in Table 1. Altogether, there are 8 parameters in the model.

A material balance, assuming negligible yeast extract metabolism can be imposed:

$$R_1 = \frac{R_2}{2} + \frac{R_3}{2} + R_4 + 1.37 \qquad (8)$$

stating that with the adjustment for molar ratios, glucose utilized must terminate in one of these products. The 1.37 reflects the glucose carbon assimilated into biomass. The equation can be solved for the intracellular concentration of metabolite I:

$$I = [-B \pm (B^2 - 4AC)^{1/2}]/2A \qquad (9)$$

where $A = K_2/K_{11}$

$B = K_9/2 + K_6K_7/2 - K_6ATP/2 + K_8K_9$

$C = 1.37 - 0.6\ K_8 - K_1ATP/K_{11}$

With high antifoam in the medium, each time K_9 appears, it is replaced by K_{10}. The intracellular concentration of the metabolite I and all fluxes are functions only of the ATP concentration. As I is intended to represent numerous metabolites in the upstream portion of the glycolytic pathway, its predicted values could be compared to the measured intracellular G6P concentration. The parameters were estimated by optimizing the model's fit to the measured specific glucose uptake and specific ethanol and glycerol production rates and the intracellular G6P concentration, as functions of the measured ATP concentration in both low and high antifoam culture. The IMSL library routine ZXSSQ, minimizing

the sum of squares of M functions in N variables with finite difference, Levenberg-Marquardt algorithm was employed (9). The M functions to be minimized were the 44 residuals between the measured and predicted values. The N variables were the 8 parameters of this model. Weightings of 2.0 were placed upon the specific ethanol and specific glycerol productivities, as these products participate in the energetics of the cell. Energetic balances relying on these results are formulated in the next section. The intracellular glucose 6-phosphate concentration residuals were weighted by a factor of 0.5, since these were viewed as the least important. Other weightings are revealed in the discussion of the results.

The outcome of the optimization is shown in Figures 2-4. In Figure 2, the specific ethanol and glycerol predictions shown a high fidelity to the data with the exception of the specific ethanol productivity with the high antifoam culture at an ATP concentration of around 8.0×10^{-6} mol/g. The accelerated ethanol productivity is out of line with all other high antifoam data points, and could never be generated with the existing model. Possible occurrences here outside the scope of the model which may account for the sudden stimulation are an increase of the limiting kinase activity or a change in the size of the adenylate pool, both decreasing the resistance toward ethanol production. In addition, as this data point existed at the lowest aeration, only 3.5 g/l of extracellular ethanol were present, lower than for the other high antifoam data points. Ethanol may be an inhibitor of glucose transport (10) and its inhibition would be the least at this point. Since the model cannot predict this point, the residual was weighted by a factor of 0.0 in the parameter estimation. The important tendencies of a peak in the specific

ethanol productivity at intermediate ATP concentrations (and aeration rates) and the diversion of metabolites away from ethanol production towards glycerol production by antifoam are predicted.

In Figure 3, the predicted and measured specific glucose uptake rates are shown. Most points are adequately represented with the exception of the two at the highest ATP concentrations. One of these follows the sharp metabolic stimulation with high antifoam, which this model is incapable of predicting. The other point occurs at the lowest low antifoam aeration rate where the residual glucose approaches the feed value. The measurement is subject to large errors. The two troublesome points were weighted by factors of 0.0 in the parameter optimization.

Figure 4 shows the predicted intracellular G6P concentration. Finally, Figure 5 shows the predicted percentage of glucose carbon excreted in unmeasured products. Especially with high antifoam, production of the other products becomes significant with high ATP levels. This might provide an additional reason for the anomalous metabolic stimulation seen at the high ATP concentration with the high antifoam. The excretion of the other products may have dire energetic consequences for the cell, requiring a large ATP generation through ethanol production. To meet this demand, the cell may have overridden the constraints imposed by this model and changed the values of some parameters.

The optimal parameter values are also listed in Table I. The model indicates a 10% inhibition of glucose uptake by antifoam in K_{11}. The total adenylate level, K_7, is 10.4 x 10^{-6} mol/g. Thus, the change in intracellular ATP from 7.5 to 9.2 x 10^{-6} mol/g measured in the transition to the lowest aeration, glycolytically inhibited, low antifoam steady

state would result in a decrease of the predicted ADP concentration from 2.9 to 1.2 x 10^{-6} mol/g. In the energetic surplus of the Pasteur effect, the ADP level has been reported to decrease from 1.8 x 10^{-6} to 0.8 x 10^{-6} mol/g with an increase of ATP from 7.4 to 9.6 x 10^{-6} mol/g (2). The Michaelis Menten constant of ADP for the pyruvate kinase reaction is 1 x 10^{-6} mol/g (3) assuming an intracellular volume of 2 cc/g dry weight. Therefore, the predicted ADP concentration falls in a range which has the power to exert control of the pyruvate kinase reaction.

The parameter K_8 indicates the ratio of unmeasured product formation to glycerol formation, and that the average degree of reductance per carbon mole of this product is 2.8 (11). Typical oxidized products are succinate and pyruvate, with reductance degrees of 2.5 and 3.35 respectively spanning the required level. The degree of reductance can be brought down to any level by the oxidation of glucose to CO_2 and $NADH_2$, CO_2 having a zero reductance.

Finally, the ratio K_9 to K_{10} indicates the relative tendencies of the low and high antifoam cultures to produce glycerol and takes the value of 0.47. From Equation 6, K_9 and K_{10} are composed of:

$$K_9 \ (K_{10}) = \frac{K_3 K_5}{K_4 + K_5} \qquad (10)$$

where K_5 of the transport coefficient of glycerol out of the cell. If transport is a limiting process in the pathway, then $K_5 << K_4$, and the ratio of the glycerol transport coefficient of the two cultures is given by the ratio K_9/K_{10}. In Figure 6, the relationship between the measured driving force for glycerol export (GLY_I - GLY) and the measured specific glycerol production rates is shown, along with optimal linear fits.

The ratio of the slopes of those lines is 0.449, close to the ratio of K_9/K_{10}.

4.3 THE ATP BALANCE

In the previous section, the catabolic pattern, including the specific ethanol and glycerol production rates and glucose uptake rate was modeled as a function only of the intracellular ATP concentration and the additional interferences of antifoam. The ATP concentration was an input to that portion of the modeling. The level of ATP attained in the cell undoubtedly reflects a balance between the tendency for its production in these catabolic pathways and its utilization in maintenance, biosynthesis, and waste. In this section, the processes of ATP utilization are modeled in terms of both environmental conditions and the ATP concentration itself. The equations formulated in this section, when solved simultaneously with those of the previous section, allow for the prediction of the ATP concentration, and thus, the catabolic pattern under different environmental conditions, particularly the dissolved oxygen concentration. Also predicted is the inability of the high antifoam cultures to attain the same, high intracellular ATP concentration or specific ethanol productivities as the low antifoam cultures at the lower aeration rates. This inability has potentially dire consequences for the cell as a very sudden extinction of the biomass concentration was observed only with the high antifoam culture and in the same aeration range that increases in ATP and the specific metabolic rates normally occur. The relationship of the ATP concentration and catabolic rates to the specific growth rate and biomass concentrations are considered in

the next section.

Incorporated into the equations are the unusual features governing ATP consumption that were exposed in Chapter 3. The efficiency of ATP utilization expressed in the ATP yield, Y_{ATP}, was found to attain a minimum as the aeration rate was decreased, since the specific ethanol production rate attained a maximum, while the specific growth rate remained constant (Chapter 3, Figure 18). It was conjectured that two separate processes were responsible for this contradictory reversal of the efficiency of ATP utilization. The first process was the wastage of ATP by ATPases, futile cycling, and other ATP sinks (12) which become progressively stronger as the ATP concentration increases. Thus, the increasing ATP concentration as the aeration decreased may be responsible for the simultaneous decrease in the ATP yield. The second process was the change in activity of these ATP waste reactions as a function of the dissolved oxygen concentration and clearly manifested itself as a large increase in the ATP yield as the aeration rate was reduced to the lowest level (Chapter 3, Figure 18). That the energetic efficiency was improved at this point is also indicated by the accumulation of ATP. All behaviors of the intracellular ATP concentration and the ATP yield can be accounted for by simple mathematical models describing the influences of ATP and oxygen on the ATP utilization reactions.

In the formulation of the ATP balance, the ATP production rate has already been described by the equations governing catabolism in the previous section:

$$R_{ATP} = R_3 - R_2 \qquad (11)$$

where R_3 = specific ethanol prod., mmol/g-hr

R_2 = specific glycerol prod., mmol/g-hr

R_{ATP} = ATP prod. rate, mmol/g-hr .

This expression derives from the generation of one high energy phosphate bond for each molecule of ethanol production and the hydrolysis of one bond for each molecule of glycerol excreted (3). Mathematical expressions relating R_3 and R_2 to the intracellular ATP concentration and the presence or absence of high antifoam have been presented. Entering these expressions into Equation 11 gives an equation in which the rate of catabolic ATP production is governed by the intracellular ATP concentration and a parameter that takes on different values when high or low antifoam is present:

$$\begin{aligned} R_{ATP} &= R_{ATP}\,(ATP,\ K_9,\ K_i) \quad \text{low antifoam} \\ R_{ATP} &= R_{ATP}\,(ATP,\ K_{10},\ K_i) \quad \text{high antifoam} . \end{aligned} \tag{12}$$

The parameters K_9 and K_{10} quantify the propensity towards glycerol production, which is greater in the high antifoam culture. The K_i are the remaining 7 parameters evaluated in the previous section. The model predictions of R_{ATP} in comparison to the data are shown in Figure 7. The adherence of the model to the data is comparable to its ability to predict the specific ethanol and glycerol productivities. In Figure 8, a modification to the model that was actually used in the ATP balancing is shown. In most ways, the modified model is identical to the old one, differing only in the slope of the high antifoam curve at the lowest ATP concentrations. This modification was necessary, as the results of the ATP balancing are sensitive to the slope in this portion of the curve,

and will be discussed further. The equations generating the new model and the parameter values are presented in Table 2.

Attention is now turned to the other half of the ATP balance, the ATP utilization rate. Superficial reasoning would dictate that ATP utilization is constant at all aeration rates since the specific growth rate, and hence, biosynthesis and maintenance consumption should be constant. However, equating a constant with the right side of Equation 12 would result in an unchanging ATP concentration, contradicting experimental observations. Also, the ATP yield was indeed found to change. A second approach would be to propose a dissolved oxygen-dependent ATP utilization rate:

$$R_3 (ATP) - R_2 (ATP) = U_{ATP} (O_2) , \qquad (13)$$

where U_{ATP} = specific ATP utilization, mmol/g-hr

O_2 = dissolved oxygen, ppb.

A graphical representation of the two halves of Equation 13 is shown in Figure 9. The horizontal line represents the ATP utilization at a given dissolved oxygen concentration. As formulated, this utilization is independent of the ATP concentration. The ATP production rate profiles appear familiar, with the inclining portion at the lower ATP concentration being due to ATP activation of the glucose transporter, and the declining portion at the higher ATP concentration due to the glycolysis slowdown at the kinase reactions precipitated by suboptimal ATP/ADP ratios. The ATP level and production rates attained are given by the intersection of the utilization and production curves. To match the experimentally observed changes in these two parameters, the level of the horizontal

line must be altered by formulating an appropriate function U_{ATP} (O_2).

The view espoused by Equation 13 is unsatisfactory for a number of reasons. The production and consumption curves actually have two intersections, one at high and one at low ATP concentrations (Figure 9). However, the solution at the lower ATP concentration in which the ATP production curve is crossed from above is actually unstable. One can envision a scenario in which the ATP concentration is perturbed to a higher level from this unstable equilibrium. Since the slope of the production curve exceeds that of the utilization curve at this point, the ATP concentration would continue to increase perpetually until the intersection at the higher ATP concentration is found. Viewed mechanistically, the intersection at the lower ATP level is in a region in which ATP activates the glucose transporter. As glucose transport is activated, glycolysis is accelerated, producing more ATP without an accompanying change in the utilization rate. The positive feedback process would continue until ATP would accumulate to a point in which the glycolytic kinases could no longer operate optimally, slowing the overall glycolytic rate and attaining the intersection at the high ATP level. With this formulation, the inclining ATP production rate with the increasing ATP concentration would never be seen.

An alternate approach would be to inject a negative feedback mechanism into the system to stabilize intersection at low ATP concentrations. The stabilization can be accomplished by formulating ATP consumption reactions that increase in rate with increasing ATP concentrations. Stated mathematically:

$$R_{ATP} = U_{ATP} \ (ATP, \ O_2)$$

and

$$\partial U_{ATP}/\partial ATP > 0 \quad . \tag{14}$$

ATP utilization is also a function of the dissolved oxygen, because at the lowest rate, the ATP concentration increased, but the ATP yield also increased (Chapter 3, Figures 18 and 21). A graphical representation of the balance in Equation 14 is shown in Figure 10. ATP consumption curves intersect the production curves from underneath, guaranteeing stable solutions at all intersections. The slope of the consumption curve is shown to increase with increasing aeration. When this is done, all necessary patterns emerge. By following the intersections of the curves as the slope(aeration) increases, the ATP yield, inversely proportional to the ATP utilization rate, attains a minimum, and the ATP concentration decreases monotonically (Chapter 3, Figures 18 and 21). The predicted ATP concentration for a given aeration rate is lower for the high antifoam culture, as are the rate of ATP production and overall metabolic rate (Chapter 3, Figure 21).

The remaining task is to formulate the function $U(O_2, ATP)$. The total ATP consumption is actually the summation of several processes. ATP consumption for biosynthesis and maintenance in the strict sense should remain constant, since the specific growth rate is constant. The variability in the overall utilization rate must arise from ATP sinks, which are independent of growth and maintenance, such as wastage by ATPases and enzymes involved in futile cycling. In E. coli, waste by ATPases can account for more than 50% of all ATP utilized (12). If the consumption reactions are modeled as a single hydrolyzing enzyme, then the kinetics with respect to ATP should be saturable. The dependence of utilization

on ATP can be written as:

$$U_{ATP}\Big|_{O_2} = \frac{\mu}{Y_{ATP}^{max}} + m + \frac{K_{14}\ ATP}{K_{15} + ATP} \quad . \tag{15}$$

Y_{ATP}^{max} is the true growth yield, μ is the specific growth rate, m is the maintenance coefficient, K_{15} is the half-saturation coefficient of the model waste reaction, and K_{14} is the activity of the reaction. For simplicity, the entire process is instead modeled by a proportionality with respect to ATP:

$$U_{ATP}\Big|_{O_2} = K_{14}\ ATP \quad . \tag{16}$$

The consequences of the simplification are the alteration of the trajectories of the utilization curves as they cross the production curves and the inability to predict ATP balances at other specific growth rates. However, there is not enough information from the experimentation or from theoretical considerations to enable the precise prediction of these trajectories or the extrapolation to other specific growth rates. In reality, anything more complicated than the linear relationship cannot be justified.

Assuming the linear relationship with respect to ATP, the functionality of the utilization curves with respect to oxygen can be established by fitting the ATP versus aeration rate data. In Chapter 3, Figure 19, the ratio $1/(Y_{ATP}\ x\ ATP)$ determined from experimental data is shown to assume a saturation profile with respect to the aeration rate. A physical interpretation of such a profile would be the induction of ATP-wasting enzymes by oxygen at low dissolved oxygen levels, analogous to the induc-

tion of numerous respiratory enzymes and the stimulation of unsaturated fatty acid and sterol synthesis (13). Therefore, utilization is modeled as:

$$U_{ATP}(ATP, O_2) = \frac{K_{12} O_2 ATP}{K_{13} + O_2} = R_{ATP}(ATP) . \quad (17)$$

Given the constants K_{12} and K_{13} and by substitution of the expression for R_{ATP} from Table 2 into Equation 17, the ATP versus dissolved oxygen profile can be predicted by solving 17 implicitly. The parameters can be evaluated by optimally fitting the experimentally determined profile.

In actuality, the data from this experimentation are reported in terms of the aeration rate, since the dissolved oxygen was not measured. However, the D.O. can be estimated by matching the data from this experimentation with those of Nishizawa et al. (14), who did measure the D.O. in the parts-per-billion range. The comparison begins by formulating a simplified gas-to-liquid mass transfer equation:

$$k_1a (P_O/H - O_2) = \nu_O O_2 X . \quad (18)$$

Here, k_1a is the mass transfer coefficient, P_O is the partial pressure of oxygen in the gas feed to the fermentor, H is the Henry's law constant, ν_O is the specific oxygen uptake rate, and X is the biomass concentration. The feed oxygen partial pressure here is easily calculated from the ratio of the aeration rate to the pure nitrogen supply rate, as the aeration rate always refers to the flow of air mixed with 500ccpm of nitrogen before entering the fermentor. It has been repeatedly stated that respiration is an insignificant contributor to metabolism, owing to severe oxygen limitation and glucose repression of respiratory enzymes.

However, oxygen scarcity in the gas phase also limits mass transfer by providing for a low driving force. Therefore, the two processes are comparable in magnitude so that respiration and biosynthetic oxygen uptake become important in determining the dissolved oxygen concentration. Functionality with respect to oxygen is assumed to be linear, again because of limiting concentrations. The final simplification arises primarily from the choice of the feed partial pressure of oxygen rather than that existent over the fermentor. However, when this is done, the dissolved oxygen can be related to measured quantities and the well-known Henry's constant, knowing only one parameter, ν_o/k_1a. This parameter can be estimated by comparing, point for point, the specific ethanol production versus aeration rate data in these experiments with the specific ethanol versus dissolved oxygen data of Nishizawa et al. (14). The predicted specific ethanol production rate versus dissolved oxygen profile, assuming a value of 0.282 for ν_o/k_1a, is compared with the literature data in Figure 11. At this value of the parameter, a maximum exists in the specific ethanol productivity at 10 ppb of dissolved oxygen as it does in the literature, and there is reasonable correspondence at the other dissolved oxygen levels. Henceforth, any reference to the dissolved oxygen concentration in the data from this experimentation is actually a prediction based on the assumed ν_o/k_1a.

The experimental data for ATP versus dissolved oxygen for both the low and high antifoam runs and the predictions of Equation 17 are shown in Figure 12. The parameters K_{12} and K_{13} were set to 5.6 and 5.7, respectively, by forcing the equation to fit the data points at the highest and lowest dissolved oxygen concentrations of the low antifoam run. The

high antifoam data with the attainment of high ATP levels shifted to the lower dissolved oxygen concentrations are well predicted. The data for the low antifoam case is less certain, given the scatter and the absence of data in the important 25-45 ppb dissolved oxygen range. However, the predictions represent one legitimate interpolation of the low antifoam data. In any event, the data and predictions agree in the higher ATP concentration attained by the low antifoam culture at any given dissolved oxygen concentration, the separation being widest at intermediate dissolved oxygen concentrations. In the next section, the possible influence is explored, of the difference in ATP content on the specific growth rate and in the sharp extinction in the biomass concentration observed with the high antifoam culture at around 20 ppb dissolved oxygen.

The model in Section 2 was modified primarily in the slope of the high antifoam ATP production curve at the lowest ATP concentration. This was done because the predicted ATP concentration at the highest dissolved oxygen concentration is sensitive to the slope in that region and the ATP concentration at 50 ppb was grossly underpredicted. As mentioned previously, the modified model is shown in Table 2.

A final measure of the success of the model is its prediction of the rate of ATP utilization as a function of dissolved oxygen for both the low and high antifoam cultures. The ATP utilization rate divided by the ATP concentration, U_{ATP}/ATP, should give the same saturation profile according to Equation 16, regardless of whether high or low antifoam is present. The data and predictions of U_{ATP}/ATP are shown in Figure 13. Despite considerable scatter, the saturation profile is discernible and accurately represented. In actuality, U_{ATP}/ATP represents the activity

of the ATP-wasting reactions. The saturable increase in waste activity may, again, reflect an oxygen induction of ATP-hydrolyzing enzymes.

In Figure 14, the predicted and measured Y_{ATP} values are shown as a function of the predicted dissolved oxygen concentrations, with the usual assumption of 0.282 for the ratio ν_o/k_1a. The descent in this parameter along with dissolved oxygen in the low antifoam culture responds to the increasing ATP concentration, ATP being the reactant and stimulant of ATP waste reactions. The reversal of the trend at the lowest D.O. indicates the relative importance of oxygen induction of ATP waste reactions at the low D.O. levels. In the high antifoam culture, Y_{ATP} is generally higher and descends less steeply, according to both the measurements and predictions. Undoubtedly, this is due to the relative constancy of the intracellular ATP concentration, especially towards higher dissolved oxygen levels. As usual, the prediction misses the data point at the lowest dissolved oxygen level of the high antifoam culture.

4.4 SPECIFIC GROWTH RATE AND BIOMASS CONCENTRATIONS

Until now, the modeling has focused on the catabolic processes of ethanol and glycerol production without considering the anabolic or biosynthetic pathways. The specific growth rate remotely entered into the ATP balance between the energy utilizing and producing processes; the outcome of the balance dictated the catabolic rates as functions of the dissolved oxygen. However, all utilizing reactions were made proportional to the ATP concentration, a formulation more relevant to ATP waste reactions by ATPases than to biosynthesis. The specific growth rate did not enter explicitly into the equation of ATP utilization.

In this portion of the modeling, factors affecting the specific growth rate and biomass concentrations are considered. Some critically important phenomena were observed in the experimentation, which must be explained by the model. In runs 4 and 7, the biomass versus aeration profile was found to undergo hysteresis. Characteristic of the hysteresis were the sudden drops in the biomass concentration with decreasing aeration, which did not retrace their paths (i.e., sudden increases in biomass) as the aeration was increased across the same volumetric rate (Chapter 2, Figures 22 and 14). Ignitions, or sharp increases in the biomass concentration were triggered by increasing the aeration rate. However, the ignition occurred at higher aerations than the extinction. Between these two critical aeration rates, both high and low biomass concentration steady-states existed at the same aeration rate. Which of these steady-states were assumed by the fermentor at these aerations depended on the past history of the culture.

Although hysteresis was observed in runs 4 and 7, runs 5, 6, and 8, which were carried out under slightly altered conditions, showed monotonic biomass-versus-aeration profiles with no hysteresis or associated extinction or ignition phenomena (Chapter 2, Figures 22 and 14). In run 5, yeast extract was added to the medium of run 4, while in runs 6 and 8, the high feed antifoam concentration of run 7 was eliminated.

The yeast extract in the medium had three possible influences upon the system, preventing the catastrophic events. The first possibility is that it directly enhanced the specific growth rate by providing biosynthetic intermediates such as amino acids and nucleotides, which would otherwise be biosynthesized by the cell. In mathematical terms, its

presence in the medium altered certain parameters in the equations governing the specific growth rate and, thereby, gave rise to a different biomass versus aeration profile.

The second possible influence of yeast extract may have been its conferral upon the culture the ability to attain higher specific ethanol productivities. Shown in Chapter 2, Figure 17 is a comparison between the specific ethanol productivity versus residual glucose profiles of runs 4 and 5. A gap between 45 and 65 g/l of residual glucose is seen in run 4. This gap represents the region passed over in both the extinction and ignition of the biomass concentration, and therefore, never seen. The gap border at low glucose concentrations corresponds to the last steady-state before extinction and the gap border at the high glucose concentration represents the last steady-state before ignition. Bifurcation theory, as will be discussed, allows only for unstable solutions in this gap region, so that they are never attained. In contrast, run 5 shows a sharply increasing specific ethanol productivity at a residual glucose concentration, which would be excluded by the gap in run 4. Thus, it is possible that the entire hysteresis was prevented by the ability of the yeast extract culture to attain the higher specific ethanol productivity in this critical region. A higher specific ethanol productivity would generate more ATP for the cell, which, in turn, would benefit biosynthesis in a manner preventing the sudden extinction of the biomass and all other aspects of the hysteresis. An opposing view is that the yeast extract free culture also has the ability to attain high specific ethanol productivities in the gap region, but is nonetheless powerless to prevent the washout of biomass. It is unclear from the catabolic

modeling how yeast extract can increase the specific ethanol productivity.

The third possibility for the role of yeast extract relates to both of the previous possibilities. By providing biosynthetic intermediates to the cell, ATP, which would ordinarily be directed towards biosynthesis, could be diverted to other causes that are vital for the maintenance of high biomass concentrations in the fermentor. From among these three possibilities, the first is most harmonious with the catabolic modeling previously described and the specific growth rate modeling of this section. The influence of yeast extract will be reassessed at the end of this section.

When the high antifoam concentration of run 7 was reduced in runs 6 and 8, the sharp extinction of the biomass concentration and the narrow hysteresis loop were eliminated in favor of a monotonic and more uniform biomass versus aeration profile (Chapter 2, Figure 22). As has now been mentioned many times, the low antifoam culture was able to develop higher intracellular ATP concentrations than the low antifoam culture. Therefore, ATP is implicated as a factor in the prevention of the catastrophic events.

In this section, mathematical equations are presented that generate hysteresis and all associated phenomena in the biomass profile. The hysteresis is reversed when the intracellular ATP concentration is allowed to attain higher levels. Thus, the effects of reducing the nutrient antifoam concentration are simulated. Particular emphasis is placed upon the intervention of ATP into the specific growth rate equation and its most realistic targets of biosynthetic enhancement. Room is also made in the model for the intervention of yeast extract. The model includes all factors thought to control the specific growth rate in this

microaerobic range, such as participation of molecular oxygen in the biosynthetic pathways of sterol and unsaturated fatty acids (13), and ethanol inhibition.

The modeling begins in the description of the four processes thought to govern the specific growth rate. The first, as just discussed, is the involvement of molecular oxygen in the biosynthesis of unsaturated fatty acids and sterols. That these components may limit growth is made clear by the need to supplement the medium with precisely these components in the form of ergosterol and tween 80 under completely anaerobic conditions (15). Without this supplementation, yeast cannot grow anaerobically. The study by Rogers and Stewart (13) indicates that only trace quantities of dissolved oxygen, of the same magnitude as employed in this study, are necessary to initiate biosynthesis of these components. This dissolved oxygen level is far below that required to support respiration. Their data also show that the percentage of the total cell weight occupied by these components has a saturation-type profile with increasing dissolved oxygen with a half-maximal response elicited by a few parts-per-billion of dissolved oxygen. Therefore, the first contribution to the specific growth equation is a Monod functionality with respect to the dissolved oxygen concentration, representing the contribution of these limiting components:

$$A = \frac{O_2}{K_o + O_2} \qquad K_o = 5.0 \text{ ppb} . \tag{19}$$

A is only one term in the specific growth rate equation, O_2 is the dissolved oxygen in parts-per-billion, and K_o is the half-saturation coefficient chosen to be 5.0 ppb to accord with the data of Rogers and Stewart.

The behavior of A as a function of the dissolved oxygen in the range relevant to this study is shown in Figure 15. The process is most relevant at the lowest aeration rates studied and at a dissolved oxygen level of around 50 ppb at the highest aeration rates, the process is nearly saturated. Again, it must be emphasized that the dissolved oxygen concentration was not actually measured, but rather, it was deduced from the aeration and nitrogenation rate and an assumed ν_o/k_1a of 0.282 discussed in Section 3.

The second process considered is enhancement of biosynthesis by the energy source, the phosphate bonds of ATP. It seems necessary that ATP in some way enters the growth equation so that the attainment of high ATP levels can affect the detrimental effects of some other processes, preventing the biomass extinction. It has long been suggested that the ATP level, or actually, the adenylate energy charge, is a fundamental rate regulator of biosynthetic processes (16). The energy charge is defined as:

$$(ATP + 1/2\ ADP)/(AMP + ADP + ATP)\ . \qquad (20)$$

The energy charge is a measure of the total number of high-energy phosphate bonds available in the total adenylate pool, with ATP having 2 such bonds, ATP one, and AMP none, explaining the weighting of the different species in the index. A number of biosynthetic enzymes, such as phosphoribosyl pyrophosphate synthetase, aspartokinase, and phosphoribosyl ATP synthetase increase in activity monotonically with an increasing energy charge. In addition, the energy charge of yeast growing in batch, continuous, and microaerobic turbidostat culture is highly correlated with the

ATP concentration (17, 18, 19). Therefore, this contribution to the specific growth rate can be viewed equally well as the domain of the energy charge. For lack of a better alternative, the functionality with respect to the ATP concentration is chosen to be Monod type:

$$B(ATP) = \frac{ATP}{K_{ATP} + ATP} \qquad K_{ATP} = 3\ \mu mol/g\ . \tag{21}$$

B represents the second contribution to the specific growth rate. A half-saturation coefficient of 3 μmol/g is chosen as being of the same order of magnitude as the ATP concentrations measured in this study. A K_{ATP} much lower than this would imply that this process is saturated under the conditions employed and that ATP exercises no control. K_{ATP} much higher than this would imply that the process is not saturable, and B is essentially a linear function of ATP. Typical half-saturation coefficients of yeast enzymes with respect to ATP do not allow much higher values of K_{ATP} (3). The shape of B as a function of the ATP concentration is shown in Figure 15. The influence of ATP is strongest at the highest aeration rates, as the ATP concentrations were lowest there.

A third process to be considered is ethanol inhibition. A study of this strain has revealed a maximum ethanol concentration of 93.6 g/l, or about 2000 mmol/l, above which growth ceases (20). The functionality of the inhibition with respect to the ethanol concentration between 0 and 93.6 g/l is uncertain, with concave downward functions, as $(1-E/E_{max})^{1/2}$, concave upward $(1-E/E_{max})^2$, and linear $(1-E/E_{max})$ inhibition functions proposed (20). For simplicity, the linear version is chosen so that:

$$C(E) = (1 - E/E_{max}) \qquad E_{max} = 2000\ mmol/l\ . \tag{22}$$

This linear functionality is also shown in Figure 15. The maximum ethanol concentration encountered in these studies is 35 g/l, meaning that growth is at most inhibited by about 35%.

The three processes just described are all well behaved, monotonic functionalities, which would not allow for the sudden extinction or ignition of the biomass concentration at the critical aeration rates. Rather, more uniform, monotonic profiles would be predicted. Therefore, a fourth process must be injected into the equations providing for the hysteresis behavior. A simple equation generating hysteresis is an "S" shaped function (21)

$$\alpha (D - D_S)^3 - \beta (D - D_S) - (O_2 - O_{2S}) = 0 \quad . \tag{23}$$

$D = D(O_2)$ is the fourth contribution to the specific growth rate and is a function of the dissolved oxygen concentration O_2. Examples of the curves generated by Equation 23 are shown in Figure 16. When $\beta > 0$, the curve folds back upon the dissolved oxygen concentration O_2, creating a region of steady-state multiplicity with three possible steady-states. From bifurcation theory (22), it is well known that the middle steady-state must be unstable. When a curve such as this describes a real process, a hysteresis loop is observed. As the dissolved oxygen is lowered, the function D gradually declines until the curve begins to turn. Past the apex, called the limit point, the solution falls to a lower level. In the real process, this would be an extinction. As the dissolved oxygen is increased from this point, the path is not retraced, but follows a gradual inclination until the other limit point is reached,

whereupon, there is an ignition. Between the limit points, two stable steady-states are possible, and the one attained depends on the past history of the dissolved oxygen inputs. All of these descriptions are interchangeable with the ones provided for the biomass concentration versus aeration rate, so that it becomes reasonable that some underlying process described by the function D gives rise to the observed behaviors.

As written, D is a function of the dissolved oxygen concentration, lacking better information. The variable actually causing these behaviors may be correlated only with the dissolved oxygen. However, if the variable is dissolved oxygen, then most likely, D relates to the intracellular processes influenced by oxygen such as respiratory enzyme induction (13), mitochondrial differentiation (23), or the biosynthesis of sterols, fatty acids, and membrane components (13). It is difficult to assign a physiological interpretation to the function D, since such behavior arises from the mathematics. However, it can be stated that the process represented by D has a tendency to maintain the status quo until conditions are stretched to the limits, whereupon the state of the system unravels completely. For example, assume that D represents differentiation of promitochondrial structures into respiratory-competent mitochondria, motivated by oxygen (23) and in some way benefiting cell growth. At the lowest dissolved oxygen levels, and lowest values of D, mitochondria would be undifferentiated and remain so until the dissolved oxygen is raised to a concentration corresponding to the limit point. Above this dissolved oxygen, the system can no longer resist the forces inducing differentiation, and suddenly most or all mitochondria undergo metamorphosis. In contrast, mitochondria in place at the highest dissolved

oxygen levels will resist degeneration if dissolved oxygen is lowered, even below the point at which the ignition occurs. When the dissolved oxygen falls below the limit point, the mitochondria degenerate completely. In the middle solution branch between the limit points, mitochondrial development is inversely related to the dissolved oxygen level. These solutions are unstable, but if a suitable control system were imposed, they would exist. It is difficult to assign a physical interpretation to this branch of solutions.

Also shown in Figure 16 are the effects of the parameter β on the shape of the curve generated from Equation 23. When $\beta>0$, hysteresis and steady-state multiplicity are generated. When $\beta<0$, a monotonic profile is seen. When $\beta=0$, the curve borders steady-state multiplicity. The parameter α dictates the height of the "S" shaped curve. The greater the value of α, the shorter the curve. Finally, the parameters O_{2_S} and D_S specify the location of the center of the "S" shaped curve. The actual "S" shaped curve injected into the equations of growth is also shown in Figure 15. The curve was intentionally made asymmetric by boosting the value of α by a factor of 50, when $D<D_S$. This was done for no other reason than to fit the data towards the lower aeration rates. The methods used to fix the parameter values of Equation 23 will be discussed shortly.

The four Equations, 19, 21, 22, and 23, representing the most important growth-related processes, are combined into a single function for the specific growth rate in a steady-state material balance on biomass:

$$\frac{\mu_{max}}{d} [A(O_2)\ B(ATP)\ C(EtOH)\ D(O_2)] - 1 = 0 \quad . \tag{24}$$

Another parameter, μ_{max}/d, the ratio between the maximum and actual specific growth rate in the chemostat, has been introduced. The lower case d is the dilution rate, which, at steady-state, equals the specific growth rate. Implied is that, if all four processes, A-D, operate at optimal values of 1.0, then the specific growth rate in the fermentor will be the maximum possible specific growth rate of the microbe. All functions, A-D, must be between zero and one. It could be interpreted from Equation 24 that no single process limits growth, but rather, the specific growth rate is a composite of all processes. A deficiency in one process can be compensated by a surplus in another. However, Equation 24 does not exclude the possibility that the subfunctions modulate a single process, or fewer than four limiting processes. For example, sterol synthesis is induced by oxygen, but may also be enhanced by ATP, so that two of the four functions apply to the same process.

The specific growth rate remains constant at all levels of aeration supplied to the fermentor. As the dissolved oxygen is changed, the degree of enhancement or inhibition of all processes must vary in a combination that preserves the mathematical product. For example, if O_2 is increased, the process A benefits, which means one or more of the processes B-D must weaken. The greatest flexibility is offered by the function C. If conditions are beneficial, then the specific growth rate increases, causing biomass and extracellular ethanol to accumulate. Biomass and ethanol continue to accumulate, until C is sufficiently inhibited so that the specific growth rate is restored to the dilution rate. The opposite scenario is easily envisioned.

Equation 24 consists of numerous variables, EtOH, ATP, and O_2. To

reduce the number of variables, the equations proposed in the previous modeling must be invoked. The ethanol concentration in the fermentor is obtained from the steady-state material balance:

$$EtOH = R_3 (ATP)X/d \ . \qquad (25)$$

R_3 is the specific ethanol production rate, whose functionality with respect to ATP is shown in Table 2 and discussed in the catabolic modeling section. This equation could be injected directly into Equation 25, but for mathematical simplicity, an optimal polynomial fit of R_3 is used instead. In Figure 17, a comparison is shown between the previous model predictions and the polynomial fit for both high and low antifoam in the medium. The polynomial equations are written in Table 3. It is important to emphasize that the mechanistic connection between the specific ethanol productivity and the ATP concentration, arrived at in the previous modeling, is unimportant here as long as the data are fit. The ethanol concentration has been eliminated from Equation 24 in favor of the intracellular ATP concentration and the biomass concentration.

The ATP balance of Equation 13 describes the relationship between the ATP concentration and the dissolved oxygen concentration. Rather than using the equation directly, polynomial fits to the equation shown graphically in Figure 18 were actually used. The polynomials are written in Table 3. Therefore, the ATP concentration can be eliminated from Equations 25 and 24 in favor of the dissolved oxygen concentration, using the polynomial ATP = ATP(O). Finally, the dissolved oxygen concentration can be eliminated in favor of the biomass concentration and the aeration rate with the aid of Equation 18, representing the gas-to-liquid oxygen

transfer and oxygen uptake balance:

$$O_2 = \frac{16.33\ Q_A}{1 + 0.282\ X} \quad , \tag{26}$$

where Q_A = aeration, ccpm

X = biomass, g/l .

Now, Equation 24 can be rewritten as:

$$F[X, Q_A, \underline{P}] = 0 \quad . \tag{27}$$

$\underline{P}$ is a vector of parameters including all yet unspecified parameter values μ_{max}/d, D_S, O_{2S}, α and β. Equation 27 can be solved implicitly to yield the biomass-versus-aeration profile. These five parameters can be set to attain a fit between the experimental and predicted profiles. From among these, the parameter D_S, the center of the "S" shaped function was arbitrarily chosen to be 0.75. If another value were chosen, then the parameter evaluation method to be described would adjust the μ_{max}/d value to accommodate the different choice, but the X versus Q_A profile would remain unchanged. The parameter value α must be chosen so that the biomass concentration at the highest aeration rate is around the experimental value of 6.5 g/l and not 20 or 2 g/l. Parameter α specifies the height of the "S" shaped curve and dictates the difference between the maximum and minimum biomass concentration at the extremes of the dissolved oxygen concentration. This leaves 3 parameters to assure that the most important phenomenon is accurately represented, the narrow hysteresis loop and the sharp drop of the biomass concentration as the aeration rate was lowered in the high antifoam run (Chapter 2, Figure 22).

The aim of the model is to use the parameters β, O_{2S}, and the μ_{max}/d to fit the biomass-versus-aeration profile of the high antifoam run 7 as closely as possible, including the incipient hysteresis loop. The relationship ATP(O) and R_3(ATP) of the equation relevant to the high antifoam run were injected into Equation 24 during the fitting process. Then, the elimination of high antifoam from the medium could be simulated by changing the polynomials ATP(O) and R_3(ATP) to those relevant to the low antifoam runs, but maintaining all other equations and parameter values. Tested in this exercise is the ability of the low antifoam culture to counteract the tendency for the biomass concentration to drop sharply past the limit point of equation D by attaining higher ATP concentrations. It has been the suspicion that the beneficial effects of the high ATP concentrations of the low antifoam culture prevented the hysteresis and all associated phenomena.

The most convenient tools for manipulating the parameter values β, O_{2S} and μ_{max}/d to duplicate the correct hysteresis behavior are offered by singularity theory. Singularity theory and its applicability to chemical reactor engineering problems have been reviewed thoroughly (21, 24) and only bare essentials are repeated here. Singularity and bifurcation theories are concerned with equations of the type 27, consisting of a functional relation between the state variable (in this case, the biomass concentration X), the manipulated input or bifurcation parameter (in this case the aeration Q_A) and a set of auxiliary parameters (in this case $\underline{P}$). A bifurcation diagram is a plot of the state variable versus the bifurcation parameter, with the auxiliary parameters held constant. Bifurcation diagrams change as the parameter values $\underline{P}$ are manipulated.

Biomass-versus-aeration profiles are all bifurcation diagrams.

An important result in singularity theory is that the qualitative features of the bifurcation diagram change when the parameter set $\underline{P}$ crosses one of three surfaces in P-space. Qualitative features refer to the number of steady-states for a given value of the bifurcation parameter and changes in the number of steady-states as the bifurcation parameter is changed. One of these surfaces is the hysteresis variety (H) and is of particular interest in this study. When the parameter set $\underline{P}$ crosses this surface, the bifurcation diagram changes from a monotonic one, through an inflection, and to an "S" shaped curve with 3 solutions for a range of bifurcation parameters. This transition is quite analogous to the effect of changing the values of β in Equation 23, with the resulting changes in the bifurcation diagram shown in Figure 16. $\beta=0$ is the parameter value for which the bifurcation diagram undergoes a transition, and for this equation, constitutes the set (H), the hysteresis variety.

The conditions upon the parameter set, making it a member of the hysteresis variety, can also be specified. The general bifurcation is $G(x, \lambda, \underline{q}) = 0$, where x is the state variable, λ the bifurcation parameter, and $\underline{q}$ the set of parameters. The hysteresis variety is defined by:

$$G(x, \lambda, \underline{q}^0) = \frac{\partial G}{\partial x}(x, \lambda, \underline{q}^0) = \frac{\partial^2 G}{\partial x^2}(x, \lambda, \underline{q}^0) = 0 \ , \qquad (28)$$

where $\underline{q}^0$ are members of the hysteresis variety. x and λ can be eliminated from two of the above three equations, leaving the last equality as a condition upon $\underline{q}$ defining a hypersurface in q-space. Changing any parameter value in $\underline{q}$ or any combination of parameters, such that $\underline{q}^0$ is crossed, results in the transition from a monotonic to a hysteresis

profile.

The hysteresis loops encountered in the biomass-versus-aeration profiles are all narrow (Chapter 2, Figures 14, 22), indicating that the parameter set of the hysteresis variety must be nearby. The observed bifurcation diagram can be accurately fit by forcing the parameter set to be members of the hysteresis variety. Furthermore, the hysteresis loop should occur at the right place, with the inflection being at the experimentally observed biomass and aeration rates. This is equivalent to specifying x and λ in Equation 28, placing 3 constraints on the parameter set $\underline{q}$ (or in reality, $\underline{P}$).

To fit the data of run 7, particularly in the appearance of an inflection in the biomass-aeration profile at around Q_A = 1.8 ccpm and x = 2.8 g/l, the 3 constraints of Equation 28 were applied to Equation 27 to solve for the three remaining parameters, O_{2s}, μ_{max}/d, and β. The equations solved in the process were:

$$F(x, Q_A, O_{2s}, \mu_{max}/d, \beta)\Big|_{x=2.8,\ Q_A=1.8} = 0$$

$$\frac{\partial F}{\partial x}(x, Q_A, O_{2s}, \mu_{max}/d, \beta)\Big|_{x=2.8,\ Q_A=1.8} = 0 \qquad (29)$$

$$\frac{\partial^2 F}{\partial x}(x, Q_A, O_{2s}, \mu_{max}/d, \beta)\Big|_{x=2.8,\ Q_A=1.8} = 0 \quad .$$

The evaluations of these derivatives are a hideous exercise in algebra and implicit differentiation and are not shown. The nonlinear equations were solved numerically using the ZSPOW algorithm in the IMSL library. To demonstrate that the method was successful in placing an incipient

hysteresis loop at the appropriate place, a plot of the biomass-versus-aeration rate profile, predicted by Equation 27 with the evaluated parameters, is shown in Figure 19. Also shown in Figure 19 is the influence of the parameter β upon the biomass-versus-aeration bifurcation diagram. When this parameter is perturbed to higher values than were output by Equation 29, then the hysteresis loop became wider, while perturbations to smaller values made the hysteresis loop disappear. This is expected, since in this exercise, β is crossing the hysteresis variety of the problem of Equation 27. Perturbations in any parameter of the function F in Equation 27 would have a qualitatively similar effect, but β is particularly potent in forcing these transitions, since it alone injects the "S" shaped character into the growth equation through the function $\bar{D}$. Interestingly, for the biomass-versus-aeration diagram to border hysteresis, the function D must assume a complete hysteresis loop, since it competes with the other functions A-C, which tend toward monotonicity. The parameter O_{2s} has the ability to move the location of the inflection along the aeration rate axis. A summary of the parametric values output by Equations 29 and of the equations and other parameter values of this section is presented in Appendix 1.

Although the inflection occurs as the correct place, the adherence of the predictions to the data at higher and lower aeration rates than the inflection depends more upon the parameters other than those evaluated through Equation 29. The parameters K_O, K_{ATP}, and E_{max} were assigned natural values, so that the parameter α in Equation 23 could be freely manipulated. Of course, the solution of the set 29 changes with different input values of α. The predictions at aerations lower than the inflections

were forced to follow the data by imposing a value of 8×10^5 upon α when $D < D_S$, D_S being the inflection point of the function D. For $D > D_S$, $\alpha = 16{,}000$ was chosen. However, the data at higher aerations are exceeded (Figure 19). Increasing the value of α would force the predictions closer to the data, since the "S" shape of the function D would become shorter. However, in doing so, a problem would arise at the highest aeration rates. The ATP versus dissolved oxygen curve shows an increasing ATP concentration with decreasing dissolved oxygen. As ATP is beneficial towards growth, the subfunction B(ATP) tends to generate a higher biomass concentration with decreasing aeration rates. This is never observed because the functions A and D have the opposite slopes. Toward the highest aeration rates, A(O) is saturated (Figure 15), leaving a delicate balance between $\overline{B(ATP)}$ and D(O). If α were increased to improve the data fit at higher aerations, B(ATP) would become relatively stronger, and an increase in the biomass concentration with decreasing aeration rates would be predicted at the highest aeration rates. The fact that this is never observed experimentally was an incentive to keep the value of α artificially high, despite some overprediction of the biomass concentration. This dilemma is indicative of the delicate balance among the different processes.

The numerical generation of the biomass-versus-aeration rate predictions from Equation 27 deserves comment. The subfunction $D(O_2)$ has multiple solutions within a range of dissolved oxygen concentrations, and care must be taken that the algorithm converges upon the correct solution in the given context. The difficulty is circumvented by noting that $O_2(D)$ is single-valued. Therefore, the first step in the algorithm is

to choose the value of D, relevant to the high aeration rate steady-state. The fact that the dissolved oxygen is about 50 ppb at the higher aeration steady-states and Figure 15 are helpful in this choice. From this, the dissolved oxygen can be calculated from a rearranged Equation 23:

$$O_2 = O_{2S} + \alpha(D - D_S)^3 - \beta(D - D_S) \quad . \tag{30}$$

With this value of O_2, ATP is calculated from the polynomial fit ATP(O) in Table 3. From ATP, R_3, the specific ethanol productivity is calculated using the polynomial fit R_3(ATP), also shown in Table 3. The subfunctions A, B, and D are now specified, so that Equation 24 can be solved to reveal the value of C. Then, Equation 22 and 25 can be solved to give the biomass concentration X:

$$X = \frac{dE_{max}}{R_3}(1 - C) \quad . \tag{31}$$

Finally, the aeration rate is evaluated, knowing the dissolved oxygen and biomass concentration, using Equation 26:

$$Q_A = \frac{O_2[1 + .282X]}{16.33} \quad . \tag{32}$$

The process just described generates one data point [Q_A, X]. To obtain another point, D is decremented, and the process repeated. The entire X-versus-Q_A curve is thus predicted. The algorithm terminates when the aeration rate reaches sufficiently low values.

As the biomass-versus-aeration profile of run 7 has been reasonably fit, the effects of removing the high antifoam from the medium can be

simulated. The removal of antifoam, according to both the catabolic model and the experimental data, confers upon the culture the ability to attain higher ethanol productivities, and thus, higher intracellular ATP concentrations. The effects of the altered metabolic pattern upon the biomass concentrations can be tested by injecting into Equation 27 polynomials ATP(O) and R_3(ATP) germane to the low antifoam culture. It is of particular interest to observe whether the benefits of the higher ATP concentration can compensate for the extinction in function D so as to smooth the biomass-aeration bifurcation diagram.

The results of the simulation are shown in Figure 20. Clearly, the new ATP-versus-oxygen curve of Figure 18 cannot predict the desired change in the bifurcation diagram. In fact, the hysteresis loop becomes more pronounced. This outcome is not surprising. The new ATP-versus-O_2 curve is steeper than the old one, but it is still monotonic. In contrast, the D-versus-O_2 curve folds back upon the dissolved oxygen concentration so that in one region, D decreases with increasing dissolved oxygen. When the system of equations encounters this region, the ATP concentration cannot compensate for the decline in the value of D, because the ATP-versus-dissolved-oxygen profile also decreases with increasing aeration. What is needed is an ATP-versus-O_2 bifurcation diagram that also undergoes hysteresis in the opposite direction from the D-versus-O_2 diagram, and only in this way can the effects of D be fully cancelled. Such a hysteresis loop would possess a portion in which ATP increases with increasing dissolved oxygen at the same place that D decreases with increasing dissolved oxygen. This possibility is further explored shortly. The other problem encountered in the new ATP-versus-O_2 diagram is that it

predicts an increasing biomass concentration with decreasing aeration rates at the higher aeration rates. Again, this arises from the steepness of the ATP-versus-O_2 curve at the higher aeration rates and the delicacy of the balance among the forces governing growth at the higher aerations.

As mentioned, to cancel the effects of $D(O_2)$ and thereby to restore the monotonic X versus Q bifurcation diagram, an ATP-versus-O_2 curve undergoing hysteresis is needed. Such a curve in relation to the experimental data and to the function D is shown in Figure 21. The equation generating the curve is shown in Table 4. As expected, the required curve is virtually a mirror image of the function D so that any marginal decline along D is equalled by a marginal gain in the ATP. The experimental data do not exclude the possibility that such an ATP-versus-O_2 curve actually exists, especially since data are missing from the low antifoam run 9 in the 35-50 ppb dissolved oxygen region. The fact that one data point at 23 ppb overhangs the cliff is not troublesome, since ATP data from run 9 are used in relation to the biomass-versus-aeration data of runs 6 and 7. Events become routinely shifted along the axis of the aeration rate because of adaptation and other random variations between runs. The models of Sections 2 and 3 of this chapter cannot generate the required ATP-versus-O_2 curve. However, if the R_3(ATP) relation is still valid, sudden jumps in the specific ethanol productivity would be predicted as the dissolved oxygen passed the limit point of the ATP-versus-O_2 curve. Sharp jumps were indeed seen in runs 5 and 10.

The predicted biomass-versus-aeration profile with the function $ATP(O_2)$ given in Table 4, applied to Equation 27, is shown in Figure 22. The precipice of the high antifoam run disappears, and is replaced by the

desired, uniformly descending profile. A slight imperfection at around 2.3 ccpm of aeration is the location of the collapse of the hysteresis loop. This imperfect region is traversed 3 times, but the identical path is not followed each time. The transitions between the high antifoam and low antifoam runs depicted in Chapter 2, Figure 22, are qualitatively and semi-quantitatively reproduced. The results would be even more satisfactory if the entire low antifoam curve of Figure 22 could be shifted to lower aeration rates. Such a shift could be accommodated by the well-known effects of antifoam upon the k_1a of the system. Antifoam interferes with oxygen transport.

It is of interest to compare the behaviors of the subfunctions A-D in relation to the aeration rate with low and high antifoam in the medium. Recall that these functions must vary in a coordinated manner to preserve the mathematical product. Figure 23 explains that in the high antifoam run the decline in the function D is compensated mainly by a rise in the function C. Thus, the decline in the biomass concentration at the precipice in D reduces the extracellular ethanol concentration so that ethanol inhibition is alleviated. With the low antifoam run shown in Figure 24, the compensation is accomplished by the rise in the ATP concentration, eliminating the need for biomass, and hence, ethanol, to wash out the lower levels.

If an ATP-versus-dissolved oxygen curve necessary to annihilate the opposing behavior of $D(O_2)$ actually exists, then it must be a regulatory mechanism built into the cell's metabolism to supply vastly greater quantities of ATP when the need arises. Yet, there is a troublesome aspect to such a regulatory mechanism, as indicated in Figures 25 and

26. In these figures, the ATP-versus-O_2 curve required to perfectly cancel $D(O_2)$ is shifted slightly toward higher dissolved oxygen levels. When this is done, an odd biomass-versus-aeration bifurcation diagram with contiguous ignitions and extinctions emerges. A variety of other strange bifurcation diagrams issue forth when the spurt of ATP is misplaced. The fact that these diagrams were never seen does not mean that they cannot exist. Nonetheless, this would seem to be an inefficient regulatory mechanism, particularly as environmental factors as antifoam separate the remedy from the ailment.

The role of ATP in the growth equations must be reassessed. Until now, ATP was thought to be beneficial for growth, but not by influencing the process D directly. The deficiency in D would be cancelled by the beneficial effect on some other growth process, leaving the composite of all processes unchanged. Since this approach is inadequate, a direct influence of ATP on the process represented by D must be postulated. The nature of the entry of ATP into D is discussed after a mathematical interlude.

Equation 23 is merely a mathematical representation of some real process. The real process shall be refereed to as D^*, and the bifurcation diagram of D^* with respect to dissolved oxygen is governed by:

$$H^*[D^*, O_2, \underline{\gamma}] = 0 \ , \tag{33}$$

where H^* is some function and $\underline{\gamma}$ is a vector of parameters governing the process. With any necessary redefinitions and with no loss of generality, $H[0, 0, 0] = 0$. Equation 23 will be rewritten as:

$$H[(D - D_S), \tfrac{1}{}(O_2 - O_{2S}), \tfrac{\beta}{}] = 0 \ . \tag{34}$$

α α

$H(0, 0, 0) = 0$. Further, assume that:

$$H^*(0, 0, \underset{\sim}{\gamma}^0) = \frac{\partial H^*}{\partial D^*}(0, 0, \underset{\sim}{\gamma}^0) = \frac{\partial^2 H^*}{\partial D^{*2}}(0, 0, \underset{\sim}{\gamma}^0) = 0 \qquad (35)$$

for special values of the parameters $\underset{\sim}{\gamma}^0$. Also, it is insisted that:

$$\frac{\partial^{2+n} H^*}{\partial D^{*2+n}} \frac{\partial H^*}{\partial O_2} \neq 0 \qquad n > 0 \; . \qquad (36)$$

Equation 35 assures that D^* can undergo hysteresis, a fact that is already known. If Equation 36 is valid, then H is a universal unfolding, contact equivalent to H^* (21). Contact equivalence guarantees that all qualitative aspects of the bifurcation diagram of D^* versus O_2 for any set of parameter $\underset{\sim}{\gamma}$ can be represented by the function H. Qualitative aspects refer to the number of steady-state solutions and transitions in the number with changes in the bifurcation parameter or in the vector of auxiliary parameters. The fact that it is a universal unfolding guarantees that there exist smooth mappings V, W, U, Z such that:

$$H^*(x, \lambda, \delta) = V(x, \lambda, \delta)\, H[W(x, \lambda, \delta), Y(\lambda, \delta), Z(\delta)], \qquad (37)$$

where x, λ, and δ are generalized state variables. Further properties of the mappings are given in Golubitsky and Schaeffer(21). The most important conclusion from Equation 37 is that the parameters $\underset{\sim}{\gamma}^0$ of the real process are related to the parameter β/α of artificial representation by some mapping; i.e., $\beta/\alpha = \beta/\alpha(\underset{\sim}{\gamma}^0)$. Thus, changing the values of $\underset{\sim}{\gamma}^0$ is equivalent to changing the value of β/α in the facsimile.

ATP can intervene into the real process D^* by altering the values of the parameters $\underline{\gamma}$, or stated mathematically:

$$\underline{\gamma} = \underline{\gamma}(ATP), \tag{38a}$$

so that

$$\beta/\alpha = \beta/\alpha(ATP). \tag{38b}$$

The higher concentration of ATP in the low antifoam run can cause the transition to a monotonic from a hysteresis-type bifurcation diagram of the biomass-versus-aeration. For this to occur, it would be very helpful if the D^*-versus-O_2 diagram did the same. The latter can be accomplished only if Equation 38 describes a curve in γ-space that crosses the hypersurface $\underline{\gamma}^0$ governed by Equation 35. At the exact point that the line crosses the surface, $\beta/\alpha = \beta = 0$, since this is the only point in the hysteresis set of H. At these points, the bifurcation diagrams of both D and D^* are in the transition from monotonic to hysteresis profiles, while the biomass aeration diagram has already crossed into the region of monotonicity. The other requirement of Equation 38 is that the hysteresis variety is crossed in the relevant range of the ATP concentration.

There is no information to choose the function $\beta/\alpha(ATP)$, so the choice is a simple one:

$\beta = 46.5$ when ATP = average ATP of high antifoam run

$\beta = -30.0$ when ATP = average ATP of low antifoam run .

The value of β for the high-antifoam case is identical to the one evaluated through Equation 29. Therefore, no aspect of the model, neither the equations nor the parameters, changes for the high-antifoam run in this reassessment. The value for the low-antifoam case was chosen so that the qualitative change in D would not be drastic, but the biomass-versus-

aeration profile would be fit. The value of α in the function $\beta/\alpha(ATP)$ was maintained at the previous value of 16,000 for $D > D_S$ and 8×10^5 for $D < D_S$.

The biomass-versus-aeration diagram for the high antifoam case is unchanged from Figure 19. In simulating the elimination of high antifoam, the different polynomials $ATP(O_2)$ and $R_3(ATP)$ are introduced, as before, but in addition, the new value of β is entered. There is some question about the choice of $ATP(O_2)$. The polynomial fit to the steeper curve in Figure 18, originating from the ATP balancing, could be used, but this as been shown to predict the opposite slope of the $X-Q_A$ curve at higher aerations. To prevent repetition of this flaw, the slope of the $ATP(O_2)$ curve was reduced at the highest aeration, but most features of the genuine curve were preserved. A graph of the new $ATP(O_2)$ curve is shown in Figure 27, and the generating functions are shown in Table 5.

The biomass aeration bifurcation diagrams are shown in Figure 28. The qualitative, and semi-quantitative, features of the removal of high antifoam are reproduced, and the fits would be even more satisfactory if factors beyond the scope of the model, as k_1a reduction by antifoam, could shift the biomass aeration diagram to lower aerations. Since the balance of forces affecting growth is delicate, it is unreasonable to expect perfect data fitting, as small parameter changes can have large effects. The experimentally observed $X-Q_A$ diagrams change from run to run, despite identical conditions, for perhaps the same reason (Chapter 2, Figure 19).

The subfunctions A-D for the high antifoam case vary with the aeration in the same manner as shown in Figure 23. The new subfunctions A-D for

the low antifoam prediction are shown in Figure 29. $D(O_2)$ no longer undergoes hysteresis, as the parameter β has crossed zero. As a consequence, the other subfunctions A-C are not obligated to undergo compensatory hysteresis loops. The biomass concentration need no longer undergo the extinction to make the mathematical product of A-D unchanged.

The reassessed version of the model is nicely poised for the admittance of the effects of yeast extract. The addition of yeast extract, in run 5 to the medium of run 4, had the familiar effect of replacing the hysteresis loop with the monotonic profile in the $X\text{-}Q_A$ diagram (Chapter 2, Figure 14). This effect can easily be accommodated by postulating that:

$$\underline{\gamma} = \underline{\gamma}(ATP, \overline{YE}) \ . \qquad (39)$$

YE represents the biosynthetic intermediates supplied by yeast extract. Equation 39 implies nothing more than that some biosynthetic intermediates introduced with yeast extract participate in the process D^* and change the values of some parameters of the equations describing the process. The addition of yeast extract effected a change in the parameters $\underline{\gamma}$ such that the hysteresis variety $\underline{\gamma}^o$ was approached or crossed. This made it possible for the overall equation, composed of A-D, to cross the hysteresis variety defined by an equation such as 29.

Equation 39 can be viewed physically. The process D^* responds primarily to dissolved oxygen, but also requires an adequate supply of ATP and biosynthetic intermediates to proceed optimally. The differentiation of mitochondria serves as a good example. The process is induced by oxygen, but obviously requires ATP and biosynthetic intermediates to proceed. The adequate supply of the latter assures that mitochondrial differentia-

tion is incremented smoothly with marginal increases in dissolved oxygen, i.e. a monotonic profile. When ATP and biosynthetic intermediates are inadequately supplied, induction of mitochondriagenesis must await higher dissolved oxygen concentrations. When these high concentrations are attained, the forgone mitochondrial differentiation occurs all at once.

In Appendix 1, the final versions of the models of Sections 2-4 of this chapter and the parameter values are provided for the convenience of the reader.

CONCLUSIONS

In this chapter, models were presented with which, at least qualitatively, all aspects of the macroscopic bioreactor variables and intracellular metabolite variations, could be predicted. In the construction of the model, heavy use was made of the results of the bioreactor studies, the enzyme and metabolite assays, and known biochemical phenomena of yeast. The models were successful in verifying some presumed mechanisms emerging from the metabolite and enzyme assays by demonstrating that when these mechanisms are expressed mathematically, reasonable predictions are made. In addition, the modeling exposed potential interactions and mechanisms that otherwise would have never been imagined.

The specific mechanisms that have been supported by the modeling are enumerated:

1) ATP activates glucose transport.

2) A downstream kinase limits glycolysis, particularly during energy surpluses.

3) Antifoam enhances the transport of glycerol out of the cell.

4) ATP waste reactions probably exist and become stronger with higher

ATP concentrations.

5) Oxygen induces ATP waste reactions.

6) Some underlying process, yet unknown, causes hysteresis-type behavior in the bioreactor parameters. This process most likely is induced by oxygen.

7) The unknown process demands the input of biosynthetic intermediates and ATP. The availability of these components determines the disposition of the process to cause the catastrophic behaviors.

8) Ethanol inhibition is an important process regulating the growth rate, despite ethanol concentrations far lower than the maximum tolerable.

These mechanisms support each and every strange behavior uncovered in these studies and enumerated in the introduction and the previous chapters.

APPENDIX 1

The final version of all equations and parameter values are presented for the convenience of the reader.

A. Catabolic Model

The preferred functionalities for calculation of the specific catabolic rates in terms of the intracellular ATP is in Table 1. The functionalities injected into the ATP balance were those of Table 2.

B. ATP Balance

$$R_3 - R_2 = \frac{5.6\ O_2\ ATP}{5.7 + O_2}$$

R_3 and R_2 were taken from Table 2.

$$O_2 = \frac{16.33\ Q_A}{1 + 0.282X}$$

C. Specific Growth Rate Model

$$\mu_{max}/d[A(O_2)\ B(ATP)\ C(EtOH)\ D(O_2)] - 1 = 0$$

$$A = \frac{O_2}{5.0 + O_2}$$

$$B = \frac{ATP}{3.0 + ATP}$$

$$C = (1 - EtOH/2000)$$

$$\alpha(D - D_S)^3 - \beta(D - D_S) - (O_2 - O_{2S}) = 0$$

$$\frac{\mu_{max}}{} = 3.41, \qquad O_{2S} = 16.9,\ D_S = .75$$

d

$\alpha = 16{,}000 \quad D < D_S$

$\alpha = 8 \times 10^5 \quad D \geq D_S$

$\beta = 46.5$ (High AF)

$\beta = -30.0$ (Low AF)

$ATP = ATP(O_2)$ from Table 5

$R_3 = R_3(ATP)$ from Table 3

$EtOH = R_3X/d$

REFERENCES

1. Spoerl, E., Williams, J.P. and Benedict, S.H., "Increased Rates of Sugar Transport in *Saccharomyces cerevisiae* a Result of Sugar Metabolism," *Biochem. Biophys. Acta*, 298, 956, 1973.

2. Den Hollander, J.A., Ugurbil, K., and Shulman, R.G., "^{31}P and ^{13}C NMR Studies of Intermediates of Aerobic and Anaerobic Glycolysis in *Saccharomyces cerevisiae*," *Biochemistry*, 25, 212, 1986.

3. Sols, A., "Regulation of Carbohydrate Transport and Metabolism in Yeast," in *Aspects of Yeast Metabolism*, eds. Mills, A.K. and Krebs, H., Blackwell: Oxford, 1967, p. 47.

4. Den Hollander, J.A., Ugurbil, K., Brown, T.R., Bednar, M., Redfield, C., and Shulman, R.G., "Studies of Anaerobic and Aerobic Glycolysis in *Saccharomyces cerevisiae*," *Biochemistry*, 25, 203, 1986.

5. Fiechter, A., "Chemostat Studies of Glycolysis in Yeasts," in *Continuous Cultivation of Microorganisms, Proceedings 7th International Symposium*, Prague, 1980, p. 81.

6. Becker, J.U. and Betz, A., "Membrane Transport as Controlling Pacemaker of Glycolysis in *Saccharomyces carlsbergenisis*," *Biochem. Biophys. Acta*, 274, 584, 1972.

7. Perea, J. and Gancedo, C., "Glucose Transport in Glucosephosphate Isomeraseless Mutant of *Saccharomyces cerevisiae*," *Curr. Microbiol.*, 1, 209, 1978.

8. San, K.Y., "Studies on the On-Line Identification and Optimal Control of Bioreactors," Doctoral Dissertation, California Institute of

Technology, Pasadena, CA, 1983.

9. Marquardt, D.W., "An Algorithm for Least-Squares Estimation of Nonlinear Parameters," *J. SIAM*, 11, 2, 1963.

10. Thomas, D.S. and Rose, A.H., "Inhibitory Effect of Ethanol on Growth and Solution Accumulation by *Saccharomyces cerevisiae* as Affected by Plasma Membrane Lipid Composition," *Arch. Microbiol.*, 122, 49, 1979.

11. Erickson, L.E., Minkevich, I.G., and Eroshin, V.K., "Utilization of Mass-Energy Balance Regularities in the Analysis of Continuous-Culture Data," *Biotechnol. Bioeng.*, 21, 575, 1979.

12. Stouthamer, A.H., "The Search for Correlation Between Theoretical and Experimental Growth Yields," in *Microbial Biochemistry*, ed. Quayle, J.R., University Park: Baltimore, 1979, p. 1.

13. Rogers, P.J. and Stewart, P.R., "Energetic Efficiency and Maintenance Energy Characteristics of *Saccharomyces cerevisiae* (Wild Type and Petite) and *Candida parapsilosis* Grown Aerobically and Microaerobically in Continuous Culture," *Arch. Microbiol.*, 99, 25, 1974.

14. Nishizawa, Y., Dunn, I.J., and Bourne, J.R., "The Influence of Oxygen and Glucose on Anaerobic Ethanol Production," in *Continuous Cultivation of Microorganisms, Proceedings 7th Symposium*, Prague, 1980.

15. Oura, E., "Effect of Aeration Intensity on the Biochemical Composition of Baker's Yeast. I. Factors Affecting the Type of Metabolism," *Biotechnol. Bioeng.*, 16, 1197, 1974.

16. Atkinson, D.E., "The Energy Charge of the Adenylate Pool as a Regulatory Parameter. Interaction with Feedback Modifiers," *Biochemistry*, 7, 4031, 1968.

17. Weibel, K.E., Mor, J.R., and Fiechter, A., "Rapid Sampling of Yeast Cells and Automated Assays of Adenylate, Citrate, Pyruvate, and Glucose 6-Phosphate Pools," *Anal. Biochem.*, 58, 208, 1974.

18. Fiechter, A., Fuhrmann, G.F., and Kappeli, O., "Regulation of Glucose Metabolism in Growing Yeast Cells," *Adv. Microb. Physiol.*, 22, 81, 1981.

19. Akbar, M.D., Rickard, A.D., and Moss, F.J., "Response of the Adenosine Phosphate Pool Level to Changes in the Catabolic Pattern of *Saccharomyces cerevisiae*," *Biotechnol. Bioeng.*, 16, 455, 1974.

20. Bazua, C.D. and Wilke, C.R., "Ethanol Effect on the Continuous Fermentation with *Saccharomyces cerevisiae*," *Biotechnol. Bioeng. Symp*, 7, 105, 1977.

21. Golubitsky, M. and Schaeffer, D.G., Singularities and Groups in Bifurcation Theory, Volume 1, Springer-Verlag: New York, 1985.

22. Iooss, G. and Joseph, D.D., Elementary Stability and Bifurcation Theory, Springer-Verlag: New York, 1980.

23. Schatz, G. and Plattner, H., "Promitochondria of Anaerobically Grown Yeast. III. Morphology," *Biochemistry*, 8, 339, 1969.

24. Balakotaiah, V. and Luss, D., "Structure of the Steady-State Solutions of Lumped-Parameter Chemically Reacting Systems," *Chem. Eng. Sci.*, 38, 1709, 1982.

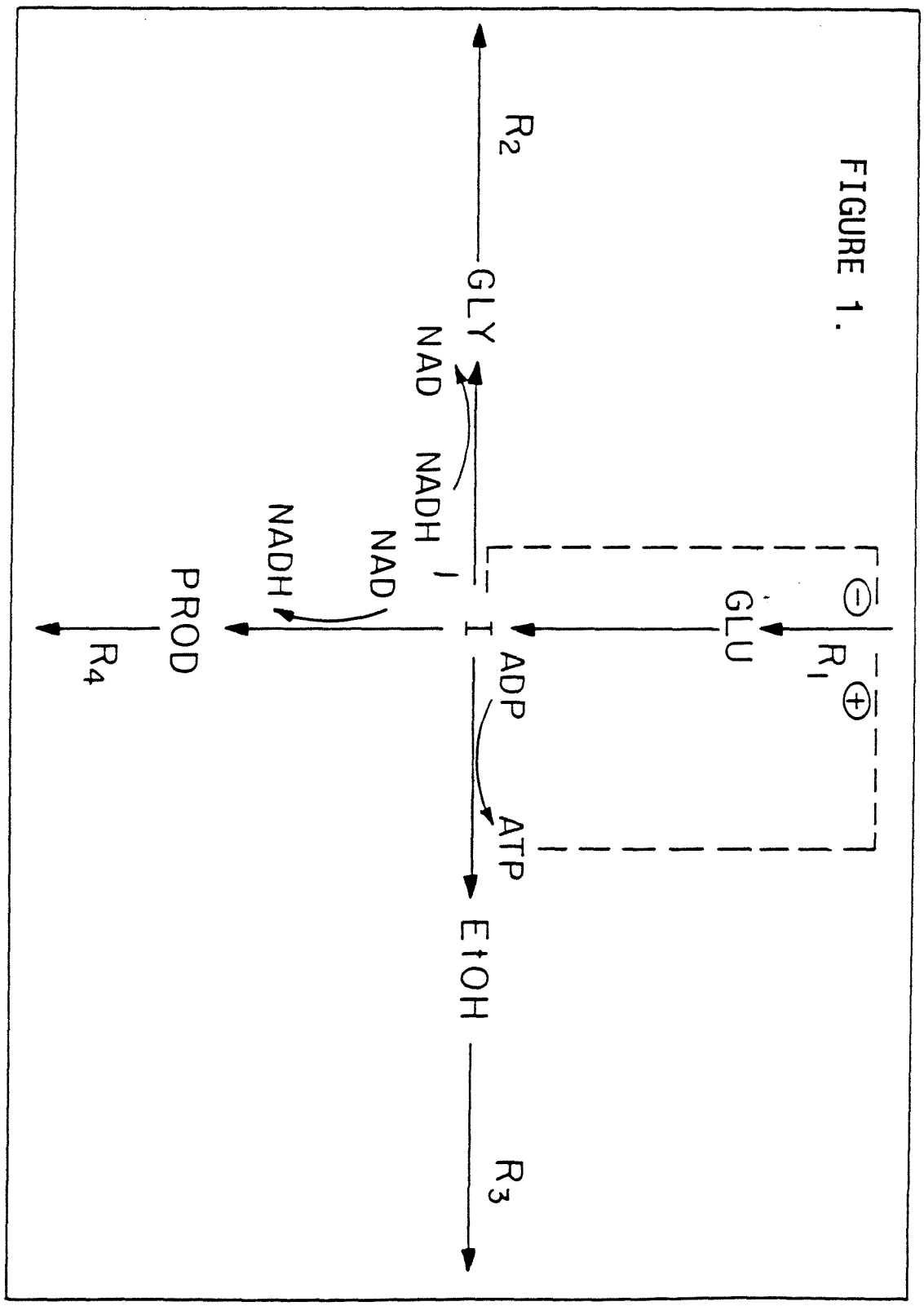

FIGURE 1.

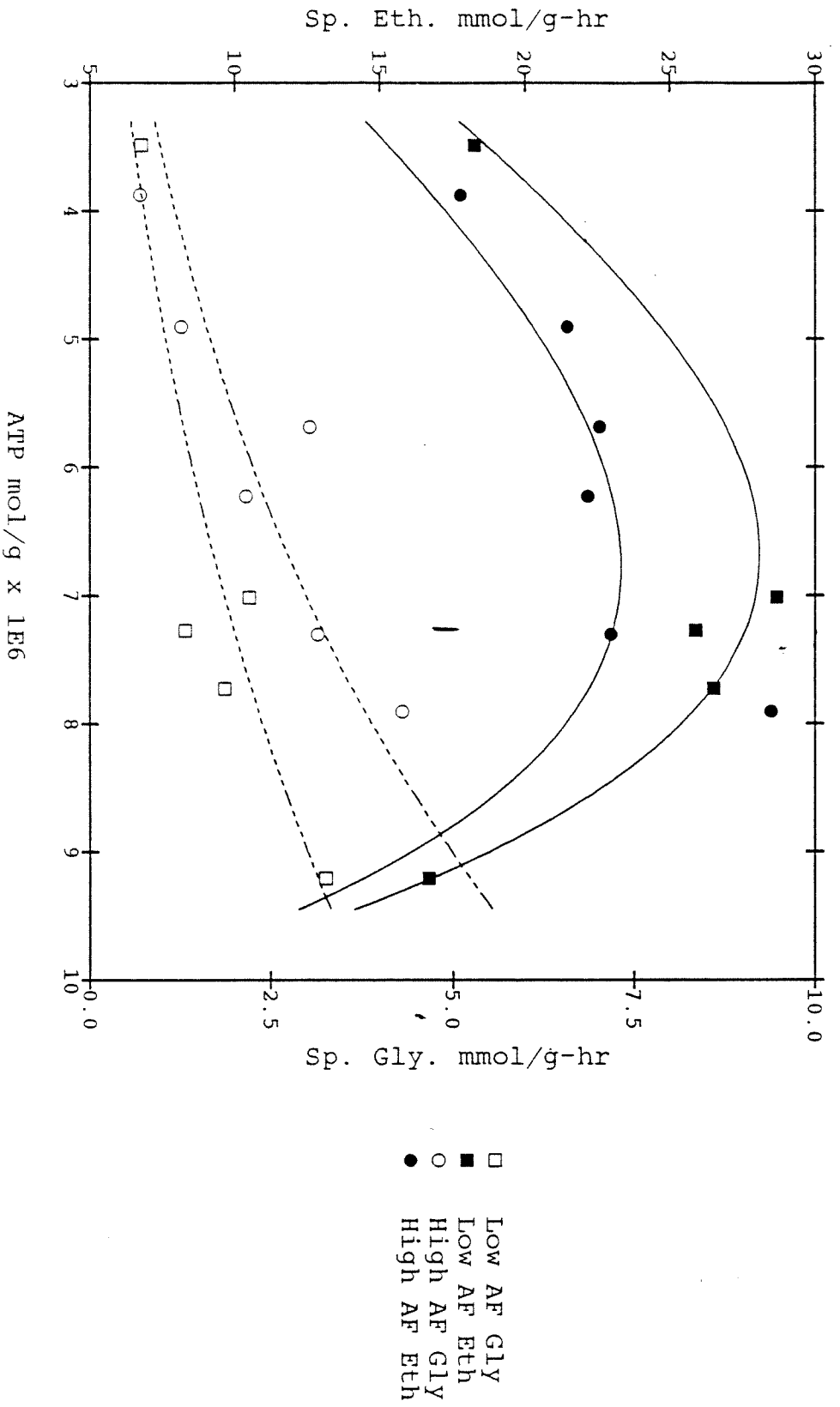

FIGURE 2. SP. ETHANOL and GLYCEROL

FIGURE 3. SP. GLUCOSE UPTAKE

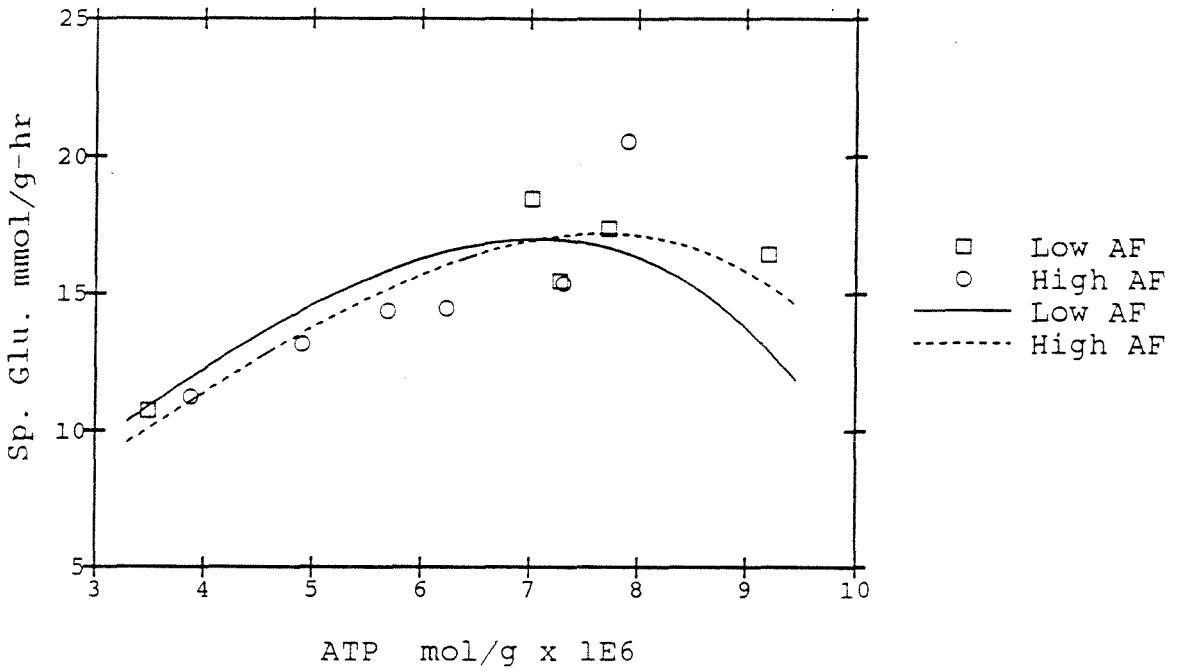

FIGURE 4. GLUCOSE 6-PHOSPHATE

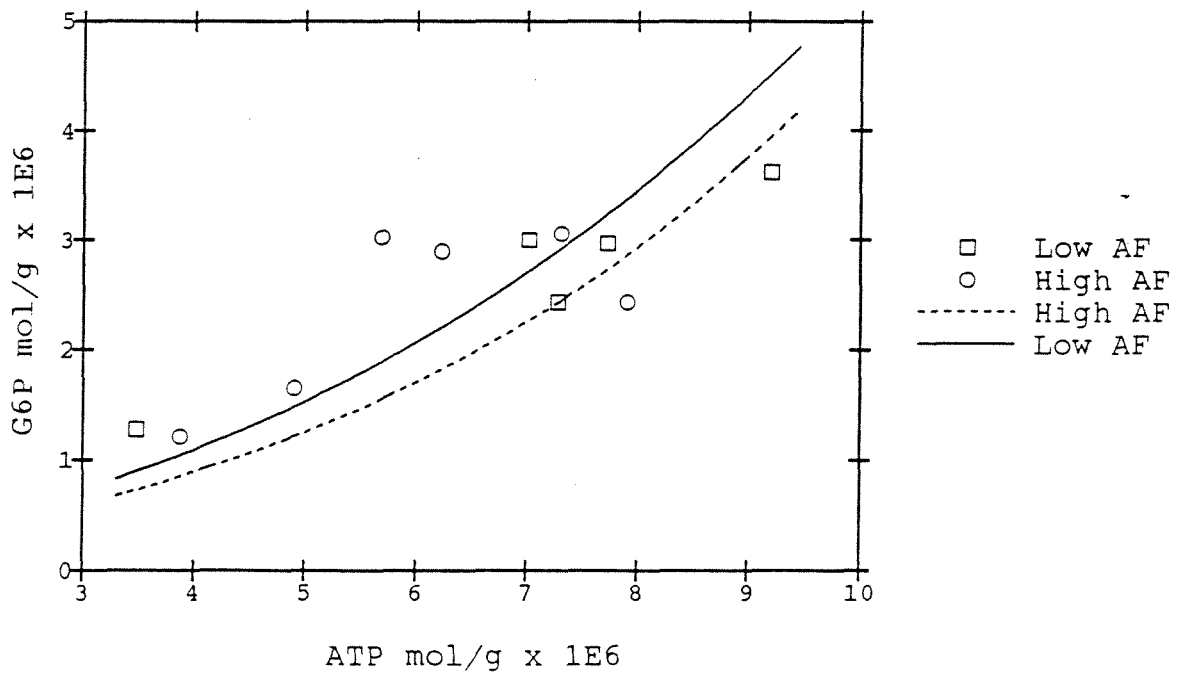

FIGURE 5. GLUCOSE UTIL.: OTHER PRODUCTS

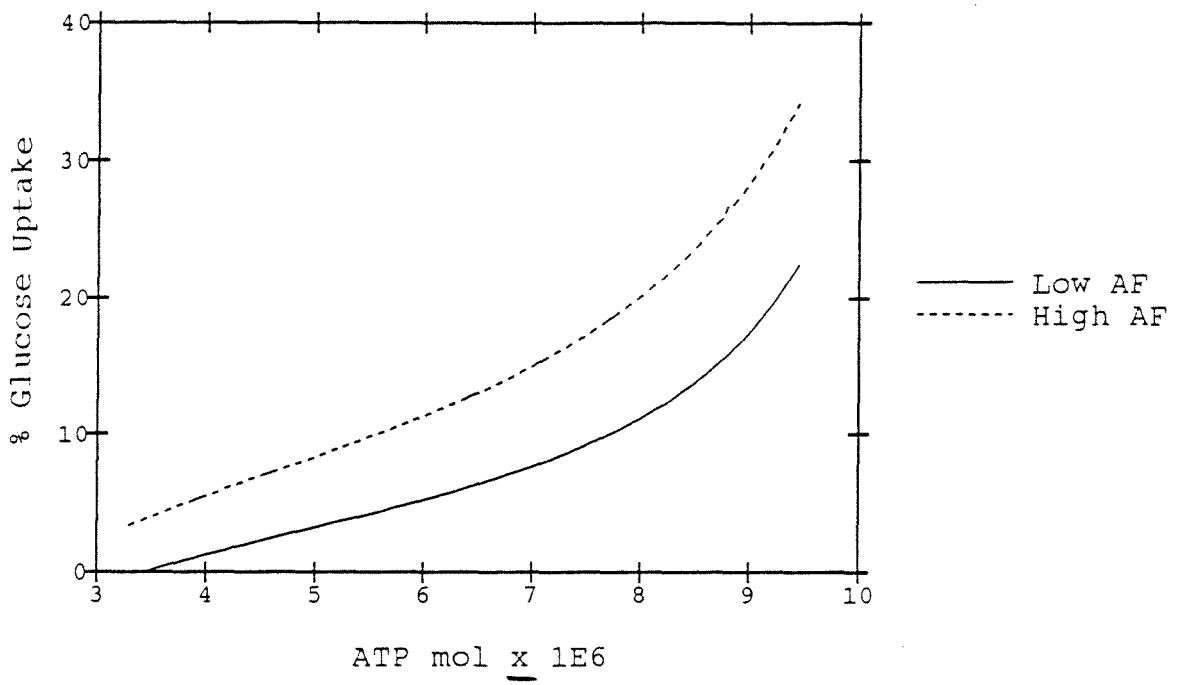

FIGURE 6. SP. GLY. vs. DRIVING FORCE

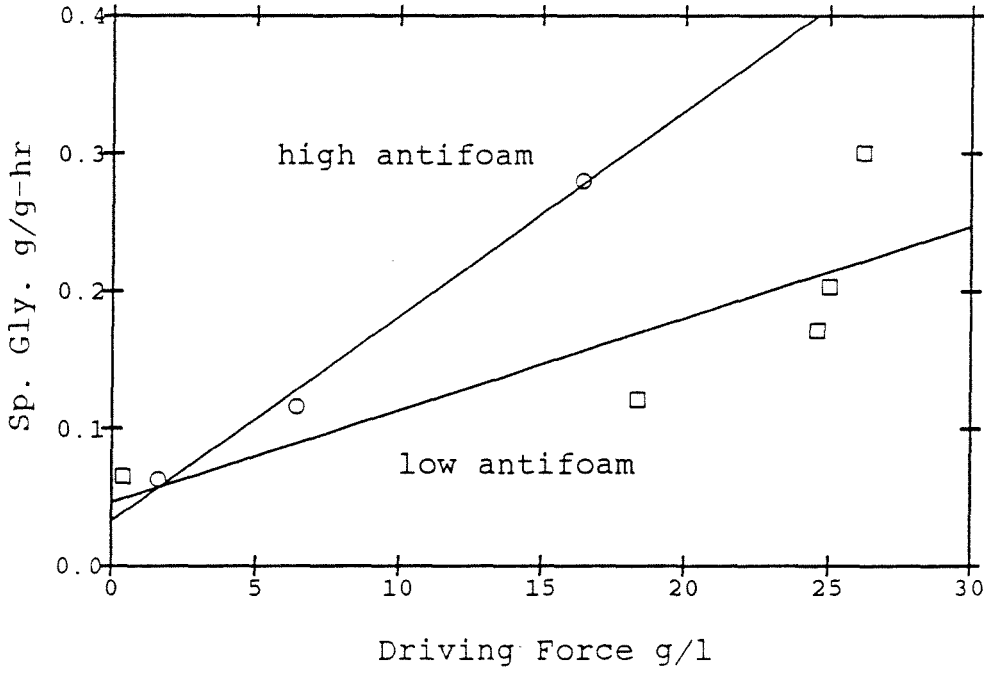

FIGURE 7. ATP PRODUCTION

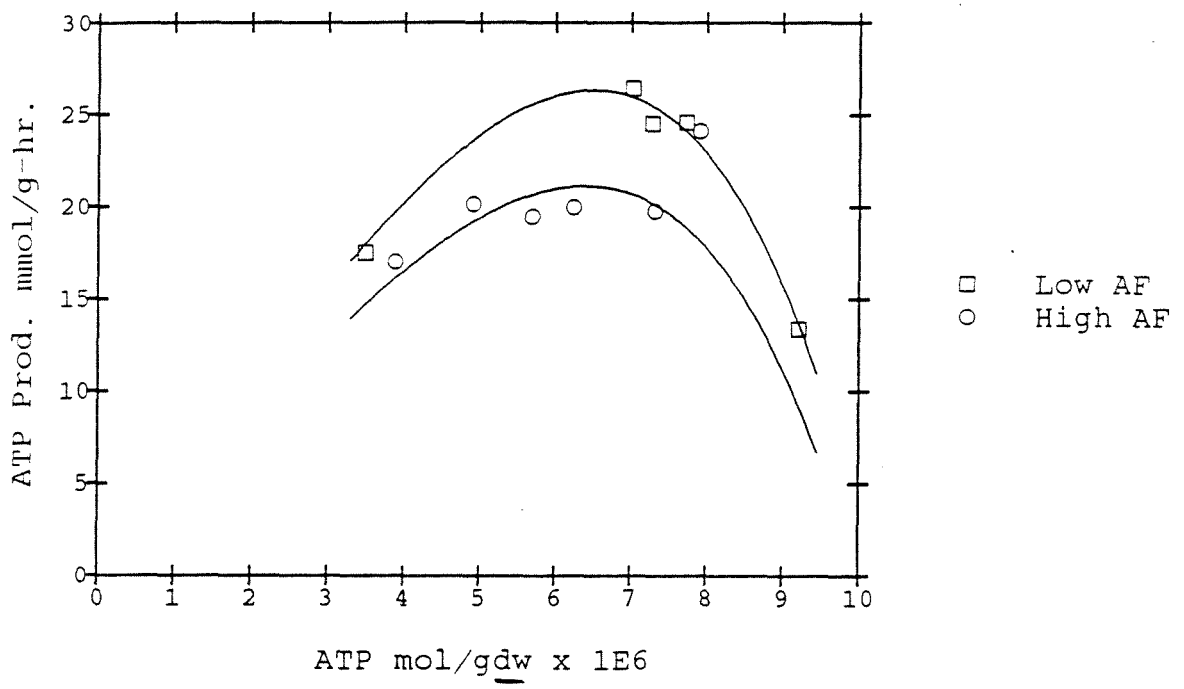

FIGURE 8. ATP PRODUCTION

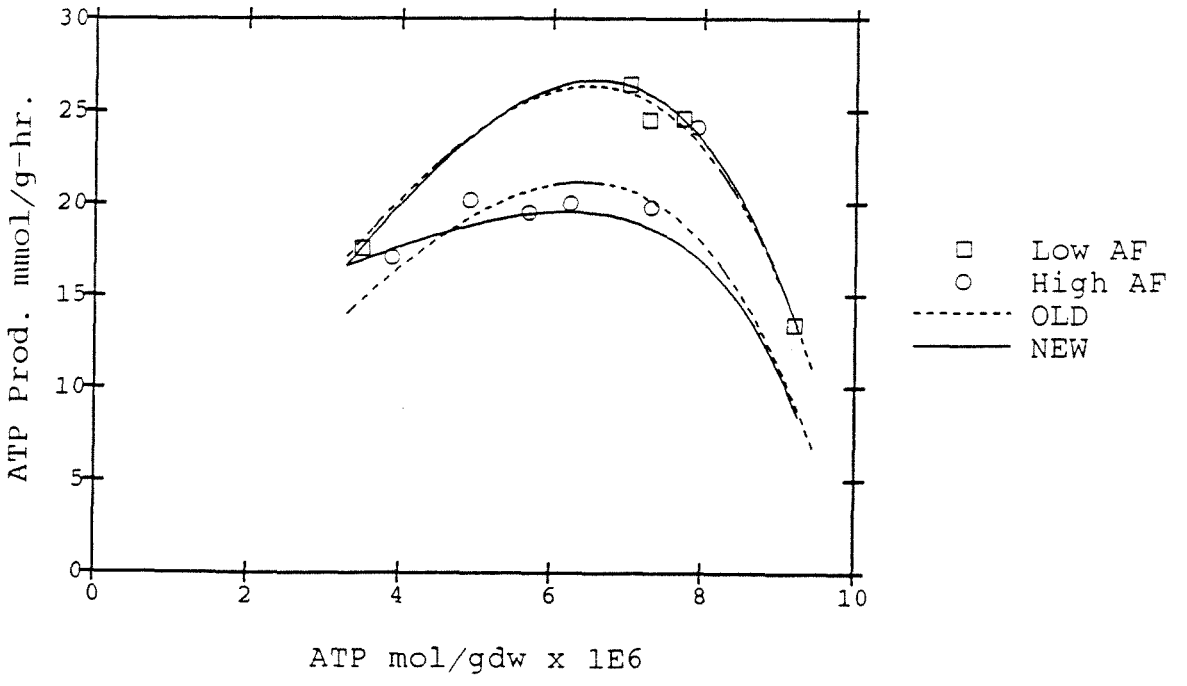

FIGURE 9. ATP PROD. and CONS.: BALANCE

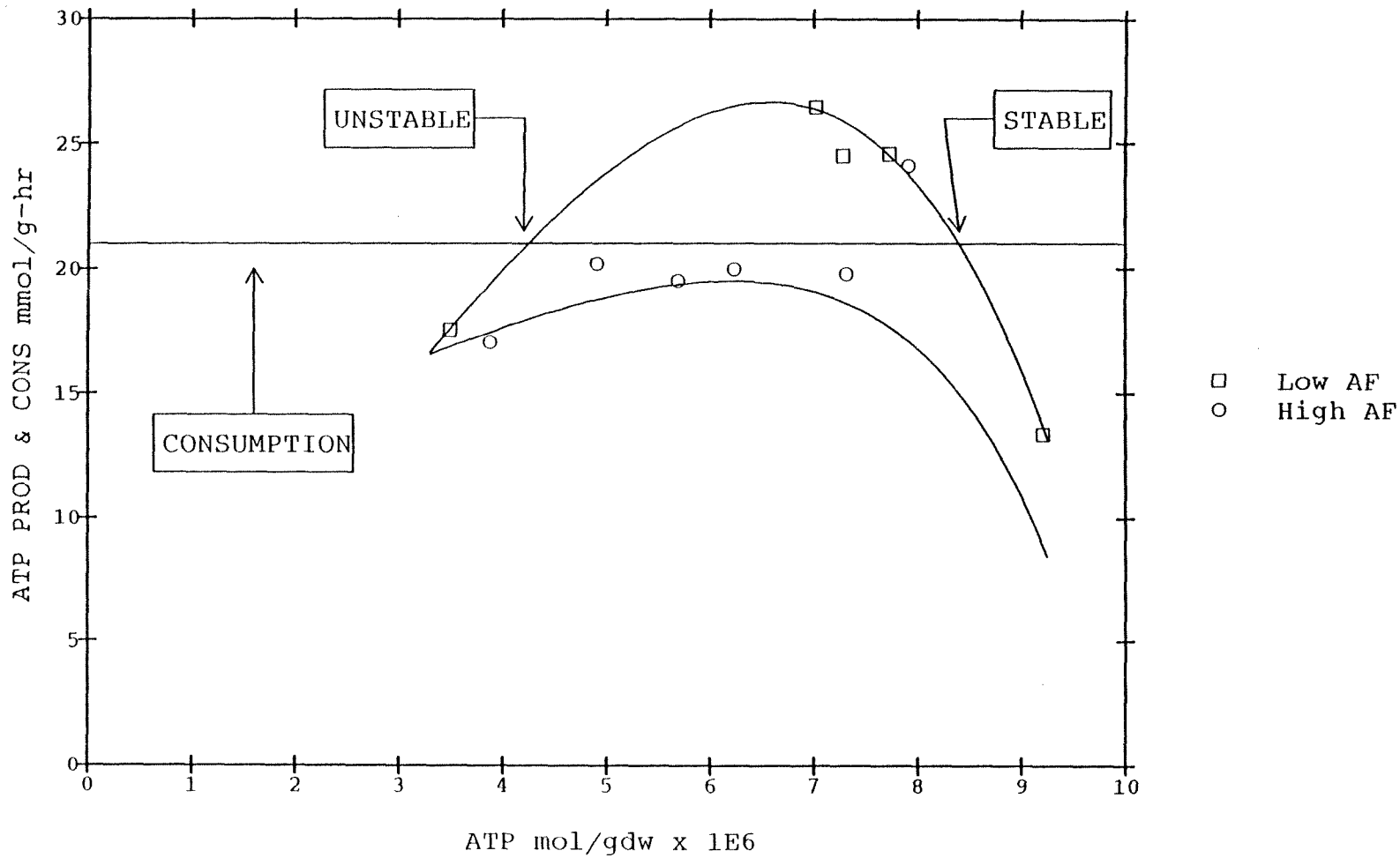

FIGURE 10. ATP PROD. and CONS.: BALANCE

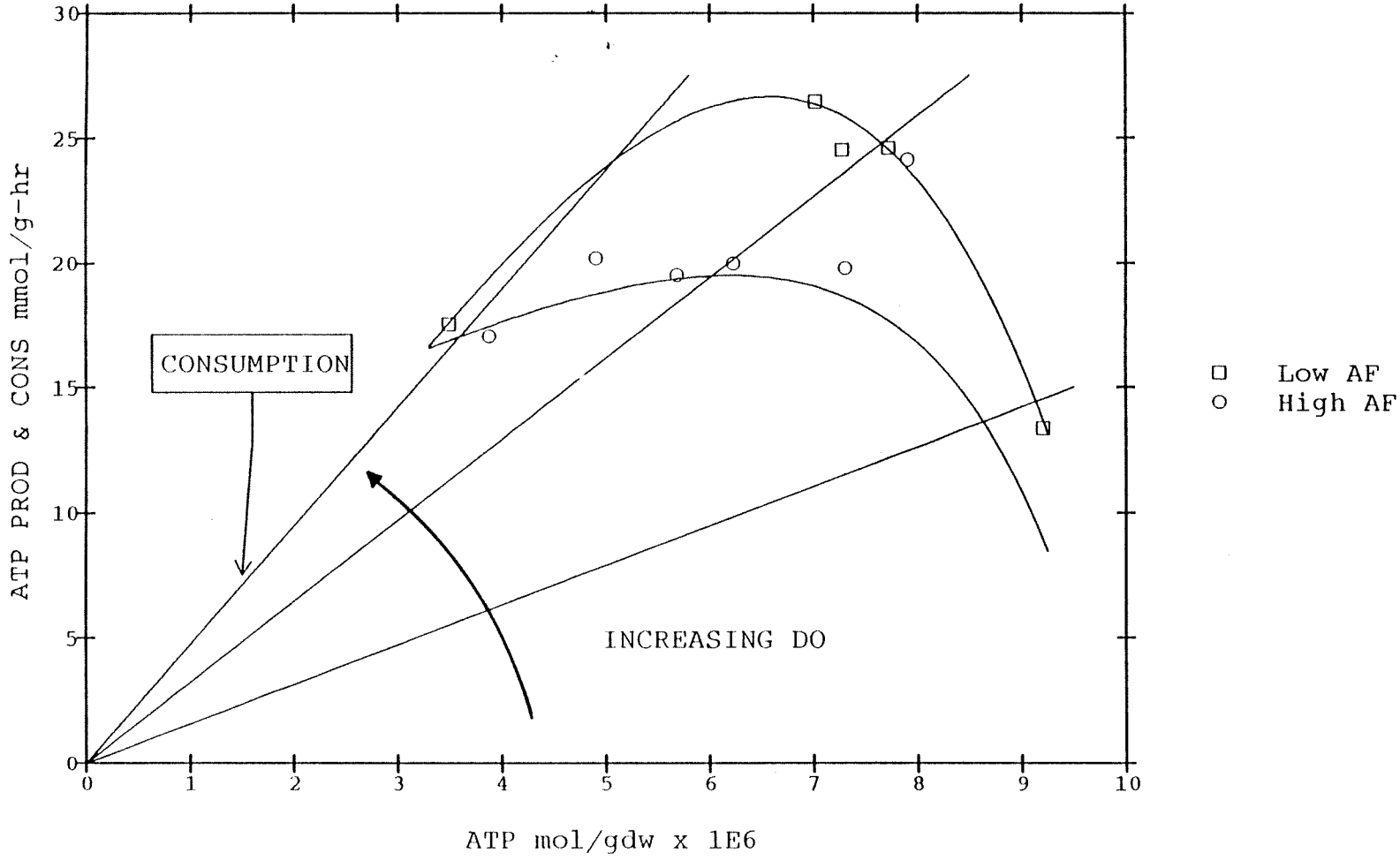

FIGURE 11. LITERATURE COMPARISON

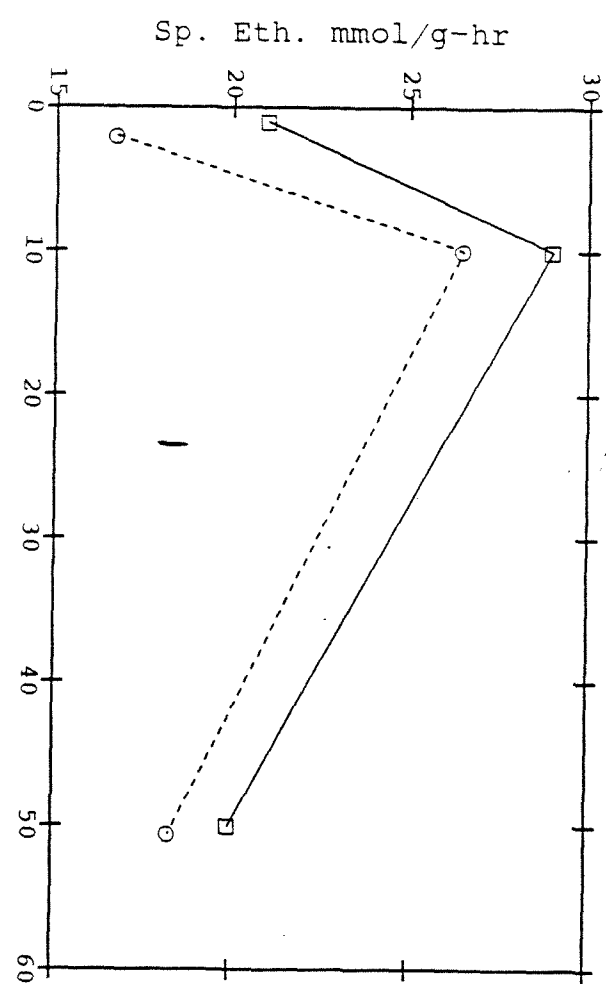

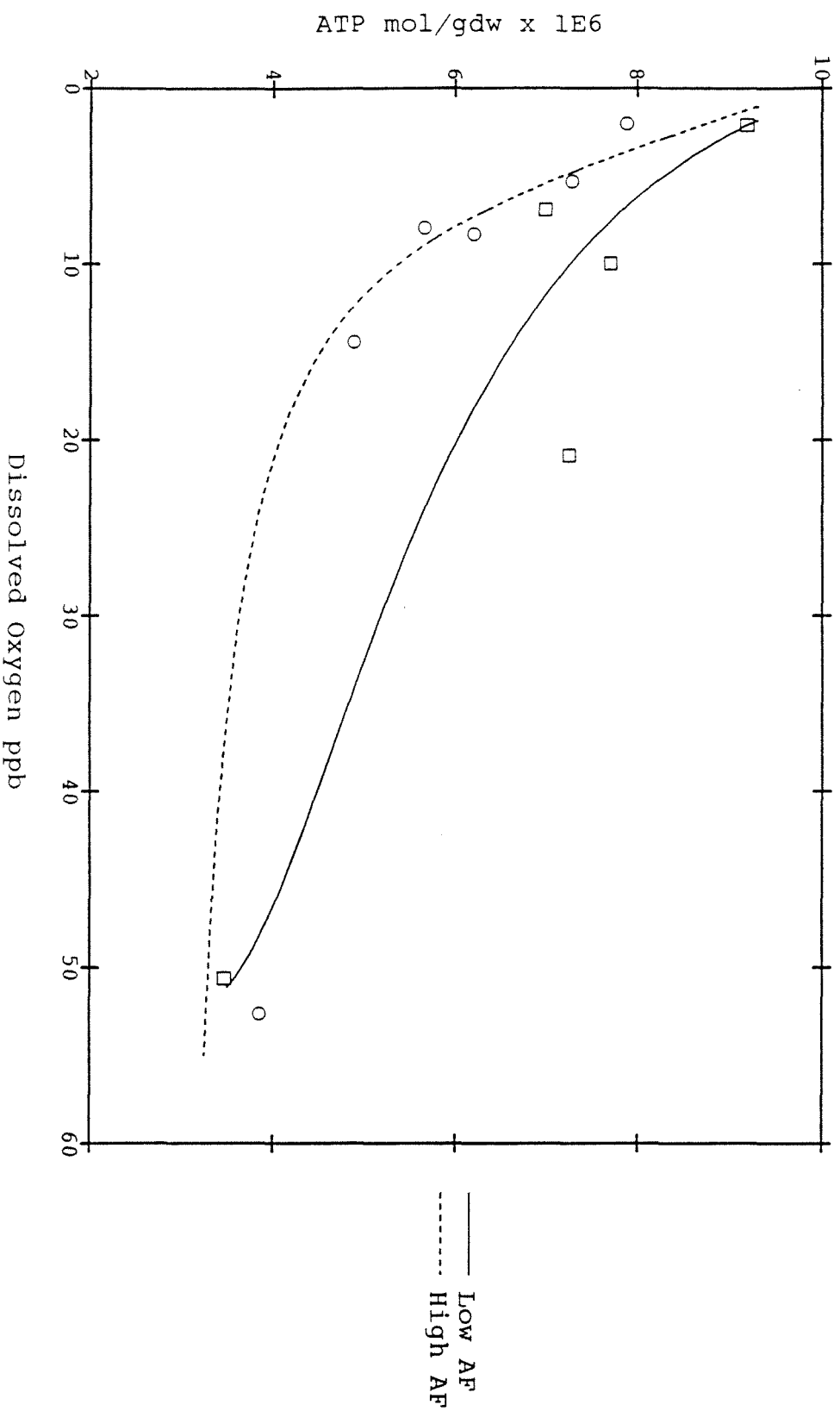

FIGURE 12. ATP vs. DISSOLVED OXYGEN

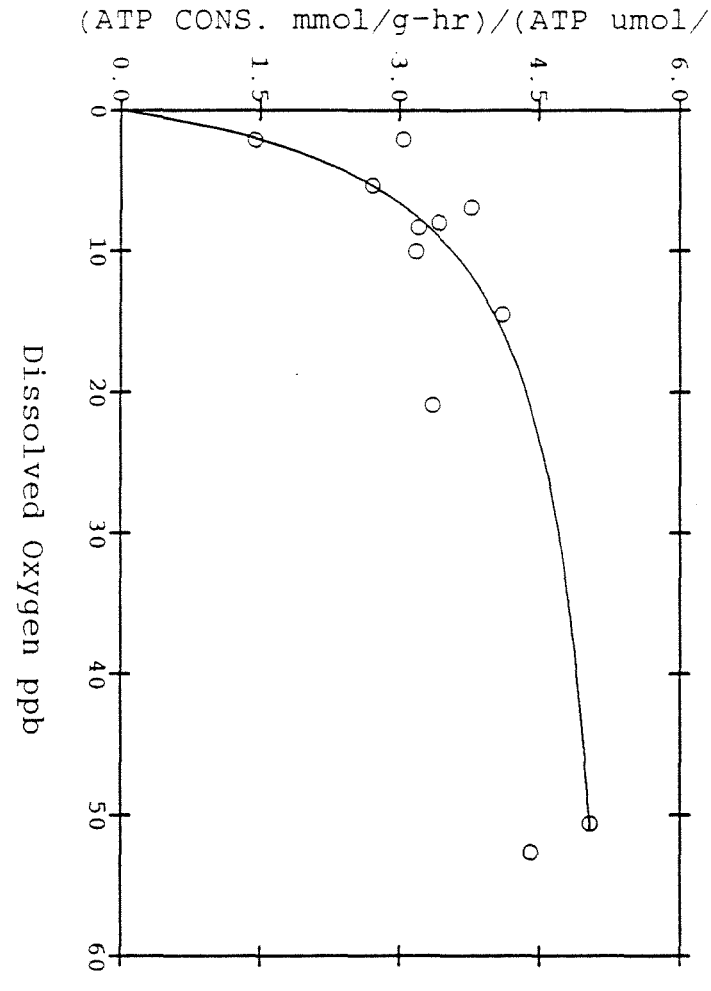

FIGURE 13. ATP CONSUMPTION ACTIVITY

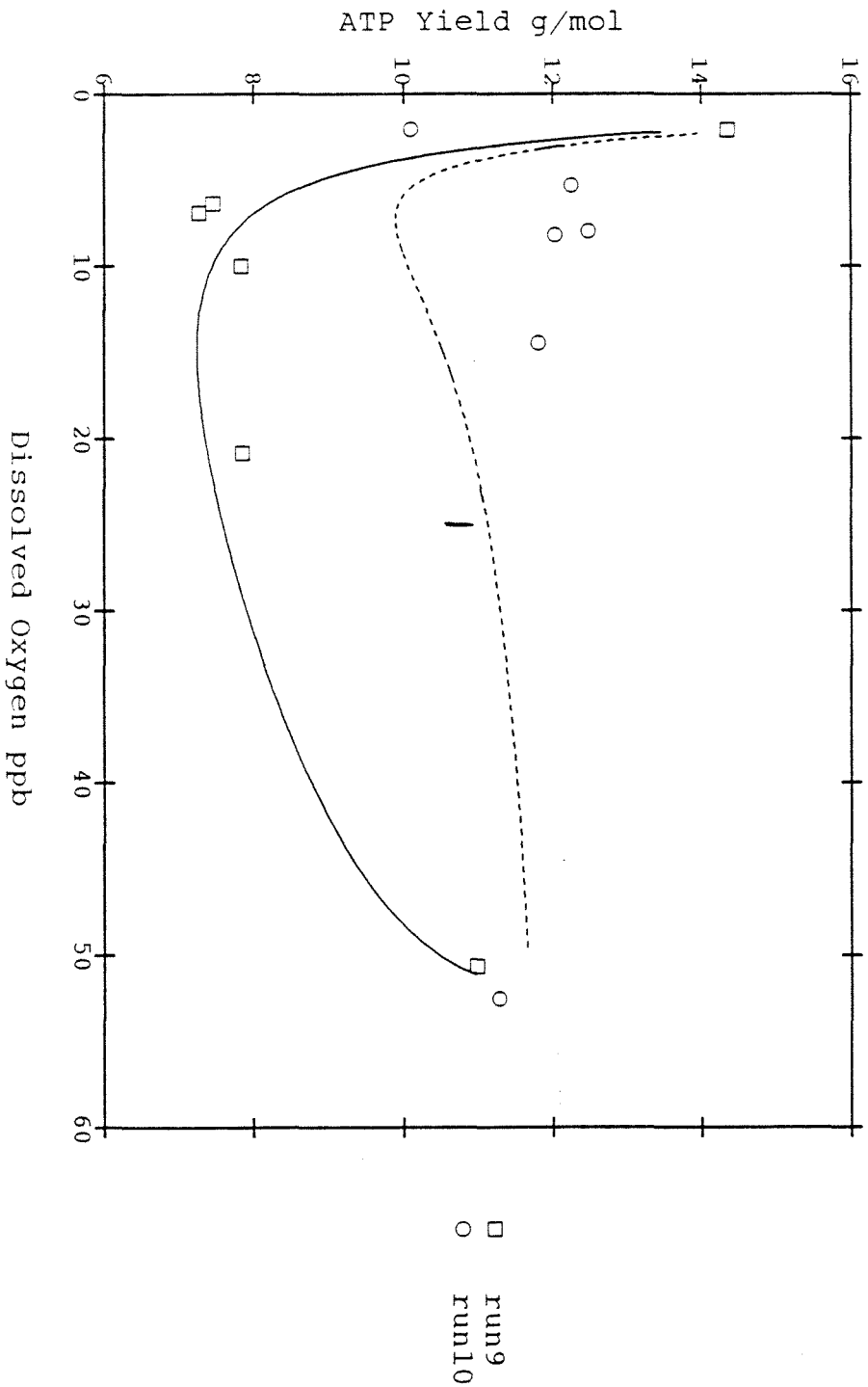

FIGURE 14. ATP YIELD vs. DO : Predictions

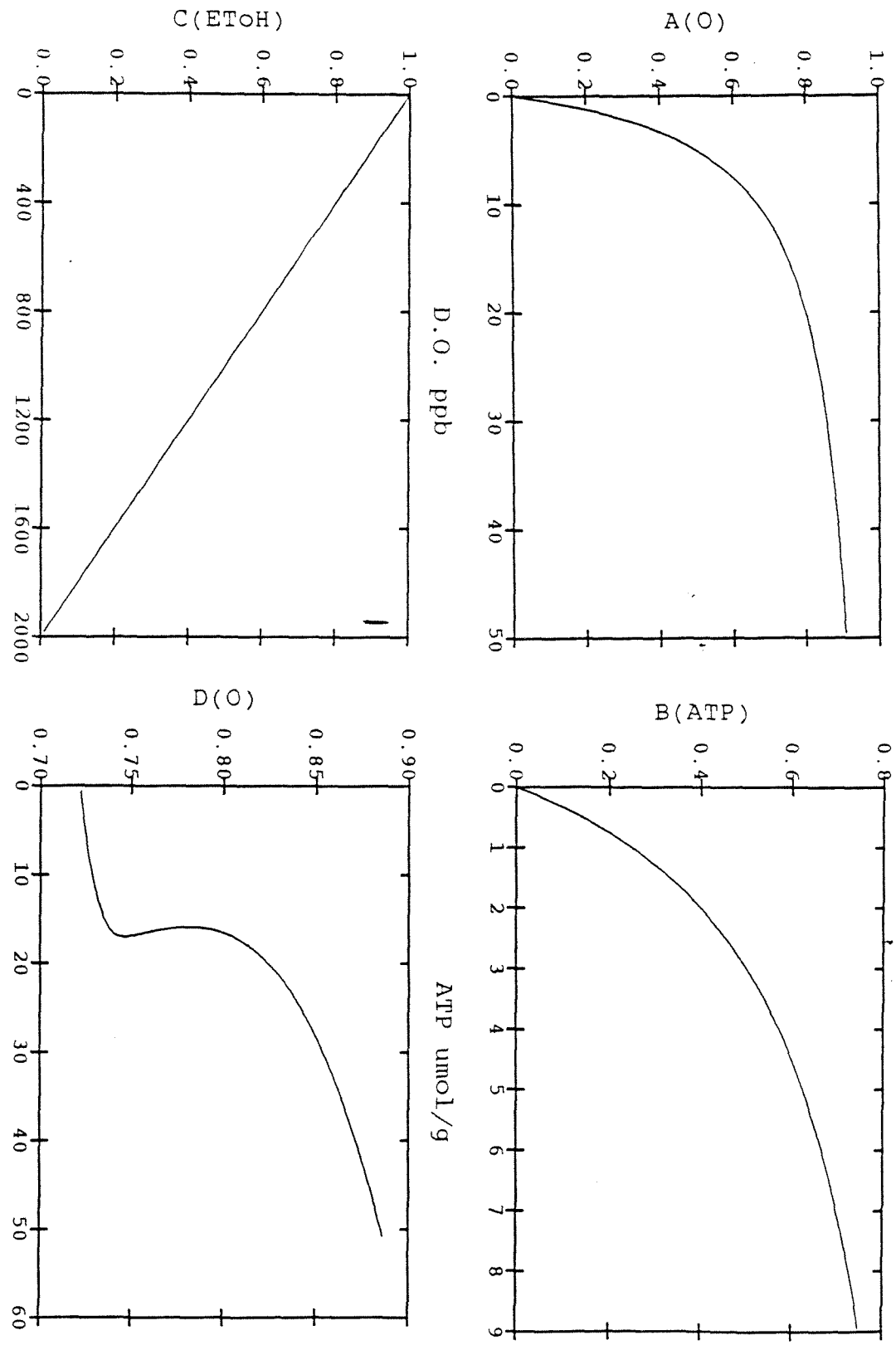

FIGURE 15.

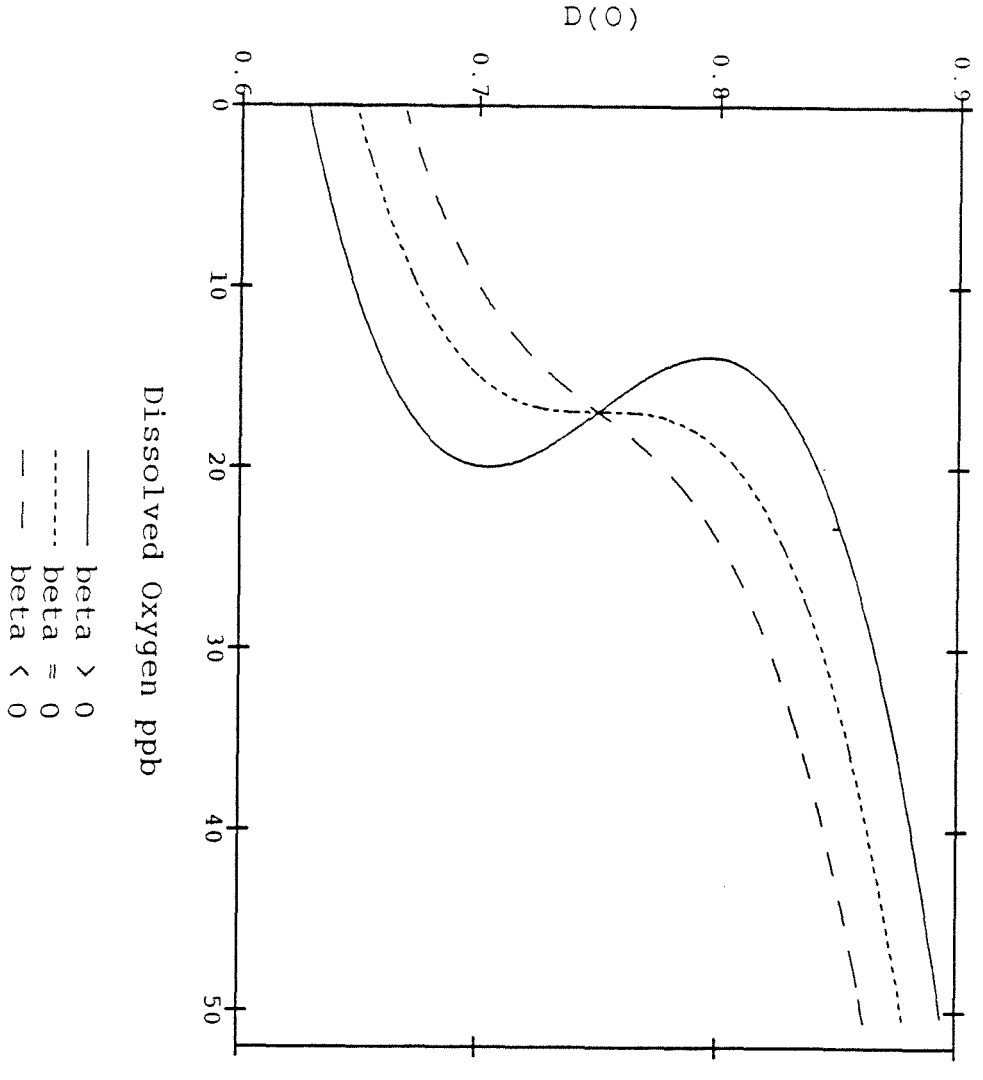
D(O)
0.9
0.8
0.7
0.6
0
10
20
30
40
50
Dissolved Oxygen ppb
beta > 0
beta = 0
beta < 0

FIGURE 16.

FIGURE 17. SPECIFIC ETHANOL PROD.

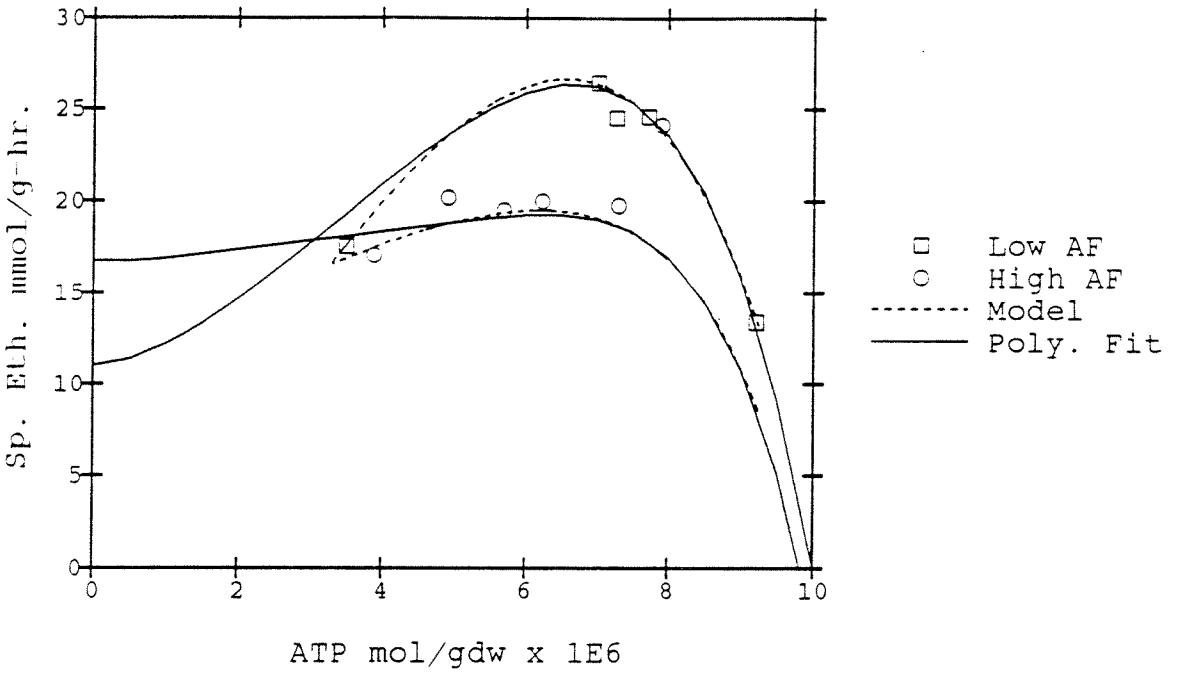

FIGURE 18. ATP vs. DISSOLVED OXYGEN

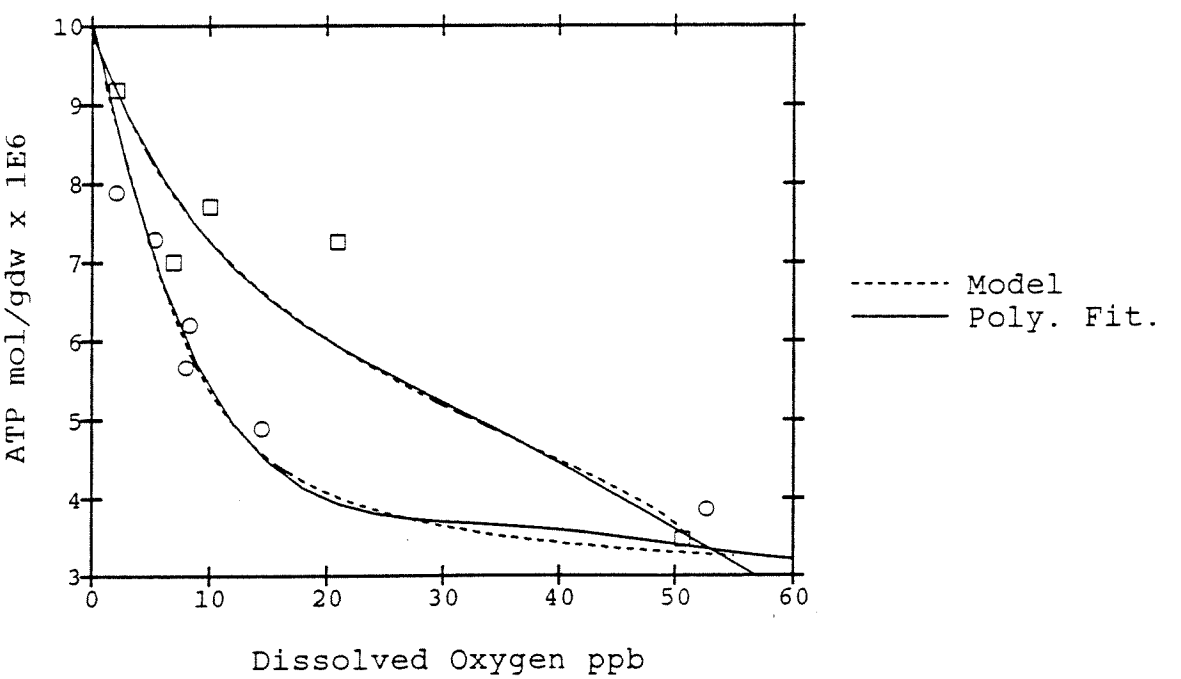

FIGURE 19. A

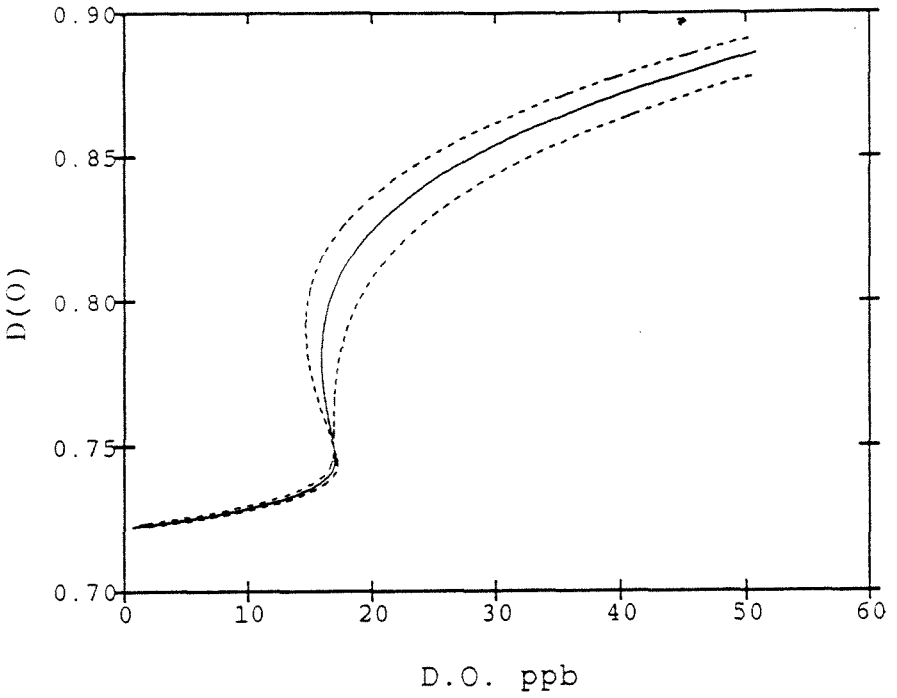

B BIOMASS vs AERATION

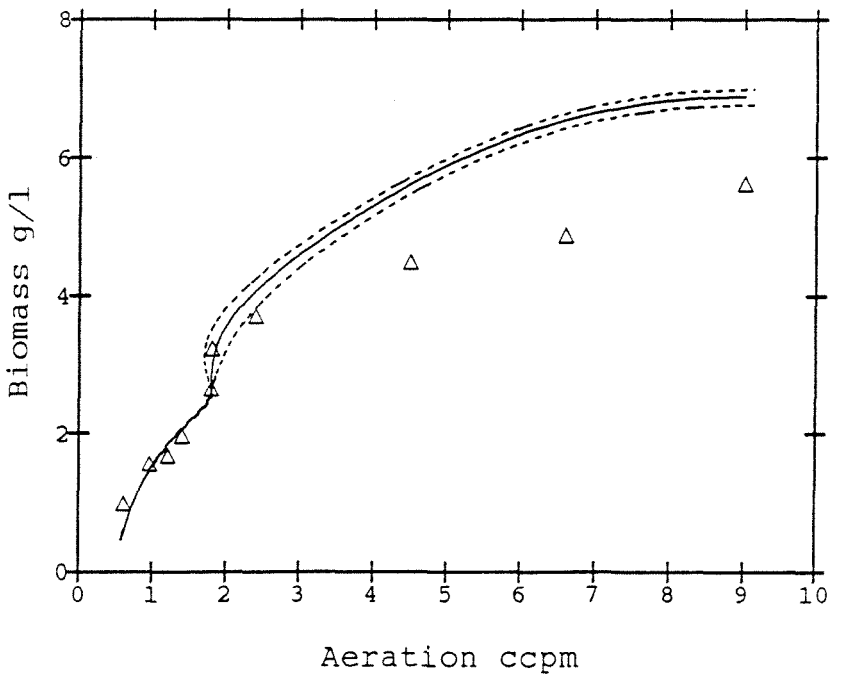

FIGURE 20. BIOMASS vs AERATION

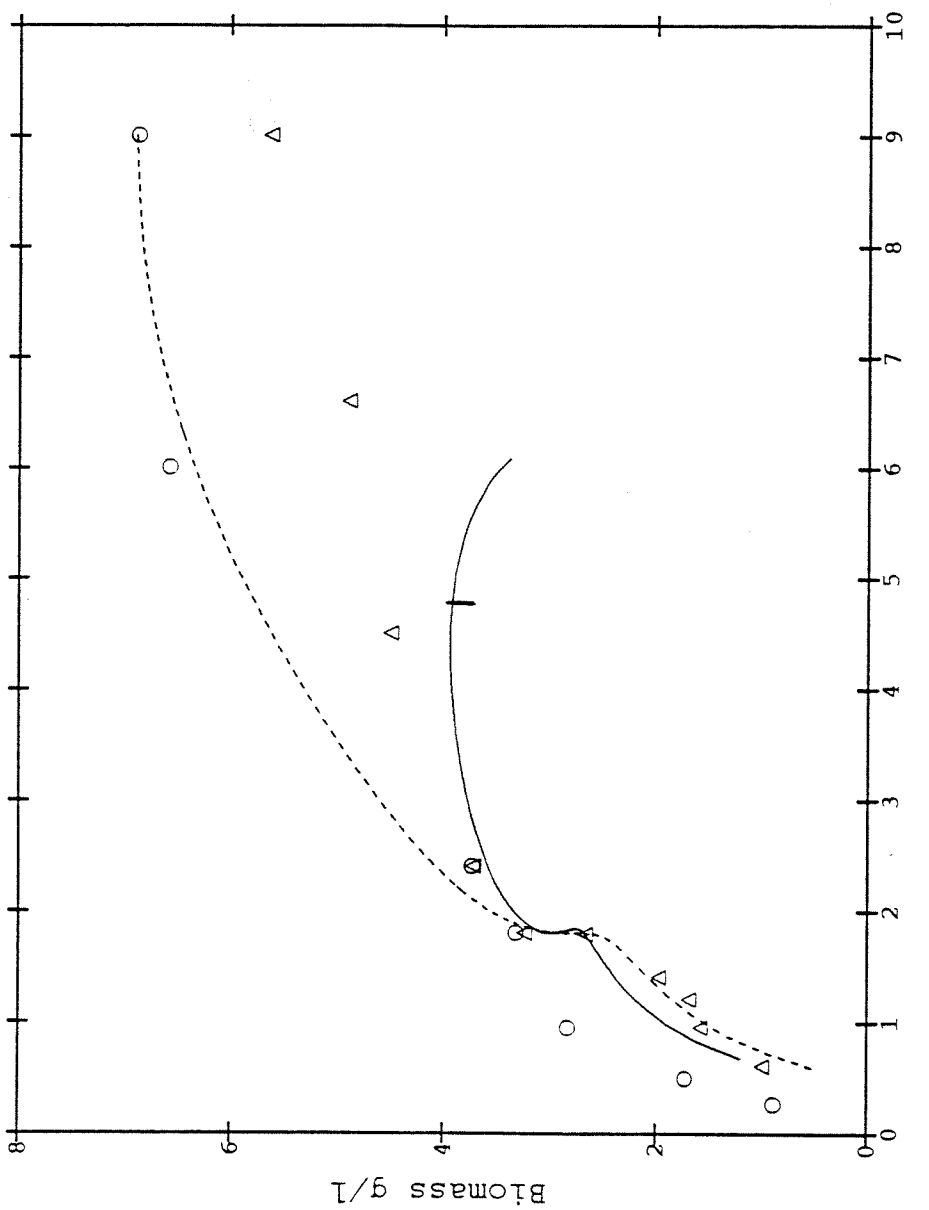

FIGURE 21. A

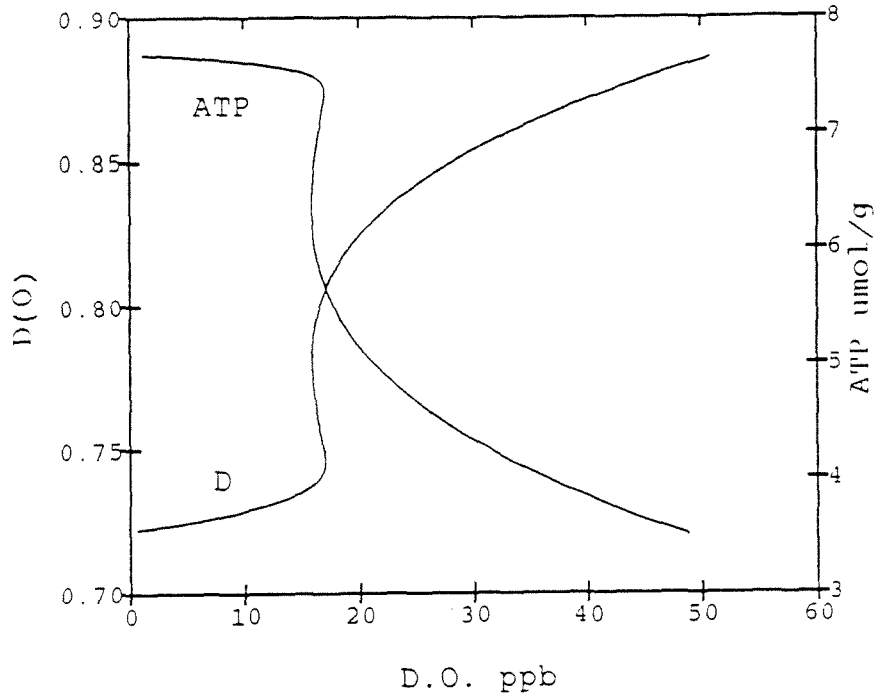

B ATP vs. DISSOLVED OXYGEN

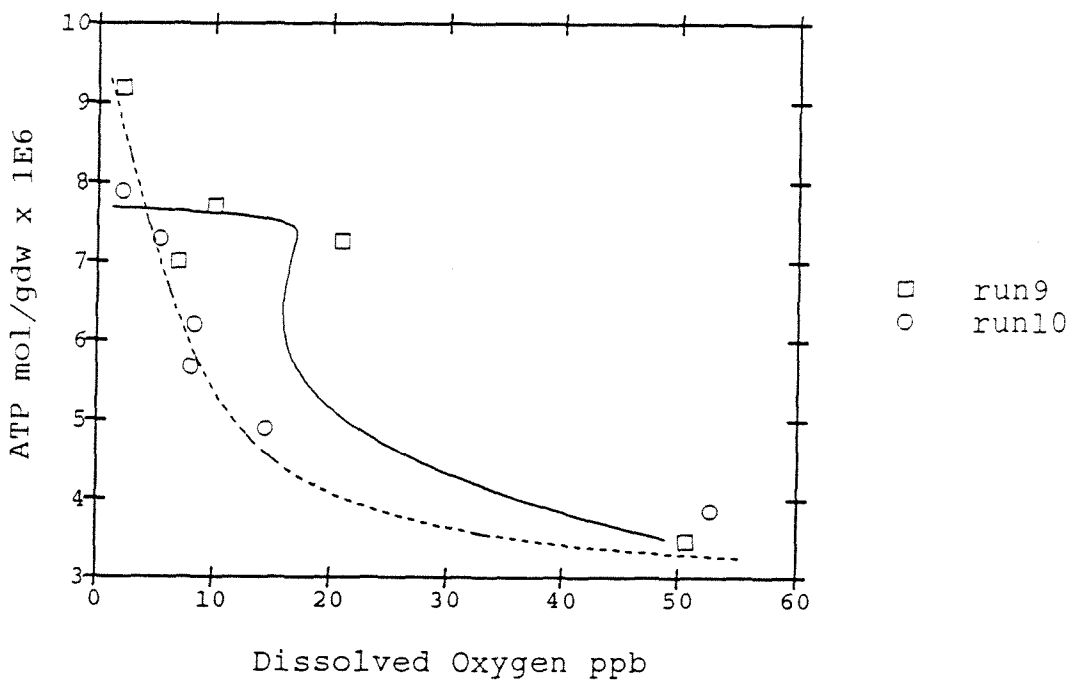

FIGURE 22. BIOMASS vs AERATION

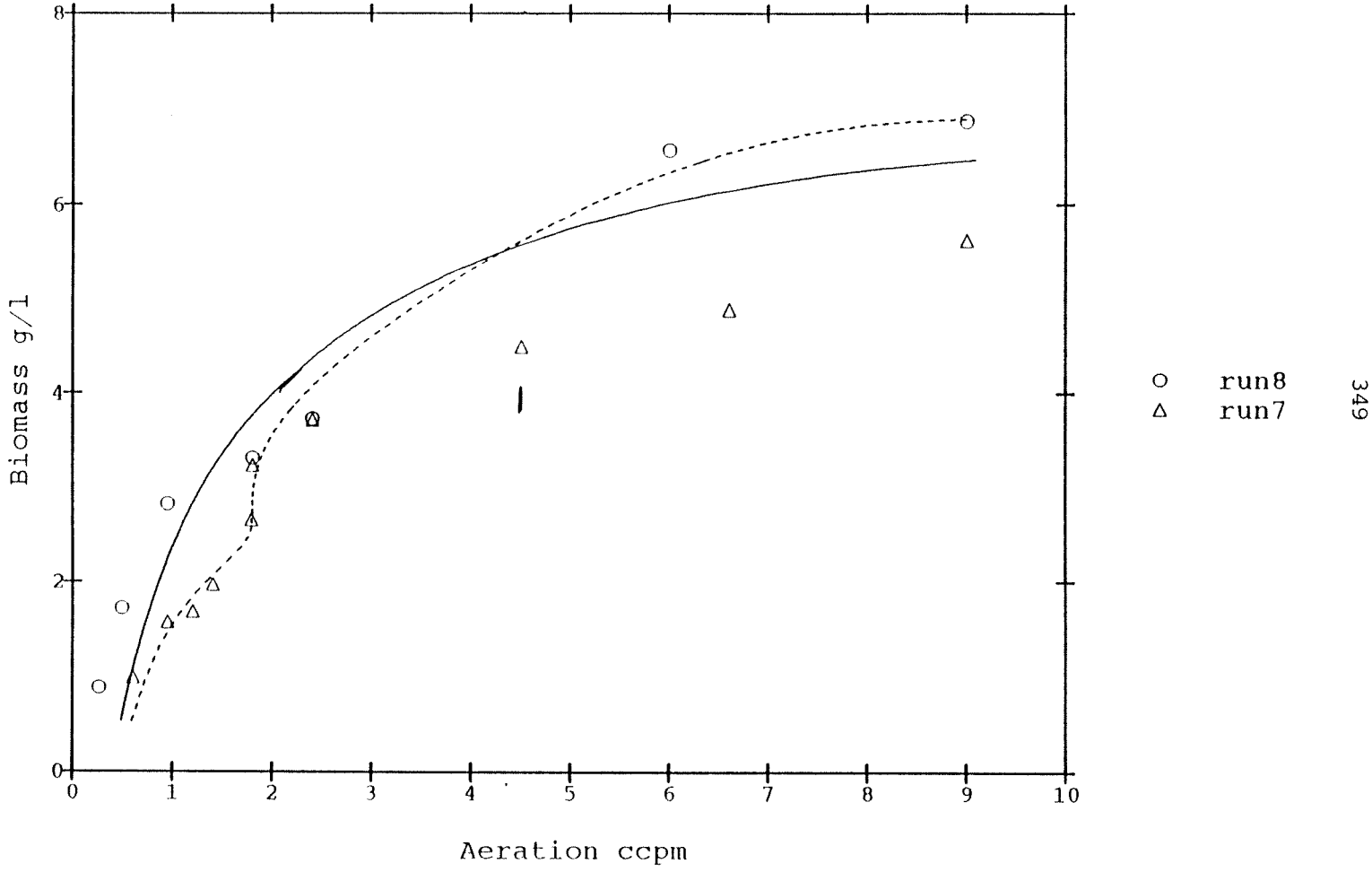

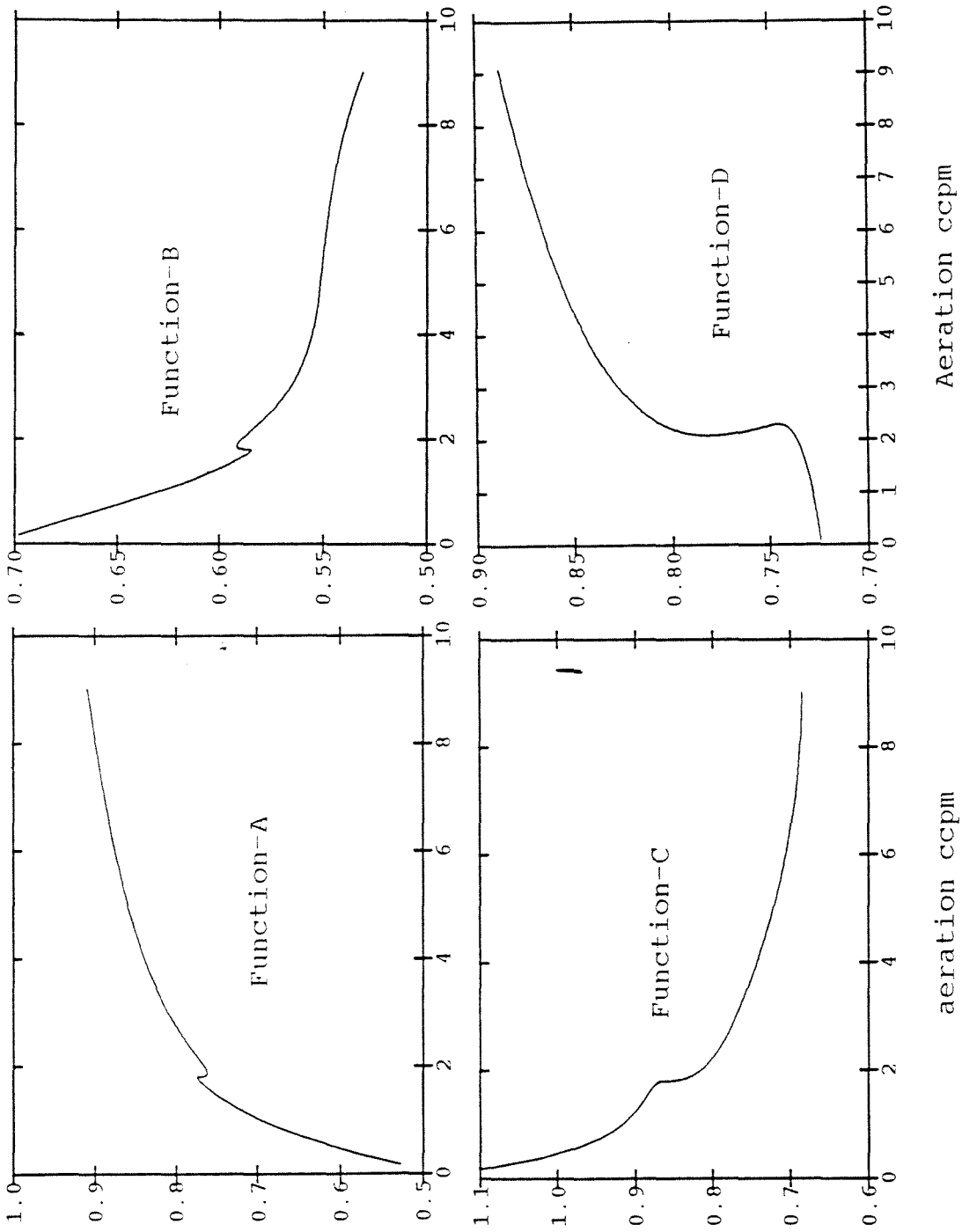
Function-A
Function-B
Function-C
Function-D
aeration ccpm
Aeration ccpm

FIGURE 23.

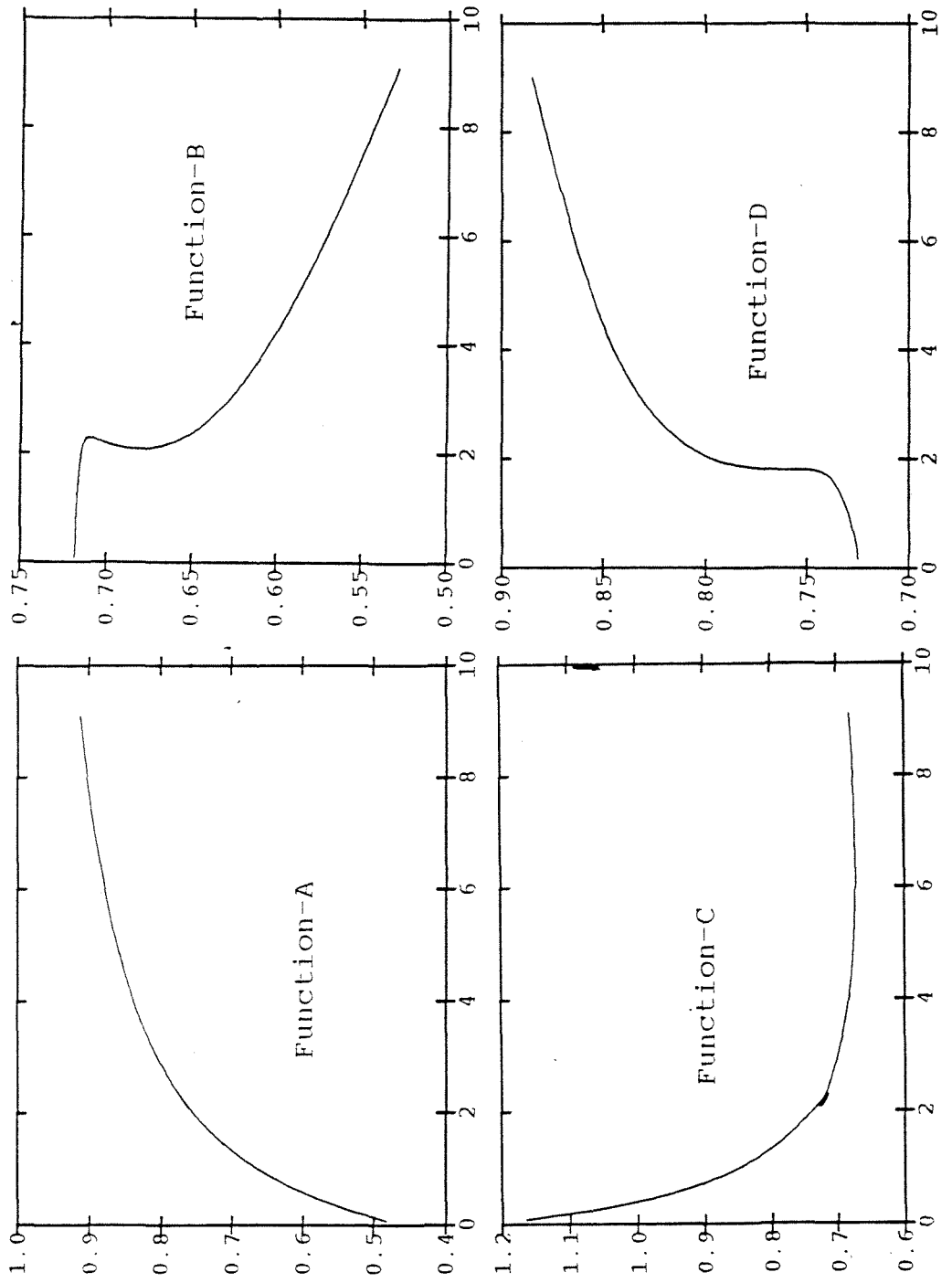
Function-A
Function-B
Function-C
Function-D
Aeration ccpm
Aeration ccpm

FIGURE 24.

FIGURE 25.

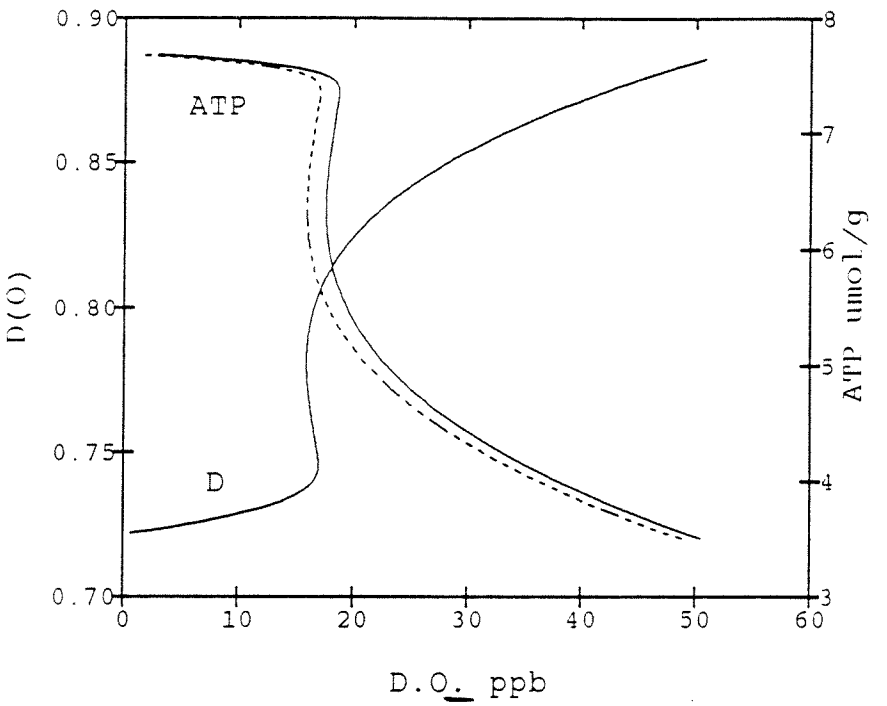

FIGURE 26. BIOMASS vs AERATION

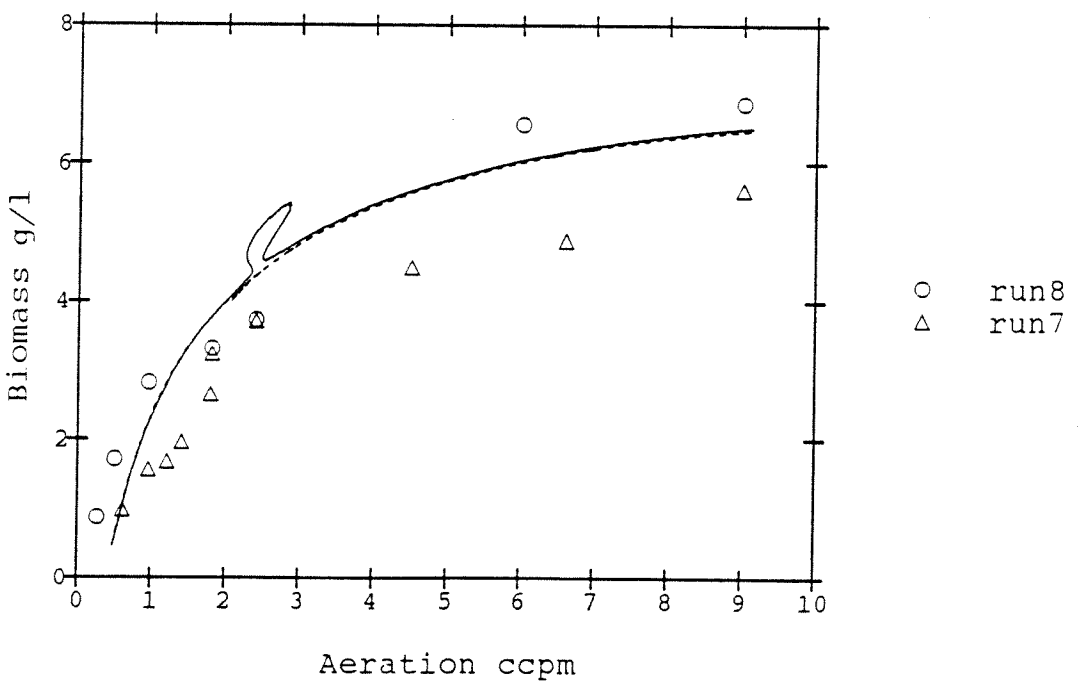

FIGURE 27. ATP vs. DISSOLVED OXYGEN

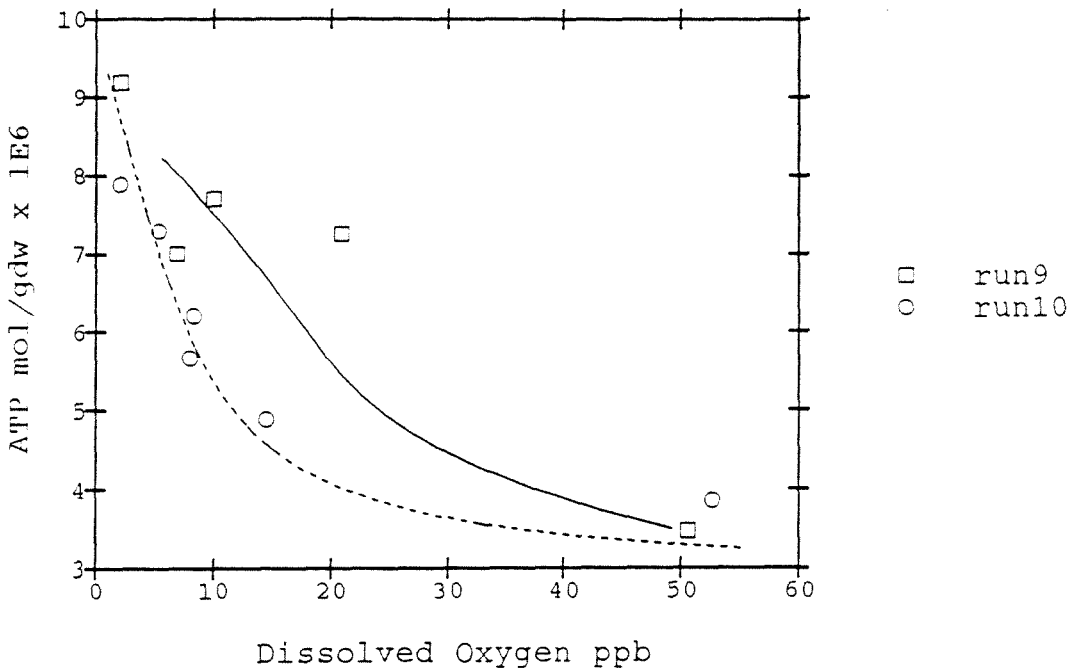

FIGURE 28. BIOMASS vs AERATION

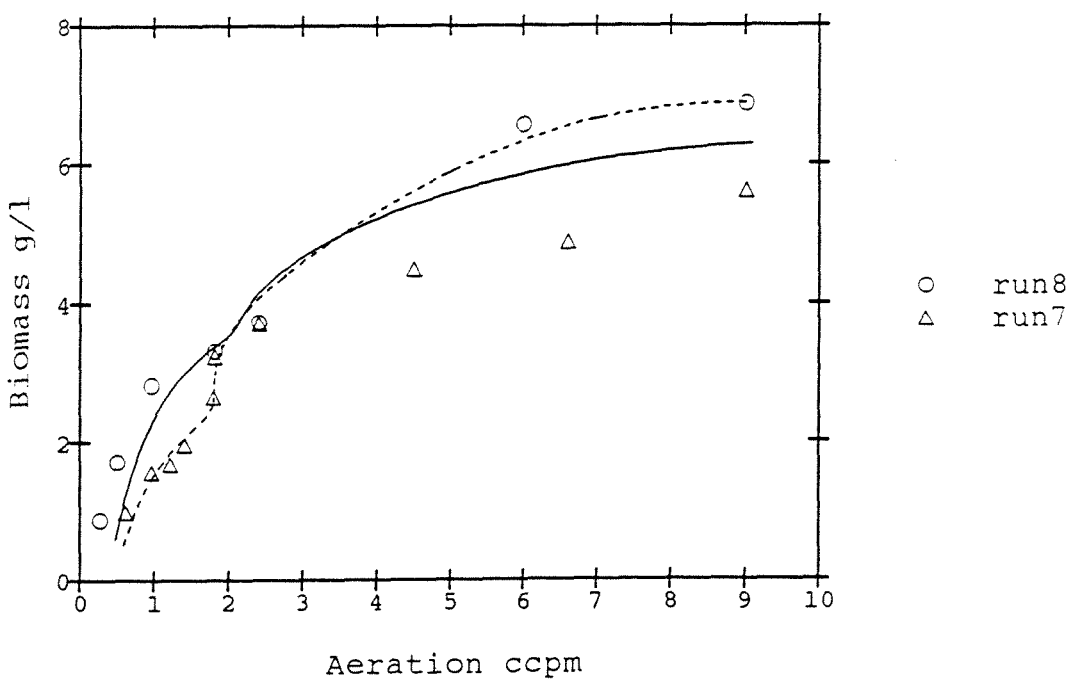

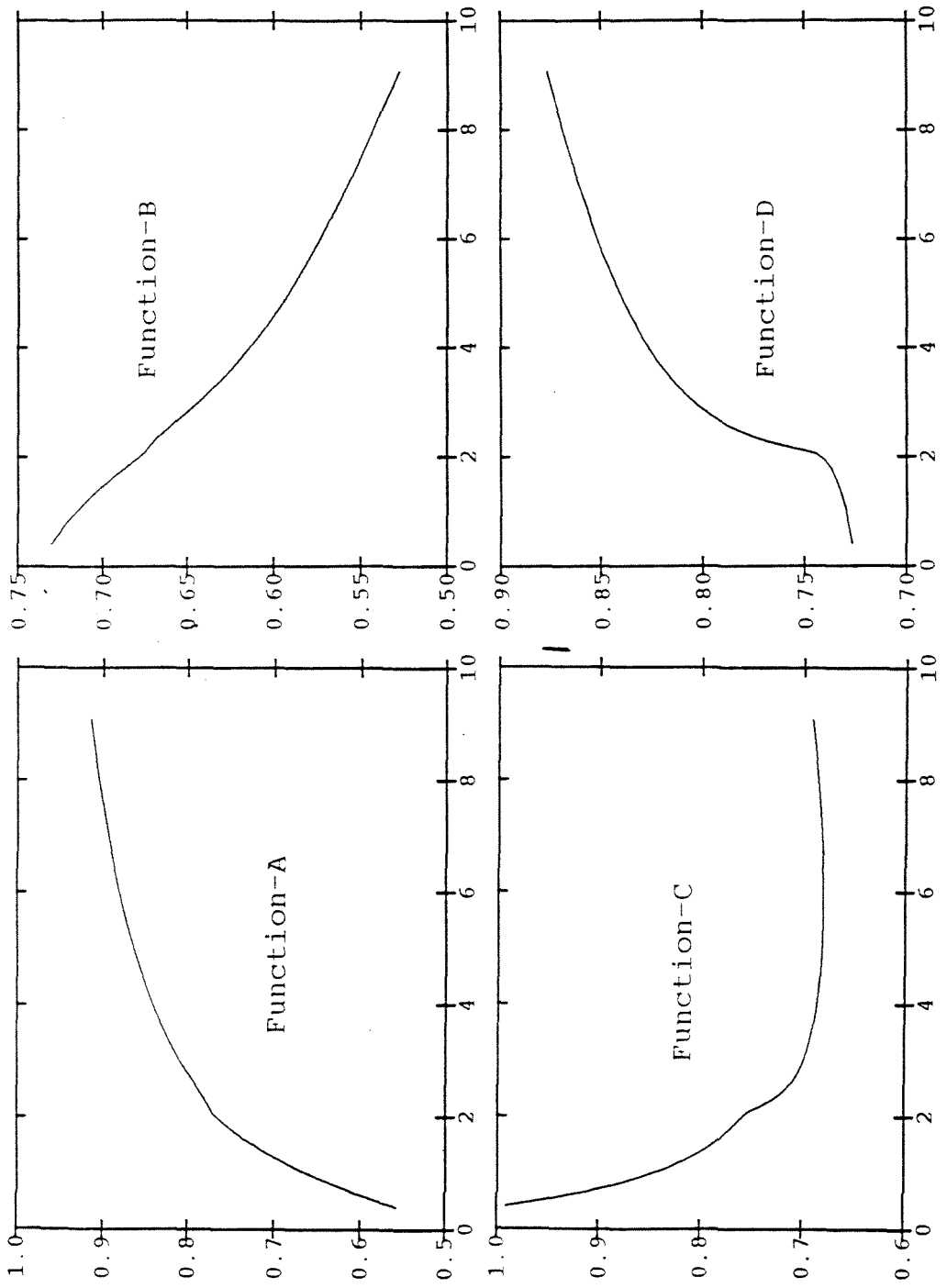
Function-A
Function-B
Function-C
Function-D
Aeration ccpm
Aeration ccpm

FIGURE 29.

TABLE 1. Catabolic Model, First Version

$R_1 = [K_1\ ATP - K_2\ I^2]/K_{11}$ $\quad [K_{11} = 1.0$, low AF
> 1.0, high AF]

$R_2 = K_9 I$ (low AF) $= K_{10} I$ (high AF)

$R_3 = K_6 I\ (K_7 - ATP)$

$R_4 = K_8\ (R_2 - 0.6)$

$R_1 = R_2/2 + R_3/2 + R_4 + 1.37$

$K_1 = 3.32$
$K_2 = 0.858$
$K_6 = 2.99$
$K_7 = 10.43$
$K_8 = 0.819$
$K_9 = 0.634$
$K_{10} = 1.348$
$K_{11} = 1.099$ (1.0, low AF)

TABLE 2. Catabolic Model, Second Version

$R_1 = 10.0 + [K_1\ (ATP - 3.5) - K_2\ I^2]/K_{11}$

$R_2 = K_9 I$ (low AF) $= K_{10} I$ (high AF)

$R_3 = K_6 I[K_7 - (ATP - 3.5)]$

$R_4 = K_8\ (R_2 - 0.6)$

$K_1 = 3.199$
$K_2 = 1.522$
$K_6 = 4.107$
$K_7 = 6.875$
$K_8 = 0.05$
$K_9 = 0.8565$
$K_{10} = 2.028$
$K_{11} = 2.578$ (1.0, low AF)

TABLE 3. Polynomial Fits of R_3 and ATP(O_2)

$$R_3 = 18.7 + 3.21\ (ATP - 3.3) - 0.064\ (ATP - 3.3)^3 - 1.548 \times 10^{-3}\ (ATP - 3.3)^5 \qquad \text{LAF}$$

$$R_3 = 18.0 + 0.457\ (ATP - 3.3) + 0.0159\ (ATP - 3.3)^3 - 2.12 \times 10^{-3}\ (ATP - 3.3)^5 \qquad \text{HAF}$$

$$ATP = 3.4 - 0.217(O_2 - 50) + 2.92 \times 10^{-5}\ (O_2 - 50)^3 - 2.958 \times 10^{-8}\ (O_2 - 50)^5 \qquad \text{HAF}$$

$$ATP = 3.5 - 0.0874\ (O_2 - 50) + 2.028 \times 10^{-5}\ (O_2 - 50)^3 - 1.427 \times 10^{-8}\ (O_2 - 50)^5 \qquad \text{LAF}$$

TABLE 4. Hysteresis Type ATP($\overline{O_2}$)

$$O_2 = 16.84 - 0.75\ (ATP - 7.2)^3 + 1.62\ (ATP - 7.2) \qquad (ATP < 7.2)$$

$$O_2 = 16.84 - 645\ (ATP - 7.2)^5 + 1.62\ (ATP - 7.2) \qquad (ATP \geq 7.2)$$

TABLE 5. Final Version ATP(O_2)

$$O_2 = 18.0 - 0.9\ (ATP - 6.0)^3 - 5.0\ (ATP - 6.0) \qquad (ATP < 6.0)$$

$$O_2 = 18.0 - 0.09\ (ATP - 6.0)^3 - 5.0\ (ATP - 6.0) \qquad (ATP > 6.0)$$